Fault Tolerant Electromechanical Actuators for Aircraft

John William Bennett

A thesis submitted for the degree of Doctor of Philosophy

Newcastle University

School of Electrical, Electronic and Computer Engineering

ACKNOWLEDGEMENTS

The author would like to thank BAE Systems, Eaton Aerospace Ltd. (formerly Fr-HiTEMP), Goodrich Actuation Systems and Airbus UK for working alongside Newcastle University on the two More Electric Aircraft projects and providing many learning experiences along the way. Particular regards to Graham Mason for his awe-inspiring knowledge of safety-critical control systems. Kind regards also to EPSRC and the DTI for their financial contributions towards the research.

Thanks to those who've been my supervisors and mentors over the last decade, Barrie, Dave and Alan. Thanks for providing a steady deluge of work, albeit often enjoyable and also for frequently reminding me that doing the job is only part of the task, understanding it is useful too.

Thanks to the many people who've passed through the doors of the Power Electronics Drives & Machines laboratories; Glynn, Steve, Simon, Matthew, Little Ross, Big Ross, Andrew, Chris, Ed and all the many others who've made working in such a grim building into such a pleasant experience and have also imparted some knowledge along the way.

Much gratitude to Darren, Jack, Allan, James, Chris, Stuart and the other technicians, I'm the worst person in the world at delegating tasks, so thanks for sharing the workload when actually given the chance. Without these gents, such a volume of electric drives would not have passed out the door, or my cars passed so many MOTs.

Kind regards to Steve and to the rest of my car club and also my many long-term friends, for showing me that pulling cars apart and going out many times a week is much more appealing than sitting down to write a long-overdue thesis. Again, thanks for that....

And finally, thanks to my family and the biggest 'thank-you' to Linda, for encouraging me to concentrate and complete this thesis and also for enduring months and months of nights in, often seeing me only at the dinner table and putting up with too many cases of 'it's nearly done'. When all is done and dusted, I've got some making up to do...x

ABSTRACT

This thesis reviews the developments in commercial aviation resulting from More Electric Aircraft initiatives. The present level of electromechanical actuation is considered with discussion of the factors affecting more widespread use.

Two rather different electromechanical actuators are presented for commercial aircraft; DEAWS electrical flap actuation and ELGEAR nose wheel steering. Both projects are industrially driven with specifications based on existing medium-sized commercial aircraft.

Methods comparing fault tolerant electric drive topologies for electrical actuators are presented, showing two different categories of electric drive and comparing each category in a variety of operating conditions to assess size and component count.

The safety-driven design process for electromechanical actuators is discussed with reliability calculations presented for both proposed actuators, showing where fault tolerant design is required to meet safety requirements. The selection of an optimum fault tolerant electric drive for each actuator is discussed and fault tolerant control schemes are presented.

The development of the electric flap and nose wheel steering systems is described, with the focus on the work performed by the author, primarily on the power electronic converters and control software.

A comprehensive range of laboratory and industrial results are given for both actuators, showing demonstrations of fault tolerance at power converter and actuator levels. Following testing, further analysis is given on various issues arising prior and during testing of both converters, with design considerations for future electromechanical actuators.

From design testing and analysis, the two projects can be compared to attempt to determine the optimal electromechanical actuator topology and to consider the challenges in evolving the two actuators to aerospace products.

CONTRIBUTIONS TO KNOWLEDGE

Contributions to knowledge in the field of power electronics, machines and drives include:

- The first demonstration that new electromechanical actuators for flap actuation and nose wheel steering can meet reliability and performance targets with the introduction of fault tolerance.
- A new understanding of fault-tolerant permanent magnet drive configurations, indicating how different options influence size and complexities for actuation-type applications.
- New knowledge of how to produce fault tolerant actuation systems to meet safety requirements, based on reliability data, aircraft interfaces and safety-critical control schemes.
- Practical knowledge of optimal fault tolerant control strategies, gathered from the implementation of the drive technologies in the new actuators, including two torque ripple minimization techniques.
- Understanding of input filter sizing and torque synchronisation methods for fault tolerant systems.

SYMBOLS & ABBREVIATIONS

A	Amperes
A/D	Analogue to Digital Converter
ac	Alternating current
ACE	Actuator Control Electronics
ASIC	Application-Specific Integrated Circuit
CMS	Control and Monitoring System
CPU	Central Processing Unit
DAC	Digital to Analogue Converter
dc	Direct current
DEAWS	Distributed Electrically Actuated Wing System
DSP	Digital Signal Processor
DTI	Dept. of Trade & Industry
EABSYS	Electrically Actuated Braking System
EHA	Electro-Hydrostatic Actuator
EBHA	Electrical Backup Hydraulic Actuator
ELGEAR	Electric Landing Gear Extend and Retract
EMA	Electromechanical Actuator
F.T.	Fault Tolerant
FCC	Flap Control Computer
FPGA	Field-Programmable Gate Array
H.V.	High Voltage
IGBT	Insulated Gate Bipolar Transistor
LVDT	Linear Variable Differential Transformer
MCU	Motor Control Unit
MTBF	Mean Time Between Failure
NWS	Nose Wheel Steering
PFC	Primary Flight Computer
P.U.	Per Unit
r/min	Revolutions per minute
RVDT	Rotary Variable Differential Transformer
s	Seconds
SPI	Serial Peripheral Interface
THS	Tail Horizontal Stabiliser
UART	Universal Asynchronous Receiver /Transmitter
V	Volts
v.f.	Variable Frequency

PUBLISHED WORK

From the work documented in this thesis, the author has co-written the following papers which have been presented and published, or accepted for publication:

"Safety-Critical Design of Electromechanical Actuation Systems in Commercial Aircraft"

Bennett, J.W. Mecrow, B.C. Atkinson, D.J. IET Electric Power Applications, 2010.

"A Prototype Electrical Actuator for Aircraft Flaps"

Bennett, J.W. Mecrow, B.C. Jack, A.G. Atkinson, D.J. IEEE Transactions on Industrial Applications, May-June 2010, pp 915-921, Vol. 46, Iss. 3.

"A Fault Tolerant Electric Drive for an Aircraft Nose Wheel Steering Actuator"

Bennett, J.W. Mecrow, B.C. Atkinson, D.J. Maxwell, C.J. Benarous, M. 5th IET Power Electronics Machines and Drives Conference, 2010.

"Failure Mechanisms and Design Considerations for Fault Tolerant Aerospace Drives"

Bennett, J.W. Mecrow, B.C. Jack, A.G. Atkinson, G.J, IEEE International Conference on Electric Machines and Drives, 6-8 September 2010.

"A Prototype Electrical Actuator for Aircraft Flaps and Slats"

Bennett, J.W. Mecrow, B.C. Jack, A.G. Atkinson, D.J. Sheldon, S. Cooper, B. Mason, G. Sewell, C. Cudley, D. IEEE International Conference on Electric Machines and Drives, 15 May 2005, pp.41 - 47.

"Fault-Tolerant Control Architecture for an Electrical Actuator"

Bennett, J.W. Jack, A.G. Mecrow, B.C. Atkinson, D.J. Sewell, C. Mason, G. IEEE 35th Annual Power Electronics Specialists Conference, 20-25 June 2004, pp.4371 – 4377, Vol.6.

"Choice of Drive Topologies for Electrical Actuation of Aircraft Flaps and Slats"

Bennett, J.W. Mecrow, B.C. Jack, A.G. Atkinson, D.J. Sewell, C. Mason, G. Sheldon, S. Cooper, B. Second International Conference on Power Electronics, Machines and Drives, 31 March - 2 April 2004, pp.332 – 337, Vol.1.

In addition the following papers have been presented on work involving the author and described within this thesis:

"The Distributed Electrical Actuation of Aircraft Flaps and Slats"

Mason, G. Everndon, Bennett, J,. UK Magnetics Society, Electrical Drive Systems for the More Electric Aircraft, one day Seminar, University of Bristol, 14 April 2005,

"Electrically Actuated Landing Gear for a Civil Aircraft Application"

Thomas, J. Maxwell, C. Benarous, M. UK Magnetics Society, More Electric Aircraft, one day Seminar, University of Bristol, 2 April 2009,

TABLE OF CONTENTS

1 Electrical Actuation Systems in Commercial Aircraft

Power in an aircraft can be defined as 'primary' or 'secondary' power.

Primary power is created by the propulsion system. Conventionally this involves combusting aviation fuel in a gas turbine, producing thrust either with exhaust gases – a 'turbojet'/'turbofan', or by driving a propeller – a 'turboprop'.

Secondary power is derived from the primary power by generators connected to the engines. It is used to supply energy to all systems on the aircraft. On commercial aircraft there are typically four forms of secondary power [1]:

- **Hydraulic -** for actuation of flight control surfaces.
- **Pneumatic** - for environmental control and wing de-icing.
- **Electric -** for avionics and utility functions.
- **Mechanical -** for engine driven ancillaries, such as fuel pumps.

By definition, an 'electric aircraft' would require both primary and secondary power to be 100% electrical. Unmanned Aerial Vehicles, with battery energy storage and electric motors driving propellers can be considered 'electric aircraft' [2] and studies have considered the impact of scaling this technology to passenger aircraft [3]. Unfortunately there is still a requirement for considerable scientific and engineering advancements, particularly in energy storage, before a purely electric passenger commercial aircraft is viable. Attaining the thrust capability of a gas turbine engine from a similarly-sized electric alternative is impossible with existing technology [3].

The concept of an aircraft with purely electrical power for the secondary systems was considered as far back as the 1970's. Despite retaining the use of gas turbines for propulsion, this arrangement was named the **'All Electric Aircraft' (AEA)**. Various companies conducted studies into the feasibility of the AEA in the 1980's, including NASA with their Integrated Digital Electronic Aircraft program. Hoffman *et al*. [4] predicted that an all-electric-aircraft could reduce aircraft weight by 10% and fuel consumption by 9%. These improvements are based on predicted data for power supplies, actuators and de-icing that are now considered inaccurate or unfeasible; however, many principles of the study remain valid, in particular 'load-sharing'. Hoffman *et al.* suggest that conventional hydraulic, electrical and pneumatic systems are under-utilised as the generators must be sized for the peak power conditions, although for the majority of flight time the power requirements are much lower. Peak loads do not occur simultaneously for the three systems, so a combined system could be rated for considerably less than the combined peak powers, thus giving a considerable size reduction. An electrical power supply was chosen for the combined system since electricity is essential for avionics, lighting and the cabin, while electrical actuators and electrical air conditioning can perform tasks normally assigned to hydraulics and pneumatics respectively.

The studies of the 1980's concluded that an AEA was feasible with existing technology, but such a radical change in aircraft systems was a step-too-large for the aerospace industry [1]. Instead, industry has aimed for a gradual adoption of electrical technology into the secondary systems of their aircraft. This process of change was named the **More Electric Aircraft (MEA).**

Subsequent MEA research programmes were initiated for military [5] and commercial aviation, with the UK Department of Trade and Industry setting up a MEA initiative in the 1990's, supporting commercial aerospace manufacturers and research institutions in various MEA-based projects (*see section 1.5 for examples*).

1.1 INCENTIVES FOR AIRCRAFT TO BECOME 'MORE ELECTRIC'

There are many incentives for adopting more electrical systems on aircraft, but in the case of commercial aircraft, the main underlying factor is financial. Many of the potential advantages of electrical systems will inherently reduce operational costs – for example any reduction in aircraft weight could be re-allocated to a saving in fuel, an increased payload (passengers or cargo) or an increased range, all of these increasing profitability [4,6]. Any reduction of fossil fuel burning can also be seen to have environmental benefits.

Although MEA do not feature the single secondary electrical power source of the AEA, converting a proportion of hydraulic and pneumatic systems to electric can still provide a reduction in net power supply weight by load-sharing. Weight reductions are also possible by simplifying the distribution networks of secondary power systems. Where networks of hydraulic pipes, pumps, valves, coolers and reservoirs are replaced by electrical cables, there can be a net reduction in weight. In addition, with future advances in technology, electrical power generators could be made significantly smaller and more efficient by eliminating gearboxes and integrating more closely with the engine.

Where electronics allows the removal of pipework, valves and mechanical linkages, inspection and maintenance is reduced. Hydraulics require frequent inspection for leaks and topping-up of fluid, whereas electronics require much less inspection time and can offer self-diagnosis of degradation or failure. A reduction in the time required for maintenance will result in lower servicing costs and more time for the aircraft to remain in active service. Installation and removal of components can also be simplified if the disconnection procedure of pipes or couplings is replaced by unplugging of electrical connectors.

There is potential for electrical systems to offer improved reliability over existing systems, which would increase the lifespan of components; however, it is an essential requirement that the safety of an electrical actuator equals or betters that of the system it replaces. By eliminating hydraulics from areas of potential combustion, it has been suggested that electrical systems offer a safety advantage [7,8].

Electrical systems could also offer increased performance, versatility and efficiency. Free from the restrictive pipework networks of hydraulics and with the potential for improved functionality, electric actuators could be distributed to provide new levels of flight control. Automated adjustment of flight control and engine systems already provides a fuel saving in existing aircraft by improving aerodynamics and throttle response [9] and this can improve with more widespread use of electric control systems on the aircraft.

Hydraulics systems can be very noisy, with actuators often audible from the cabin, so any reduction in noise with an electrical alternative would be considered a benefit to passenger comfort.

1.2 ACTUATION IN COMMERCIAL AIRCRAFT

An actuator is defined simply as an operating device and in the case of aircraft, actuators are used to move components to allow manoeuvring on the ground and in the air. Actuators are almost always hydraulic and much of the More Electric Aircraft research involves investigating electrical alternatives.

Manoeuvring is performed with a variety of control surfaces or mechanisms on the ground and throughout the flight, some of which are shown in Figure 1-1.

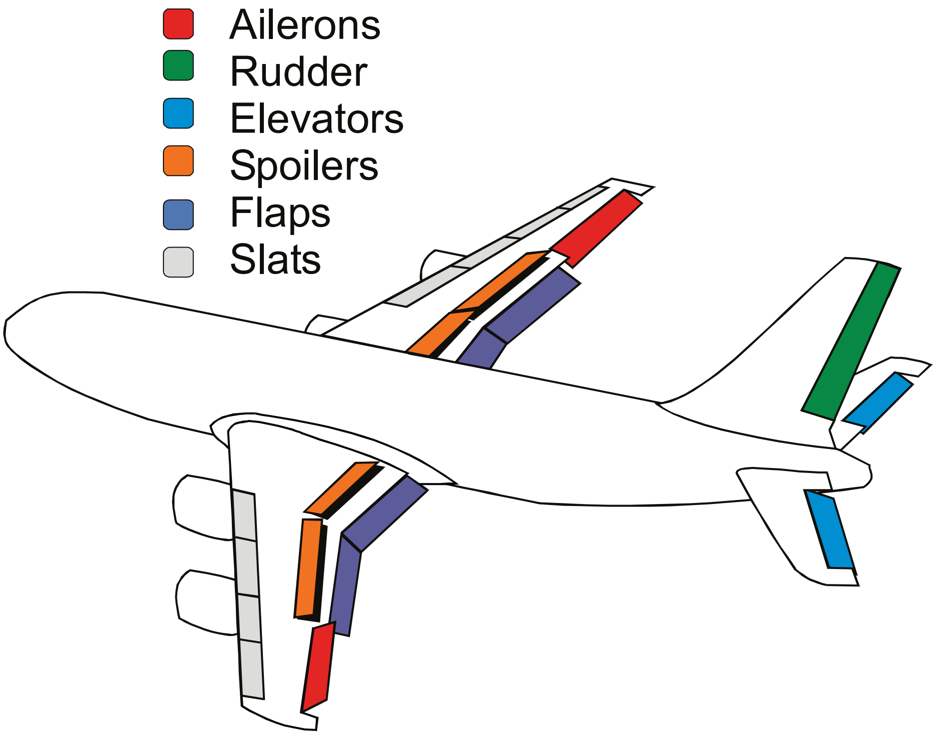

Figure 1-1: Flight control surfaces.

The 'primary' control surfaces consist of:

- **Ailerons**. These are present on the outer trailing edge of the wings and control the rotation of the aircraft along the longitudinal axis – i.e. the *roll*. The ailerons on the two wings conventionally move in opposite directions.
- **Rudder**. The rudder is present on the tail and deflects left or right to alter the rotation of the aircraft along its horizontal axis – i.e. the *yaw*.
- **Elevators**. These are situated on the horizontal tail fins and deflect up or down to point the nose of the aircraft down or up, respectively – i.e. the *pitch*.

The secondary controls and other actuation points include:

- **Spoilers**. Often referred to as air-brakes, these increase the drag on the wing, allowing altitude to be reduced without pointing the nose downwards and increasing airspeed.
- **Flaps**. These extend to increase the wing area, increasing the maximum lift co-efficient and are used for take-off and landing. They are situated on the inside trailing edge of each wing.
- **Slats**. These perform a similar task to the flaps by lowering the stall-speed of the aircraft, thus aiding landing and take-off.
- **Landing Gear**. As well as take-off and landing, the landing gear is required for taxiing to and from the runway. There are multiple actuators required for stowing, deployment and steering.

In addition, ‘trim’ controls also exist to compensate for errors such as heading offsets from aerodynamic and weight imbalances. For example, as cargo may not be ideally centralized, the pilot can set the trim to counteract the effects, rather than manually compensating via the primary controls for the duration of the flight. Some aircraft simply use zero offset adjustments of the primary surfaces to set trim, while others have additional actuated trim surfaces – for example the A380 features a horizontal trim stabilizer on the tail (*see 1.3.3*).

The term ‘**fly-by-wire**’ was introduced in the 1960’s to commercial aircraft [9]. Whereas previously there were mechanical linkages between the control levers in the cockpit and the actuator, fly-by-wire replaced this link with a sensor on the cockpit lever and a wired analog/digital link to the actuator. Although control is electric, via servo valves at the actuators, power is still provided by pressurised hydraulic supply lines.

The term ‘**power-by-wire**’ applies to an actuator that is powered from an electrical supply. An aim of the MEA initiative is to increase the quantity of power-by-wire actuators on aircraft.

1.3 MORE ELECTRIC ACTUATION IN COMMERCIAL AIRCRAFT

1.3.1 The Electro-Hydrostatic Actuator

One of the first developments of the More Electric Aircraft initiative was the Electro-Hydrostatic Actuator (EHA), a hybrid electrical/hydraulic device and a successor to similar actuators used in the Vulcan bomber of the 1950's [10], but designed to meet modern civil aviation safety standards. The actuator is hydraulic in operation; however, the hydraulic fluid is self-contained and pressurised by an inbuilt electric motor to move the actuator. Significant pressure is only required for movement, resulting in an energy saving over the conventional hydraulic servo-actuator which maintains pressure when holding [11]. As only an electrical supply is needed, the EHA is power-by-wire, thus following the MEA path of migrating devices to electrical generators and saving weight and maintenance by removing hydraulic supply networks. There are also safety advantages in running electrical cables along the fuselage rather than hydraulic pipes and less hazardous hydraulic fluids can be used in localized systems than the conventional Skydrol™.

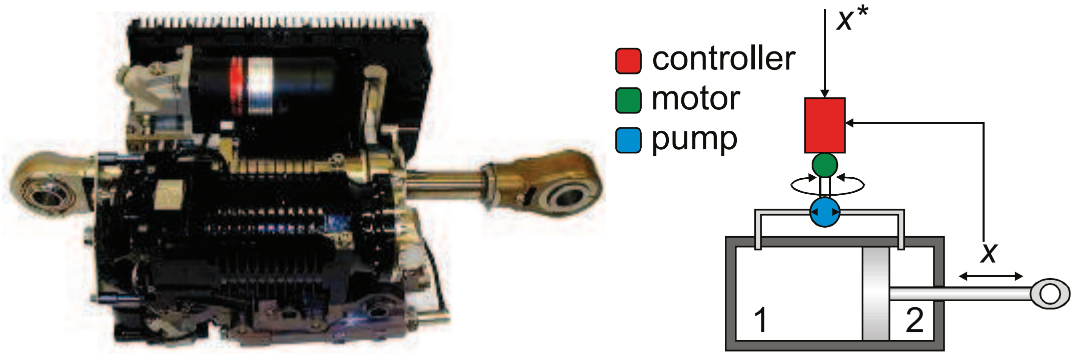

Figure 1-2: A380 EHA photo and topology (photo c/o Goodrich).

Internally, a power electronic converter drives a permanent-magnet, brushless dc motor to speeds up to 10,000r/min and 50kW [7], to drive a pump, as in Figure 1-2. By changing the direction the motor/pump, hydraulic fluid can be pumped into chamber 1 to extend the actuator arm, or into 2 to retract. The device operates in position control, with a linear position transducer (LVDT) feeding the arm angle back to the controller. Without a hydraulic supply network in which to dissipate heat, the casing of the actuator acts as a passive heatsink. When stationary the motor is rotating at a low speed (100r/min) to overcome leakage flow in the actuator and pump [12].

EHAs could be considered an interim stage in the transition from hydraulic to electromechanical actuation, although there are benefits in this hybrid approach:

- Hydraulic actuators can have a very high power density, which is increased as fluid pressure is increased.
- With its compact design, an EHA can almost be considered a direct physical replacement for a conventional hydraulic unit, so design of the aircraft can be relatively conventional and thus more appealing to aircraft manufacturers.
- Upon failure, hydraulic rams will no longer be able to exert force and will default to a damping action, rather than locking solid or exerting a drag force. This allows the actuator to 'fail-safe', so where multiple actuators drive a surface, the remaining actuators can still provide movement.
- As multiple EHAs can be used to drive a surface for safety backup purposes, there is no requirement for backup technology within a single EHA, so a conventional motor-converter can be used

1.3.2 The Electrical Backup Hydraulic Actuator

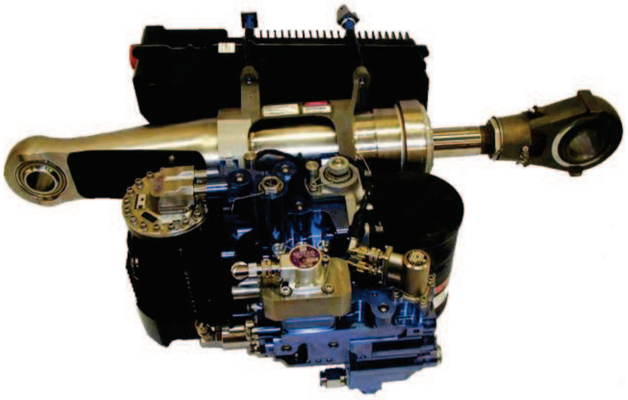

Figure 1-3: EBHA from A380 rudder (c/o Goodrich).

The Electrical Backup Hydraulic Actuator (EBHA) uses the modern electrical technology of the EHA but in a rather different arrangement - the unit is a hydraulic actuator with an electrical backup [9].

The actuator connects to the aircraft hydraulic supply for a primary source of power, with electronics providing the control signals, as is normal with 'fly by wire'. As a back-up, the actuator also includes an electric pump which, in the event of hydraulic supply failure, can pressurise the fluid in the actuator allowing full operation of the hydraulics from an electrical supply.

1.3.3 More Electric technologies in production aircraft

The Airbus A380 debuted in 2007, the largest commercial aircraft in the world and a showcase for new technology, including many ‘more-electric’ approaches to flight control actuation. Figure 1-4 shows the actuator configuration for the flight controls.

With the technologies available at the time of design, hydraulic and electro-hydraulic actuation were considered a necessity due to the size of the aircraft and the forces required. To minimise the size of the actuators, 5000psi was used, rather than the conventional 3000psi. Hydraulic actuators are present on each type of control surface, although where safety and design permits, electrical technology is used in parallel or as a backup. In the event of a complete hydraulic supply failure, the aircraft is capable of flight using 100% electrical and electro-hydraulic actuation, although EBHAs are only intended for backup and are therefore rated for a short operating cycle [13]. The total estimated weight saving due to the electro-hydraulic actuators and moving to higher fluid pressure is claimed to be over 1.5 tonnes [10].

There are 8 spoiler surfaces on each wing, all of which use conventional hydraulic actuators, bar surfaces 5 and 6 which use EBHAs. Two hydraulic power supplies (‘green’ and ‘yellow’) are alternated between surfaces, so that if a supply fails, there remains an even distribution of functioning spoilers across the wing.

As the spoilers employ hydraulic or electro-hydraulic actuators, failure of an actuator will result in the actuator reverting to a damping mode, rather than a jam. The failed surface will ‘blow back’ to an aerodynamically safe position, while the remaining spoilers will be sufficient for air-braking. In the event of complete hydraulic failure, the EBHAs on surfaces 5 and 6 will provide emergency functionality from electrical supplies.

The three aileron surfaces of a wing are each powered by dual actuators, so loss of an aileron would require failure of both actuators. The mid and inboard surfaces are sufficient for flight control following an outboard failure, so both use an EHA in parallel with a hydraulic actuator, allowing electrically powered operation in the event of total hydraulic failure.

Elevators are similar to the mid and inboard ailerons in their use of hydraulic actuators and EHAs on each surface. As elevators are flight critical, every surface will be able to operate from an electrical source in the event of hydraulic failure.

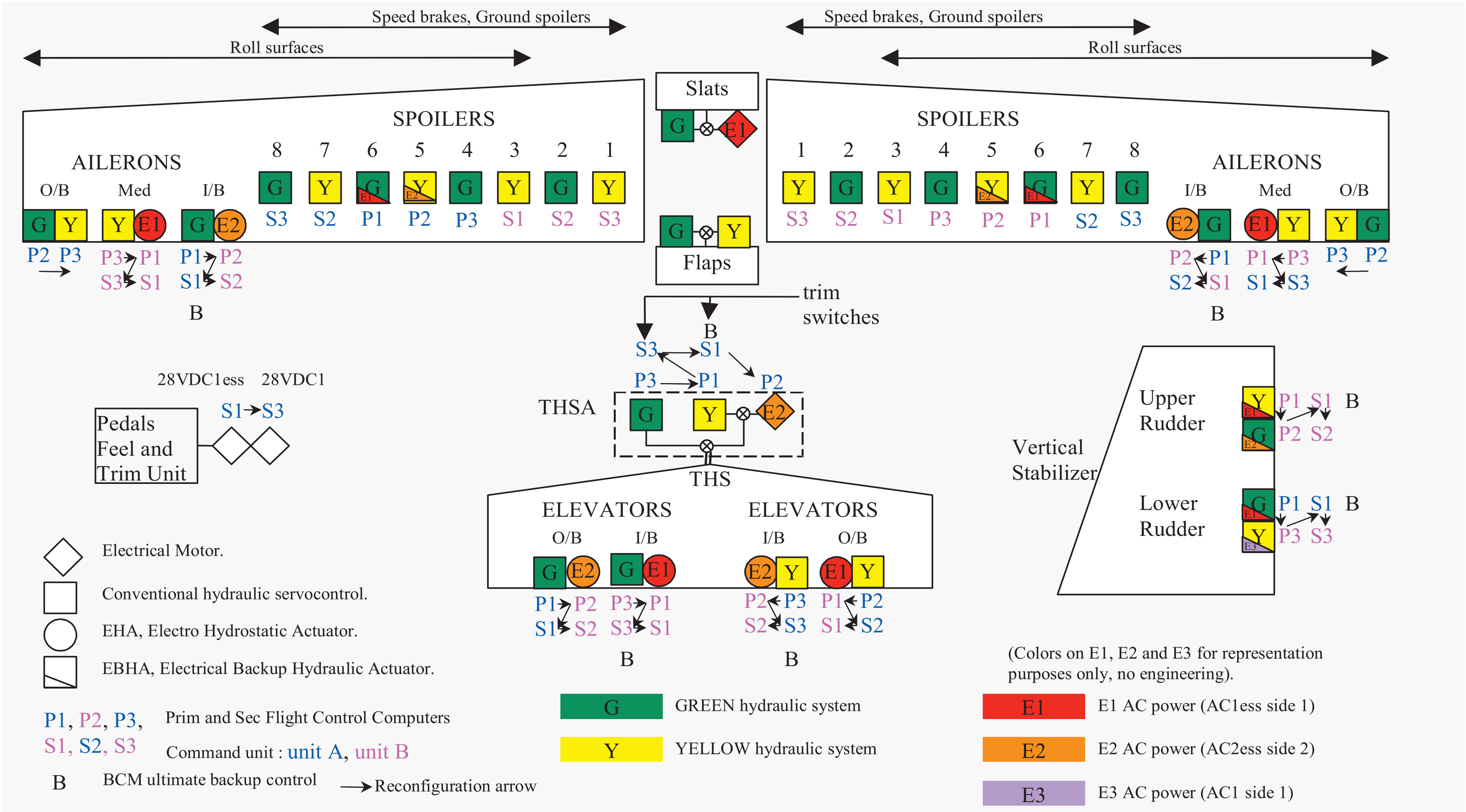

Figure 1-4: Architecture of flight control surfaces in the Airbus A380. Courtesy of Goodrich Actuation Systems.

s.

There are two rudders, each actuated with a pair of EBHAs. The configuration allows a rudder to operate with a failure of an actuator, or multiple power supply failures.

The tail hydraulic stabilizer (THS), an additional secondary flight control on larger aircraft, features a hydraulic actuator and an electric-hydraulic actuator. The electric-hydraulic actuator contains both a hydraulic and electric motor with a speed-summing gearbox, so either can move the actuator if the other is stationary or jammed. All flaps and slats are powered via driveshafts from two speed-summed motors within the body of the aircraft, both of which are hydraulic on the flaps, while one motor is electric on the slats.

A summary of the key points in the A380 configuration can be made:

- Hydraulic actuators are the foremost source of actuation power.
- The entire architecture is arranged so that full functionality can be maintained with the loss of an actuator, a power supply, a control signal and where aerodynamically safe, complete loss of drive to a control surface.
- For surfaces which are critical to remaining airborne, functionality can be maintained after failure of two power supplies.
- The aircraft can fly for limited periods using only electrically powered actuators, although performance will be limited as a result of no functioning flaps and a reduced number of active surfaces.
- The rudders are the only surfaces to feature solely electro-hydraulic actuators; however, as EBHAs are used, they are still primarily driven from hydraulic power supplies, with electrical providing the emergency backup.
- Only the slats and the tail horizontal stabiliser feature electromechanical actuators. As a jam is considered a failure possibility in an electric motor, or the associated mechanism (e.g. a ball screw), electrics are confined to control surfaces which can either be locked in the event of a failure or as backup where torque-summing gearboxes can overcome jams.

From a safety-backup viewpoint, the advantages of the More Electric approach are made clear in the A380 architecture. With 2 hydraulic and 3 electric power sources there are a total of 5 power supplies used on the flight control surfaces. This could all be accommodated by 5 hydraulic supplies, but, as multiple electric power supplies would already be present for avionics and cabin electrics, re-using these as backup supplies to actuators achieves the same 5 supply safety level with just 2 hydraulic systems.

Another significant change from convention in the A380 is the introduction of variable-frequency power generators. The variable frequency results from the absence of Constant Speed Drives (CSD), mechanical devices translating a variable-speed engine output to a constant speed mechanical input for an electrical generator [14]. Removing the CSDs result in a weight saving and an estimated 50% increase in electrical power system efficiency [10], although, since the generator output now varies with engine speed, all connected electronics must operate from a power supply frequency varying between 400 and 800Hz.

Although a very recent example, the A380 is not the first instance of More Electric technologies in modern commercial aircraft. In the early 1990's, Boeing were implementing an electrical backup arrangement for the flaps and slats in the 777 [15]. The system is similar to the A380 in that central hydraulic motors drive the flaps and slats, with electrical motors as backup. The main difference is that an electric clutch couples the electric motor, rather than a speed summing gearbox. The 777 was also the first 100% fly-by-wire Boeing aircraft.

1.4 RELIABILITY AND SAFETY

The actuator arrangements described in section *1.3* are all derived from comprehensive studies of component reliability and the reliability requirements for safety regulations.

Reliability is conventionally expressed as a Mean Time Between Failure (MTBF), with aerospace adopting the units of 'flight hours'. A component with a MTBF of 1 billion flight hours would be predicted to suffer one failure if 1 billion of the components were operated for 1 hour on an aircraft – i.e. a 1 in a billion chance of failure during a 1 hour flight. MTBF is not an indication of lifespan, so a single component would not be estimated to last 1 billion hours in service as degradation occurs over time, decreasing the reliability.

When considering aircraft safety, the acceptable probability of a failure event occurring determines the reliability requirements of the associated components. As is convention with probability, failure probabilities are expressed as a fraction per flight hour, so a probability of 1.0 is a guaranteed failure during an hour of flight and 1×10^{-3} is a 1 in 1000 chance of failure during an hour of flight.

As an example; if the acceptable failure of the propulsion system is 1×10^{-9}, then the combined MTBF of the propulsion-providing components must be 1 billion hours.

If no individual engine systems are available with this reliability, two engines can be used and configured so both are completely independent and either capable of propelling the aircraft. To calculate the implications of this, from 'compound probability', the probability of two completely independent events occurring is equal to the product of their probabilities:

1-1 $$P_{a\&b} = P_a \times P_b$$

If *a* and *b* are the failure probabilities of each engine and are considered to be of the same value (as they are identical engines) then the probability of both occurring is:

1-2 $$P_{a\cdot b} = P_a^{\ 2}$$

If for our example the allowed probability of both occurring is 1×10^{-9}, the minimum reliability requirement for a single engine per flight hour is calculated as:

1-3 $$P_a = \sqrt{1\times10^{-9}} = 3.16\times10^{-5}$$

The MTBF requirement for a single engine is the reciprocal: 31,622 flight hours.

So, for a subsystem of failure probability *p*, putting *n* completely independent subsystems in parallel gives a failure probability of p^n.

Seemingly unfeasible reliability requirements can be met by putting backup sub-systems in parallel. An electronic system with duplication of components to provide alternatives when one fails is known has having **redundancy**. This allows continued operation after a fault, referred to as **fault tolerance**.

There are restrictions to adding components in parallel, as the added complexity results in more components that may fail. Using the engine example, if there are *n* engines, each of reliability P_a, then the probability of a single engine failing, P_s, is:

1-4 $$P_s = nP_a$$

If an engine was designed from *eqn.* 1-2 to precisely attain the failure probability of 3.16×10^{-5} and two engines were used in the aircraft, the probability of an engine randomly failing is now 6.32×10^{-5}. While it may be allowable to fly with certain component failures, increasing the component count to attain safety targets will ultimately result in more time with the aircraft out of service, undergoing repairs. The use of more reliable components will result in fewer required in parallel to meet safety requirements and thus reduce the maintenance requirements.

The safety requirements of actuation systems vary throughout the aircraft as they are determined by the resulting severity of a failure. As can be observed in the A380, the primary flight control surfaces must function throughout the flight, so multiple actuators are present on multiple surfaces, with multiple power sources.

The safety requirements for *loss of function* are lower for flight surfaces that are not critical to flight, but in which failure would result in reduced performance or an emergency landing, although the faulted surface must not jeopardize the overall control of the aircraft. For example, each spoiler surface on the A380 contains only an individual actuator as air-braking can be performed from the remaining spoilers; however, a failed spoiler must blow back under aerodynamic forces, so there must be no jam of a failed actuator.

At the design stage, the failure probability of components is calculated using fault-tree analysis, as shown for a rudder example on an unmanned aircraft in [16]. The probability of a failure is derived from all potential failures leading to its occurrence, resulting in a tree of associated events, with values based on sourced component failure data.

1.5 RESEARCH INTO FUTURE TECHNOLOGIES

While the A380 is the commercial debut for many ‘power-by-wire’ technologies, many existing aircraft are decades behind with some not fully fly-by-wire [9], let-alone power-by-wire. With new replacements due for many aircraft, there are opportunities to apply More Electric technologies, of similar levels to the A380 and beyond.

The Totally Integrated More Electric System – TIMES was an initiative setup in 2001 [6] by a consortium of UK aerospace companies to investigate further development of aircraft electrical technologies, including optimizing the design of potential future aircraft around electrical technologies (rather than adapting conventional aircraft or designing components to retro-fit). This section considers some of the More Electric research from TIMES and other initiatives.

1.5.1 Electrical generation and distribution

There is much scope for development in the electrical power generation on aircraft. Although the direct-drive, purely electric system of the All Electric Aircraft could be considered the goal, new developments aim to evolve the existing electric/hydraulic/ pneumatic systems in a More Electric Aircraft.

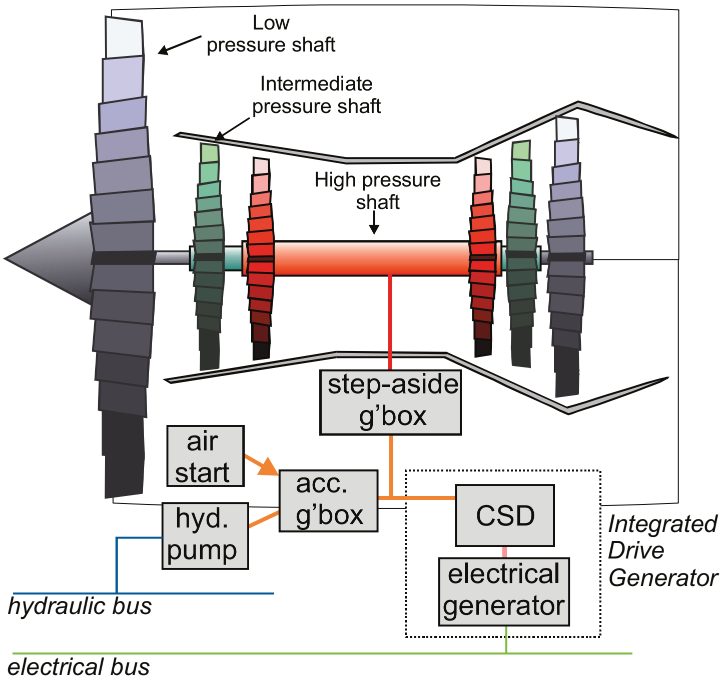

Figure 1-5: Secondary power generation from triple-shaft turbofan engine.

Conventionally electrical power is derived through a series of steps (Figure 1-5):

- A step-aside gearbox derives a right angle output from the main engine shaft at the high pressure spool section.
- The right-angle take-off shaft drives an accessory gearbox (for hydraulic and pneumatics) and an Integrated Drive Generator.
- The IDG incorporates a CSD, capable of translating a variable speed mechanical input into a constant speed mechanical output.
- The CSD mechanical output feeds an electrical generation unit which outputs a constant 400Hz ac at 115V.

As discussed in *1.3.3*, the A380 eliminates the CSD by effectively connecting an electrical generator directly to the step-aside gearbox, resulting in a variable-frequency ac supply. Conventional fixed-frequency generators are not suitable for this arrangement so Oliaya *et al.* [17] describe the design of a new generator to accept the HP engine-speed shaft, at 11400 to 23400r/min and output an electrical signal of 380 to 720Hz at 115V ac (120kVA). All electrical systems on the aircraft must interface to the V.F. supply, so adaptation may be required in some cases where 400Hz-specific devices cannot accept 780Hz.

Research is ongoing into the next logical stage of optimizing the power generation; to remove all gearboxes and drive a generator directly from the gas turbine. Provost [18] proposes an idealised All Electric Aircraft arrangement with multiple electric generators located within the gas turbine, directly on the 10~25kr/min intermediate and high-pressure spool shafts and also on the low pressure spool at the rear of the engine. Using the shaft-mounted generators, the design proposes an electrical link between the intermediate and high pressure shafts of the engine, allowing improved engine control and vastly simpler mechanics by reducing compressor stages and eliminating bleed valves. Without pneumatics to start the engine, this feature will instead be performed by the generator, acting as a starter motor. As there are no accessory gearboxes, hydraulic and pneumatic supplies are derived electrically so an electric alternative for wing de-icing will be required, as this is conventionally achieved pneumatically using a hot air bleed from the engine. Although Provost proposes a theoretical target, there is scope for incorporating aspects of the vision into existing engines as part of the MEA initiative.

Powell *et al.* designed a prototype switched-reluctance machine for locating on the high pressure spool shaft, intended to operate at 350 - 400°C [19] while Hall *et al.* provided further research into this area, designing a switched-reluctance starter/generator with an outer rotor to overcome mechanical expansion issues with such a large, high speed machine [20]. With the More Electric aircraft requiring a greater amount of electrical power generation, the machine is sized for 200kW generation, with an input speed of 13,000r/min.

There are proposed generators to locate on the 1050-3100r/min low-pressure spool shaft, with Mitcham and Cullen of Rolls-Royce discussing 250kW direct-drive and geared permanent magnet generators using oil and air cooling to keep windings below 250°C [21]. A direct drive 250kW prototype generator was subsequently developed, with test data presented in [22]. A direct-drive, low pressure shaft generator and power converter is also undergoing research [23] with a 70kW permanent magnet machine using 5 independent phases, each driven from a separate power converter for fault tolerance.

In addition to normal generation, the low-pressure shaft can be used to provide 25kW of emergency power from the windmilling effect of the engine, post failure. A 25kW prototype permanent magnet generator was designed and constructed by Burrow *et al.* [24], optimised for the windmilling condition, with the aim of eliminating the emergency Run Air Turbine on the body of the aircraft. The generator operates over a 3000-36000r/min range using a step-up gearbox from the LP shaft [25].

It is notable that all the generators proposed in [19-23] state or imply a dc output from the power electronic converters, rather than the variable frequency ac of the A380. With only theoretical aircraft considered for most research, a voltage standard for future MEA & AEA power supplies is yet to be established; however, the high-voltage dc supply is expected to become a reality, with the Boeing 787 featuring a ±270V dc power bus, derived by autotransformers/rectifiers on the ac bus [26].

The advantages of dc transmission, listed by Provost [18], include smaller transmission cables (due to skin effect with ac transmission) and the elimination of voltage converters within connected devices. Conventionally power electronic converters use an internal interim dc stage, so a dc supply eliminates the requirement for rectification. Bi-directional power flow is also simplified without an ac/dc conversion stage.

There is a requirement for larger circuit breakers on dc supplies as there is no zero-crossing point to break the circuit and there have been safety concerns over discharge dangers, although research has shown dc systems actually achieve higher power transmission capability than ac with the same cable density [27].

Both the high and low pressure shaft generators discussed by Hall and Mitcham [20,21] suggest a need for fault-tolerance within the engine generators, with Todd [23] demonstrating a separate electric controller for each phase of the generator for fault-tolerance and Sun [22] presenting phase fault-mitigation strategies. With most commercial aircraft featuring multiple engines, each driving separate electrical bus generators, there is already an inherent redundancy of the power supplies. Although no supporting data is given in [20, 21, 22 & 23] it could be inferred that the reliability of an embedded electrical generator and drive cannot meet the reliability of an existing gearbox-based generator (see Figure 1-5) without fault-tolerance, or that there is a desire to significantly increase the reliability of electrical generation.

Avery *et al.*[28] state that fault tolerance is applied in permanent magnet generators to mitigate against the failure modes resulting in torque ripple or excessive winding temperatures due to short circuits. The implications of generator failures on the operation of a gas turbine must be considered if there is a risk of affecting the engine operation and some of the possible fault conditions are investigated by Sun *et al*. [22] on their 250kW fault tolerant generator.

It is also logical that, with an embedded electrical generator on a More Electric aircraft proposing to supply an increased number of electrical devices, including pumps to derive hydraulic supplies, safety requirements will be higher than those of conventional generation.

1.5.2 Electric fuel pumps

Haylock *et al*. developed a 16kW prototype aircraft fuel pump in 1994-1997 [29]. The design was a ‘proof of concept’ that could evolve to replace conventional mechanical pumps, offering improved control over flow rates, as opposed a flow rate directly linked to the engine speed. The motor initially consisted of a 6-phase brushless permanent magnet motor operating up to 13,000r/min and submerged in aviation fuel. The pump pioneered a fault tolerant permanent magnet motor drive arrangement, with each phase winding electrically, magnetically and thermally isolated and individually controlled from an independent power converter. Full output power capability is achievable with one motor winding or converter faulted. The power electronic converters are capable of detecting short-circuits within motor windings and taking remedial action to prevent over-heating. A 4-phase variant was later produced [30], offering the same performance and fault tolerance, but with a lower component count.

The 4-phase fuel pump motor was redesigned by Atkinson *et al.* [31] to a 100kW prototype, capable of operating to 30,000r/min. The substantial redesign accounted for the increased machine losses when scaling the permanent magnet 16kW motor, reducing a potential 19kW of loss to 5.7kW. This prototype pump was sized for a large future More Electric aircraft.

The fault tolerant laboratory demonstrations described by Haylock focused on faults within the motor and power-electronic converter. This work was taken a stage further by Green *et al.*, initially by evolving the power electric controller to operate sensorless [32]. With work based on the original 6-phase motor, a sensorless scheme for each motor phase was proposed, on the assumption that a true fault tolerant electric drive would require an independent controller for each phase. This eliminated the requirement for 6 mechanical position sensors. This ‘lanes of power’ approach was continued in [33], where a three-phase active rectifier was developed for each motor phase controller, providing an interface to a variable-frequency supply of 360 to 860Hz, 115V_{rms}, the proposed power supply for the A380 at the time of research. The active rectifier approach was to allow bi-directional power flow, minimise harmonic distortion and attain unity power factor.

1.5.3 Surface actuation

The present drive in actuation research is to move from the electro-hydraulic power-by-wire solutions of the EHA and EBHA to purely electric EMAs (electromechanical actuators). Whereas previously EMAs were considered too slow and bulky to compete with hydraulics on surface actuation, the advent of digital motor drives and improvements in motors have made the EMA more viable. Theoretically, alongside an electro-hydraulic actuator, a modern EMA should be smaller as there is no internal reservoir, stiffer as there is no fluid-based loading, more efficient without fluid pumping losses and easier to maintain and store without hydraulic leaks [34].

The LEMAS – Large Electro-Mechanical Actuation System, is a prototype laboratory actuator developed for application on the spoiler surfaces. Initial research considered a selection of permanent magnet, brushless dc machines [35], although finally a 4-phase switched reluctance motor was selected for the 25kW actuator [36]. The actuator has a linear arm arrangement, with the motor driving a gearbox to operate a ball screw mechanism to move the spoiler.

Conventionally the spoiler surfaces use only one actuator per surface, as fault-tolerance is achieved at the wing-level by multiple spoilers (*see 1.3.3 for A380 example*). Although re-emphasised in [36] that fault tolerance is not a requirement, a topology is considered for the SRM with each of the 4 phases capable of running from individual power electronic converters. Although the fault tolerance allows electric drive and supply failures, there is no mechanism in LEMAS to overcome a mechanical jam in the system, preventing the spoiler from blowing back in the event of a failure.

A very similar spoiler actuation system, also employing a switched-reluctance motor is proposed by Fronista *et al.* [37] although the work presented is in the conceptual stages with an identical motor-level fault tolerant scheme.

The ball screw and roller screw are the common choice for linear actuators, based around a threaded screw shaft, a threaded nut and ball bearings or rollers in-between. Although these devices are not found on primary control surfaces of commercial aircraft, they often feature secondary surfaces such as flaps and slats. Throughout the service life of Concorde, roller screws performed gate actuation of the engine air intakes with no failures [38].

Garcia *et al.*, discuss the EMA for primary flight control surfaces [39] drawing comparisons with the EHA and highlighting the susceptibility of jamming as a major issue with the adoption of the EMA in aircraft. The solutions proposed are to eliminate gearboxes using a direct-drive motor and ball screw arrangement and to improve fault-monitoring to pre-empt jam conditions in the motor or ball screw.

Work on a technology demonstrator of direct-drive EMA was described by Gerada *et al.* in [40]. A rollerscrew is used, so although gearbox-free, the screw mechanism infers a rotary-linear gearing ratio, allowing huge loads to be driven by relatively low torques. Permanent magnet motors with high pole numbers were simulated with results for fault mitigation of open circuit phases and terminal short circuits. Although intended for driving a spoiler, a fault tolerant drive topology was proposed, with individual controllers for each motor phase. The technology demonstrator motor is rated for a nominal torque of 27Nm, which although requiring a slightly larger motor than a geared equivalent, is still feasible and is claimed to result in an overall reduced weight and inertia.

A demonstrator direct-drive rudder actuator was considered by Aten *et al*, intended for loads of 159,000N using a permanent magnet motor operating with 17.9Nm at 9047r/min [41]. Later results show a constructed demonstrator operating with a load of 55,000N [42]. Fault tolerance is not employed within the electric drive as research focuses on the performance aspects of the EMA and the matrix converter motor drive (*see section 1.5.4*); although it is acknowledged that an EMA for a rudder application is a long way from aviation acceptance as ‘safe’.

An actuator consisting only of a linear motor could be considered truly ‘direct drive’ and such a solution is proposed by Zeigler *et al.* [43]. Basic fault tolerant schemes are suggested, although the ability to connect multiple linear motors in parallel without risk of a jam is the most significant advantage of the technology. Unfortunately, with an active mass of 1.3kg to drive 1.3kN, scaling such a technology by an order of 100× for an actuation surface would result in an excessively heavy actuator, rendering the current technology unsuitable for aviation.

The EABSYS project [8] involves EMAs to apply the wheel brakes of an aircraft. As conventional systems are hydraulic, the usual benefits of replacing hydraulic with electric are cited, along with improved brake torque control and the elimination of flammable hydraulic fluids from the brake systems. The proposed brake caliper uses a pair of miniature actuators (electric motors, gearboxes and a roller screws) to apply linear force to the disc. Miniature friction brakes lock the motor when the required braking force is achieved so electrical power is no longer required.

A dual-lane controller operates the system, with each controller operating an actuator on both wheel calipers. A mechanical lever arrangement within the calipers requires one actuator to hold and the other to apply force in order to brake the wheel. In the event of a loss-of-drive failure, an actuator will default to a holding configuration via miniature power-off friction brakes. This allows the remaining actuator to operate the brake. In the event of an actuator jamming on, the brake will not operate unless the remaining actuator applies a force.

Ertugrul *et al*. discuss a fault tolerant actuator configuration in [44]. Rather than focusing on a particular actuator, instead a fault tolerant motor demonstrates a dual rotor arrangement on a common shaft and two corresponding stators. Ertugrul also discusses simulation of a three-way control scheme with a dedicated controller for each stator/rotor and a third supervisory controller. As the actuator has no specific application, it is described as direct-drive and exists purely as a laboratory concept demonstrator.

1.5.4 Actuator power converter research

There has been a considerable body of research concerning the configuration of electric drives on More Electric Aircraft. With conventional aircraft offering an ac supply, power electronic controllers for motors are based around an ac-dc-ac arrangement and various alternatives have been considered for the ac-dc supply interface and rectification stage.

With the advent of variable-frequency power supplies in the A380 and an increase in electrical devices, 12-pulse autotransformers [45] were adopted for some electric systems as a standard ac-dc (6-pulse) diode rectifier will not meet the ac power quality requirements due to poor power factor and non-sinusoidal current waveforms. A 12-pulse autotransformer effectively splits and phase shifts a 3-phase waveform into 6-phases, with 2 sets of diode rectifiers and an LC filter also present. The result is a much more sinusoidal current drawn from the supply and no requirement for electronic control. With the 400Hz+ ac supply on aircraft the autotransformer can be rather compact, with a complete transformer/rectifier 5kW arrangement weighing 2.8kg [46].

The three-phase active rectifier, used by Green for a fuel pump application [33] is acceptable for many applications as it can offer sinusoidal input currents with unity power factor and with filter requirements comparable in size or even smaller than those of a 12-pulse autotransformer [46]. It offers the advantage of bi-directional power flow, although there are more power devices than a 12-pulse system and control circuitry is required.

It should be noted that as neither the autotransformer nor the three-phase active rectifier are inherently fault tolerant and present a single point of failure, particularly following a power supply failure, a fault tolerant electrical actuator may require a separate rectification unit on each lane of power.

Considerable research has been undertaken into Matrix Converters with the intention of aircraft surface actuation. The Matrix Converter is a direct ac-ac converter, providing the capabilities of a back-to-back active rectifier and motor drive inverter, but with a matrix of bi-directional switches rather than a pair of transistor bridges and an interim dc ‘link’. By going directly ac-ac, rather than ac-dc-ac, the aim is to provide a more compact form of power electronics, replacing the conventional dc link capacitor with an LC filter on the ac input. Results in [41] show a simulation of a 24kW matrix converter driving an induction machine to operate a rudder actuator. Input filters of 60μF and 63μH are used on each phase. This was later realised in the 20kW demonstrator of [42] and [47]. Also presented in [48] is an EHA using a fault tolerant 5-phase motor with a ‘single sided’ matrix converter for each motor phase, providing 5 lanes of power. As EHAs are usually non-fault tolerant, employing conventional motor/drive configurations (see 1.3.1) this arrangement is claimed to improve upon the reliability as multiple power supplies can be utilised. This laboratory demonstration converter also uses an FPGA with hysteresis control, therefore requiring far less complex control electronics than a processor arrangement – particularly important if multiple control elements are required in a converter.

It is important to note that, if in future, dc power supplies are accepted as the aviation-standard, then there will be no requirement to interface to an ac supply, so a conventional dc-ac transistor-bridge configuration will be a sufficient motor drive arrangement, although filtering will be required to maintain an acceptable dc input current.

1.6 CONCLUSIONS

The overriding factor in the adoption of More Electric Technology on aircraft actuation is passenger safety.

The oft-quoted NASA studies of the 1980's [4] suggest weight saving data for an All-Electric-Aircraft based on purely theoretical single-phase 20kHz ac transmission systems with resonant power converters and ac-ac motor drive electronics. A dual-electric actuator drive is considered sufficient to operate a surface.

Decades later, even though these predicted electronic arrangements are unrepresentative of modern systems, it is actually the safety requirements which have disproved claims of a commercial all-electric-aircraft being feasible.

If the feasibility of a concept is measured by the willingness of aerospace manufacturers and aviation authorities to accept it, then the A380 shows the acceptable level of More Electric technology in current aircraft. When observing the actuation systems of the A380, it is clear that hydraulics remain the predominant method of actuation on all flight controls, with electrically powered actuators present in far smaller quantities. In addition, on primary control surfaces any electrically powered actuators are electro-hydraulic with electronics supplying a localised pump and actuation performed hydraulically. Some secondary surfaces feature electric motors for electromechanical actuation, although these are surfaces in which jam is not catastrophic and a hydraulic motor is also present in parallel, using a speed-summing gearbox to allow operation following a jam of either motor.

There are many actuator configurations for the flight controls of the A380, all employing redundancy to tolerate failures including power supplies, control signals and complete actuator failure. Redundancy is achieved either by multiple actuators on a surface, multiple surfaces performing a task or in the case of some secondary surfaces, with a single actuator driven from multiple motors. The revert-to-damping of hydraulic and electro-hydraulic actuation allows parallel connection of actuators or a surface to blow-back to an aerodynamically neutral state following a failure. The implementation of electromechanical actuators in these cases is hampered by the risk of mechanical jams.

While it is conceivable that electro-hydraulic actuators could one day allow a More Electric aircraft with no hydraulic supply buses, there remains considerable research before electromechanical actuation is considered for more safety-critical control surfaces, in particular the three primary controls. Although actuators have been proposed for some of these surfaces and for the spoilers, even using ‘direct drive’ systems without gearboxes, there remains a risk of a mechanical jam in the roller screw or ball screw mechanisms which must be overcome to attain airworthiness. Solutions to the jam problem are under consideration, with Thomas *et al.* proposing a dual load-path ball screw arrangement in [49] for the main landing gear actuation of the ELGEAR project (*see section 2.2 for more details*), although the weight and component counts of such measures must be considered. Actuators consisting of linear motors have also been suggested, removing all gearing and bearings, although the power density of these machines is inadequate at present.

There appears more scope for manufacturer approval of electromechanical actuators in less safety-critical applications. The flap, slat and tail stabilisers of the A380 and the flap and slats of the 777 are mechanically coupled systems, many featuring electric motors in parallel with hydraulic motors and it is quite conceivable that such systems could be made fully electric as the aircraft can remain flyable following a complete jam of the surfaces.

The EABSYS project shows how a dual electromechanical actuator can operate a brake system after the event of any single failure, including an actuator jam. Manufacturer approval seems attainable as EABSYS reached the stage of installation and successful flight on an Airbus test aircraft.

In other More Electric areas, such as engine generators and fuel pumps, the design challenges are focused on designing suitably compact motors and electronics capable of enduring the extremely harsh operating environment requirements. While mechanical and electrical failures remain an important consideration, particularly if engine performance is affected, the implications are potentially less severe due to the parallel backup afforded by multiple engines and generators. The application of embedded engine electrical generators seems feasible in the not-too-distant future and this will in-turn drive the abandoning of hydraulic power supplies to actuators.

This thesis focuses on the research and design of two very different electrical actuation systems for the More Electric Aircraft. The safety aspects of both systems are considered throughout, driving the design process and producing two actuation systems with a potential of commercial acceptance exceeding many research prototypes. Fault tolerance is considered in detail at an electric drive level and at a system level, with the required control strategies presented and demonstrated on industrial test rigs.

2 The DEAWS and ELGEAR Projects

This thesis features research on aspects of two industry-driven More Electric Aircraft projects:

- **DEAWS**, an electric flap and slat system, developed between 2001 and 2004.
- **ELGEAR**, an electric landing gear system, of which a nose wheel steering actuator was developed between 2007 and 2009.

2.1 THE DISTRIBUTED ELECTRICALLY ACTUATED WING SYSTEM

The flap and slat high-lift surfaces in commercial aircraft (*section 1.2*) conventionally feature mechanical shafts across the wingspan, driven from a central hydraulic motor arrangement. Due to the permanent coupling to the shafts, the entire flap system moves in unison, as do the slats. A typical flap and slat arrangement is shown in Figure 2-1.

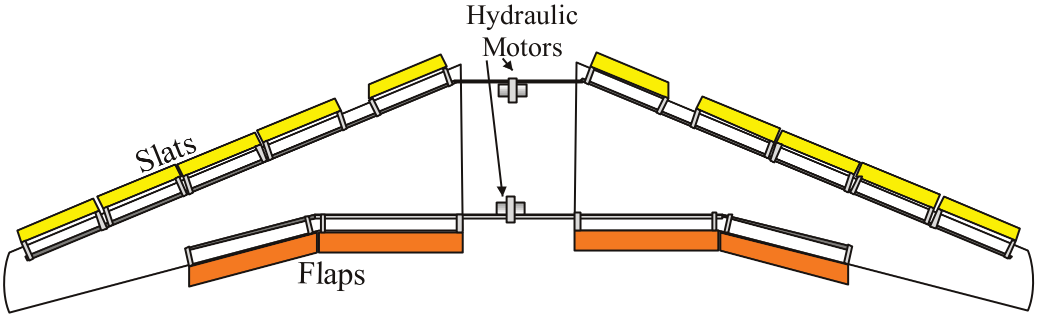

Figure 2-1: A typical flap and slat arrangement for a small commercial aircraft.

The Distributed, Electrically Actuated Wing System (DEAWS) was a DTI funded industrial/university research project to investigate the feasibility of electrically powered flap and slat systems, dispensing with the shafts across the wingspan and central motor systems and instead distributing electrical actuators across the flaps or slats (Figure 2-2).

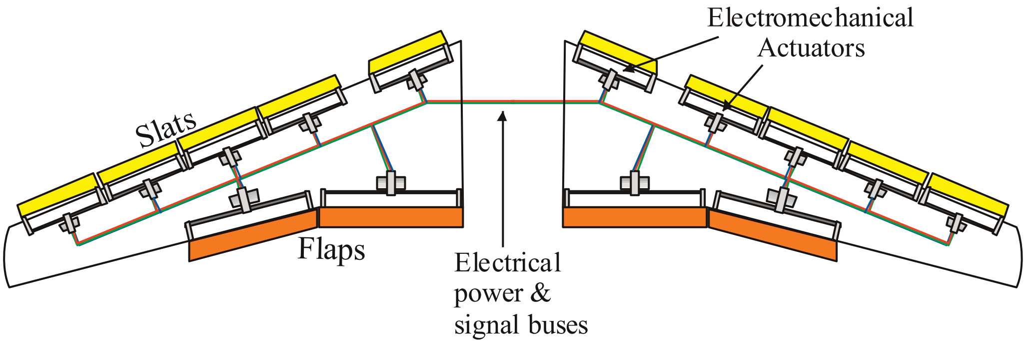

Figure 2-2: An example DEAWS flap and slat systems with one actuator per surface.

The topology for flaps and slats is very similar, hence DEAWS was proposed as a technology suitable for either system.

There were four partners on the project:

- **BAE Systems, Rochester.** Avionics specialists and responsible for the overall system architecture.
- **FR-HiTEMP, Tichfield.** Design and manufacture of the actuators and also providing testing facilities.
- **BAE Systems, Woodford.** Aircraft manufacturers, responsible for providing information on existing actuators, including costs, weights, reliability and also feasibility studies of the new system, including aerodynamics.
- **Newcastle University.** Design and manufacture of the power electronic controller and design of the electric motor.

There is no specific target aircraft, rather a transferable design suitable for potential future aircraft. Trade studies conducted by BAE Systems were based around the A320, a medium-sized 180 seat aircraft; however, it was noted that the technology will be scalable for different sized aircraft as safety requirements have the greatest influence on the design and these remain essentially the same.

2.1.1 Advantages of distributed electrical high lift surfaces

The drive for researching fully-electric flap and slat systems follows the More Electric Aircraft aims of sharing more devices on electrical power generation systems and reducing hydraulic generation systems. Reducing system complexity can also yield weight and maintenance savings.

The diagram shown earlier in Figure 2-2 may suggest DEAWS to be potentially more complex than a conventional system; however, the schematic of a 146/RJ flap system in Figure 2-3 highlights the true complexity of a conventional flap system (and the case is similar for slats). To meet safety requirements, a dual motor arrangement is necessary for the power source, requiring two networks of hydraulic pipework and associated reservoirs and valves (not shown). The outputs of the two motors are fed into a speed-summing gearbox, allowing the system to operate with one motor unpowered or jammed. The system is normally operated in an 'active-active' configuration, with both motors running. In the event of a motor failure, the remaining motor operates the flaps at half speed. All data is obtained from BAE Systems Woodford [50].

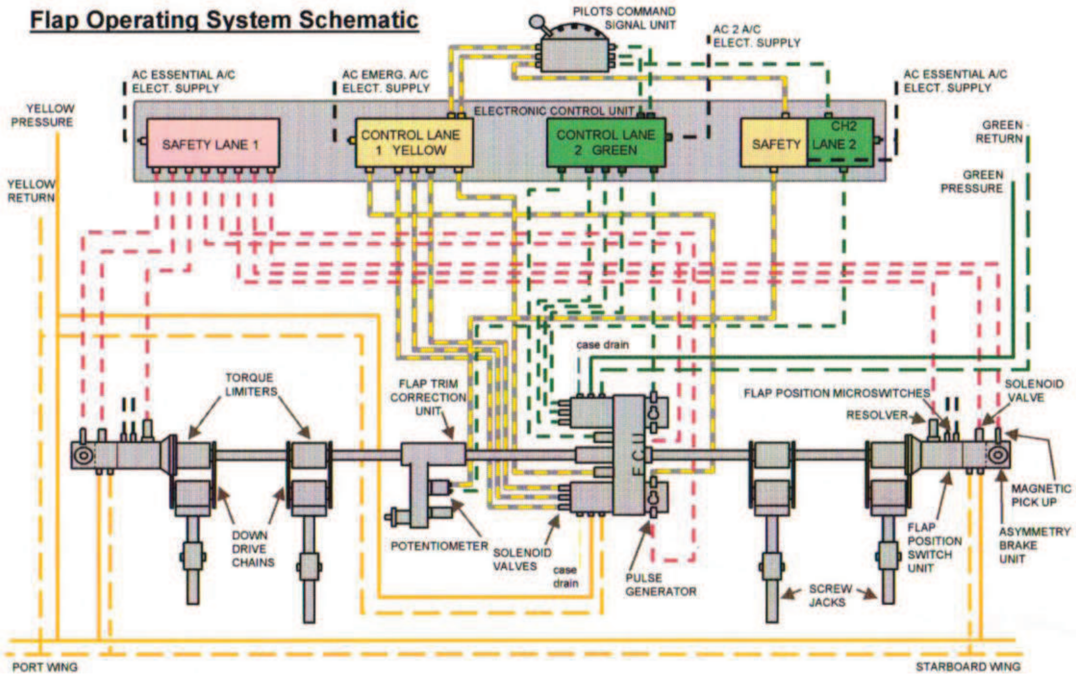

Figure 2-3: The 146/RJ flap system (courtesy BAE Systems Woodford).

A distributed system requires more motors than the conventional arrangement, although each motor is only rated for the torque of a single flap/slat and therefore will be of a much smaller power requirement than a central unit.

A shaft breakage could be potentially catastrophic, as could overloading a flap mechanism, therefore the 146/RJ features mechanical torque-limiting units on every flap-track mechanism. A distributed system has no common shaft to break and will contain inherent digital torque-sensing on each flap/slat motor to prevent damage to localised mechanisms. Mechanical torque limiters have a considerable mass and also require manual inspection and resetting after a 'trip'. This can result in nuisance lock-ups on aircraft, where control of the flaps or slats is lost until the aircraft can be hand-inspected and reset on land.

Maintaining the port and starboard flaps at the same angle is critical to flight safety, so a series of sensors are used on the 146/RJ to detect asymmetry from mechanical failure. A pulse generator on the central motor provides a speed signal, while resolvers at both ends of the shafts record the flap angle. Microswitches are toggled when the flap is fully extended or retracted. The safety lane computer identifies any anomalies between all the sensors and shuts the entire system down, to within 1° of port and starboard asymmetry. Brake units on either ends of the wingspan shafts lock the system in this failure condition.

Without a common shaft across the wingspan, ensuring the flaps are at the correct angle at all times is the main priority of the DEAWS system. Although emergency brakes may still be required on each flap/slat surface, the associated sensors and wiring can be integrated into the distributed actuators, rather than from a central monitor. Modern electrical sensors can also be smaller than existing sensors – particularly the pitch-trim correction units; sensors on the main shaft with integrated step-down gearboxes to estimate the output flap angle, rather than measure it directly.

A major potential advantage of the distributed system is the ability to move individual flap and slat surfaces to different angles. Although maintaining symmetry between port and starboard will always be essential, varying the angles between inboard and outboard surfaces may prove aerodynamically advantageous. Performing an angle variation on conventional systems would require additional differential gearboxes, with offset motors (Figure 2-4); however, this ability would be inherent in a distributed arrangement.

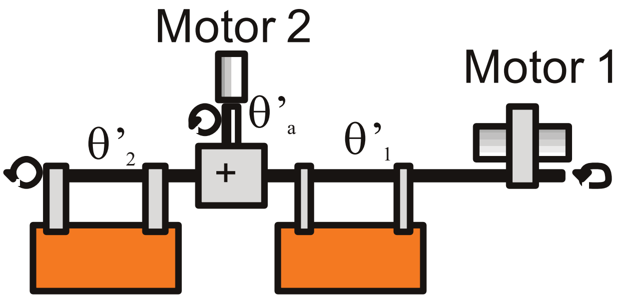

$$\theta'_2 = \theta'_1 + \theta'_a$$

Figure 2-4: An arrangement for altering deployment angle of adjacent flap/slat surfaces.

In the event of an actuator failure, DEAWS could allow the aircraft to lock a failed surface and the corresponding surface on the other wing, but maintain operation of the remaining surfaces, giving surface-level fault tolerance.

2.1.2 Reliability requirements for high lift surfaces

Safety requirements will determine the architecture of the DEAWS system and the proposed solution must attain the reliability levels of conventional aircraft systems. From Airbus data, the main failure conditions of flap and slat systems are presented, with the maximum allowable probability for the failure occurring:

- **Asymmetry** – *probability* $< 10^{-10}$ *per flight hour.* The port and starboard flap/slat surfaces must not vary by more than 5% of their travel. A 5% variation in surface angle between wings will require the pilot to use 10% of the roll control (via the ailerons) to counteract the resultant forces. Any greater asymmetry could result in loss of aircraft control, hence this condition is considered ‘safety-critical’. 5% of travel is also an extreme condition and it is desirable for the symmetry to remain much closer than this tolerance.

- **Uncommanded movement** – *probability* $< 10^{-10}$ *per flight hour.* Another safety critical factor is ensuring that the probability of more than 1% of flap/slat actuator travel occurring uncommanded/‘uncontrolled’ is less than 10^{-10} per flight hour. Whereas asymmetry considers the positional accuracy of flaps when controlled, uncommanded movement can involve a breakage or an erroneous actuator action and as these could result in rapid surface movement, which the pilot may not be able to respond to, such events must be arrested quickly, hence the 1% tolerance.

- **Inability to extend/retract flaps/slats** – *probability* $< 10^{-5}$ *per flight hour.* Flaps and slats are actuated at take-off and landing and an inability to extend will result in an aborted take-off or emergency landing. If the surfaces will not retract after take-off, then the pilot will have to return to the airport and if the surfaces will not retract after landing, then the aircraft will be grounded for repairs. Failure to deploy during flight will result in an emergency landing and is therefore an increased risk. While none of these conditions are catastrophic, they are all undesirable.

- **Incorrect indication to pilot** – *probability* $< 10^{-9}$ *per flight hour*. The pilot must be correctly notified of the flap/slat status at all times in order to take appropriate action to maintain stability and safety. For example, a flap/slat problem may require an emergency landing; however, if the pilot is unaware of a problem and attempts a conventional landing, the consequences may be catastrophic.

2.1.3 Initial specifications

With the A320 providing a baseline target aircraft for the DEAWS system, a representative load profile was generated by BAE systems. Figure 2-5 shows the peak load profile for the flap system using a rotary actuator. Each A320 wing contains two flaps, the inboard driven by stations 1 and 2 and the outboard by stations 3 and 4.

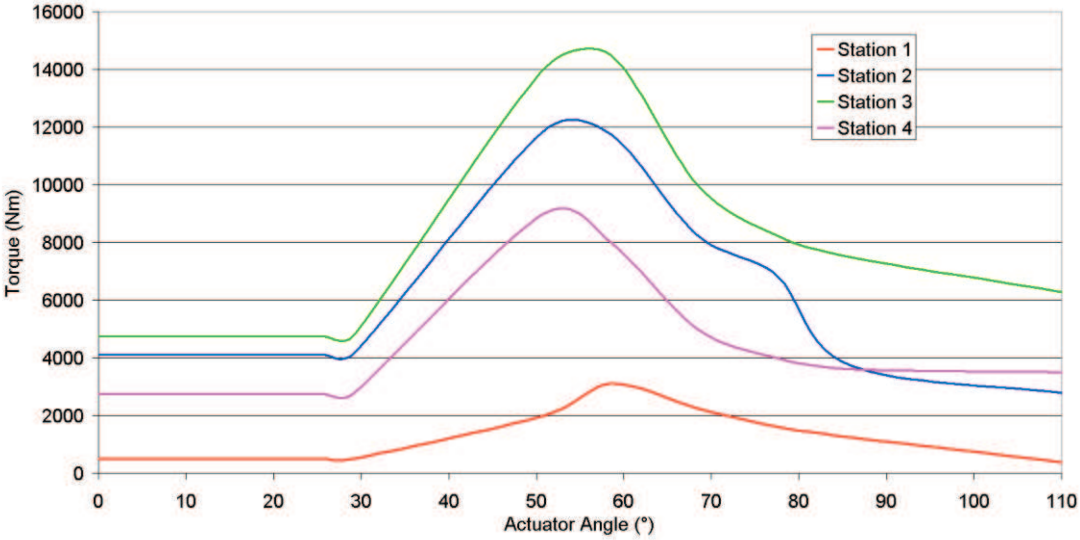

Figure 2-5: Load profile for DEAWS flaps.

A 30 second extension and retraction time was set as a target for the flaps, although this is the minimum speed requirement – as little as 15 seconds is allowed. A minimum delay of 60 seconds between extension and retractions is imposed, as repeated operation in the air is not necessary and would only be performed during an aborted landing.

It was decided that a demonstrator flap actuator should be sized for the worst-case condition; a single actuator driving both stations of the outboard flap (3 & 4), giving a total peak load of 22800Nm. A full flap extension is 112°, so to achieve this in 30 seconds requires a peak power of 1.5kW.

The rack and pinion gears in the 5 slat surfaces move through 568° in 30 seconds, with the peak torques much lower than the flaps, with the inboard slat experiencing the highest loads of 1432Nm and 839Nm at the stations, corresponding to 473W and 277W. At the conception stages of the project it was decided to manufacture only one prototype system, which will be for the flaps as they require much higher power levels than the slats. Results were later scaled by BAE systems to assess suitability for the slats.

The power supply requirements are based on the A380 variable frequency system, with a three-phase 115V ac 360-800Hz supply, which can be rectified to 270V dc for the power electronics and the motor. The maximum rate of frequency change is 100Hz/s. The harmonic spectrum limit for input current is shown in Figure 2-6 as a multiple of the nominal sinusoidal current. It is notable that the 9,13th and 23rd peaks resemble that of a 12-pulse autotransformer [51], suggesting the specification is formed around such devices. From conversations with Airbus it is believed that a degree of flexibility in meeting this distortion specification is allowed, should a device prove beneficial in other areas, such as cost, weight and performance.

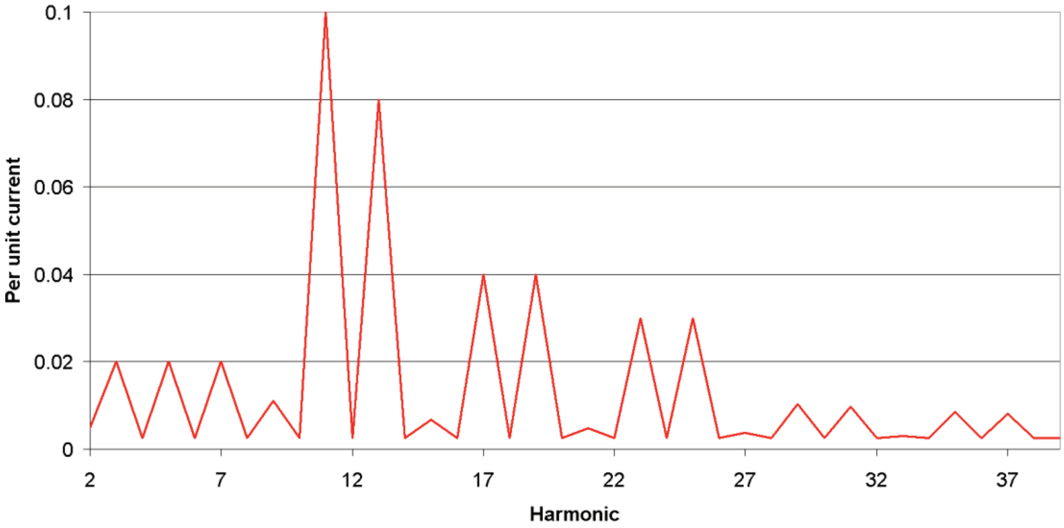

Figure 2-6: Current harmonic limits for operation from an Airbus V.F. supply.

2.2 THE ELECTRIC LANDING GEAR EXTEND AND RETRACT: NOSE WHEEL STEERING

The Electrical Landing Gear Extend And Retract project, ‘ELGEAR’ is an industrial funded project investigating all-electric landing gear systems on commercial aircraft.

The project was instigated by Airbus UK, with three industrial organizations; Goodrich Actuation Systems, General Electric and Messier-Dowty (and their sub-contractors) designing and manufacturing alternative solutions for potential use on future Airbus aircraft.

Figure 2-7 shows the nose wheel landing gear and half of the main landing gear on an A320. All actuation is hydraulic and both systems feature a bay door actuator, an 'actuating cylinder' to raise and lower the gear, uplocks to hold the gear up in the bay and a lock stay to a fix the landing gear arms in extended positions. The nose wheel features a hydraulic steering system.

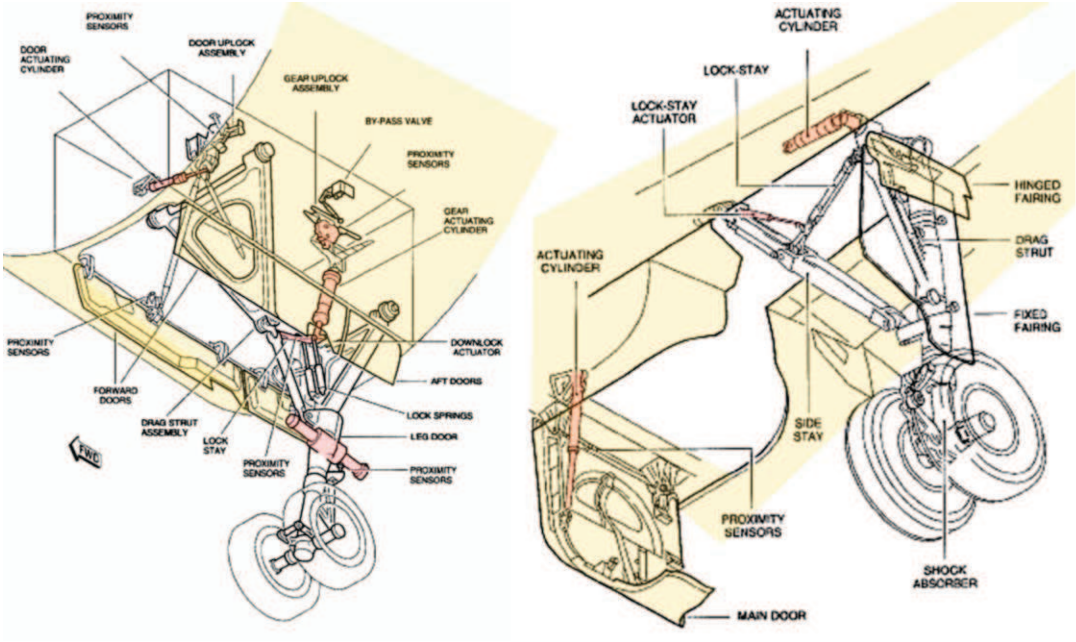

Figure 2-7: A320 nose (l) and main(r) landing gear.

In addition to developing electrical actuators for the main landing gear extend/retract and lock stay, Goodrich Actuation Systems in Wolverhampton were responsible for an electrical nose-wheel-steering system, with the power electronic controller researched, designed and manufactured by the author.

The Airbus A320 was selected as a baseline target aircraft, although, like DEAWS, the system is investigated as a proof-of-concept, intended for future, more-electric aircraft, rather than to retrofit an existing product.

2.2.1 Advantages of electrical landing gear actuation

As with the DEAWS project, the ELGEAR electromechanical actuation is proposed as an improvement on the conventional hydraulic arrangements, as operating more actuators from electrical power leads to an overall optimization of the power supplies on the aircraft (*see 1.1*).

A more specific advantage of ELGEAR is the elimination of hydraulics from the landing gear bays. The wheel brakes can become extremely hot and in certain instances the pilot must delay take-off until the brakes have cooled from the previous landing. This is due to the flammability of hydraulic fluid and the proximity to hot brakes with the gear stowed away.

A specific advantage to electric nose-wheel-steering is that the conventional hydraulic systems can suffer from an amount of 'shimmy' – a wheel-wobble vibration effect caused by backlash in the mechanical components of the steering arrangement. Many hydraulic systems use a 'rack and pinion' arrangement which is prone to shimmy due to clearances between gear teeth.

The operation of a rack and pinion system is illustrated in Figure 2-8. A pair of hydraulic linear actuators push and pull the steering rack, rotating the pinion gear and the steering leg. Despite the dual actuators, the system is not fault tolerant as the two actuating cylinders are hydraulically linked and operate in tandem.

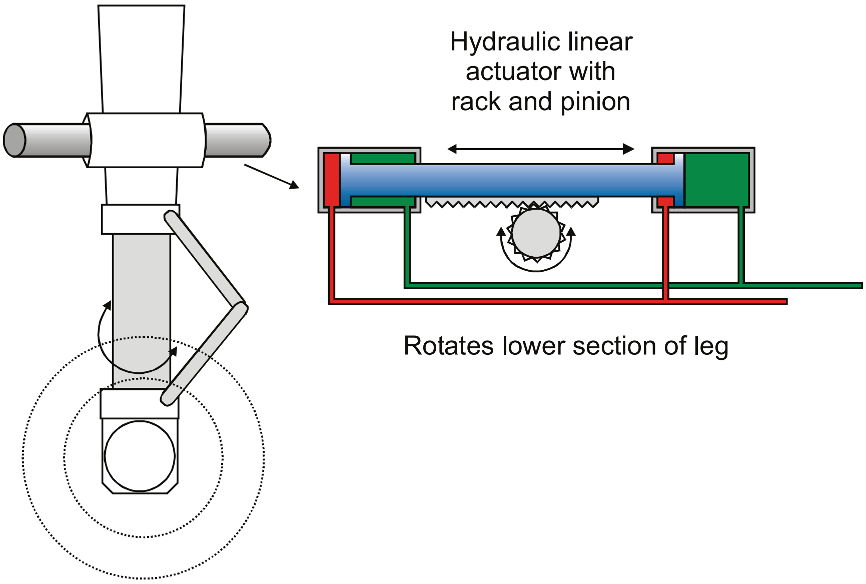

Figure 2-8: Hydraulic rack-and-pinion nose-wheel steering.

Figure 2-9 shows a photograph and diagram of another hydraulic arrangement where two linear actuators push or pull the steering directly. The photograph reveals some of the pipework complexity in a relatively simple hydraulic arrangement.

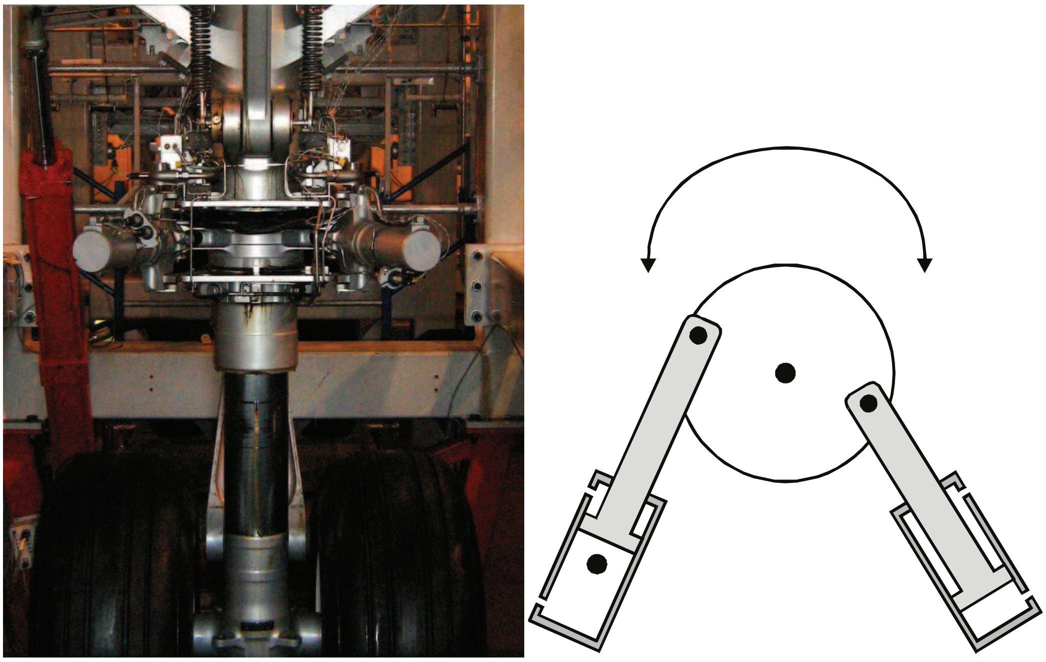

Figure 2-9: A340 NWS with rotary hydraulic push-pull arrangement.

To rotate the leg one actuator pushes on the leg while the other pulls. Both actuators pivot to follow the rotating leg, although there are points of rotation where only one actuator can provide a force. For this reason the system is not fault tolerant at an actuator level. In the case of the A380, a small electric pump can pressurise the local accumulator for the nose-wheel steering hydraulics, thus providing a backup hydraulic power source [52].

Hydraulic actuators are placed near the centre of the leg, resulting in a considerable moment of force on the extension/retraction actuator, which is physically restricted to pushing and pulling near the pivot at the top of the leg. A system with the mass relocated higher up the leg would require less structural strength and actuation requirements, resulting in a weight saving [49].

2.2.2 Reliability requirements for nose wheel steering

The basic premise of the ELGEAR nose wheel steering (NWS) is to produce a nose-wheel leg using electric motors for actuation. As is the case with all electric actuation, the reliability must meet or exceed that of the conventional hydraulic arrangement and this will determine the selected design architecture.

In the case of nose-wheel steering, a directional change and thus actuation, is only required when on the ground and moving to and from the runway – ‘taxiing’. This would suggest that failure to steer is not so much a safety concern, more a problem with lost operational hours resulting from repairs.

For ELGEAR it is actually a requirement to have an aircraft fully operational and safe to fly with a known fault - The Manufacturers Minimum Equipment List requests that *‘no single failure of a generator, bus bar, power drive electronic or motor will ground the aircraft’* [49]. This therefore constrains the NWS to using at least two power supplies, motors and controllers.

One condition that could be determined safety-critical is for the steering to move to an undesired angle when performing a landing or take-off as this could result in the aircraft leaving the runway at speed. This is not a problem on the hydraulic systems as the steering is disabled during take-off and landing. Unpowered hydraulic actuators will revert to a damping mode and the corrective forces from the moving aircraft will pull the nose-wheel straight. This is referred to as ‘free to castor mode’. The ELGEAR actuator will have to offer a ‘free to castor’ method and ensure this mode is always selectable.

2.2.3 Initial specifications

The main operating specifications for the nose wheel steering actuator are:

- **Supply voltage:** ± 270V dc.
- **Peak torque:** 7000Nm
- **Max operating speed:** 18.5°/sec
- **Peak output power:** ~1kW

The required torque profile for different steering angles is shown in Figure 2-10. Defining 0° as straight ahead, the steering can physically move from +95° (clockwise) to -95°, although the commanded movement and range of loaded operation is only ±75°. Clockwise and anticlockwise loads are identical. The red trace shows the torque profile where the actuator is moving against the force induced by the tyres on the runway, whereas the blue trace shows where these loads are assisting. The profile is more severe than that observed in reality, since no loads are exerted when the steering is straight ahead and torques will be lower towards the centre of steering; however, it is preferable to design an actuator capable of peak torque at all operational steering angles.

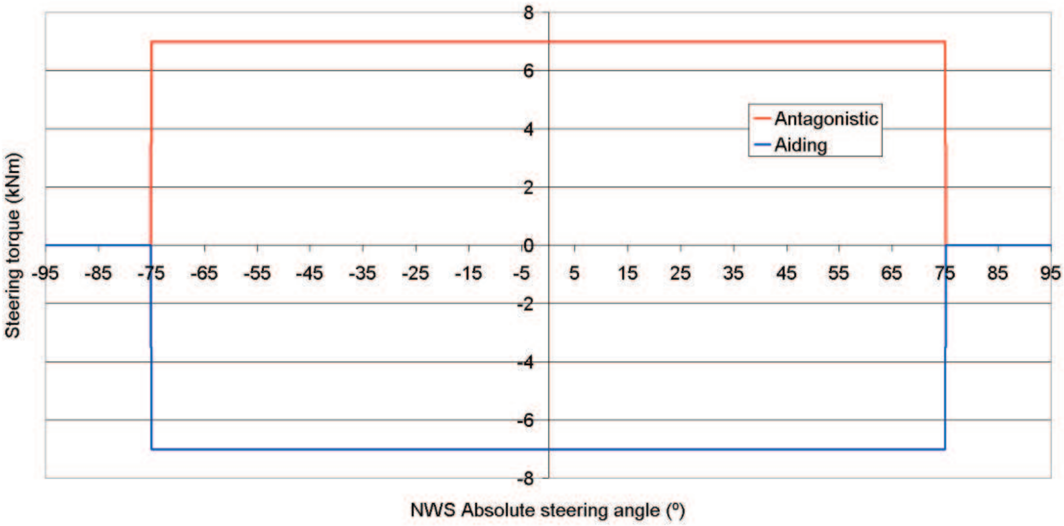

Figure 2-10: Torque/angle profile for ELGEAR NWS.

The torque/speed envelope for the actuator is shown in Figure 2-11. The optimal operating speed is 18.5º/sec, although under load this can fall and at the peak load of 7kNm, only 10º/sec is required. Effectively, the actuator slows as it is loaded.

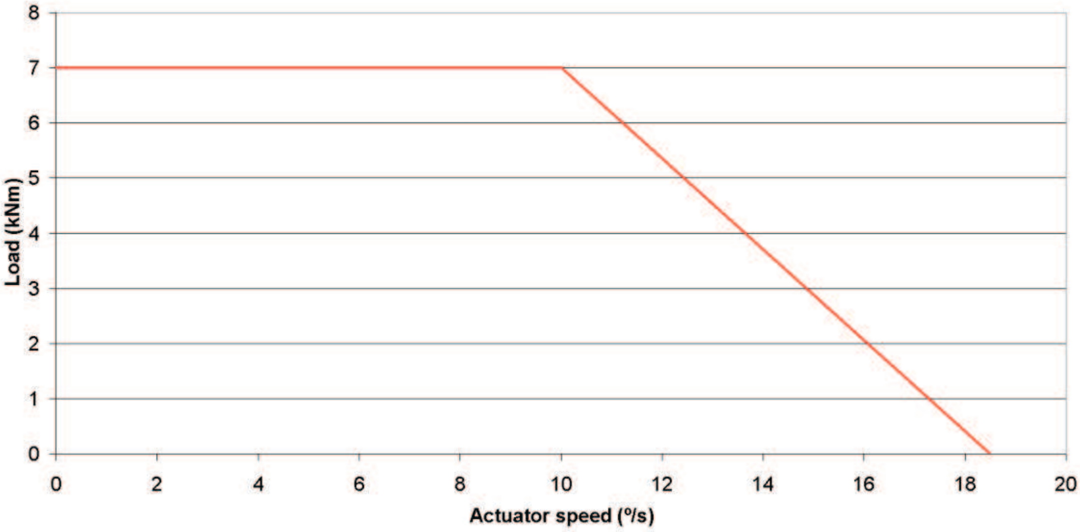

Figure 2-11: Torque/speed profile of ELGEAR actuator.

The ±270V supply allows 540V for use by the power electronic controller and motor.

2.3 CONCLUSIONS

Two projects are presented that are both potentially viable for future More Electric aircraft. With existing More Electric landing gear and flap/slat systems featuring electric motors in backup configurations, eliminating hydraulics completely is a logical step forwards.

As the specified power levels of 1-2kW are relatively low, far smaller electric drives will be required than for actuation of primary control surfaces or spoilers [53] and both proposed systems have very short operational duty cycles.

The ‘jam’ problem associated with failure of electromechanical actuators can be sidestepped in DEAWS as the flap system must be locked in the event of a serious failure. Meanwhile the ELGEAR NWS will employ a free-to-castor mechanism to overcome any actuator jams.

There are effectively two stages of reliability/safety for both systems:

- Ensuring the system does not shut down.
- Ensuring the system does not lose control.

Whereas DEAWS specifies a minimum loss of operation probability of 10^{-5} per flight hour, ELGEAR specifies that no single failure will result in a shutdown. This entails that both systems will require a degree of fault-tolerance, in the case of DEAWS this is because 10^{-5} is considered out of reach for motors and drives. Even the military-grade electric motor drives used in EHAs cannot meet such a high specification, with Sadeghi *et al.* [54] giving a failure probability of 1.5×10^{-4} per flight hour for the electric drive components.

Ensuring the system does not lose control carries a significantly higher requirement for DEAWS, although full motor drive functionality is not required in this case as the system can be considered under control if locked with brakes. The free-to-castor mode of the ELGEAR NWS allows the system to default to an controlled state, determined by corrective forces on the wheel, although there is no strict safety requirements to ensure this, since operation is only required when taxiing.

In terms of technological steps forward, it could be said that DEAWS presents the largest step and thus takes the largest risk in gaining acceptance and approval by manufacturers. Eliminating the wingspan driveshafts and distributing actuation is a massive variation from existing arrangements and proving the safety, while maintaining a cost-effective system is a considerable challenge.

3 Fault Tolerant Drive Topologies

With safety requirements and specifications for DEAWS and ELGEAR suggesting a need for fault-tolerance within the electric drives of the actuators, a study was undertaken to compare the many different topologies for a fault tolerant drive, with the intention of finding an optimum.

As demonstrated by many existing aircraft, multiple motors can be used to drive electromechanical actuators by means of clutch [15] or speed-summing gearboxes (see *1.3.3 & 2.1*). These arrangements allow operation after failure of one motor, although there is an additional mass and reliability penalty in the gearbox.

The concept of a motor capable of operation after a fault has been a research topic for many years. In 1980, Jahns [55] proposed driving each phase of an induction motor from a separate power converter H-bridge. This allowed operation following an open or short circuit within a motor winding or failure of a power converter. Subsequent research has considered the faulted behaviour of switched reluctance machines [56], and latterly, permanent magnet motors [29], [57].

While fault tolerant drives attempt to segregate the motor windings and power electronic converter into separate lanes, there remains a common rotor and bearings. Although the likelihood of winding failure is considered lower than that of bearing failure during prolonged operation [58], winding short-circuits or loss of power can result from errors within the power electronic converter so reliability of the winding and converter lane should be considered as a whole, resulting in a failure probability significantly higher than the bearings. Comprehensive discussion on this is presented in chapter 4.

This chapter looks at the different configurations for fault tolerant drives, comparing sizes, component counts and reliability under a variety of operating conditions. With actuators capable of stopping and starting at any position, full torque is required at all speeds, including a stationary rotor, so the motors considered here must produce full torque at all rotor positions, following a single fault in a winding or power electronic converter.

3.1 MOTOR TECHNOLOGIES

With this body of work concerning research into the optimal electric drive topology for an electromechanical actuator, the optimal motor technology must first be considered.

Initial specifications for DEAWS and ELGEAR indicate output torque requirements in kNm, but power requirements less than 2kW due to low operating speeds. High speed motors with gearing are therefore essential in achieving compact actuators.

Since the research of Jahns, it has become well recognised that induction motors are not inherently suited to safety critical fault tolerant applications. With extensive coupling between phases required to produce a rotating field and a common neutral point, sufficient electrical and electromagnetic isolation between drive ‘lanes’ cannot be achieved.

Switched reluctance motors are well established as inherently fault tolerant, using single tooth windings and independent power circuits for each phase. Unfortunately the SRM can only provide substantial torque from each phase for about 1/3 of an electrical cycle, so, unless there are at least 6 phases, a failed phase will result in rotational angles where no remaining phases can provide significant torque. A high phase number requires a high number of power electronic devices and if each phase is to be allocated to a separate electronic converter and power supply, then the complexity may be prohibitive.

Permanent magnet machines have been shown to offer the highest torque per unit density of the three motor types [59], since the armature is not required to provide magnetising current. When rotating, permanent magnets induce a back emf in the windings which remains present when a phase is faulted or unpowered and can induce massive currents in any short-circuited windings. Strategies to detect short circuits and minimise these currents are well established, with special machines designed with an increased reactance, in which the current of a winding short circuit can be to limited to 1 P.U. by imposing a terminal short circuit via the electronic converter [29].

It seems clear from both a size and complexity perspective that permanent magnet motors are the optimum choice for the relatively low power electrical actuators. Further discussion in this chapter applies to permanent magnet motors, although some of the concepts may be applicable to the other motors.

3.2 PHASE MODULES

To describe how a motor and controller can be split into individual phases or sets of phases, a 'module' will be defined. A module is one element of a fault tolerant electric drive – i.e. a 'lane' of control and can be considered to be composed of either:

- A single motor phase, isolated electrically and magnetically from all other phases and supplied from a single-phase transistor H-bridge.
- A set of 3, star-connected phases, isolated from all other phases and supplied from a 3-phase transistor bridge.

To represent redundancy, it will be assumed that there are $n+1$ modules in a fault tolerant drive. In the event of a module failing, the remaining n modules continue to produce full torque.

Thus, features will be compared for:

- **n+1 phase drives:** e.g. $3+1$, $5+1$.
- **$3n+3$ phase drives:** e.g. $3+3$, $2\times3+3$, $3\times3+3$.

Modules composed of sets of two-phase drives are not included, as each module would contain two single phase motors supplied from single phase bridges. Consequently this becomes a special case of multiple single phase drives.

Conventional transistor H-bridges with dc input supplies are considered for calculations. Alternative converter types and additional rectifiers will simply involve scaling the results presented and should not affect any conclusions.

Fault tolerant drives which are not composed of independent modules with isolated dc supplies, motor windings, power electronics and control electronics cannot be considered as these feature single points of failure. For these reasons, standard drives with additional power devices for fault bypassing, such as those described be

Welchko *et al.* [60] cannot be considered truly fault tolerant as only specific motor and electronic faults may be tolerated.

3.3 COMPARISON UNDER NORMAL OPERATING CONDITIONS

The power electronic devices for different drive configurations can be compared in terms of their total power switch VA ratings, calculated by the product of the peak current, dc link voltage and the number of switching devices:

3-1 $$VA = I_{pk} \times V_{DC} \times devices$$

It will be assumed that the dc link voltage is fixed; therefore calculations are based on the peak current and the number of switching devices. Furthermore, the back emf of each phase will be assumed to be sinusoidal, as will be the current when operating in the unfaulted condition. The peak current is considered to be the current drawn when the motor and drive are operating after a fault. i.e. with *n* of the *n+1* phases contributing to torque production.

A standard 3-phase, star connected drive with a 6-transistor bridge is used as the basis for comparison in all calculations. This will be considered to have a motor size of 1, with the converter size calculated in *3.3.1*.

In addition to power devices, gate-drive circuitry is also a consideration. Gate drives require isolated power supplies and while these supplies are minimised when switching devices share a common emitter/source connection (e.g. all the ground-referenced lower devices in a bridge), these vary between the two topologies.

3.3.1 A conventional 3-phase, 'star' connected motor

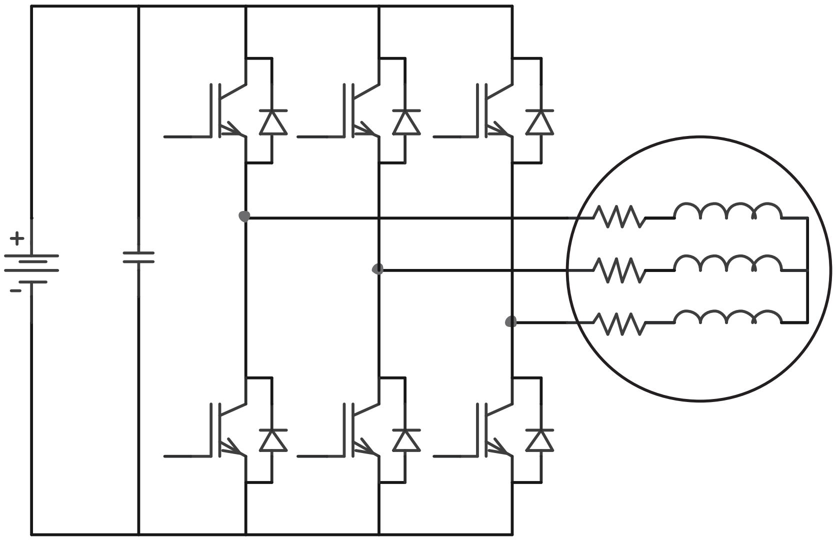

Figure 3-1: Conventional 3-phase power electronics and winding layout.

A standard 3-phase bridge requires 6 IGBTs and freewheeling diodes (Figure 3-1). There are six switching devices and from eqn. 3-1 the KVA is given by:

$$KVA = V_{dc} \cdot \hat{I}_{ph} \cdot 6 \tag{3-2}$$

and the power by:

$$P = 3 \cdot V_{rms} \cdot I_{rms} \cos\phi = 3\frac{\hat{V}_{ph}}{\sqrt{2}} \cdot \frac{\hat{I}_{ph}}{\sqrt{2}} \cos\phi \tag{3-3}$$

$$= \frac{3}{2}\hat{V}_{ph}\hat{I}_{ph} \cos\phi$$

Allowing for space vector modulation or third-harmonic injection, the peak phase voltage, $\hat{V}_{ph}$ can be up to $V_{dc}/\sqrt{3}$ without distortion (a 15% increase from the $V_{dc}/2$ of conventional sinusoidal PWM [61]), so combining these two equations will give a KVA/KW rating of:

$$\frac{KVA}{KW} = \frac{6V_{dc}\hat{I}_{ph}}{\frac{3}{2\sqrt{3}}V_{dc}\hat{I}_{ph}\cos\phi} = \frac{4\sqrt{3}}{\cos\phi} \tag{3-4}$$

If the reactance of the machine is negligible, so that the voltage and current supplied to the drive are always in phase, then the KVA/KW is ~6.9. This is an unrealistic assumption. In fault tolerant permanent magnet drives, the motor inductance is increased so that a terminal short will result in a fault current induced by the back emf, which cannot exceed the nominal rated current, normalised to 1 'per unit'

(P.U.). To ensure 1 P.U. current in a short-circuit condition, it is therefore required that the per-unit reactance and back emf are of equal value [29].

In the event of a terminal short circuit

$$I_{sc} = \frac{\omega_e k_{emf}}{\omega_e L} = \frac{V_{emf}}{X} \tag{3-5}$$

If I_{sc} is limited to 1 P.U., then

$$V_{emf} = X = 1P.U. \tag{3-6}$$

Normalising the output voltage (V_{PWM}) of a fault tolerant converter to 1P.U., the vector diagrams of Figure 3-2, show that the required voltage is ~37% greater with a fault tolerant motor than for a conventional motor (with 0.2 P.U. reactance in this example). The same proportional increase can be assumed for all the permanent magnet machine topologies in this analysis, so this is not considered in subsequent comparisons.

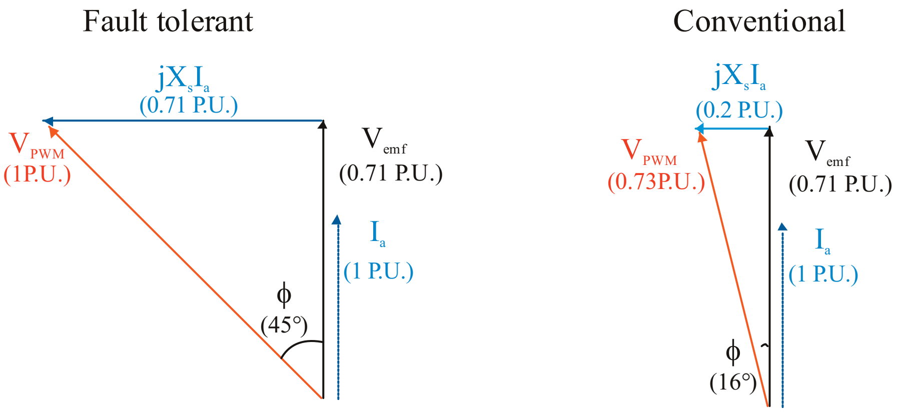

Fault tolerant

Conventional

$$V_{PWM} = \sqrt{(jX_s I_a)^2 + V_{emf}^2}$$

Figure 3-2: PM synchronous machines with 0.71 P.U. and 0.2 P.U. reactance.

Other factors to compare:

- **Machine size**: This is the baseline, so the machine size is defined as 1.
- **Gate drives**: A minimum of 4 isolated power supplies are required, 1 for each of the 3 upper devices and 1 shared between the lower devices.

3.3.2 Motors with n+1 isolated phases

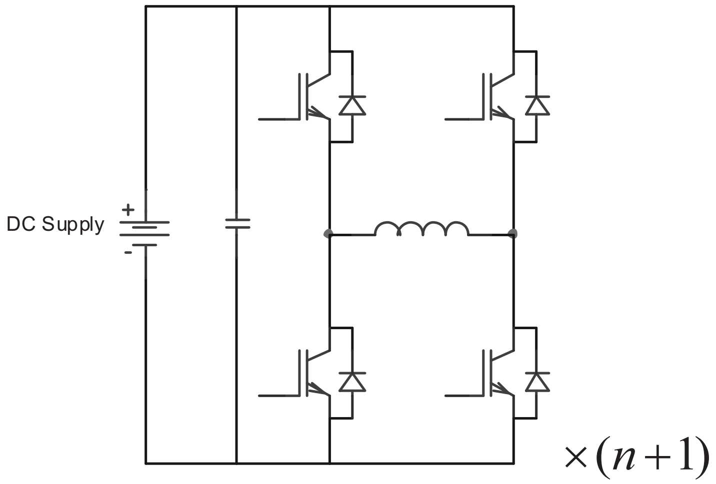

Figure 3-3: A single phase module.

The motor must be able to deliver rated power with *n* powered phases and 1 phase failed/redundant. To provide isolation between phases, each phase is operated by an independent H-bridge.

Each phase has a dedicated H-bridge, so the full dc link voltage can be applied and $\widehat{V}_{ph} = V_{dc}$. Increasing the number of phases will decrease the current required in each phase and therefore the current rating of each power device.

Each H-bridge requires 4 devices, so there are $4(n+1)$ devices in total. The KVA is given by:

3-7
$$KVA = V_{dc} \cdot \hat{I}_{ph} \cdot 4(n+1)$$

The output power is given by:

3-8
$$nV_{rms} \cdot I_{rms} \cos\phi = n\frac{\hat{V}_{ph}}{\sqrt{2}} \cdot \frac{\hat{I}_{ph}}{\sqrt{2}} \cos\phi$$
$$= \frac{n}{2} \hat{V}_{ph} \hat{I}_{ph} \cos\phi$$

(Note: Although there may be *n+1* phases, rated power must be supplied by *n* phases.)

As $\widehat{V}_{ph} = V_{dc}$, the KVA/KW is:

3-9
$$KVA \Big/ KW = \frac{V_{dc} \times \hat{I}_{ph} \times 4(n+1)}{n \big/ 2 \, V_{dc} \hat{I}_{ph} \cos\phi} = \frac{4(n+1)}{n \big/ 2 \cos\phi} = \frac{8 + 8 \big/ n}{\cos\phi}$$

- **Machine size**: In order to produce rated torque with one module failed the machine size is increased by the ratio *(n+1)/n.*
- **Gate drives**: For each H-bridge, 3 isolated supplies are required (1 for each of the upper devices and 1 shared between the 2 lower transistors). Therefore *3(n+1)* gate drive supplies are required.

3.3.3 Motors with multiple 3 phase sets ('3n+3')

The motor is divided into sets of 3-phase star-connected modules, each powered by 3-phase transistor bridges. Rated power is supplied by *n* sets of 3-phase modules with one 3-phase module redundant. For example, in a *3×2+3* system, six phases supply active power and three phases are redundant. Three sets of three-phase bridges are required. Figure 3-3 shows the case for *n=1*, i.e. a *3+3* motor:

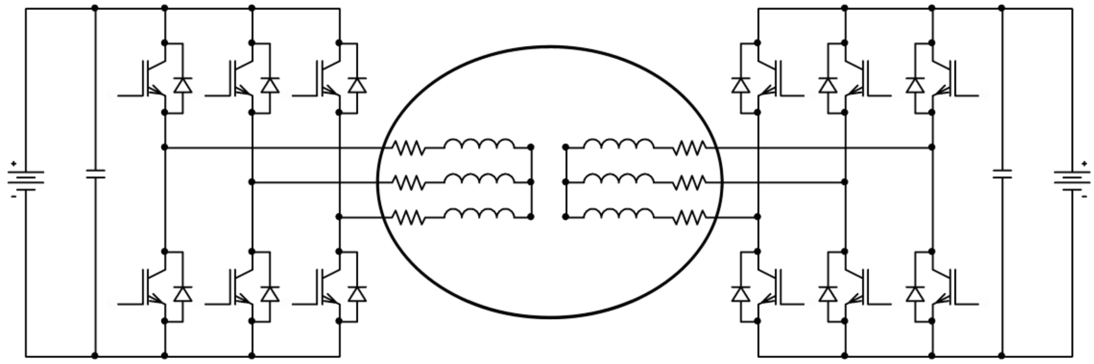

Figure 3-4: A 3+3 motor (n=1).

As with the standard 3-phase star-connected motor, peak phase voltage can be up to $V_{dc}/\sqrt{3}$, without distortion.

The current required by each phase module will decrease as *n* increases.

There are 6 switches required for every set of 3-phases, hence $6(n+1)$ switches.

The KVA is given by:

3-10 $$V_{dc} \cdot \hat{I}_{ph} \cdot 6(n+1)$$

The output power is given by:

3-11 $$3nV_{rms} \cdot I_{rms} \cos\phi = 3n\frac{\hat{V}_{ph}}{\sqrt{2}} \cdot \frac{\hat{I}_{ph}}{\sqrt{2}} \cos\phi = {}^{3}\!/_{2}\, n\hat{V}_{ph}\hat{I}_{ph} \cos\phi$$

As $\widehat{V}_{ph} = \frac{V_{dc}}{\sqrt{3}}$, the KVA/KW is:

3-12 $$\frac{KVA}{KW} = \frac{V_{dc}\cdot \hat{I}_{ph}\cdot 6(n+1)}{\frac{3}{2\sqrt{3}} nV_{dc}\hat{I}_{ph}\cos\phi} = \frac{6(n+1)}{\frac{3}{2\sqrt{3}} n\cos\phi} = \frac{4\sqrt{3}+{}^{4\sqrt{3}}\!/_{n}}{\cos\phi}$$

- **Machine Size**: The machine size is once more increased by the ratio of active + redundant to active modules: *(n+1)/n.*

- **Gate drives**: A minimum of 4 isolated power supplies are required for each set of 3-phases, 1 for each of the 3 upper devices and 1 shared between the lower devices. This requires *4+4n* power supplies.

3.4 COMPARISON WHEN OPERATING AT LOW SPEED

Although a shorted module exerts no significant drag torque on the drive at high speeds, when the fault current is limited by the phase reactance, there is a low speed at which a shorted module will exert significant braking torque. As the speed drops the fault current remains constant as long as the per unit reactance (which drops with speed) is still significantly larger than the per unit resistance. Therefore the loss in the faulted phase remains constant, but because the speed is lower, the braking torque rises inversely proportional to speed.

Consider Figure 3-5, which shows a phasor diagram of a shorted phase winding:

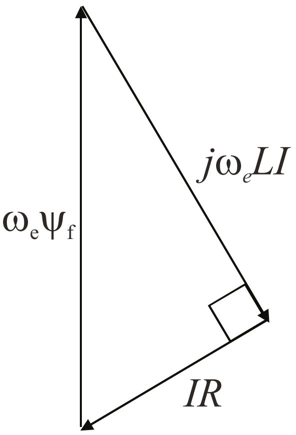

Figure 3-5: Phasor diagram of a machine with a terminal short-circuit.

The power lost in the winding is given by:

3-13 $$P = i^2 R$$

Trigonometrically resolving the phasor voltages to find i^2:

3-14 $$\left(\omega_e \psi_f\right)^2 = \left(IR\right)^2 + \left(I\omega_e L\right)^2$$

3-15 $$\Rightarrow I^2 = \frac{\omega_e^{\,2}\psi_f^{\,2}}{\left(R^2 + \omega_e^{\,2}L^2\right)}$$

the power can be shown as:

3-16 $$P = \frac{\omega_e^{\,2}\psi_f^2}{R^2 + \omega_e^{\,2}L^2}R$$

This is a maximum at high ω_e, tending towards*:*

3-17 $$\left(\frac{\psi_f}{L}\right)^2 R$$

A drag torque exists, as follows:

3-18 $$T = \frac{P}{\omega_m} = p\frac{\omega_e\psi_f^2 R}{R^2 + \omega_e^{\,2}L^2}$$

where p is the number of pole pairs.

This is a maximum when:

3-19 $$\frac{\partial T}{\partial \omega_e} = 0 \Rightarrow \frac{\psi_f^2 R}{R^2 + \omega_e^{\,2}L^2} - \frac{\omega_e\psi_f^2 R\cdot 2\omega_e L^2}{(R^2 + \omega_e^{\,2}L^2)^2} = 0$$

3-20 $$\Rightarrow 1 = \frac{\omega_e \cdot 2\omega_e L^2}{R^2 + \omega_e^{\,2}L^2}$$

3-21 $$\Rightarrow R^2 + \omega_e^{\,2}\mathrm{L}^2 = 2\omega_e^{\,2}L^2$$

Hence the maximum drag torque is at the frequency where $R=\omega_e L$ and is of magnitude:

3-22 $$T = p\frac{\omega_e^{\,2}\psi_f^2 L}{2\omega_e^{\,2}L^2} = p\frac{\psi_f^2}{2L}$$

and is independent of R.

If $L_{pu} = \psi_{fpu}$ then T_{drag} = 0.5 of the rated torque of one phase at the frequency of:

3-23 $$\omega_{pu} = \frac{R_{pu}}{L_{pu}} << 1.0$$

Hence the peak braking torque is predicted to be one half of the rated torque of the shorted module and occurs at a per unit speed given by the ratio of the module per unit resistance to the per unit reactance. This will typically be at 3-10% of rated speed. In order to validate these predictions, measurements were made upon a demonstrator fault tolerant machine with the parameters given in Table 3-1.

Parameter	Value
Pole pairs	4
Resistance	0.156Ω
Inductance	1.275mH
r.m.s. field flux-linkage	0.0258 volt-seconds

Table 3-1: Measured per-phase parameters of a fault tolerant demonstrator machine.

The machine was mechanically coupled to an external drive so that it could be run at a range of speeds when unexcited. Shaft torque was measured using a commercial torque transducer. The machine was initially rotated with all phases open-circuit and the shaft torque measured, this torque being due to friction, bearing loss, windage and iron loss. The test was then repeated with a single phase shorted at its terminals. The difference between torques measured in the two tests was that exerted by the shorted phase, assuming that the iron loss is unchanged. Figure 3-6 shows these measurements alongside predictions using the parameters of Table 3-1 and there is generally good agreement. Peak torques are within 2% of each other, although the measured peak value is at a slightly lower speed than predicted. This may be due to changes in the phase resistance with temperature.

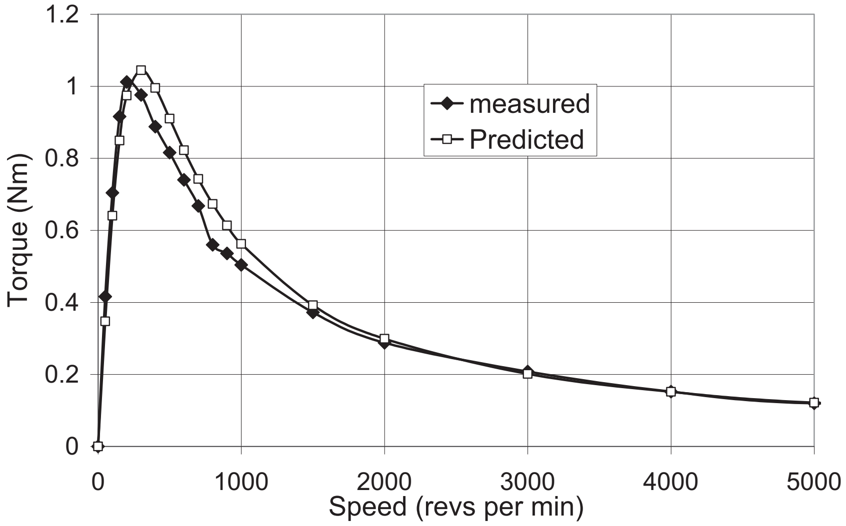

Figure 3-6: Measured and predicted braking torque exerted by a single phase short-circuit in a demonstrator fault tolerant drive.

For an actuator electric drive required to provide rated torque at all speeds, an over-rating factor must be included to overcome this braking torque. With one lane short-circuited, the *n* remaining lanes must provide 1 P.U. torque and overcome 0.5 P.U drag from failed lane:

3-24 $$nT = 1 + 0.5T$$

where T is the rated torque of one lane and can be given by:

$$T = \frac{1}{n - 0.5} \tag{3-25}$$

As $n+1$ lanes are present, the total P.U. rating of the fault tolerant drive is given by:

$$\frac{n+1}{n-0.5} \tag{3-26}$$

The relative effects of this on different topologies are discussed later in this chapter.

3.5 TORQUE RIPPLE AT STANDSTILL

When a module fails it can no longer contribute to torque. The loss of torque is not necessarily equal at all positions, leading to torque ripple. This torque ripple is not likely to be important in a machine rotating at reasonable speed, because the inertia of the machine and load will ensure that the machine continues to rotate, responding only to the mean torque requirement. However, when the machine is stationary or running very slowly, this is no longer the case and it becomes necessary to produce rated torque at all positions in order to ensure that the drive can start. Again, it is assumed a requirement for an actuator drive motor to produce rated torque at standstill. (*Appendix A presents calculations for the example motor used in 3.4, showing a minimum speed of the order of 130r/min for the inertial energy of the rotor to subsume the torque ripple from a failed phase under nominal loading.*)

The effect of different drive configurations upon the near-standstill torque capability will be examined in this section, leading to a torque scaling factor needed by the remaining modules to overcome this problem. Firstly an overview of the two module types can be made:

- A *3n+3* motor consists of multiple 3-phase windings, each set with 120° separated, star-connected phases. Each 3-phase set is capable of running the motor with constant torque at all positions. Therefore a failure will result in the shutting down of a 3-phase winding but **will not** result in a torque ripple.
- In an *n+1* motor, failure of a phase will result in a phase imbalance, resulting in a torque ripple.

Consider a motor with 3 isolated phases, each phase supplied from a single phase bridge (i.e. *2+1*). The drive must be capable of running with only 2 phases to give fault-tolerance. If the back emf and current are assumed to be 1 P.U. and in phase, the relationship between current, back emf and torque is shown in Figure 3-7.

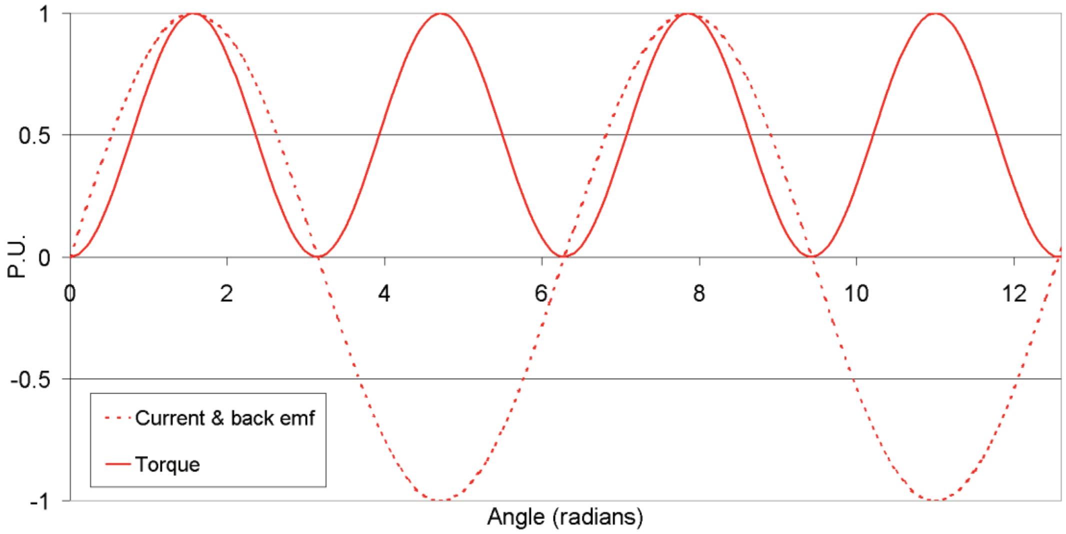

Figure 3-7: Torque and current / back emf in one phase of a 2+1 motor.

The combined torques from all 3 phases are shown in Figure 3-8 :

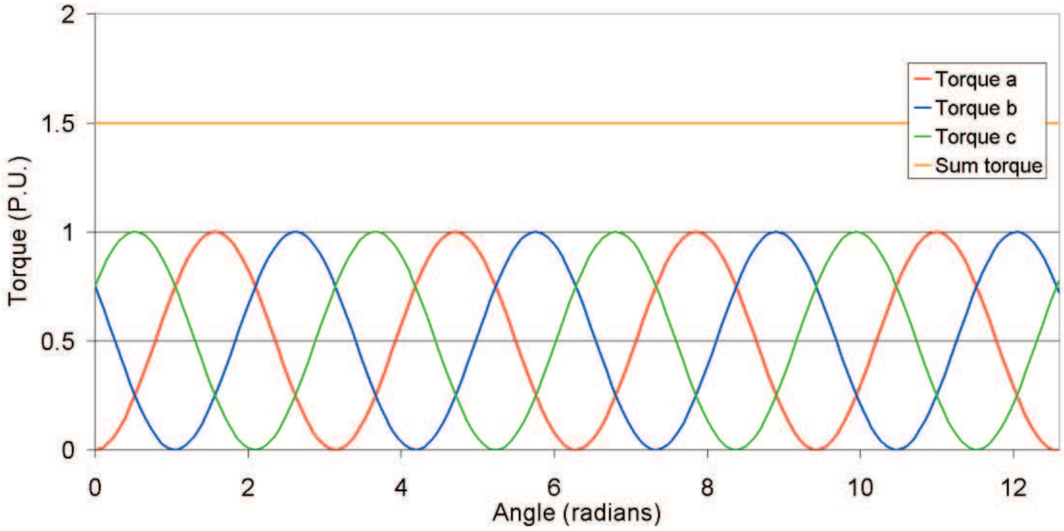

Figure 3-8: Torques from each phase of a *2+1* motor and sum output torque.

Now if one of the 3 phases fails open-circuit at speed, it will produce no torque. If the motor continues to run unadjusted, the torques are as shown in Figure 3-9.

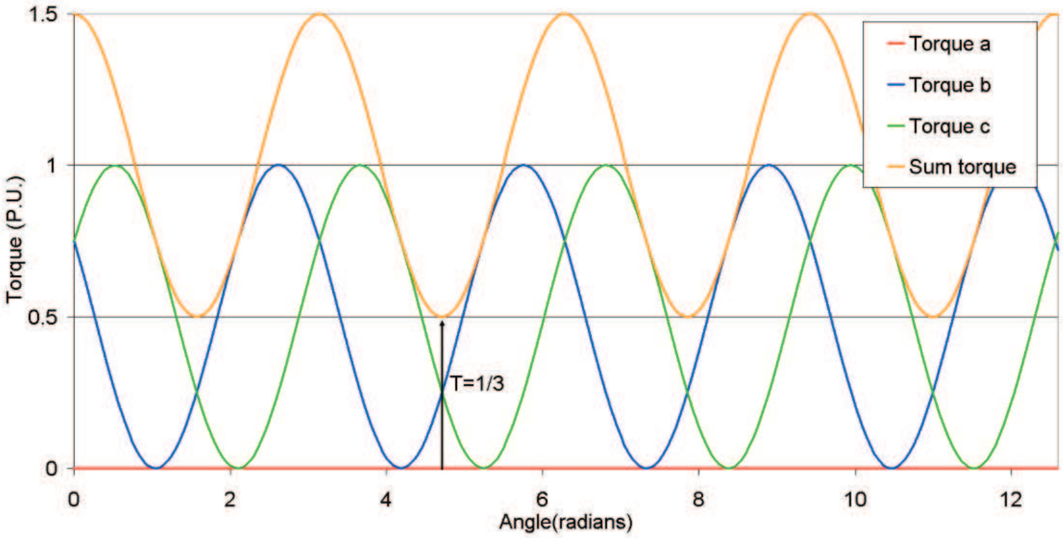

Figure 3-9: Phase torques in a *2+1* motor with 1 failed phase.

Note how at some positions the torque capability has fallen to only one third of the unfaulted case. To cancel out the ripple torque, the functional phases have to compensate for the torque lost from the failed phase. In the example above, at the point of maximum ripple, phases b and c need to provide three times their normal torque to compensate for the loss of phase a.

For a fault tolerant motor with *n+1* phases, the unfaulted mean torque capability is $(n+1)T_{phase}$ where T_{phase} is the mean torque capability of each phase.

When one phase fails there is a peak loss of torque at certain positions, corresponding to $2T_{phase}$; hence the ratio of torque capability when faulted to that when unfaulted is:

3-27
$$\frac{n-1}{n+1}$$

Therefore, to be capable of producing rated torque at all positions, the functioning phases must increase their output torque by:

3-28
$$\frac{n+1}{n-1}$$

at the point of maximum ripple to maintain full output torque.

A simple but effective technique for cancelling out torque ripple is to calculate, for all positions, the ratio between the torque available and the torque required. The torque from the functional phases can then be increased by this factor:

3-29 $$T_{phase\_new} = T_{phase\_old} \times \frac{T_{required}}{T_{available}}$$

The effects of this on the *2+1* motor phase torques are shown in Figure 3-10:

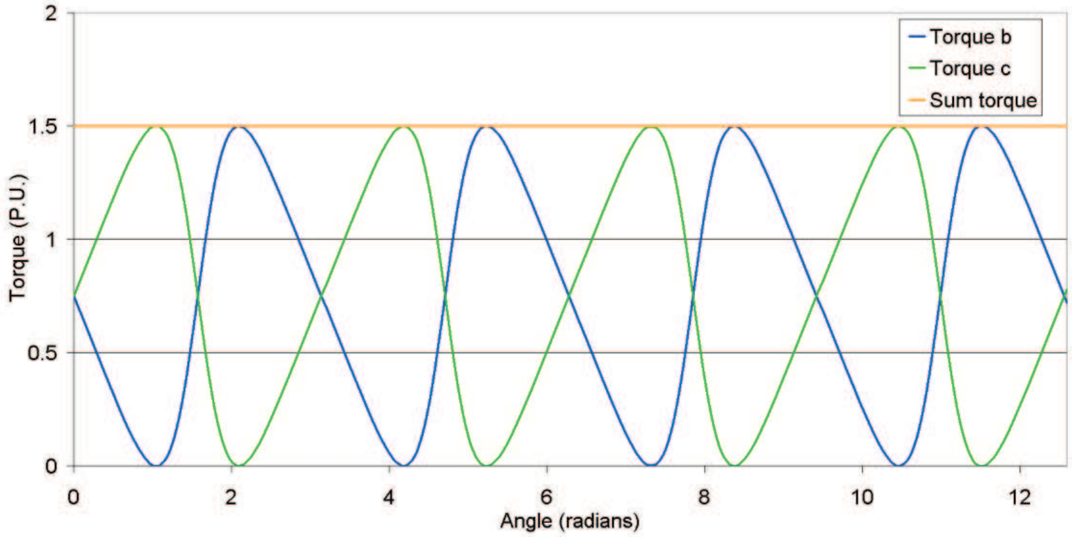

Figure 3-10: Ripple-compensating torques in a *2+1* motor with 1 failed phase.

To increase the torque from a phase, as the voltage from the dc link remains constant, the current must be increased. The increase in current to allow torque reshaping determines to what extent the rating of a machine & drive must be increased.

It must be noted that no torque feedback is required to reshape the torque and current. The power electronics controlling the healthy phases will be aware of which phase is faulted and thus the expected torque 'dip' across 360 electrical degrees.

A derivation of current shaping in a *2+1* system is given in Appendix A, *pp.9.2.*

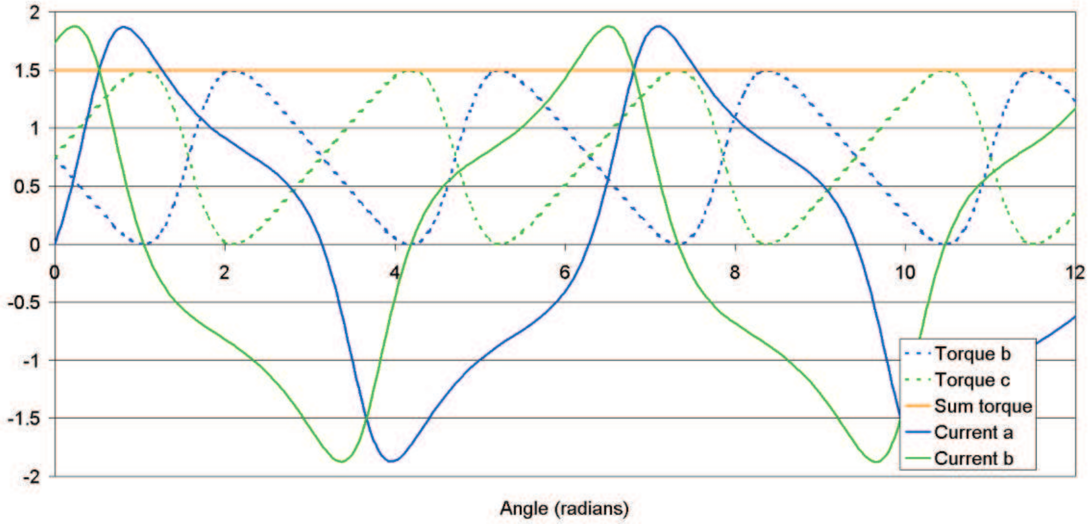

Figure 3-11: Reshaped currents and torques in a faulted 2+1 motor.

As Figure 3-11 shows, although the sum instantaneous phase torque may be required to increase by $\frac{n+1}{n-1}=\frac{3}{1}=3\times$, the peak current is only required to increase by approximately 1.8×. Experimental results of this current shaping technique were published by the author in 2003 [62], although similar reshaping techniques were presented by Ede *et al*. in 2002 [63,64] and later by Zhu *et al*. in 2008 [65]. While the approach by Zhu employs the same technique as the author, the reshaping calculations employed by Ede result in considerably different currents to those shown in this chapter. The motors developed by Ede *et al*. feature non-sinusoidal back emf waveforms, so even when unfaulted, the current waveforms are shaped to provide a smooth torque. Additionally, in the case of a motor short-circuit, the waveforms are reshaped to compensate for the instantaneous drag torque from the failed phase. As stated earlier in this section, for the high speed motors considered in this thesis, the effects of drag torque from a short circuit are considered to occur at speeds much higher than those at which torque ripple effects may occur, so the drives need not be designed to cope with both effects occurring simultaneously.

The torque ripple in a *3+1* motor with one failed phase is shown in Figure 3-12. The torque has fallen to a minimum of $(3-1)/(3+1)=0.5\times$, at positions where the failed phase output would normally be at a maximum.

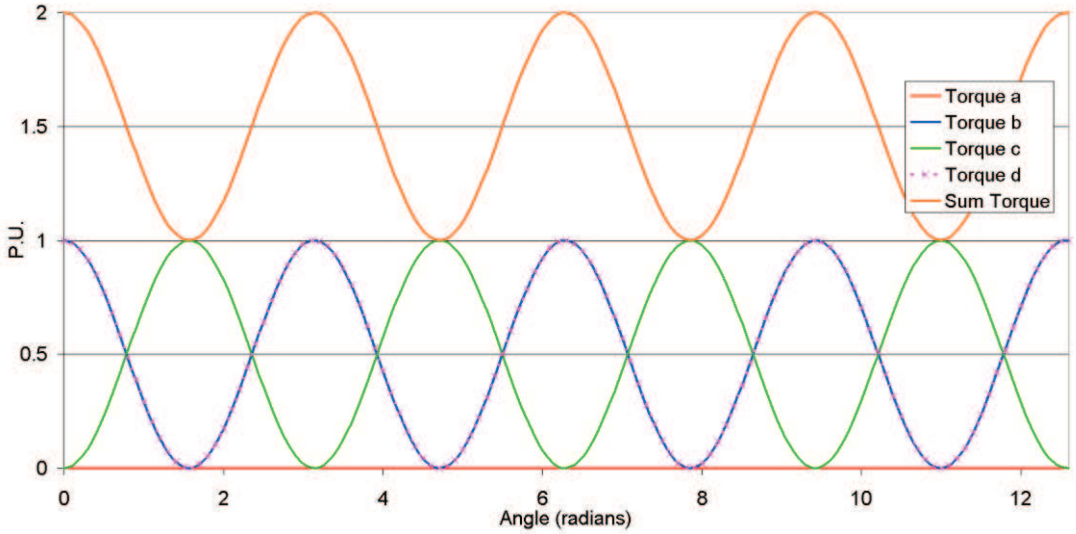

Figure 3-12: ***3+1*** **motor with one failed phase.**

The reshaped waveforms to compensate for the torque ripple are shown in Figure 3-13. It is clear that phase *c*, 180° from the failed phase *a*, has increased its current to a peak of 2 P.U. in the worst case. This is a case for motors with even numbers of phases, as the symmetrical distribution will result in only the opposite phase to a faulted phase being capable of contributing additional torque at all positions.

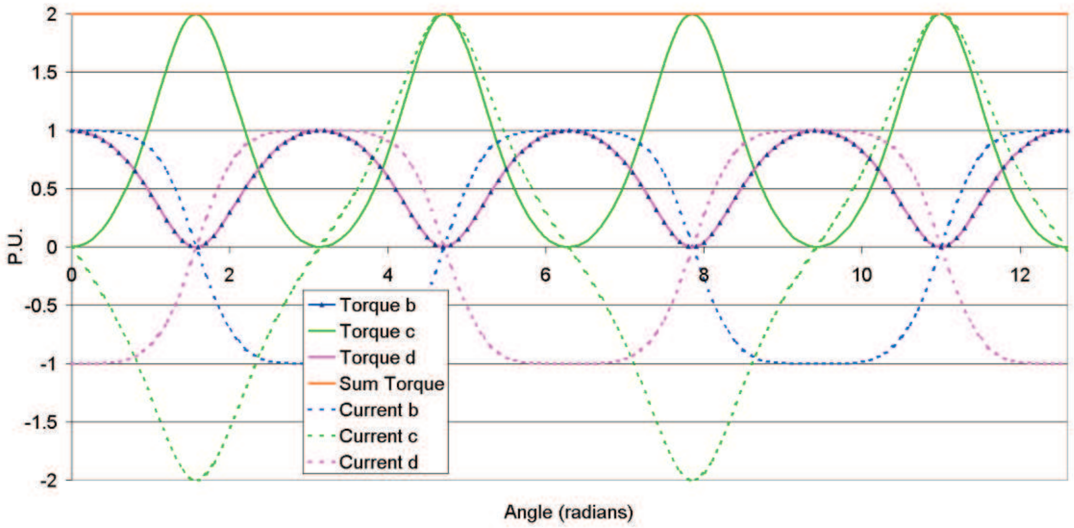

Figure 3-13: Reshaped motor currents and torques in *3+1* motor with one failed phase.

Torques and currents have been calculated for various other *n+1* phase motors and the resulting graphs are available in Appendix A, *pp.207*. The following observations can be made.

- For motors where n+1 is an even value, the peak current increase is given by:

$$\frac{n+1}{n-1} \tag{3-30}$$

- For motors where n+1 is an odd value, the required peak current increase is *less than* $\frac{n+1}{n-1}$. As no simple equation can be derived to relate this current to *n*, specific values are listed later in this chapter (*pp.67*).

It must be noted that the torque ripple is only a problem at low speed. This means that the extra voltage required to produce the non-sinusoidal current waveforms is not an issue for the drive rating as at low speeds the motor requires relatively low voltages in the healthy case and the additional faulted voltage is still well within the voltage capability of the drive. As speed builds up and the torque ripple becomes subsumed within the inertia of the machine, it is no longer useful, or necessary, to reshape the current waveforms.

3.6 OVERALL COMPARISON

The relative electrical machine size and power electronic converter complexity for numerous fault tolerant drive configurations have been evaluated for three conditions in which rated torque must be produced when faulted:

- **High Speed**: Drag torque from a short-circuit module and torque ripple effects are insignificant.
- **Low speed**: The drag torque from a shorted module has been shown to rise to a peak of ½ the motoring torque. The speed at this point is considered high enough for the inertia of the machine to overcome any significant effects of torque ripple and the system will only respond to the mean torque produced.
- With the machine **near stationary**, when torque ripple is an issue for ($n+1$) drives consisting of multiple single phase windings.

Fault tolerant electromechanical actuators are assumed to require rated torque at all motor angles. With true direct-drive actuators very unlikely due to high torque requirements, motors coupled through gearboxes and ball/roller screw mechanisms must perform many revolutions to move an actuator through the full range of motion and must therefore provide rated torque at all angles. An actuator can be stopped and restarted at any position, so starting operation must always be considered under the peak torque from the worst case load profile.

To summarise the findings; a fault tolerant machine must be over-rated to provide worst-case peak torque when faulted, at any rotor position and must also overcome the peak drag torque once rotating.

The extra torque required for overcoming torque ripple and drag will only occur briefly during the acceleration of the motor, so the thermal limit capability of the drive is unaffected. The motor must be electromagnetically capable of producing this short term overload torque (i.e. without saturation or magnet demagnetization limiting overload torque) and power electronics must be rated for the additional current.

Full details of calculated results for $n+1$ and $3n+3$ topologies are presented in Table 3-2 at the end of this chapter (*pp.67*), while a summary is shown in Figure 3-14. The machine ‘size factor’ is the ratio of peak torque over and above the thermal limit torque of a conventional motor and is derived from the operating condition requiring the greatest over-rating. In practice meeting this peak torque will require that sufficient iron is included in the armature to avoid saturation, which might amount to a 50-60% increase in tooth and core back cross-sections for a doubling in peak torque capability. It is unlikely that increases in peak torque will require deeper magnets, since the magnets need to be relatively deep to avoid mutual coupling between phases (to meet fault tolerant requirements). Results are also presented for KVA/KW ratings under the various operating conditions. An additional converter over-rating of $\sqrt{2}$, due to the increase in per-unit reactance for fault tolerance (ϕ=45°, *pp.51*) is incorporated into the results, including the standard 3-phase drive.

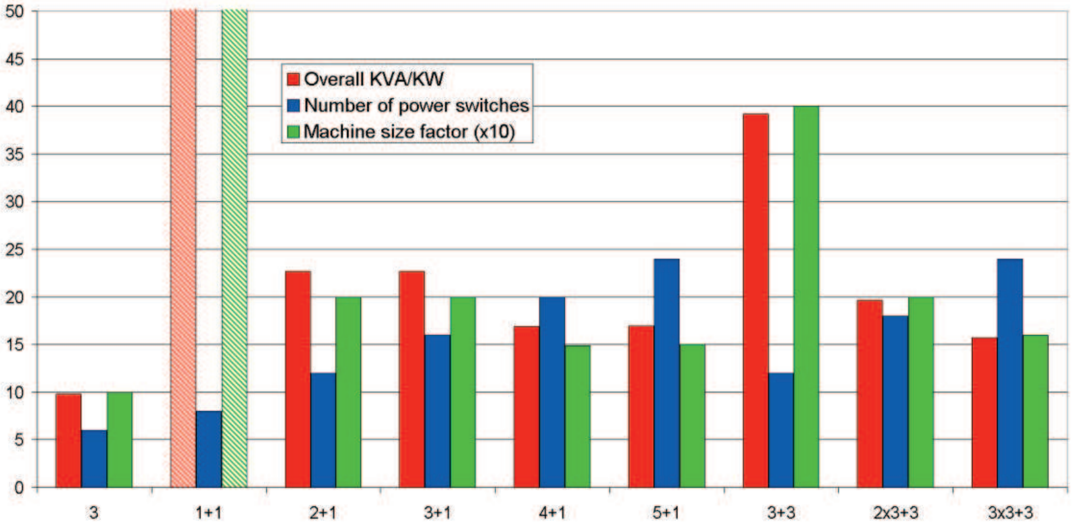

Figure 3-14: Motor size, converter size and complexity of fault-tolerant topologies.

From Figure 3-14 it can be seen that as the number of modules increase, the overall size of the fault tolerant drive tends to decrease, but the component count increases. Higher module numbers will show a levelling-out of drive size, but an ever-increasing component count. The shaded bars of the *1+1* motor represent infinity as this motor will not provide full torque at standstill from one phase and hence is not a feasible actuator motor.

Motors with three phase modules generally require a smaller overrating than those with single phase modules at standstill. This is because they do not introduce torque ripple.

For values of *n*, three phase modules produce the same relative low-speed drag torque as single phase modules; however, to minimize this effect, larger numbers of *n* are required and this results in a much higher component count for 3-phase systems; e.g. a *2×3+3* system produces the same drag torque as a *2+1* system, but requires 50% more power devices.

Despite the trend for higher values of *n* requiring smaller drives, it can be observed that a *2+1* arrangement appears to offer a more optimal solution than *3+1*, requiring a similar sized machine and power electronic VA quantity, but only 75% of the components. This is because even numbers of phases seem to cope less well with torque ripple at standstill.

As the number of single-phase modules increases to *4+1* or *5+1,* the machine "size factor" falls from 2.0 to 1.5, alongside a similar reduction in KVA rating. Although a notable improvement, this must be factored against an increase in component and connection number. Once more, the odd number of phases (*4+1*) seems to be a better choice than the even number (*5+1*), offering similar sizing with a lower component count. The quad three-phase arrangement (*3×3+3*) offers a similar motor and converter size with the same number of devices as a *5+1*, although converters with such high values of *n* are perhaps overly complex and may require increased maintenance due to the higher component counts, resulting in increased probability of individual component failure.

3.7 CONCLUSIONS

This analysis suggests that the best combination of component count, converter size and machine size occurs with either *2+1* or *4+1* phases, supplied from single phase bridges. The former has only 60% of the device number of the latter, but requires a 33% larger motor and a 40% greater converter volt-ampere rating.

Although not affected by torque ripple, three phase machines appear at a disadvantage as higher numbers of modules to overcome drag torque will result in 50% more devices than single phase systems. For this reason, the most basic *3+3* machine suffers from a very large over-rating factor and a *2×3+3* would require a motor of 50% the size; however, this is a nine-phase motor with considerable component count and a three-way control architecture.

When selecting a topology by the number of control lanes, if a duplex system is required then only a *3+3* motor can be utilised as a *1+1* motor cannot start itself at all angles following a fault. If a triplex system is required then a *2+1* or a *2×3+3* motor can be selected; however, the *2+1* offers 50% fewer switching devices and

75% of the isolated gate drivers. If a quadruplex system is required, the same comparison applies for *3+1* and $3 \times 3+3$.

The calculations presented here are based on actuators with emphasis on full torque at all speeds and angles. Where a load profile does not require full torque at low speeds – for example, a pump application, the effects of torque ripple at standstill may be irrelevant and the designer must compare the speeds affected by drag torque against the required torque/speed profile to determine whether it is actually necessary to over-rate to compensate.

Calculations are based on conventional transistor bridges with dc inputs; however, values can be adjusted to include drives with ac rectification inputs and also to motor drive variants such as matrix converters. Regardless of converter arrangement, each phase must operate from a separate converter to follow the fault-tolerant 'lanes of power' approach and motor sizes will be unaffected. The component counts may vary with different power electronic converter technologies, but the results will simply be scaled with trends remaining the same for values of n.

The calculations are unaffected by the duty cycle of the actuator. If a converter accelerates almost instantly to full speed, passing through the torque ripple and drag torque regions in milliseconds, the motor must still be electromagnetically over-rated to overcome these effects, as must the power converter peak current rating.

	Standard	Multiple single phases					Multiple three-phases		
Phase configuration	3	1+1	2+1	3+1	4+1	5+1	3+3	2x3+3	3×3+3
Number of lanes post-fault	-	1	2	3	4	5	1	2	3
Motor phases	3	2	3	4	5	6	6	9	12
Number of power switches	6	8	12	16	20	24	12	18	24
Gate drive power supplies	3	6	9	12	15	18	8	12	16
No. of machine connections	3	4	6	8	10	12	6	9	12
Machine size factor at high speed	1.00	2.00	1.50	$1.3\dot{3}$	1.25	1.20	2.00	1.50	$1.3\dot{3}$
Converter KVA/KW (inc. 0.707 P.U. reactance) at high speed	9.80	22.63	16.97	15.08	14.14	13.58	19.60	14.70	13.06
Machine size factor to overcome drag torque at low speeds	N/A	4.00	2.00	1.60	1.43	1.33	4.00	2.00	1.60
Converter KVA/KW for low speeds	N/A	45.25	22.63	18.10	16.18	15.08	39.19	19.60	15.68
Machine size factor to overcome torque ripple at standstill	N/A	N/A	1.88	2.00	1.49	1.50	2.00	1.50	1.33
Converter KVA/KW near standstill	N/A	N/A	21.27	22.63	16.86	16.97	19.60	14.70	13.03
Overall machine size factor	1.00	N/A	2.00	2.00	1.49	1.50	4.00	2.00	1.60
Overall converter KVA/KW	9.80	N/A	22.63	22.63	16.86	16.97	39.19	19.60	15.68

Table 3-2: Motor and converter size and complexity for conventional and fault tolerant permanent magnet drive configurations.

4 Safety-Critical Design of Electromechanical Actuation

Electric drives can be designed to continue operation after a fault by employing the fault tolerant topologies discussed in chapter 3, although for use within an electromechanical actuator (EMA) on a commercial aircraft there are many additional considerations.

The review of flight control surfaces in chapter 1 highlights the level of safety backup systems required in commercial aircraft. Multiple actuators are employed on flight-critical surfaces and surfaces are required to continue operation after failures of external interfaces, such as loss of power supplies and control computers.

This chapter initially discusses safety-driven design for flight control actuators and considers where electromechanical actuators may be applied and where limitations occur, such as those resulting in the ‘jam’ problem highlighted in chapter 1. Where fault tolerance may be prove advantageous, discussion is given on the control requirements to ensure the multiple ‘lanes’ operate in a manner that complements, rather than compromises, the safety and reliability benefits.

Latterly the considered topologies of the DEAWS and ELGEAR NWS systems are presented and analysed. Although actuator design choices were made in conjunction with industrial partners, observations, justifications and calculations given within this chapter are those of the author.

4.1 DESIGNING A ELECTROMECHANICAL ACTUATION SYSTEM

4.1.1 Existing fault tolerant actuator configurations

All potential failure conditions in an aircraft have an acceptable probability of occurring which corresponds to the severity of the outcome. During the design process this is considered in the Failure Modes and Effects Analysis and any new devices must be designed to meet these failure probabilities.

In the case of a control surface, a failure which will result in loss of the aircraft is considered the most severe and must therefore have an exceedingly low probability of occurrence. This can be observed in the various safety requirements for the DEAWS system (*see section 2.1.2*), where any failure resulting in a catastrophic failure of the aircraft has a failure probability of $<10^{-9}$ per flight hour. Similar failure probability requirements are also is stated by Yeh [66] for failures which may affect the aircraft structure.

Primary flight control surfaces are critical to an aircraft remaining airborne, so failure probabilities can be considered of the order of 10^{-9} per flight hour. To understand the existing arrangements of actuators, the reliability of a single actuator can be considered. With the Electro-Hydraulic Actuator (EHA) present on primary control surfaces of modern aircraft, this is a good basis for calculations.

A breakdown of the failure probabilities for components within a military EHA are given by Sadeghi and Lyons [54]. A simple fault-tree of a single-lane EHA can be constructed using this data (Figure 4-1), resulting in a failure probability of 1.98×10^{-4}.

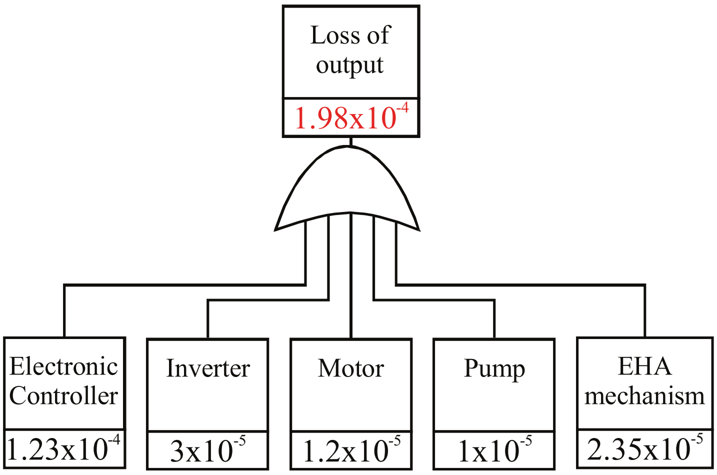

Figure 4-1: Simplex EHA fault tree. Failure probabilities per flight hour.

It should be noted that the electronic controller failure probability incorporates power supply and control signal failures. Accurate failure probability data is difficult to find and predicted component reliabilities may vary between sources and also between commercial and military actuators; however, a failure probability of 1.98×10^{-4} per flight hour is many orders of magnitude greater than the required 10^{-9} for a primary control surface and indicates a single EHA will not be suitable.

To overcome this reliability shortfall, as [54] shows, there are many possibilities for connecting EHAs in parallel to drive a single surface and probabilities of ‘loss of control’ can be reduced to values of the order of 10^{-15} using dual EHA mechanisms on a surface, each driven by two independent sets of hydraulic pumps and control electronics, resulting in a quadruple control arrangement, capable of tolerating 3 faults.

The connection of hydraulic actuators in parallel can be observed as far back as the 1970’s [67] in space shuttle control, where all flight controls are handled by four independent computers running identical control software. Each control surface features four hydraulic servo actuators, each operated from a different lane of the flight control computer. Pressure differential measurements allow automated detection and bypassing of up to two actuators operating with an unacceptable variation from the average. After two failures, it is not possible to identify a further failure by pressure differential, so instead a disagreement ‘standoff’ is highlighted to the pilot, who can manually bypass either of the two remaining actuators, with the help of results from inbuilt failure monitoring.

These fault tolerant designs all require bypassing of hydraulic and electro-hydraulic actuators in the event of a failure. The probability of a jam which cannot be overcome by removal of fluid pressure is not mentioned, so it can be assumed that it is of a negligible probability.

It is therefore logical that parallel configurations of hydraulic and electro-hydraulic actuators are used in modern aircraft to attain safety requirements (*for examples, see section 1.3.3. for A380,* [66] *for B777 and* [26] *for B787*). A selection of these configurations is shown in Figure 4-2.

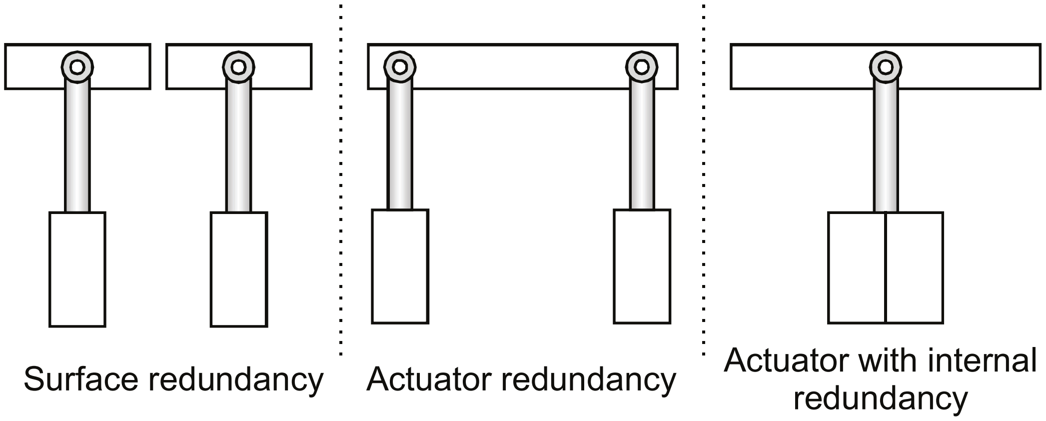

Figure 4-2: Methods of actuator redundancy.

The three common arrangements are:

- **Surface redundancy:** Where multiple surfaces perform an aerodynamic task, such as spoilers, a single actuator can be employed on each surface. Following actuator failure, the fail-to-damping of the hydraulics allows the surface to be aerodynamically blown to a neutral position and the remaining surfaces to provide control.
- **Actuator redundancy:** Where multiple actuators move a surface, a failed actuator reverts to damping and torque is provided by the remaining actuator.
- **Actuator with internal redundancy:** Actuators with multiple internal hydraulic paths (e.g. EBHAs) allowing tolerance of power supply failure although the single path of actuation represents a common point of failure. On the A380 rudder this arrangement is used in conjunction with surface and actuator redundancy.

4.1.2 Electromechanical actuator configurations

The first stage in assessing the applicability of electromechanical actuators (EMAs) in aircraft is to produce a fault tree to compare with the EHA. An EMA is assumed to consist of a power electronic controller, motor, gearbox and ball/roller screw mechanism. The power electronic controller, power supply and control signal failure rates can be assumed to be similar to the EHA values provided by Sadeghi and Lyons [54] as both technologies feature conventional electric drives. A recent breakdown of motor reliability data is given by *Pieters et al.* in [68] where a MTBF is given as 1.4 million hours, which can be proportioned between bearing and winding failures using the respective values of 95% and 2%, suggested in [58]. To estimate the failure probability of a gearbox, it is assumed that bearing failures are the dominant factor, so a gearbox with 10 bearings is used – this would be the case in a 4 planet epicyclical unit. A roller screw is considered as the most likely option for linear actuation, for which reliability data is predicted in [69]. The resulting fault tree is shown in Figure 4-3.

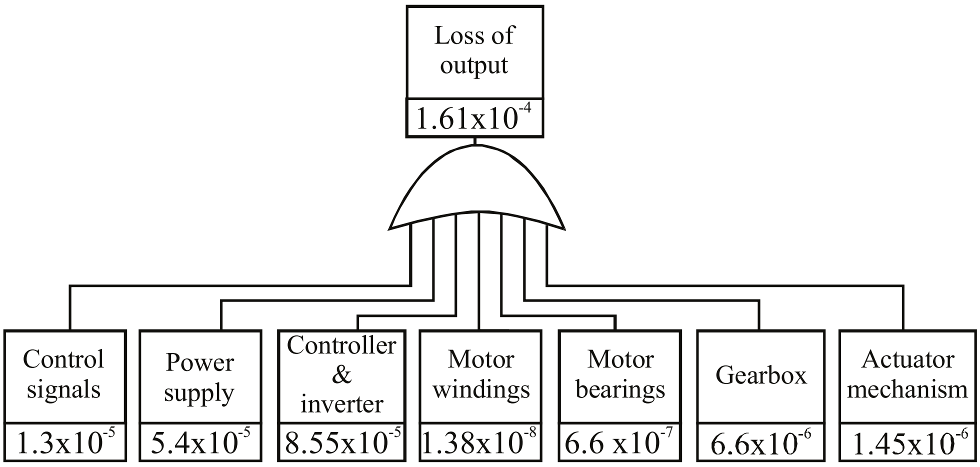

Figure 4-3: Single channel EMA fault tree with failure probabilities per flight hour.

From the data it is clear that an EMA offers a similar failure probability to that of an EHA and is completely unsuitable for a safety critical application requiring a 10^{-9} failure probability per flight hour. The logical solution is to connect multiple EMAs in parallel, in a similar manner to the schemes described in section 4.1.2; however, this is not a viable option.

As discussed in chapter 1, the motor rotor, bearings, gearbox and actuator mechanism of the EMA have the potential for seizures, so there is not the inherent fail-to-damping mode of a hydraulic actuating cylinder. If EMA redundancy is to be implemented with parallel actuators, then a failsafe mechanism will be required to decouple a jammed actuator (i.e. a clutch), or a mechanism with a negligible probability of a jam, such as the dual load-path ball screw proposed in [49], adding considerable weight and complexity. Figure 4-4 shows topologies for clutch and dual load-path EMA systems capable of tolerating a jam. It must be noted that a mechanism to combine the two lanes must be downstream of all jam-capable components, including gearboxes and therefore at the point of maximum torque.

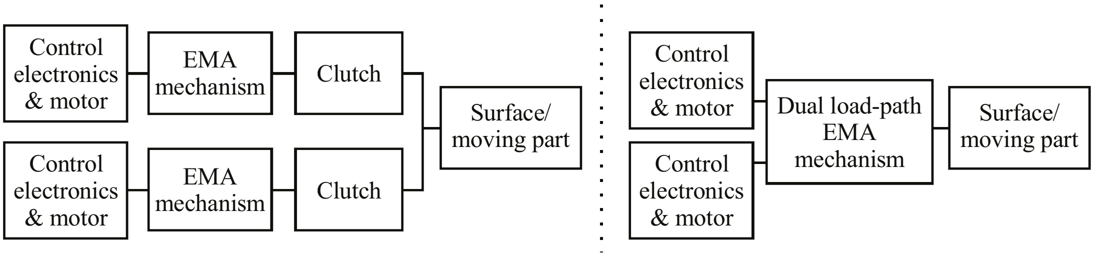

Figure 4-4: Two jam-tolerant EMA topologies.

In depth discussion of these schemes is beyond the scope of this work, but the difficulties in applying electromechanical actuators to the most safety-critical control surfaces are apparent.

With the EMA fault tree suggesting that the electronic controller, control signals and aircraft power supply offer the greatest risk of failure, it is viable to consider the potential reliability improvements of employing a fault tolerant drive configuration. With the fault tolerant drive topologies of chapter 3 all capable of operating following one fault in the motor or power electronic converter, probability of failure can represented by two drives in parallel as two failures are required for loss of output. The redrawn fault tree is shown in Figure 4-5.

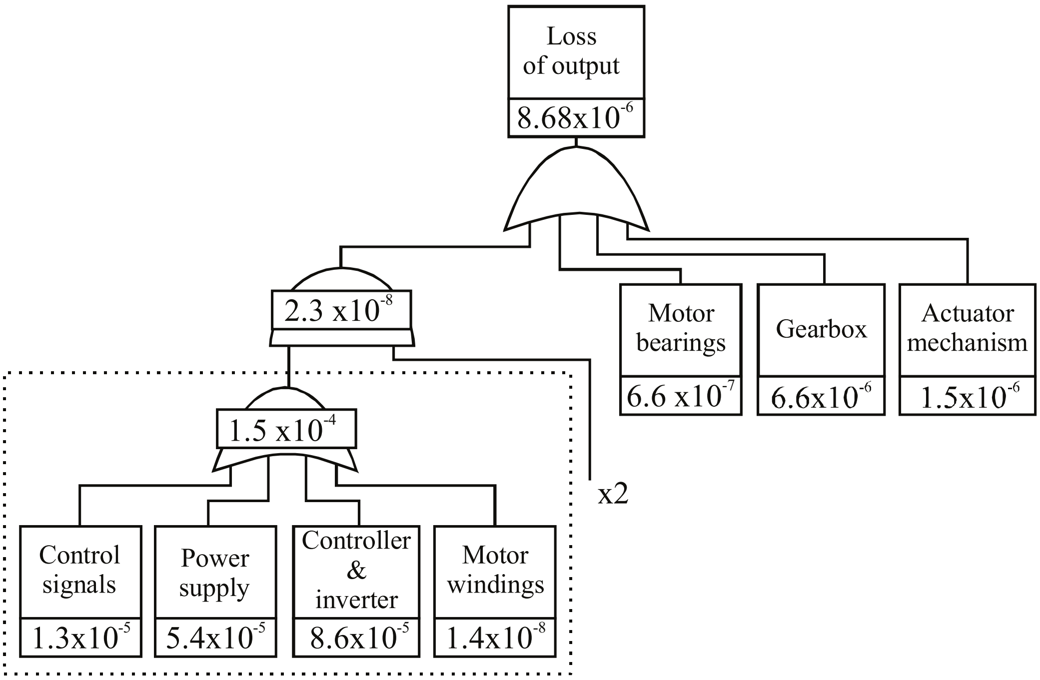

Figure 4-5: Dual channel EMA fault tree with failure probabilities per flight hour.

The resulting failure probability is far lower than the single channel solution and is now dictated by the mechanical components. While the mechanical failure probabilities could be deemed overly pessimistic, as they are derived from long term operational failures, rather than random failure during a single flight, it is unlikely that a significant increase in reliability is possible.

The results do indicate that an individual EMA with fault-tolerance could be viable for systems with a less strict probability for loss of output, and where a jam is not catastrophic, such as the flap/slats of DEAWS, with an allowed 1×10^{-5} per flight hour for loss of operation.

This data also suggests that while removing the gearbox may provide a reduction in component count, the motor bearings and to a greater extent, the roller screw, are still a dominating factor in the overall failure probability. In other areas where fault tolerant electric drives are under consideration, such as engine generators (*section*

1.5.1) there is obviously no actuator mechanism, so only the motor bearings offer a single point of failure and the failure probability will be reduced accordingly.

As an alternative to fault tolerant drives, similar functionality could be achieved with a pair of motors and a speed summing or clutch system. Such an arrangement is shown below a fault tolerant drive in Figure 4-6.

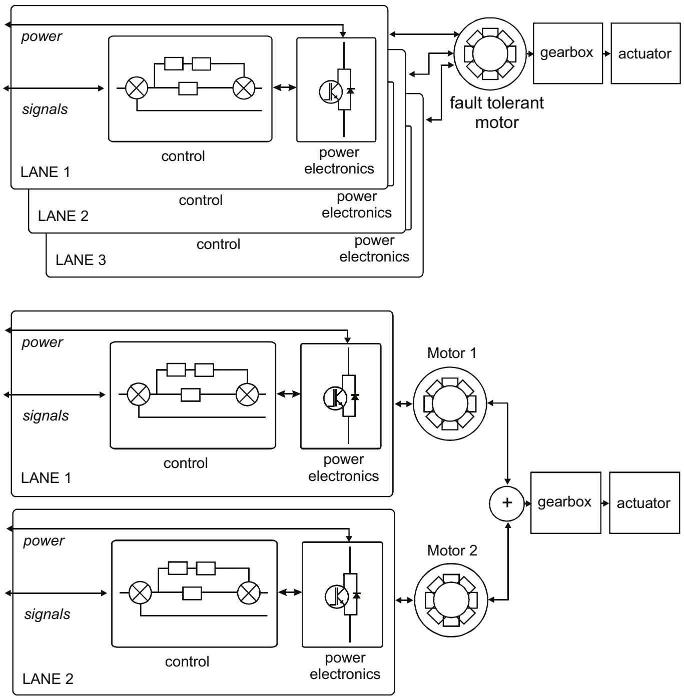

Figure 4-6: An actuator with a fault tolerant drive (top) and a pair of motors (bottom).

A dual motor arrangement is capable of operation following the failure of a set of motor bearings; however, the component count and weight is higher due to the additional motor packaging. Both schemes are valid in an EMA although neither presents a significant safety advantage as the single points of failure in the gearbox and actuator mechanism remain. The work in this thesis will focus on actuators with fault tolerant motors.

With the conclusion that an EMA with fault tolerance is sufficiently reliable for application in non-flight critical actuation systems, an optimum fault tolerant drive topology can be considered.

It should be noted that the drive shown in Figure 4-6 and many of the topologies discussed in chapter 3 feature three or more lanes of controllers and motor windings. Although theoretically only two lanes are required for any system to operate following a single fault, in the case of *n+1* drives (*pp.48*), three or more lanes may be required in order to provide rotation post-fault.

When designing any fault tolerant aerospace drive the cost and maintenance penalties (*section 1.4*) of overly complex systems must be considered. With each lane of a fault tolerant drive requiring a separate power supply it must be noted that there are only a finite number of power buses and control channels available on a commercial aircraft. For example, the A380 is fitted with 3 ac supply buses for the wing actuation systems so fitting an EMA with a fault tolerant drive of 4 or more lanes would result in significant penalties for the additional supply generation, cabling and also for the control computer signalling. In the same way, fault tolerant generators and fuel pumps with high lane numbers such as that proposed in [23] & [31] will require either a corresponding number of supply buses or a method of coupling all lanes to buses which does not compromise fault tolerance of the motor/ generator or multiple supply buses following a single failure.

While the conclusions of chapter 3 suggest the multiple single-phase '*2+1*' drive to offer a good compromise between size and complexity, the larger dual three-phase '*3+3'* drive may also appear attractive to system designers where two power supplies and control signals are preferable to three. It can be concluded that there is no optimum fault tolerant drive configuration for an actuator, and a topology must be selected on a case-by-case basis.

It is however, insufficient to consider fault tolerant drives purely from a topological perspective, particularly as the fault trees presented here are somewhat simplified. A more in-depth review of the internal architectures is required to ensure such drives can become a viable reality within an EMA.

4.1.3 Sensing the motor shaft angle in a fault tolerant drive

With high performance drives a method to determine the rotor commutation angle is required for optimum performance. Commutation angle can be determined without a physical angle sensor, i.e. 'sensorless', by a variety of techniques monitoring the motor commutation current or voltage [70,71,72]. Such a technique was successfully employed by Green *et al.* on a fault tolerant fuel pump [32]. Unfortunately sensorless commutation has limitations at standstill or low-speeds and is therefore not suited to actuator applications which typically require rated torque at all speeds.

Where a physical commutation angle sensor is a requirement, conventionally an encoder, resolver or hall-effect sensor array is mounted on the stator to measure the rotor angle. In fault tolerant applications with multiple lanes controlling one motor, a single sensor shared between lanes would be a common point of failure and would also compromise isolation boundaries. In addition, conventional sensors will only operate from a single power supply or excitation source and therefore must be electrically allocated to a specific lane.

The logical solution is to use multiple position sensors, each allocated to a different control lane. It is possible to manufacture position sensors with multiple transducers in a single housing and sharing a common shaft, although the designer will have to carefully consider the mechanical reliability as any single points of failure will compromise the fault tolerance.

4.1.4 Position control of an electromechanical actuator

Actuators will generally operate under position control – the pilot demands a position and the actuator follows.

Rather than routing all communications links between the cockpit and the actuator, localised control computers can act as intermediate stages, grouping signals from multiple actuators. An example of this can be seen in the Boeing 777 flight controls [66], where a bank of 4 'Actuator Control Electronic' (ACE) units receive pilot lever commands as analogue inputs and remotely control the hydraulic servo actuators. This approach reduces cabling and allows a surface to be controlled by actuators operating from multiple ACEs for fault tolerance. The ACEs also provide a digital bus link to the primary flight computers for automated monitoring and autopilot commands.

Conventional position control typically consists of a set of nested current, speed and position 'loops' as shown in Figure 4-7. In the 777 and many other hydraulic servo systems the position loop is contained within the ACE, with analogue signals to the servo valves to move the actuators and position feedback sensors. This allows the ACE to monitor 'first hand' the position of the actuator and detect any errors; however, with improvements in processing technology it is viable to contain all control loops within EHAs and EMAs. By modularising the control in this manner, the data transmission between the ACE and the actuator is reduced, with position demand signals requiring a relatively low bandwidth and return data only required to relay status information. One area of concern is detecting position sensor failures and this must be performed either by cross comparison of data between actuators or between lanes in a fault tolerant actuator, otherwise additional, dedicated, position sensors will be required for the ACE to oversee operation. This modularised system is the most elegant; however, it must be noted that an actuator with a fault tolerant drive will require a position controller within each lane in order to maintain true redundancy and each lane will require a connection to an ACE.

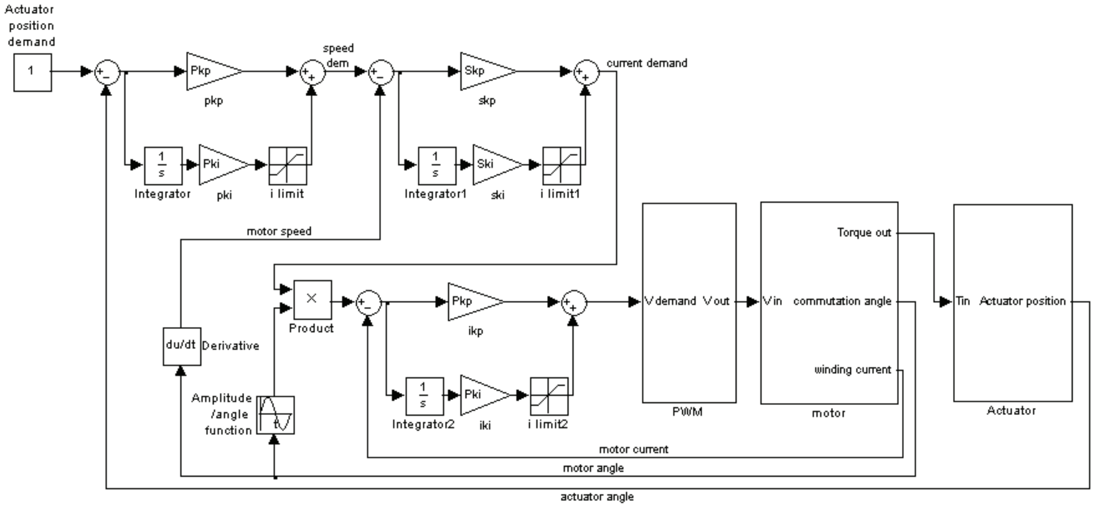

Figure 4-7: Example of nested position, speed and torque control loops in an actuator.

When considering a method for position sensing in an EMA, the motor drive electronics will already sense the motor commutation angle and this could be considered for calculating the actuator position. Despite EMAs featuring ball/roller screws mechanisms and gearboxes, output position can be predicted by accumulating motor revolutions, dividing by the effective gearing ratio and if the output is non-linear, multiplying by a function *f:p* (which could be in the form of a look-up-table):

$$Actuator\_position = f : p \times \sum\left[(\Delta motor\_angle)/gear\_ratio\right] \tag{4-1}$$

With a fault tolerant drive featuring multiple commutation sensors, this method will provide a position feedback signal for each lane; however, there are potential issues:

- Any movement of the actuator without power, or any spurious loss of power forcing a reset of the processing electronics, will result in a variation between the accumulated position and the actual actuator angle.
- Where a clutch mechanism is required to decouple the motor from the actuator, it will also disconnect the commutation sensor from the actuator.

- Any position calculated from the motor can not take into account backlash, skew or breakage between the motor output and the actuator output.

It is therefore necessary to employ dedicated output position sensors on many electric actuators and where a fault tolerant drive is employed, multiple position sensors distributed between lanes to avoid single-point failures, exactly as with commutation angle sensors.

4.1.5 Communications and voting within a fault tolerant drive

Communication is required to provide demands and return status information from actuators. It can also be used between control lanes in a fault tolerant system for synchronisation and to identify and overcome failures.

A two-way communications link can be lost via the physical connection or failure of a connected device at either end. When more than two devices share a connection, measures must be taken to accommodate one device short-circuiting or spreading erroneous data onto the link, or in the worst-case, transferring a high-voltage failure to other connected devices. For these reasons, a fault-tolerant system will require individual connections between a control computer and each power electronic lane. Similarly, where links between lanes are required, discrete links are required between every lane. Galvanic isolation may also be required at some stage within the lanes.

The primary flight computers (PFC) of the 777 provide an example of a fault-tolerant, isolated communications arrangement (Figure 4-8).

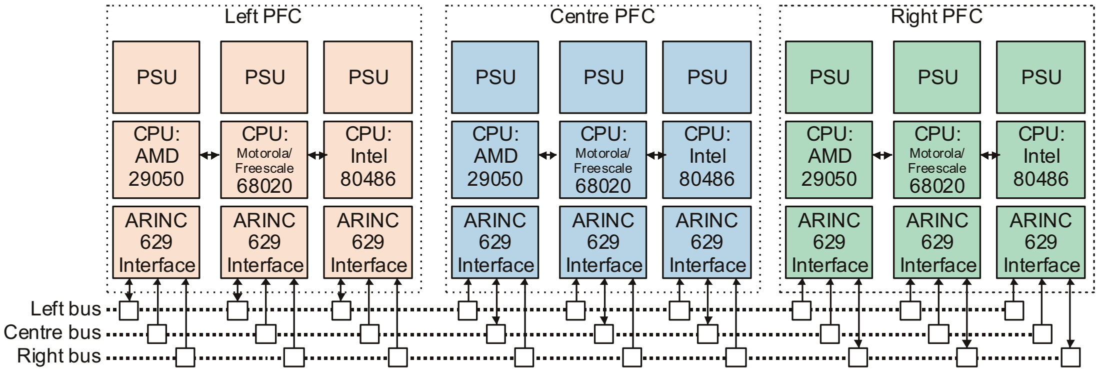

Figure 4-8: Boeing 777 'Triple-triple' primary flight control computers [66].

There are three PFCs, each containing a further three internal processing elements. Three ARINC 629 serial buses distribute flight control data across the aircraft and the PFCs interface to this bus using 'current-mode' couplers, providing galvanic isolation. Although a PFC can read from every bus, transmission is only possible to one assigned bus, preventing corruption of multiple buses with erroneous data.

Each PFC contains three processors for three-way voting on parameters. Each processor is from a different manufacturer, running alternative versions of the same program. This concept of non-identical software was proposed by Chen and Avizienis in 1978 [73] as ‘n-version programming’, offering an improvement over the identical multi-lane control already used in space shuttles [67]. Multiple instances of the same algorithm are programmed by completely independent teams of programmers, with no interaction. This reduces the possibility of common software faults. In the 777 this concept is extended to non-identical processing elements to eliminate common faults in the processors and compilers. Faults are identified and overcome by majority voting of variables at stages of the software execution.

The transferral of data between control lanes for voting is a common method of detecting errors and filtering anomalies and in the case of a fault-tolerant EMA there are three main areas where data can be shared:

- **Input demands:** Each lane can feature a separate communications link to a control computer so, in the event of a communications channel failure, only one lane will lose input demands. Each lane could even be assigned to a different control computer if required. By sharing input demands between lanes, a lane with a failed demand input can obtain demands via another lane and maintain operation, thus adding signal-level fault tolerance.
- **Sensor feedback:** Each lane will have independent motor and actuator sensing. Certain sensors, such as actuator position, should return near-identical data to each lane. By sharing the sensor values across lanes, failed sensors can be detected and values can also be consolidated to find an average, thus reducing noise.
- **Internal parameters:** Each lane may require the operational status of the other lanes in order to control its own output, especially if a change in behaviour is required post-fault (*such as the current reshaping shown in section 3.5*). There may also be requirements for synchronization between lanes.

'Consolidation' is the process of cross-comparing data to find a *true* value and to detect whether a value is a significant deviation from the norm and a potential failure.

An example of a 3-lane system consolidating data is shown in Figure 4-9. The solid lines represent incoming signals I_1, I_2 and I_3 and the dashed lines represent the same signals shared between the modules on inter-module data links. In normal operation the three inputs should be identical, as should the outputs (O_1, O_2 and O_3). In the event of either I_1, I_2 and I_3 deviating from the common value, the median of the remaining two values should generate identical outputs at O_1 , O_2 and O_3, allowing all three lanes to continue operation.

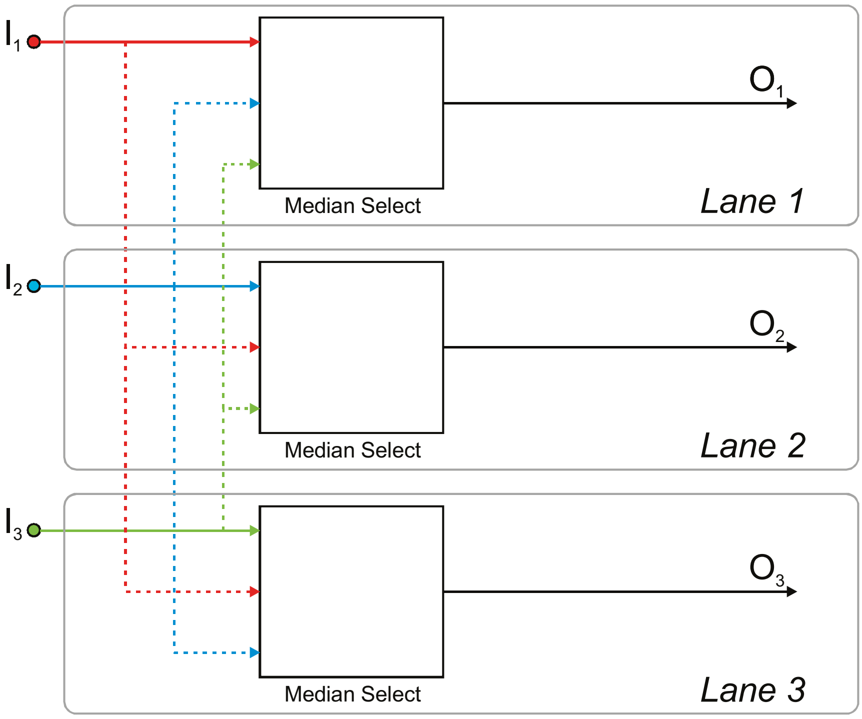

Figure 4-9: Consolidation of 3 values across 3 lanes.

When considering the failure probability of a system, data consolidation effectively provides parallel signals to each lane, adding an extra level of signal fault tolerance. The extensive failure analysis presented by Sadeghi and Lyons [54] encompasses the safety benefits of inter-lane voting in actuators.

Although [67] and [73] employ majority voting and Figure 4-9 lists median selection, there are various voting strategies available and different voting methods must be applied to certain data types.

Included in the voting strategies discussed by Blough *et al*. [74] are:

- **Mean:** The sum of all values, divided by the number of values. Once calculated, this mean value is either taken to be as the true input, or the nearest input value to the mean is selected.
- **Median:** All values are ordered by magnitude and the central value is selected to be the true input. For cases where there are an even number of values the mean is taken from the central two values.
- **Majority:** A value is taken to be correct if it occurs in more than 50% of cases.
- **Plurality:** The value occurring the most often over a time period is selected.

Although a plurality voter can be shown to be very accurate at determining the true value, data must be collected by multiple samples over a period of time and occur repeatedly. Electric drives process data with fixed-frequency control loops and data may change on each iteration of these loops, so unless the cross-comparison data is transmitted at a far higher bandwidth than the loops, repeat data will never occur frequently and a plurality voter will be of little use.

It is also possible to incorporate 'weighting' into the voting schemes, in which values are assigned a weight related to their likelihood of being correct. This may produce more accurate results in certain instances; however, for fast changing signals over a large range of numbers, pre-assigning a weight to particular values may be impossible or introduce extra processing complexity.

For voting of measurement signals with a level of noise, such as analogue feedback sensing, 'inexact voting', the majority voter will almost certainly fail as there is a very high probability that all the sampled values will be slightly different. Median and mean are the most applicable voters in this case. Table 4-1 shows an example of three typical analogue signals and how mean, median and majority will interpret the consolidated value.

Input A	Input B	Input C	Mean	Median	Majority
92.7	88.9	0	60.53	88.9	-

Table 4-1: Example of an inexact voter, e.g. for an analogue feedback signal.

Input C shows a zero value to represent failure of a sensor. This zero value causes a large drift in the mean, whereas the median effectively disregards the failed sensor. The majority cannot generate a result as no input occurs more than the others.

Table 4-2 shows an example of three demand signals, sent from a control computer to three lanes of a drive – ‘exact voting’. Each lane will normally receive identical demands, but in this case input C is faulted (a disconnection, resulting in zero data).

Data A	Data B	Data C	Mean	Median	Majority
92	92	0	61.3	92	92

Table 4-2: Example of an exact voter e.g. for a digital demand signal.

Taking the mean would again allow one erroneous signal to corrupt the true value, whereas the median and majority voters allow the correct value to propagate. For exact signals, the majority voter can actually prove advantageous, according to studies performed by Latif-Shabgahi et al. [75], as in the case of multiple signal errors a ‘no result’ will be returned, whereas the median will return an incorrect result. From implementing voters in drive software, the author has also noted that with no requirement for data-reordering or comparing, a majority voter can produce a result with less computational complexity than a median voter, particularly in cases involving simple Boolean data.

In the case of erroneous data, there are many schemes, including those suggested in [75], [76] to obtain correct data; however, like the plurality voter, repeated transmission of data is required to construct trends to ‘smooth’ out errors and this is not always applicable to dynamic systems such as those within EMAs.

With selection of the appropriate scheme for a particular data type, the median or majority voters will be adequate for comparison of data between lanes in a fault tolerant drive EMA.

4.1.6 Detection of signal and controller faults using voters

When voting between lanes in a controller, a signal demonstrating a repeated deviation from the calculated ‘true’ value can be deemed as faulty. A method of calculating this is to use threshold values and error counters. This process requires two inputs of the voter to agree, in order to determine the ‘true’ value and highlight the faulted input, so three or more inputs are required. If a fault tolerant system features only two lanes, the two-way data can only be compared to detect a disagreement, and the voter can not be used to overcome a signal error.

A control lane can identify itself as faulty using built-in hardware testing, or by identifying its own data as faulty after cross-comparing with the other control lanes.

A controller lane falsely declaring itself faulted and shutting down is undesirable, but provided the probability is low, may will be permissible as a fault tolerant system can still function afterwards using the remaining lanes.

A lane can highlight another lane as faulty if the data presented for consolidation appears out of tolerance, or missing. Figure 4-10 shows this process in a 3 lane system. Data is compared via cross-monitoring and from this, each lane can decide if itself and the other lanes are healthy and transmit an enable signal. The supply contactor on each lane requires a minimum of two enables to activate a lane.

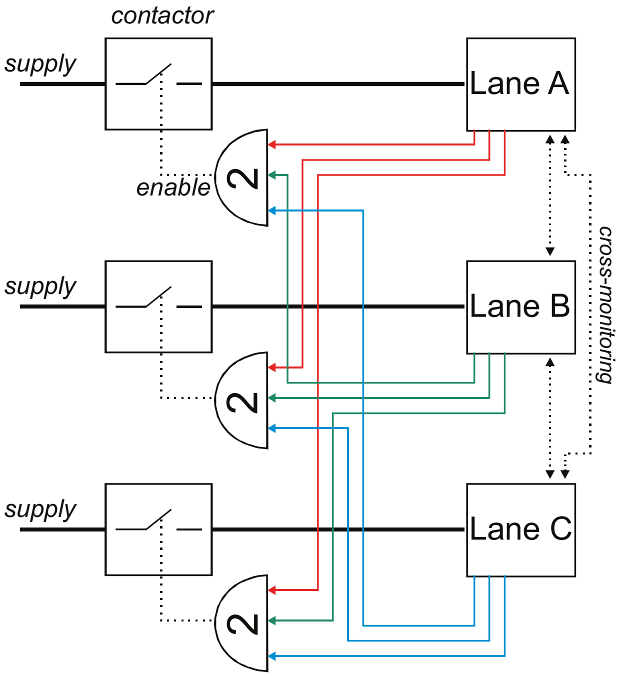

Figure 4-10: Shutdown mechanism for 3 lanes.

In a system with 2 lanes, the scheme is reduced to that of Figure 4-11.

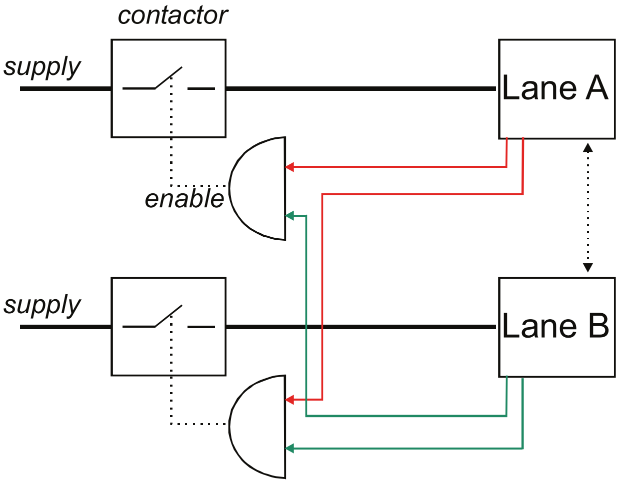

Figure 4-11: Shutdown mechanism for 2 lanes.

Table 4-3 presents the possible shutdown logic for a healthy lane A and a faulty lane B. It is assumed that in certain cases lane A has successfully detected a fault in lane B and in other cases lane B has self-detected a fault.

		A self-enable	**A enable from B**	**B self-enable**	**B enable from A**		**A Supply (AND)**	**B Supply (AND)**
1	All ok	1	1	1	1		**ON**	**ON**
2	B fault, detected only by A	1	1	1	0		**ON**	**OFF**
3	B fault, detected only by B	1	1	0	1		**ON**	**OFF**
4	B fault, detected by A and B	1	1	0	0		**ON**	**OFF**
5	B enable out fault	1	0	1	1		**OFF**	**ON**
6	B dual fault, detected only by A	1	0	1	0		**OFF**	**OFF**
7	B dual fault, detected only by B	1	0	0	1		**OFF**	**OFF**
8	B fault, detected by A and B	1	0	0	0		**OFF**	**OFF**

Table 4-3: Shutdown logic in a 2 lane system with faults on lane B.

Rows 1 to 4 show that B is correctly shut down and lane A continues to operate in all cases where a fault is detected and a correct enable signal is transmitted from the faulty lane.

Rows 5 to 8 can be considered to represent a faulted enable signal from lane B to lane A. In row 5, as lane B is otherwise unfaulted, the system continues operation on lane B and lane A is incorrectly shutdown, which although not ideal, will maintain operation.

In rows 6 to 8, the combination of a faulted enable out signal and a detected controller fault in lane B results in a total shutdown. Although these could be considered double-fault conditions (where shutdown is acceptable), the designer would have to ensure that no single controller fault in lane B will disable B and incorrectly remove the enable signal to lane A. This may prove difficult as even the most simple fault - loss of power to B, could result in such a condition.

Some of the deadlock/disagreement limitations of two-lane systems can be overcome by adding additional monitoring to effectively increase the parameters to vote on. One solution is to use observer schemes, which run within each lane and contain software models of a healthy system and where signals and performance deviate from the ideal model, errors can be deduced. Model-based schemes are used in electric power-assist steering systems [77,78] as a fail-safe shutdown mode is essential in event of electric drive failure. Observer schemes can allow detection of faults which are not covered by conventional self-monitoring of cross-comparison of sensor values – for example a slipping of a commutation sensor could result in a lane outputting negative torque and if commutation angles are not cross-compared due to bandwidth limitations, an observer scheme in each lane could declare a fault from the resulting performance variation.

4.1.7 Implementation considerations for cross-communications

In a conventional electric drive the motor commutation code (or 'current loop') is operated at the highest iteration rate (usually 10's of kHz), while the speed and position loops are operated at a significantly slower rate. The iteration rates are normally determined by motor specifications and performance bandwidth requirements. A fault tolerant system can follow the conventional arrangement but with the additional task of data consolidation between lanes.

Data consolidation requires a physical data connection between modules and the required consolidation rate will determine the transfer rate of this connection. Cost and complexity will impose restrictions on the number of wired connections between lanes and the transmission speeds, particularly if galvanic isolation is required.

Figure 4-12 shows the data that could be compared between nested control loops within two lanes of an EHA. Data for consolidation is transmitted and processed at the rate of the associated control loop, so performing all consolidation at the rate of the position controller will require the lowest bandwidth.

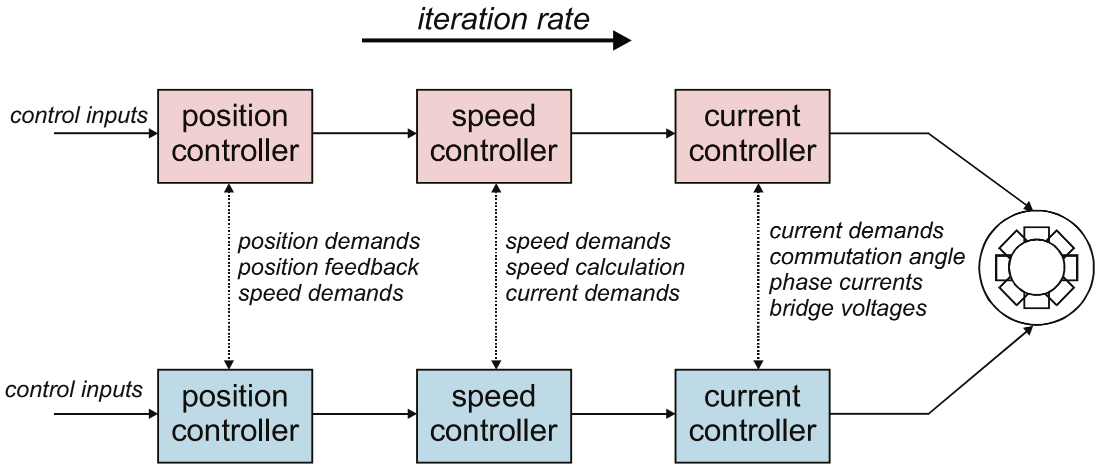

Figure 4-12: Cross-comparison of signals between control loops.

Ideally only position controller data comparisons will be required to ensure both lanes are moving with the same demand and that position feedback sensors are in agreement. If both position controllers have identical demands and feedback then the speed control loops should receive identical demands in both lanes. Similarly, as both lanes share a common motor with a common rotor, the commutation sensors should derive identical speed signals in both lanes.

With both lanes powering independent sets of motor windings, there should be no requirement to share phase currents, voltages or commutation angles. In reality the operation is considerably more complex, and findings are discussed in detail in section 7.3.

Safety requirements for an actuator may also determine the rate at which data must be consolidated in order to detect a serious fault. For example, the DEAWS system designer must consider the fastest possible uncontrolled flap movement and ensure the fault consolidation software can react quick enough to respond within the allowed 1% of uncontrolled movement allowance (*see section 2.2.2*). System specifications may also have tolerances for performance glitches due to fault handling and recovery which will determine the required response rate of the associated control loops.

The discussion in this section has focused on EMAs in which all lanes are active simultaneously when the system is operating unfaulted. If, for example, a dual-lane system is designed to run in ‘active-standby’ then data consolidation will not be required for synchronisation between lanes, although cross-communication may still be required to detect errors in control signals, sensors and the active controller.

4.2 THE DEAWS SYSTEM

To attain the specified requirements for the DEAWS system (*section 2.1*), a series of trade studies were performed by BAE Systems. The trade studies were combined with studies from the author at Newcastle University (*chapter 3*) to produce a design topology. The control system within the actuator is designed with the guidance of BAE Systems, Rochester. This section presents an independent review of the considered and selected topology.

4.2.1 Selecting the topology

In the trade studies all feasible topologies were considered for an actuator applicable to a flap or slat surface, with component count, cost and reliability compared. For simplification of development, the system is designed to interface with a rotary flap/slat mechanism such as that of the A380. The rotary mechanism is based around two gearboxes on either side of the surface rotating an arm to extend or retract the surface and is shown in APPENDIX B (*pp.210*).

Due to the high torque requirements on the input to the gearboxes, it was also determined that the DEAWS actuator would include an additional gearbox on the output of the motor.

From a safety perspective the operation of a flap or slat system is significantly different to other control surfaces in that operation is not critical to the aircraft remaining airborne. From section 2.1.2 the specified probability for a failure-to-operate is $<10^{-5}$ per flight hour, whereas for control surfaces critical to flight, failure probabilities would be 10^{-9} or lower. Calculations in section 4.1.2 suggest this is within the realm of a single EMA (section 4.1.2) although a degree fault tolerance will be required.

A greater safety concern is the ‘uncommanded movement’ probability of 10^{-10} per flight hour. Uncommanded movement involves incorrectly driving the flaps/slats to an unspecified angle, or releasing control as surfaces may not ‘blow back’ to a safe angle and may instead cause the aircraft to roll. Rather than attempt to engineer a sufficiently reliable active system to maintain the surfaces under control with motors, it was deemed more feasible to utilise brakes to lock the system in the event of a serious failure and also to hold the surfaces when at a desired position, since operational duty cycles are relatively short so powering motors throughout the flight is excessive. Frictional 'power-off' brakes will be employed to lock the mechanisms unless a power signal is applied. This also results in a locked system upon complete power supply failure, which is also a fail-safe requirement.

Figure 4-13 shows the approximate safety requirements for sections of the system, with the strictest requirement by far being the probability (λ) of 1×10^{-10} per flight hour for the brakes to fail to hold the surface.

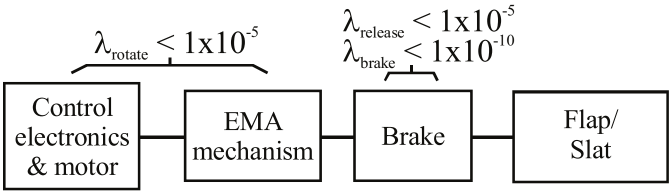

Figure 4-13: Allowable EMA failure probabilities for a DEAWS 'fail-freeze' surface.

Topologies were considered featuring a flap/slat surface driven from actuators on both sides and also from one side, using a shaft. Figure 4-14 shows a simplified example of shafted and an unshafted arrangements. For this and similar figures, '**p**' represents a position transducer, '**b**' represents a brake, '**m**' represents a motor, '**g**' represents the DEAWS gearbox and '**MCU**' represents a power electronic 'motor control unit'. The existing flap/slat gearing and mechanism are shown in red.

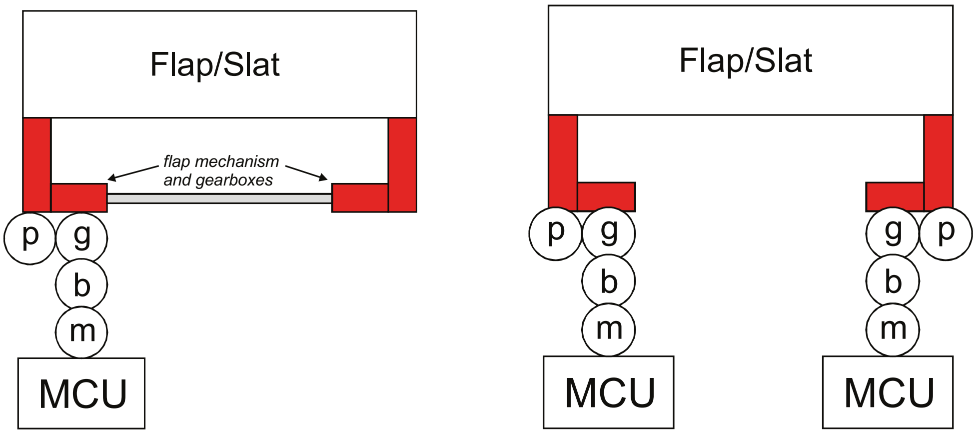

Figure 4-14: Diagram of shafted (l) and unshafted flap/slat actuation (r).

It was decided that placing the brakes on the motor output was preferable due to the smaller torques upstream of the gearboxes; however, this places additional safety requirements on the gearbox to hold the flap/slat after the brakes are applied post-fault. Eliminating the shaft between both sides of the surface offers a weight reduction, although this is nullified if adding a second motor drive arrangement makes the system heavier.

A conventional flap arrangement (*see section 2.1*) uses torque limiters to prevent a shaft breaking in the event of a jam. The shafted DEAWS arrangement could potentially snap a shaft if the undriven side becomes jammed so a broken or overloaded shaft could be detected by strain gauges and position transducers; however, debate remains as to what action would be deemed acceptable in the event of a breakage. It may be possible to hold an entire flap/slat from the actuator mechanism on one side, although this is unclear from initial data provided for the project. The alternative is to combine a brake into the undriven side to hold in the event of a shaft break; however, as it is downstream of the motor gearbox this brake will be far greater in size.

The unshafted arrangement has the issue of an undetected electronic failure driving the flap/slat sides unevenly, causing a skew or even surface damage.

Ultimately trade studies determined that the complexity of the additional motor and electronics for the unshafted arrangement resulted in a heavier and more expensive system and was therefore not desirable.

In both arrangements it must be noted that multiple position sensors would be required on each side of the flap/slat surface, otherwise the system cannot discern between a mechanism fault and a broken sensor.

Additional studies were conducted into topologies involving the sharing of electronics between adjacent flaps/slats. A basic diagram is shown in Figure 4-15. The sharing arrangement effectively provides a second MCU to oversee the actions of the surface-driving MCU and apply the brakes if any anomalies occur.

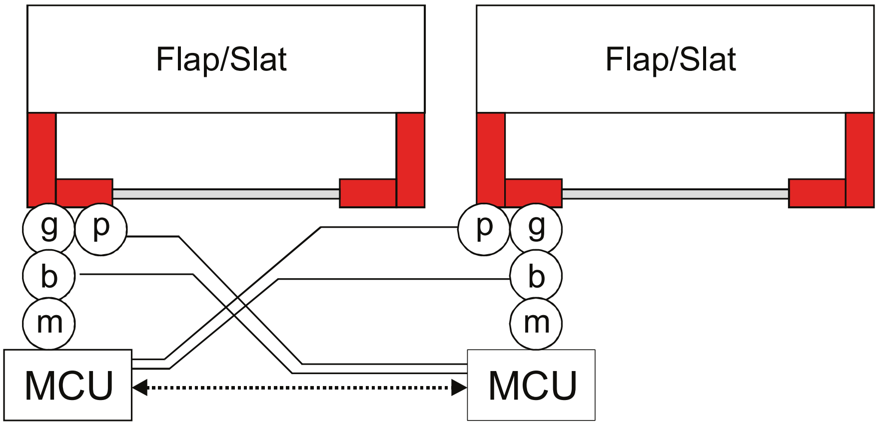

Figure 4-15: Sharing arrangement between flap/slat actuators.

The sharing arrangement shown cannot operate after a fault as the second MCU has no motor driving capability. To add fault-tolerance, multiple MCUs and motors (or fault-tolerant motors) will be needed on each flap/slat and doing so will add extra position monitoring and brake control, nullifying the benefits of sharing information between adjacent flap/slats. With a preference towards a shafted arrangement and fully independent electronics on each surface, a series of schemes for driving from one shaft were considered with two basic arrangements shown in Figure 4-16.

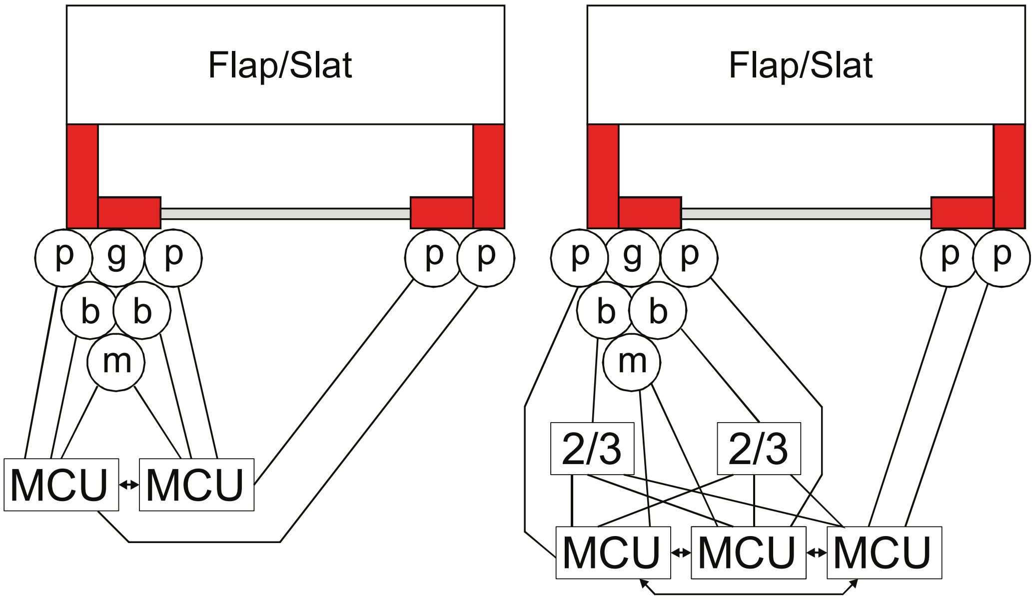

Figure 4-16: Duplex (left) and triplex (right) flap/slat control.

In addition to maintaining multiple position transducers on each side, the two example schemes consider dual brakes a necessity for guaranteed safe shutdown. The second scheme in Figure 4-16 considers a third motor control unit, which although not required to operate the motor, is present for additional monitoring of signals and voting on parameters. The '3/2' brake controller units will perform a vote on three incoming signals to determine whether to release a brake.

To fully assess the suitability of the schemes for DEAWS, failure analysis calculations must be performed. Although detailed 'failure mode effects and analysis' was performed by BAE systems, an alternative, generalised overview is presented here by the author.

To meet the failure to operate condition, a fault tree of a single DEAWS actuator can be constructed to highlight the areas dictating the reliability.

Attempting to accurately assess the reliability of an EMA from second-hand data is near-impossible due to variations in collected data, the inability to verify the initial sources and ideally requiring a breakdown of all the different failure modes for components; however, in Table 4-4 the data obtained for the EMA calculations in section 4.1.2 is shown alongside proprietary data used by BAE Systems for the DEAWS trade studies. DEAWS data is used for position sensors and brakes as these are project specific.

	DEAWS	Sadeghi [54]	Tavner [58]	Pieters [68]	Lemor [69]
control signals	4.50×10^{-5}	1.30×10^{-5}			
power supply	1.20×10^{-5}	5.40×10^{-5}			
electronic controller	2.80×10^{-5}	8.55×10^{-5}			
motor windings	3.90×10^{-6}		9.48×10^{-8}	1.38×10^{-8}	
motor bearings (jam)	1.10×10^{-6}		3.00×10^{-6}	6.55×10^{-7}	
motor (total)	5.00×10^{-6}	1.20×10^{-5}	3.16×10^{-6}	6.9×10^{-7}	
motor gearbox	5.70×10^{-7}			6.55×10^{-6}	
actuator mechanism	1.10×10^{-6}				1.45×10^{-6}
position sensors	2.0×10^{-6}				
brake jam on	2.8×10^{-6}				
brake disconnect	2.4×10^{-6}				

Table 4-4: Failure probabilities (per flight hour) for EMA components from various sources.

Most data is of similar orders of magnitude, although the DEAWS actuator mechanism data is for a rotary system, consisting of a pair of gearboxes, whereas the data used earlier in this thesis is based on a roller screw. The DEAWS motor bearing failure is a probability of a rotor jam, rather than a specific bearing failure.

The fault tree shown in Figure 4-17 is constructed for a single EMA operating the flap system, featuring a single electric drive, motor and actuator system. There are two position sensors represented in one block - one for commutation and one for flap angle feedback. Failure modes resulting in loss of output are shown. The DEAWS data is used in this calculation, although the alternative values of Table 4-4 will produce similar results and allow the same conclusions to be drawn.

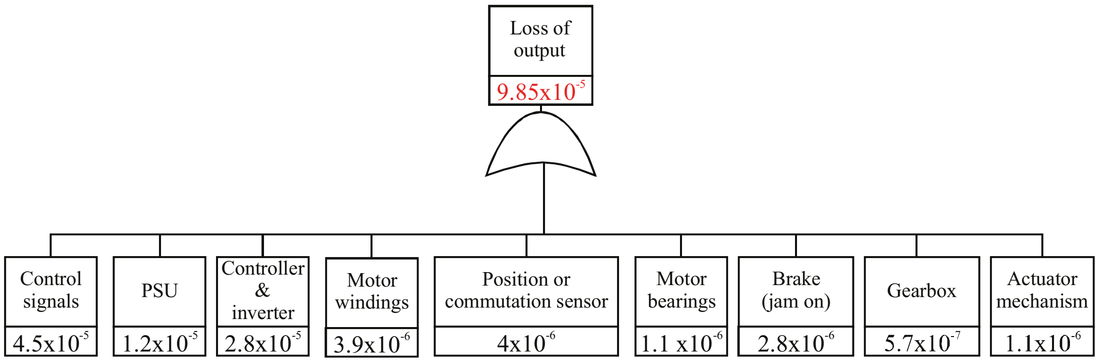

Figure 4-17: Fault tree for loss of output from a simplex DEAWS actuator.

The probability of loss of output is notably in excess of the 1×10^{-5} per flight hour required for the system. With the motor and electric controller components having the higher failure probabilities, the tree can be recalculated to include a dual-lane fault tolerant motor (Figure 4-18).

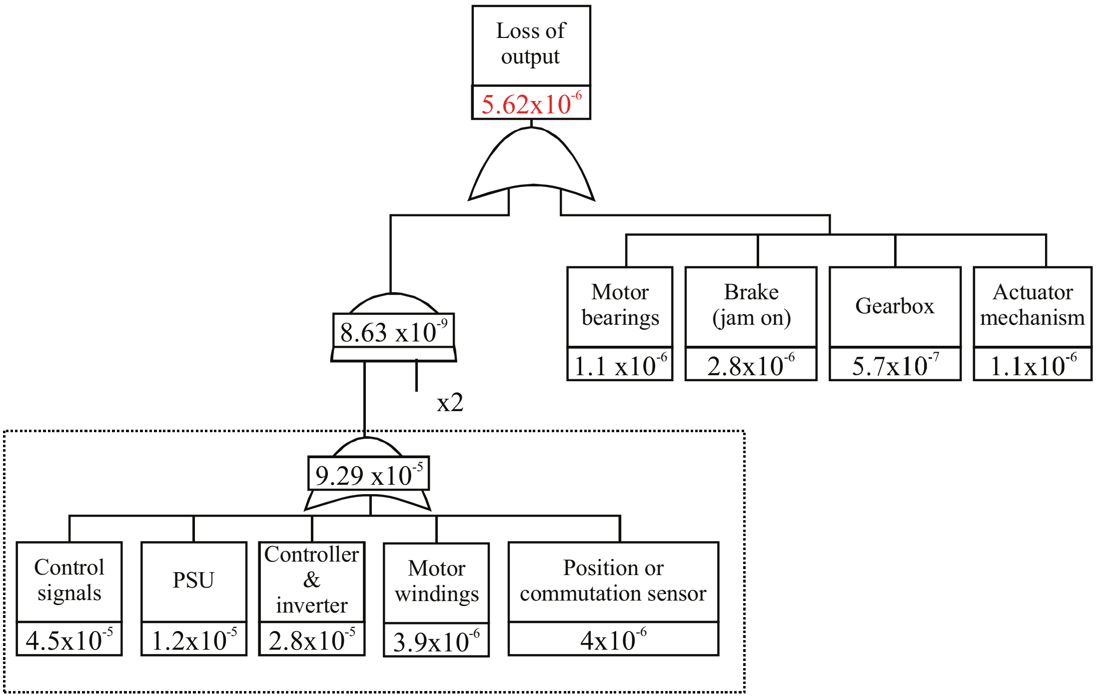

Figure 4-18: Fault tree for loss of output from a DEAWS actuator with a 2-lane motor.

The failure probability of the system is reduced below the 1×10^{-5} requirement with the duplex motor, to the point where the motor bearings and actuator components become the dominating factor. Although a more detailed fault-tree system was performed by BAE systems, this tree shows that a dual-lane EMA should be sufficient to attain the loss of operation safety requirement for a flap/slat system.

The ‘loss of control’ condition must also be considered and the dual-lane fault tree can be reconstructed with component failures that may lead to this event (Figure 4-19). To maintain control, only the brakes are required to function – the motor is not a factor, although the controller electronics are required to interface to the brakes and position sensors. Relevant failure probabilities are provided from the trade studies for brake and actuator failure modes, although these are not orders-of-magnitude away from values used in the previous fault trees.

The tree shows that the system falls short of the 1×10^{-10} failure probability target and it is the dual-lane power electronics and the actuator/brake mechanical sections which are restricting the reliability.

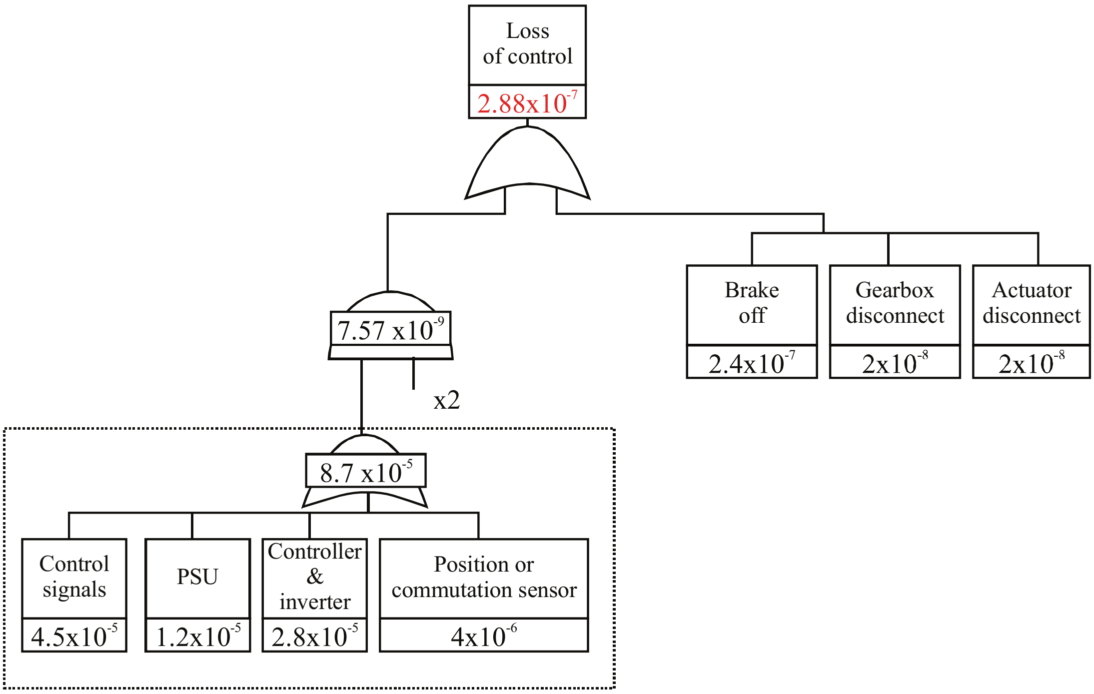

Figure 4-19: Fault tree for loss of control from a DEAWS actuator with a 2-lane motor.

As the flap system is driven from both sides, it is possible to separate the actuator mechanism into two identical halves, effectively adding two sets of brakes, gearbox and actuator mechanics. Although both halves will operate in unison from a single controller, two load paths would be provided for holding in the event of a mechanical failure. The dual-lane motor can be extended to a three-lane motor to provide a third set of control electronics and position sensor interfaces.

The resulting failure-tree can be seen in Figure 4-20. Although the tree is far simplified from the analysis performed in the trade studies, the system is significantly below the 1×10^{-10} failure probability. It can be summarised that although a two-lane fault-tolerant motor is sufficient for operation, to maintain safety a third set of control electronics are required for additional monitoring and brake control (although these do not need to interface to a motor and the motor is not required to operate after two failures). Having a third electronic system allows voting on parameters, eliminating 2-way ‘deadlocks’ and allowing additional levels of signal fault tolerance (*see section 4.1.5*). The equivalent of a parallel-actuator arrangement is also required, although as this is required to hold the system when failed, there is no requirement to overcome the jam in one actuator mechanism.

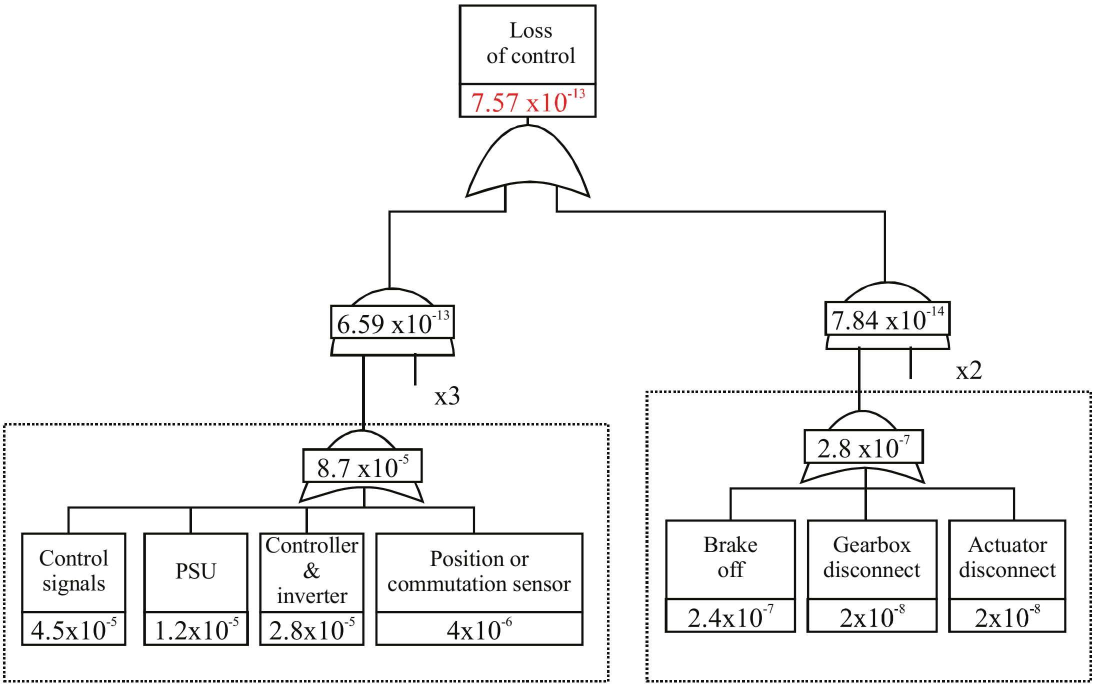

Figure 4-20: Fault tree for loss of control with two load paths and a 3-lane motor drive.

With motor operation only required following one fault, all of the fault tolerant drive topologies described in chapter 3 should be suitable for DEAWS. However, with the requirement for a third lane for voting and monitoring, a motor with three lanes must be selected, or a two lane motor with an additional monitoring lane.

The topology selected with the industrial partners is shown in Figure 4-21.

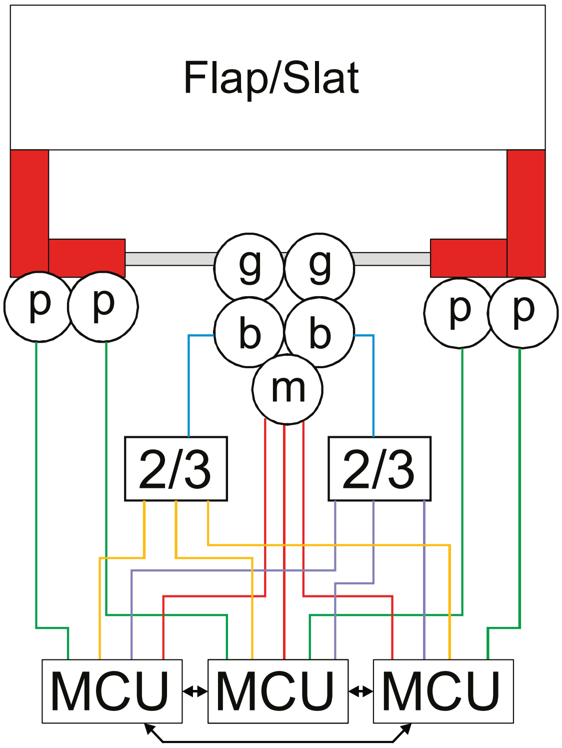

Figure 4-21: The selected DEAWS triplex topology.

The brake voting is simplified for clarity, although each brake essentially requires two out of three signals in order to release.

A 3-module fault-tolerant motor consisting of 3 single phase windings (*2+1*) was selected over a motor consisting of 3 three-phase windings (*2×3+3*) due to the significantly lower component count.

It was also decided not to use a dual three-phase *3+3* drive as the studies of chapter 3 showed this to have considerable size penalty against the *2+1* machine.

The three lanes of power electronics and motor windings are shown in Figure 4-22. Each lane features a communications link to the flap control computer and there is a pair of bi-directional links between every lane to consolidate data.

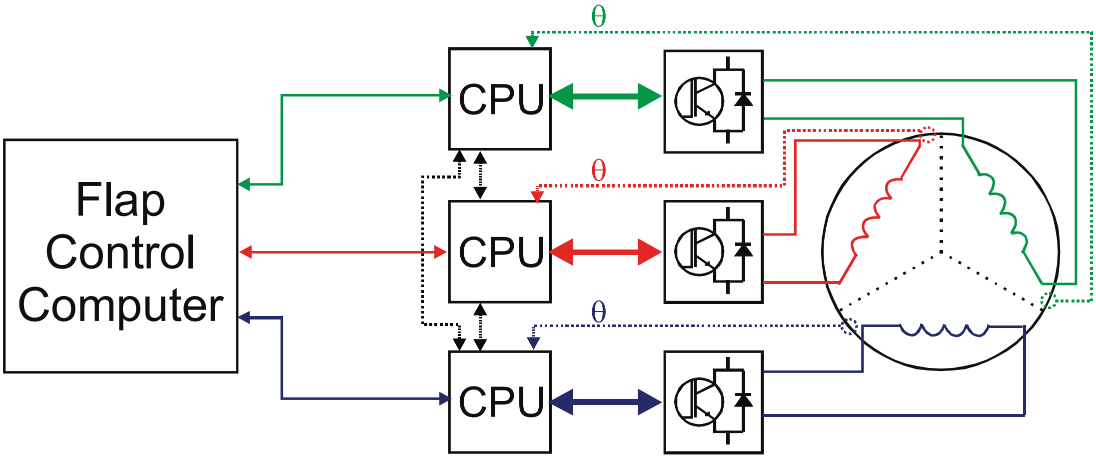

Figure 4-22: Fault-tolerant Power electronic drive arrangement.

A major conclusion from the trade studies is that the DEAWS system is not a cost-effective solution for the slat system. This is due to the large number of slat surfaces on the target aircraft, requiring a large quantity of actuators with a weight and complexity far in excess of the existing arrangement. As a result later research focused only on a flap actuator.

4.2.2 The actuator control scheme

The triplex electric drive arrangement described in section 4.3.1 and the existing mechanism for the A320 were used as a basis for the design of the DEAWS actuator. Between all the partners companies on the project, a design for an actuator was formed (Figure 4-23).

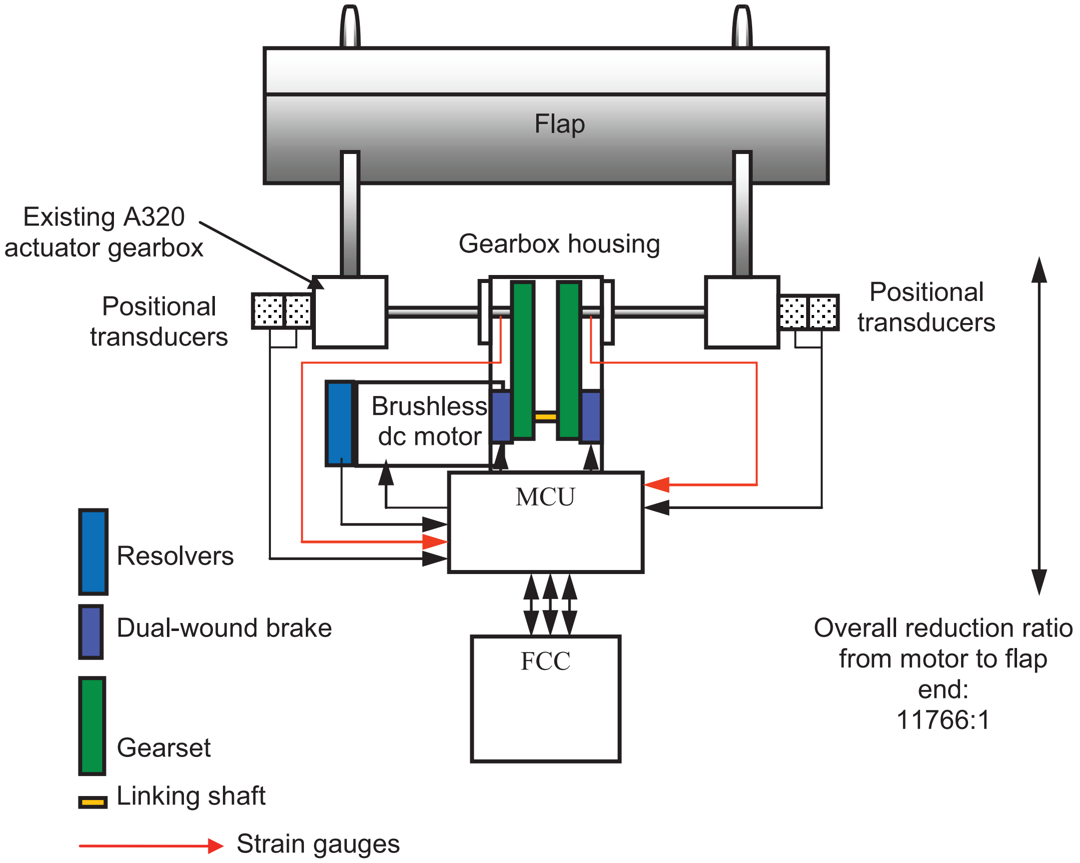

Figure 4-23: A single DEAWS actuator.

The main components of the actuator are:

- **An existing A320 rotary actuator mechanism with 318:1 gearbox.** DEAWS is designed to interface to an existing rotary mechanism (*see APPENDIX B*).
- **A triplex motor control unit (MCU),** containing three lanes of power electronics, as shown earlier in Figure 4-22.
- **A brushless dc, 3× single phase fault-tolerant motor.** A *2+1* arrangement.
- **Multiple resolvers.** A set of three resolvers to provide motor commutation angle to all 3 lanes.
- **A 2-way gearbox housing**. A pair of 37:1 step-down gearboxes in one housing.
- **Multiple actuator position sensors.** Linear and rotary position transducers on each actuator arm.
- **Torque sensing.** Strain gauges to detect excessive torques and prevent shaft breakages.
- **Brakes**. Dual-wound friction brakes which release on application of 24V dc.

- **Flap control computer (FCC).** A computer representing a three-lane flap control computer.

The gearbox contains two gearing sets and can be driven from one motor or two. When a single motor is used, a linking shaft is inserted to join the motor to both gear sets. Although not the selected arrangement for the project, removing the shaft allows the system to represent a dual motor unshafted actuator (similar to Figure 4-14), should future testing require this.

The 37:1 gearbox ratio is combined with the 318:1 actuator gearbox to give an overall 11766:1 ratio between the electric motor and the flap.

The input to the system is ultimately determined from the flap lever in the cockpit. The pilot moves the lever to one of a set of predetermined flap positions, which is then converted by the FCC to an actuator shaft angle and transmitted to each control lane.

The internal control scheme for a single lane is shown in Figure 4-24. This can be implemented in a variety of formats, including a processor, FPGA or even discrete digital/analogue circuits.

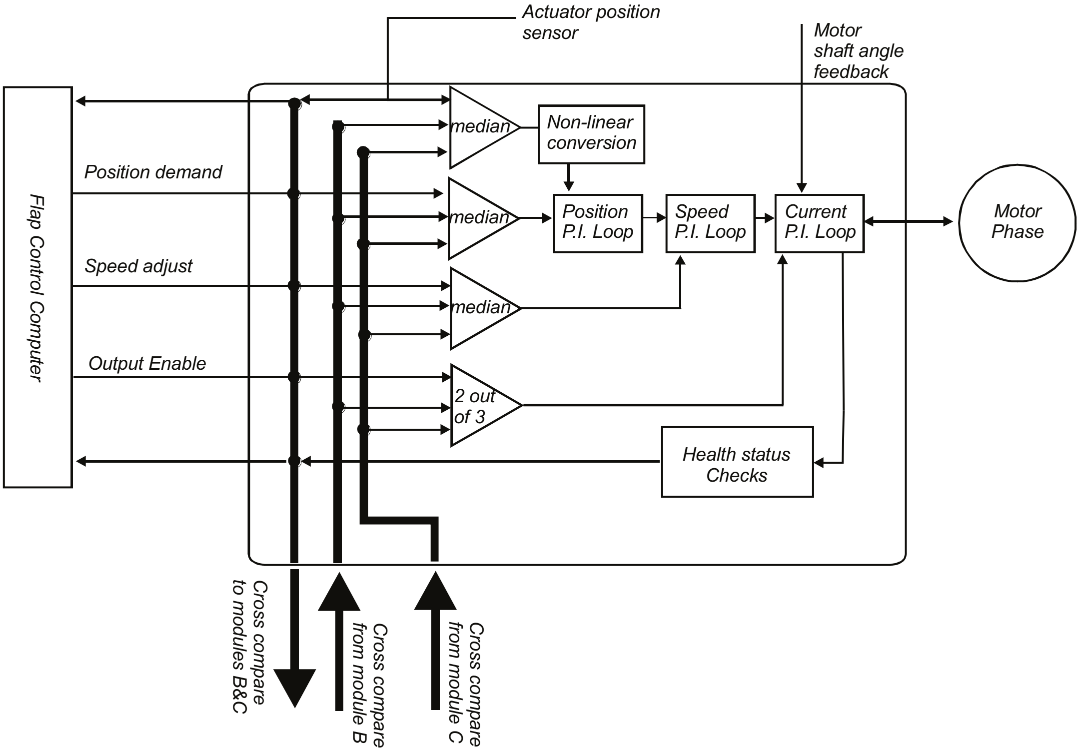

Figure 4-24: DEAWS control scheme within one MCU lane.

The flap angle demand is transmitted to each of the modules by an RS-232 communications link. The repeat rate of the messages is 100Hz, which is also the iteration rate of the position and speed control loops.

The position of the flap is measured by rotary (RVDT) transducers on the two flap gearbox outputs and linear (LVDT) transducers on the flap arms. The four transducers are fed back and distributed amongst the three lanes, (with lane b receiving two signals). The signals are then consolidated between the modules with look up tables converting the LVDT measurements to rotary angles. Although not illustrated, logic will also be included to detect skew and breakages of the flap mechanism by monitoring position sensors between lanes.

Each lane uses the demanded shaft angle and the consolidated shaft angle as parameters in the position control loop. The position loop outputs a speed demand to the speed loop.

The speed loop controls the motor up to speeds of 10,000r/min, but a speed offset command from the flap computer allows this to be reduced, which is necessary to maintain precise synchronisation between flaps.

The speed loop outputs a current demand for the current controller, which outputs a PWM voltage to the phase winding of the motor. A resolver for each lane provides a motor commutation angle for the current controller.

All the demand data transmitted from the flap control computer is consolidated between the 3 lanes using median select routines to overcome signal errors. Position measurements are returned to the FCC to detect anomalies and allow a remote shutdown via the ‘output enable’ signal.

The returned position measurement data is also used by the FCC to maintain symmetry between flaps. The symmetry controller will limit the speed of a faster flap to ensure movement is in unison and brakes will be applied if asymmetry limits are exceeded.

Each brake is dual-wound to add additional lanes of control and improve reliability. Power is removed in an emergency shutdown and also when the demanded position is reached so that motors need not be energised when the flaps are stationary, which will be for the majority of the flight duration.

4.3 THE ELGEAR NOSE WHEEL STEERING SYSTEM

The ELGEAR NWS prototype was envisaged as requiring a fault-tolerant electric drive from the conceptual stages, driven by the requirement that ‘no single failure of a generator, busbar, power drive electronic of motor will ground the aircraft’ (*see section 2.2.2*). Existing nose wheel steering arrangements are based on a single-lane hydraulic actuator but are capable of switching between power supplies (*section 2.2*).

4.3.1 Selecting the topology

As steering is required when taxiing to and from the runway, loss of steering ability is not critical to safety. At take-off and landing the steering is simply required to follow the (straight) heading of the aircraft. To ensure that no electrical failure points the steering at an undesired angle at landing and take-off, a ‘free to castor’ mode is required. In hydraulic systems ‘free to castor’ is achieved by removing the hydraulic supply. With an electro mechanical actuator, to mitigate for any jam condition the ELGEAR NWS is designed with an integral clutch which must be engaged to couple the electric actuator to the front axle.

So there are effectively two levels of failure to be designed into the system:

- **Failure of one motor drive lane**, resulting in continued operation using the remaining motor drive(s).
- **Failure of the entire system**, resulting in disengaging of the clutch and free to castor.

Figure 4-25 shows a basic EMA fault-tree constructed for the NWS. With information unavailable from the ELGEAR trade studies, the most recent failure probabilities from the EMA studies of section 4.1.2 will be used where possible. It is assumed that due to the torque requirements a gearbox will be required; however, there will be no other gearing or mechanism in the steering as it far simpler than a flap mechanism. The failure probability of the clutch is assumed to be similar to that of the frictional brakes used in DEAWS as both feature friction plates and solenoids.

The resulting probability of loss of steering suggests a very reliable system which even surpasses the requirements for a ‘failure to deploy’ for the DEAWS flap/slat system (a failure requiring an emergency landing – a much more severe outcome than an inability to steer when taxiing).

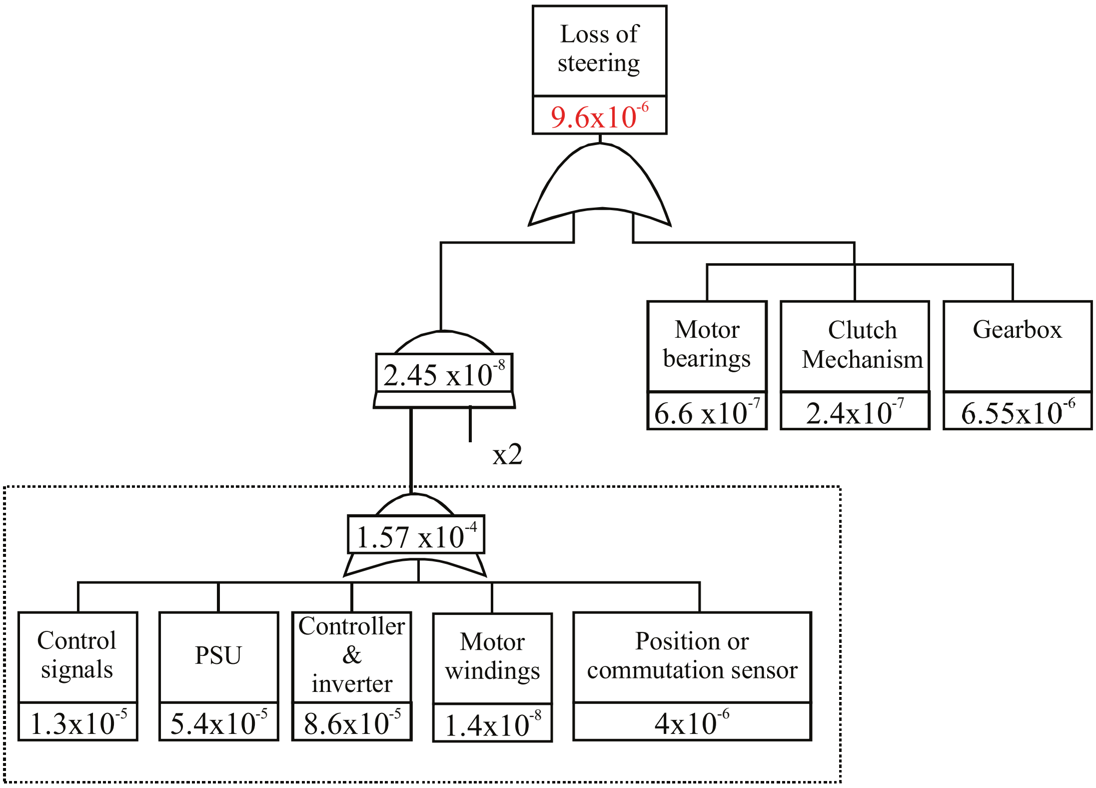

Figure 4-25: Fault tree for NWS loss-of-steering.

The duplex motor configuration can be considered sufficient to tolerate the ‘no single electrical failure’ condition and provides a very high reliability.

Although not specified in the project, the free-to-castor condition could be considered a strict safety requirement as a set of failures resulting in an undesired steering angle when taking off or landing could result in a serious outcome. A dual-solenoid clutch will most likely be required so either lane is capable of driving the system following a fault, although this allows an erroneous lane to drive the system. However, with a clutch that requires power to engage, the system can be remotely disconnected and made safe in the event of a lane disagreement. The cross-monitoring and shutdown scheme for a 2-way system proposed back in Figure 4-11 (*pp.83*) also presents a method to disable the system in any deadlock. It is also necessary for the clutch to be placed downstream of the gearbox so no mechanical failure will prevent free castor.

With a duplex motor sufficient, the only 2-module fault-tolerant motor topology capable of providing torque at all positions when faulted is a dual 3-phase (*3+3*) motor (*see chapter 3*). The main drawback of this topology is that due to half the motor potentially providing a drag torque when faulted, the *3+3* motor has an over-rating factor of 4× (calculated from eqn. 3-26, *pp.57*), a value twice that of the DEAWS *2+1* motor. Another drawback of a 2-lane control topology is the inability to vote on lane failures, with the potential for deadlocks (*see section 4.1.5*).

A fault-tolerant drive topology similar to that of DEAWS could also be applied to the NWS, offering a smaller motor and three-way-voting. The ELGEAR partners decided that the *3+3* topology was preferable due to fewer control electronics and a requirement for only two electric power supplies and communications links. The weight penalty was deemed insignificant in respect to the overall mass of the actuator. It was decided that where a 2-lane system could result in deadlocks, additional communication and feedback signals could be used to increase voting parameters although as shown in Table 4-3 (*pp.84*) provided faults are detected by either lane, a duplex system can remain operational post-fault.

The intended default operation for the actuator is to drive the motor from both motor winding sets simultaneously in order to minimise the current levels and heating. This is known as ‘active-active’ and is the same approach adopted for DEAWS.

The proposed architecture for the NWS system can be seen in Figure 4-26. The *3+3* motor will drive a 596:1 step-down gearbox to rotate the nose wheels clockwise or anti-clockwise. By default the wheels are decoupled from the motor/gearbox by the clutch with a dual-wound control solenoid for operation by either lane. A pair of position transducers on the output shaft provides angle feedback to the two Motor Control Units. The Control and Monitoring computer interfaces to the NWS using the ARINC 429 serial protocol with two transmit and one receive connection to each MCU.

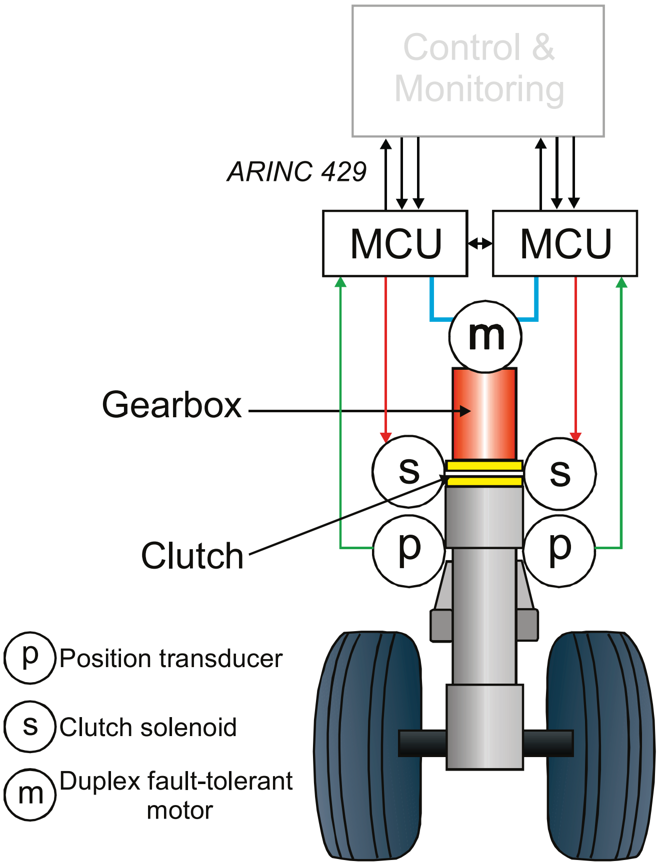

Figure 4-26: Top-level schematic of ELGEAR nose-wheel steering

4.3.2 The actuator control scheme

The control and monitoring computer (C&MS) shown in Figure 4-26 is designed and manufactured by G.E. Aviation and its internal specifications are not detailed in this body of work. It is intended to control all the ELGEAR projects – i.e. the nose-wheel steering, nose wheel extend/retract, main landing gear extend/retract, lock stay actuators and all door locks. Pilot control of the nose wheel steering is from a pair of tiller-inputs in the cockpit, allowing two people to steer the aircraft. The inputs are summed by the C&MS to give a steering angle demand. As the C&MS handles the entire landing gear system, it determines when the steering is available – i.e. the landing gear must be fully deployed and the ground speed within specifications to allow the NWS to operate. The control signals use the high-speed ARINC 429 protocol, a bussed system which multiple ELGEAR projects will share.

Figure 4-27 shows a more detailed description of the fault-tolerant control scheme.

The fault-tolerant *3+3* motor contains a pair of three-phase windings, each capable of providing full rated torque at all speeds. A dual resolver arrangement allocates a commutation angle signal to each MCU lane and a dual thermocouple arrangement allows each lane to detect overheating of its own motor winding set.

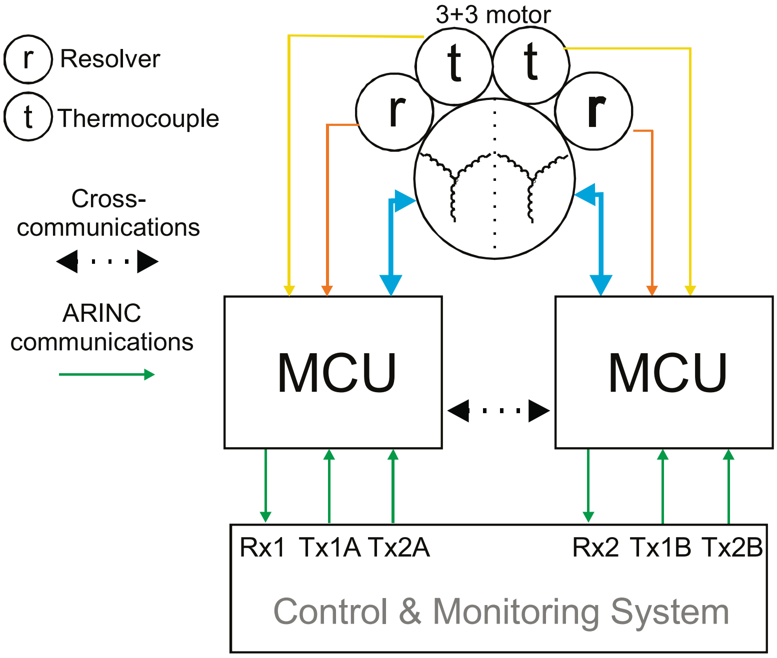

Figure 4-27: ELGEAR signals and motor drive and configuration.

A high-speed, isolated, communications link allows each MCU to compare and consolidate control data and fault information.

There are two transmission channels between the CMS and each MCU. The MCU must see identical data on these channels to determine whether a signal is valid.

The original Airbus-driven specification is to operate the nose wheel steering using one of the two sides. For example, if side 1 is selected, the MCU and motor on side 1 drive the actuator and side 2 is in standby. Control is alternated between side 1 and side 2 on subsequent flights to 'exercise' both sides and detect dormant failures. In the event of a side not functioning, the CMS will attempt to use the other side.

The Goodrich/Newcastle design approach is to use both lanes of the nose wheel steering simultaneously so, unless faulted, the control operates in a master-slave type configuration. For example, if side 1 is providing the control inputs then MCU 1 is the master and MCU 2 (the slave) will obtain the control input data from MCU 1 via the cross-communications link.

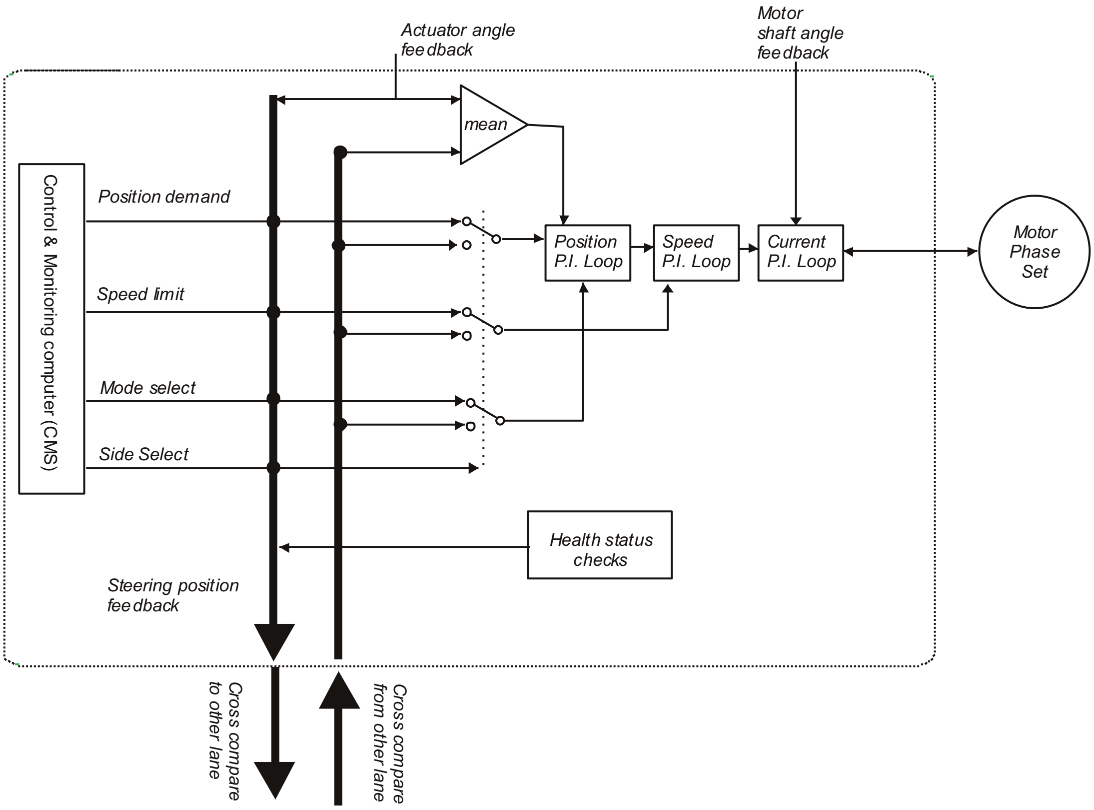

Figure 4-28: Internal control scheme of a NWS MCU lane.

The control scheme for a motor controller lane is shown in Figure 4-28. The control loops receive their input commands from either directly the CMS or via other MCU lane, dependant on the ‘side select’ command (from the CMS). Additionally each input is sent across two ARINC channels, for error detection, but this is not represented here for clarity reasons.

The input commands to the MCU are relatively simple, comprising of:

- **Position demand** – i.e. the required steering angle.
- **Speed limit** – this is almost always set to 20°/sec, instructing the NWS to operate as fast as possible, but can be reduced.
- **Mode** – a series of operating modes:
    - Normal: Clutch engaged, normal position control.
    - Limited: Clutch engaged, move to centralize steering at 1°/sec.
    - Inhibited: Clutch and power electronics disengaged – ‘free to castor’.
    - BIT: Built-in self test routine.
- **Side Select** – i.e. which side is master.

The position speed and current loops within the MCU are conventional PI loops and initial studies by Goodrich suggested that to attain a fast steering response, a relatively high sampling rate is required for the position and speed loops, therefore these will be operated at 1kHz. The demands from the CMS will be sent at 50Hz, but the actuator position sensor will be sampled at 1kHz. The current P.I. loop is considered relatively conventional, so a maximum sampling rate of 20kHz was assumed (depending on power transistors and subsequent thermal results).

Whereas the DEAWS will use median select routines to compare data, this feature is not applicable to ELGEAR. The four ARINC transmission channels allow a signal to be transmitted twice to the master lane, and where a repeated variation is noted, a signal error is declared and the slave lane will become the master to exercise the alternative pair of transmission channels. Consolidation of position feedback data between the two MCU lanes to compensate for signal errors is not possible with the initial schemes presented here, so to highlight significant measurements anomalies a tolerance band will be set. A 4-way position sensor arrangement in later revisions will overcome these limitations.

4.4 CONCLUSIONS

Safety calculations for electromechanical actuators have been shown, demonstrating why applicability of present technologies is restricted by the mechanical components of the actuators. It has been shown that by adding fault tolerance, the safety of such actuators is made suitable for applications where failure to operate will not result in a catastrophic failure of the aircraft.

The concept of independent lanes with a fault tolerant drive has been explored in detail, discussing the partitioning of control, signalling and measuring requirements for a system to become a practical reality in an aerospace electromechanical actuator application.

Fault tolerant topologies have been considered from a control perspective, with the advantages of voting in systems with three or more lanes described. This suggests that of the electric drive topologies proposed in chapter 3, those featuring three or more electronic control lanes will be advantageous from a control perspective. Reliability studies indicate that tolerance of one motor or converter fault is sufficient for an electromechanical actuator as any gains from additional fault tolerance are nullified by the mechanical restrictions of the actuator. The maximum number of lanes in a fault tolerant drive is restricted by component count and by the number of power supplies and communications links available on an aircraft. Existing power supply arrangements for actuators suggest a system with two or three lanes to be a an optimum arrangement. Considering the *n+1* and *3n+3* topologies of chapter 3, it could be initially summarised that a three single-phase *2+1* controller appears to be the optimum topology in terms of control lanes, component count and mass.

The trade study process of the DEAWS system was described, with a review of the selected topology and the safety requirements attained through fault tolerance.

The ELGEAR NWS system was also analysed, although safety requirements are less well defined as the system is required to operate only when taxiing. Despite studies of chapter 3 indicating a dual three-phase motor to be 2× the size of the *2+1* and a dual-lane architecture not optimal for voting, a *3+3* drive was selected for the NWS as a three-lane system was considered to have excessive control electronics. Analysis has shown that a 2-lane architecture is capable of attaining safety requirements and that the system can remain operational if single faults are correctly identified. In the case of voting deadlocks over feedback signals it is expected that additional signals can be added at a later date, although such cases are not considered critical provided the system can safely default to a ‘free to castor’ mode in a deadlock.

From the trade study research, the DEAWS system was determined to have a much higher component failure rate than an existing hydraulic arrangement. This is due in part to the distributed actuator approach, rather than solely the fault-tolerant electrical actuation. Although safety requirements are met, the increased component and maintenance costs resulted in DEAWS being unsuitable for the slat system due to a greater number of control surfaces than the flap system.

5 Actuator Development and Construction

This chapter documents the design and construction of both the DEAWS and the ELGEAR actuators, with the main focus on the work carried out by Newcastle University.

5.1 DESIGN OF THE DEAWS ACTUATOR

The DEAWS motor and power electronics were researched and designed at Newcastle University and the gearbox by FR Hi-TEMP. The power electronic controllers were assembled at Newcastle and the motor, gearbox and actuators were constructed at Fr Hi-TEMP.

The actuator follows the design topology described in section 4.2 and a single prototype actuator was designed for the worst-case load of 22,800Nm; experienced by an actuator driving both stations of an outboard flap (*see 2.1.3*).

As the actuator is designed to interface to a conventional flap mechanism with a 318:1 gearbox (*see 4.2.2*), the output torque of the actuator is approximately 72Nm in the worst-case. With the planned 37:1 actuator gearbox, the motor will experience 1.95Nm. These parameters do not include losses in the actuator gearbox and include no over-rating margins; hence values were increased to the following specification:

- **Motor peak torque:** 3.4Nm at all speeds and with 2 out of three lanes operating.
- **Motor operating speed:** 10,000r/min.

The specification demands a maximum extension time of 30 seconds so a 10,000r/min operating speed, results in a 22s flap extension and a peak power requirement of 2kW, which must be obtained from a 115V_{rms} 400-800Hz ac source.

5.1.1 Motor

A *2+1* permanent magnet synchronous motor with three independent phase windings was designed by Prof. B.C. Mecrow with assistance from Dr. G.J. Atkinson at Newcastle University. The machine is designed with the phase windings constrained to separate thirds of the stator with no slot containing coils from multiple phases and no overlapping of end windings. This mechanical separation reduces the thermal coupling and thus the probability of an overheating fault propagating between two phases.

The machine is also designed with the each phase per-unit inductance being equal to the per-unit back emf, in order to maintain rated current in the case of a terminal short-circuit (*section 3.4*).

After a large number of trial designs, the end-result is the phase-grouped motor in Figure 5-1. The red, green and blue coils in the second image show the distribution of the three phases.

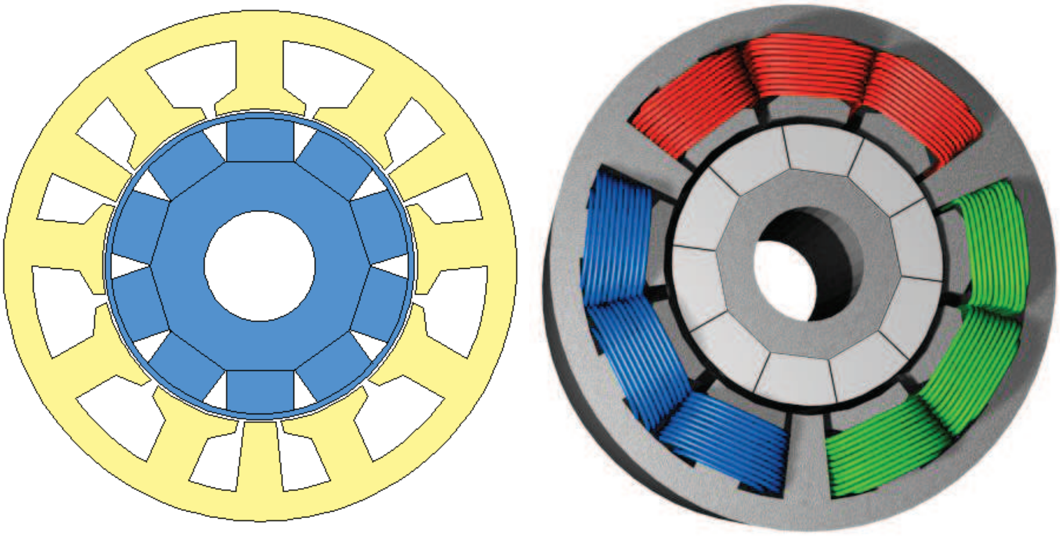

Figure 5-1: The DEAWS *2+1* motor design.

The coils for each winding are spread over three adjacent teeth and then separated from the adjacent module's windings by spacer teeth. The three teeth of a module occupy a full pole pitch, thus maximizing the winding factors to unity.

The adjacent teeth of a module are wound in a North, South, North arrangement and brought out to two wires as there is no star point.

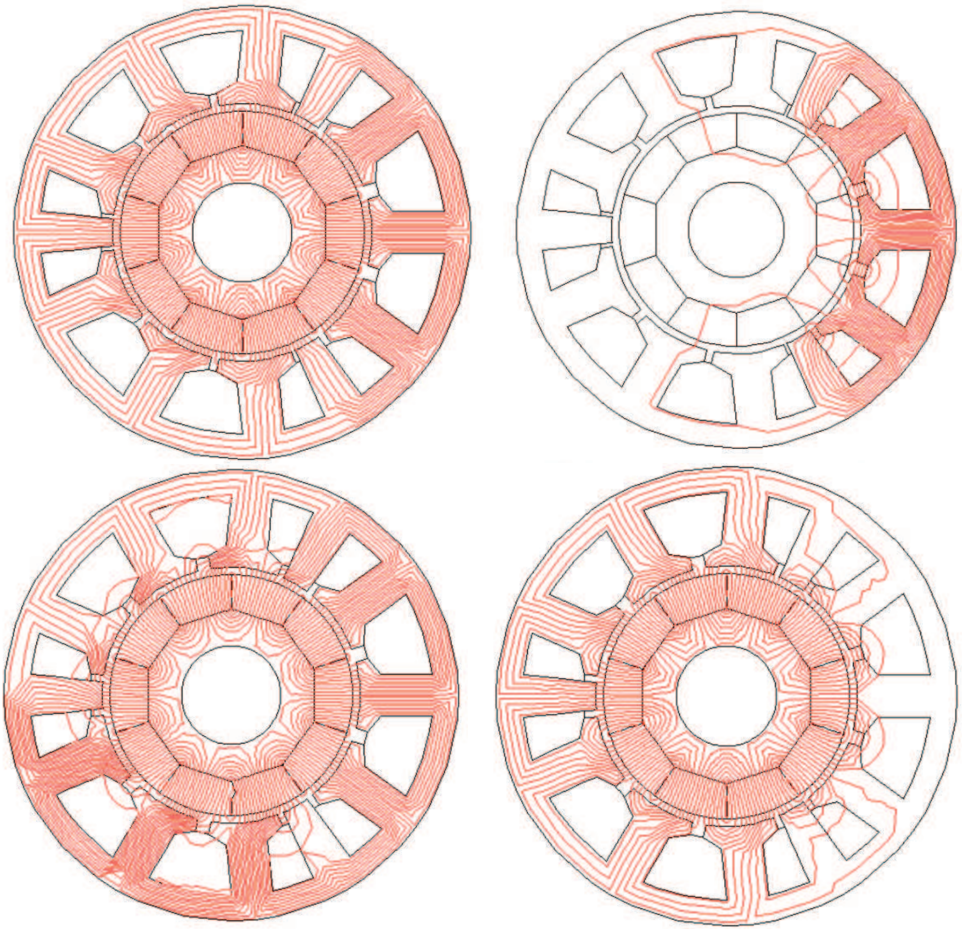

Figure 5-2: Clockwise from top left, flux distribution at no load, flux from a single, unfaulted phase at full load, no load with a shorted phase and full load unfaulted.

Figure 5-2, bottom right, shows a simulated faulted phase with the coils wrapped around the three teeth on the right of the figure. Induced currents in the shorted phase prevent any net magnetic flux from linking that phase, but have no significant effect upon any other phase. The bottom left simulation shows a clockwise torque on the rotor in an unfaulted condition. Table 5-1 gives the parameters of the designed motor with predicted values of back emf, resistance and inductance.

To attain the rated torque of 3.4Nm, the peak instantaneous currents of each phase are shown in Table 5-2. The highest current is due to low-speed drag torque where an over-rating of 2× is required, although this will be for a relatively short time in normal operation as the machine accelerates through the drag to the peak speed of 10,000 r/min.

Stator teeth	9 (+ 3 spacers)
Magnet poles	10
Magnet type	Samarium cobalt (for high temp tolerance)
Lamination material	Low-loss silicon steel
Lamination thickness	0.2mm
Coils per phase	3
Turns per coil	23
Slot fill factor	0.6
Wire diameter	1.4mm
Wire insulation	High Temperature Class (200°C+)
Back emf constant	0.0158 V per r/min $_{\text{(peak)}}$
Phase resistance at 20°C	0.13Ω
Phase self-inductance	780μH
Inter-phase mutual inductance	6.3μH

Table 5-1: DEAWS motor parameters.

Unfaulted operation	15 A
High speed, one phase open or short-circuit	22.5 A
Near standstill, one phase open or short-circuit	28.2 A
One phase short circuit, low speed	30 A

Table 5-2: Motor peak currents to attain a peak torque of 3.4Nm.

Table 5-3 lists two of the major sources of electrical loss – winding loss and lamination iron loss. All losses are predicted for operation at 3.4Nm, 10,000r/min and a maximum operational temperature of 150°C, with the exception of the short circuit value which is predicted for the region where peak drag torque occurs, although, again, this condition will occur briefly during acceleration to 10,000r/min. Losses for 0.35mm laminations are shown for comparison to the selected 0.2mm.

Total winding loss (unfaulted)	67 W
Total winding loss (one phase o/c)	100 W
Total winding loss (one phase s/c)	189 W
Iron loss	105 W (0.35 mm laminations) 66 W (0.2 mm laminations)

Table 5-3: Calculated motor losses.

The motor is of a segmental construction. Teeth segments were wire eroded from low-loss silicon steel, stacked and placed into a custom-made jig. Adhesive is applied to the inner and outer faces of the stacks and allowed to penetrate between segments (via capillary action) prior to clamping and setting.

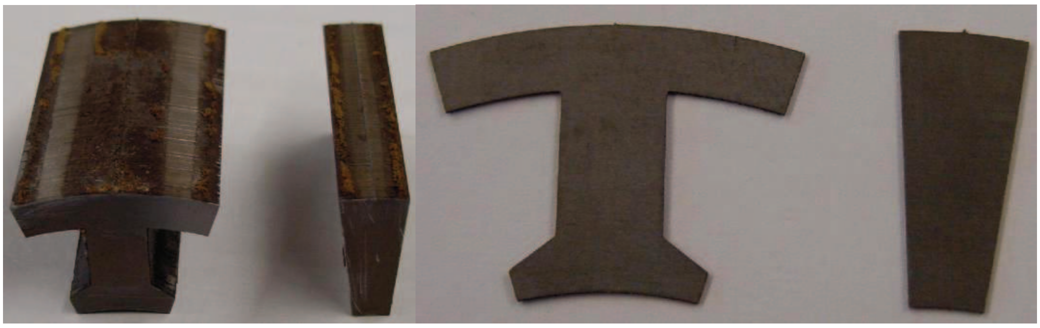

Figure 5-3: Motor segments (left) and individual laminations (right).

The segment stacks were wound and then assembled into the motor arrangement. An outer casing is interference fitted using heat, with an additional Loctite 648$^{(\text{TM})}$ adhesive applied (Figure 5-4).

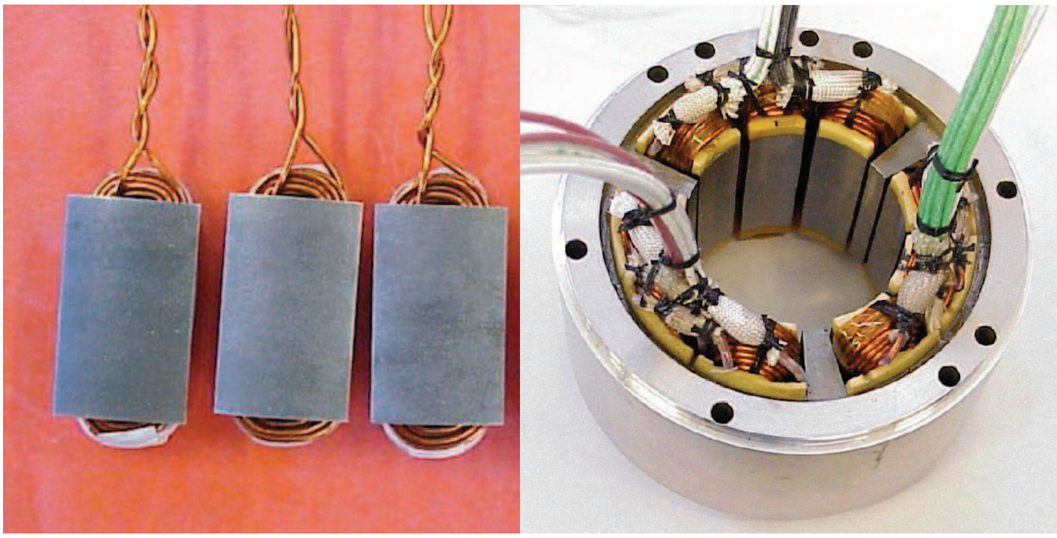

Figure 5-4: Individual wound segments (left) and assembled into outer sleeve (right).

As discussed in 4.1.3, to prevent a single point of failure in a fault tolerant system it is necessary to use multiple resolvers. In the DEAWS drive, each lane has a dedicated resolver and all three are located at the back of the motor and are coupled to the main shaft via a gear system. Each resolver contains a locating pin which will shear in the event of a resolver jamming, thus mechanically decoupling the resolver from the shared shaft (Figure 5-5). Although the rotor and central gear remain single points of failure, FR-HiTEMP deemed the added tolerance of resolver jam and shorter casing length preferable to arranging three resolvers in-line.

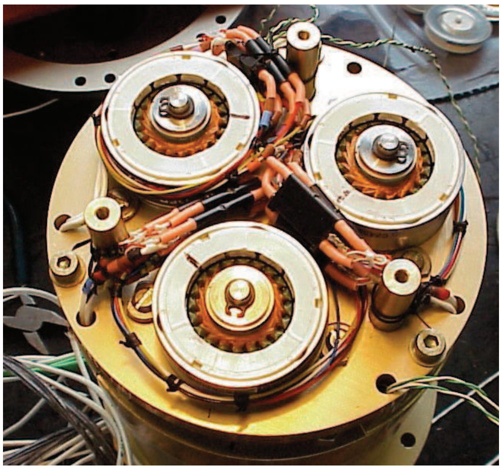

Figure 5-5: Triplex resolver arrangement.

5.1.2 Gearbox

The gearbox for the DEAWS project was designed as a versatile prototype for R&D, as opposed to an optimized production unit, consequently there are two identical halves to the gearbox (Figure 5-6), each designed with a 37:1 step-down ratio and capable of interfacing to a flap track mechanism.

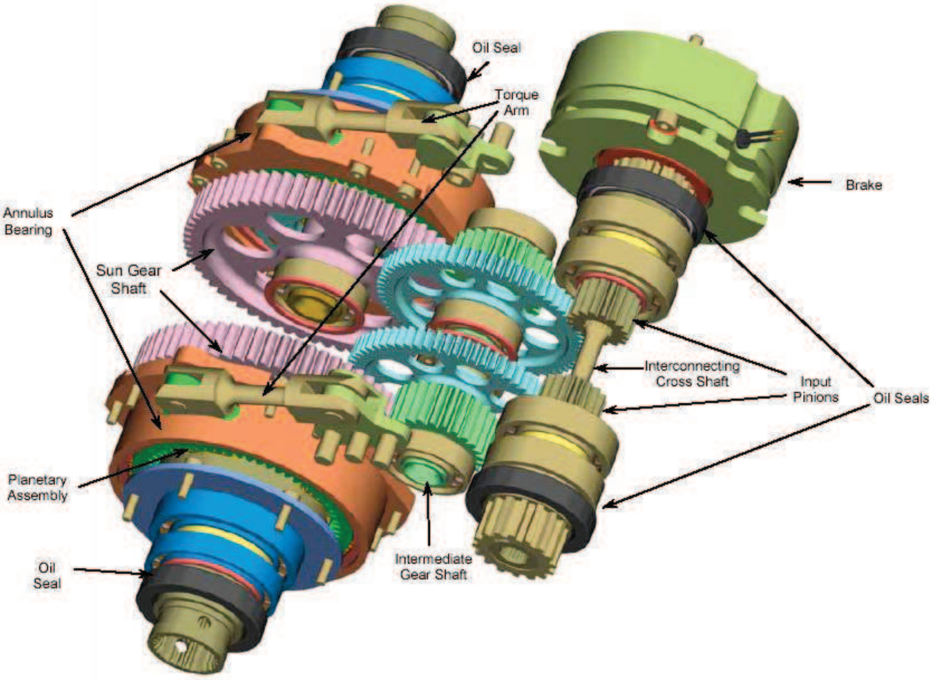

Figure 5-6: Internal diagram of DEAWS actuator gearbox (c/o FR-HiTEMP).

As described in *4.2.2*, a cross-shaft between gear sets can be removed to drive two output shafts from two electric motors. The shaft is fitted by default for all results presented in this work.

The internal construction features a two-stage spur gear set and a final planetary stage. Torque arms allow the fitment strain gauges to allow the MCU lanes to initiate a shutdown in the event of overloading.

The combined motor, gearbox and a termination box is shown in Figure 5-7. The termination box is intended to represent a production-sized power electronic converter, but for the research and development stage, it serves as a junction box between the motor, flap sensors and an external power electronic converter.

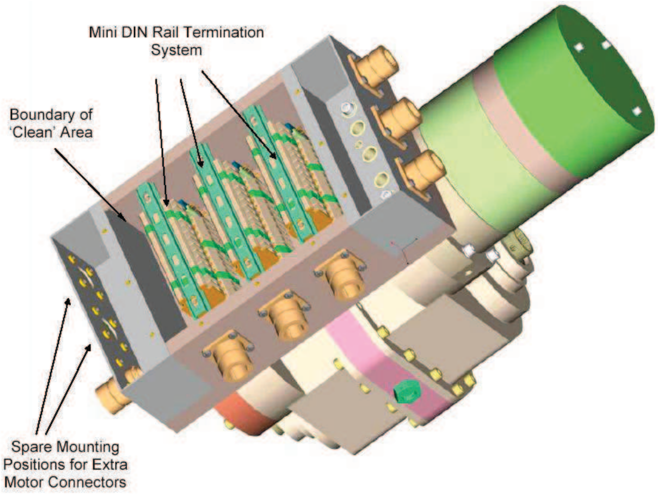

Figure 5-7: DEAWS with termination box and one motor (c/o FR-HiTEMP).

5.1.3 Power electronic converter

The aim for the first phase of the DEAWS project was to construct a prototype demonstrator rig. The electronics will power the actuator and demonstrate the handling of certain deliberately-imposed faults. As a 'proof of concept', the design is based around functionality and an operational representation, rather than a component-level prototype of an aerospace-class actuator. The 'technology readiness level – TRL' can be considered around level 3, where 0 is a paper study and 8 is an aircraft device. The arrangement of the power electronic converter follows the topology diagram presented in Figure 4-22 (*pp.95*).

As Newcastle University has undertaken prior research onto fault mechanisms within permanent magnet machines [29,79] it was deemed unnecessary to incorporate handling of motor turn-turn short-circuits and specific power device faults within the power electronic converter. The purpose of the DEAWS system was to demonstrate faults at an actuator level, including communications failures. Demonstration of motor and converter failures therefore involved real-time de-powering of winding modules and off-line imposing of short-circuits at the motor terminals in order to monitor operation with absent modules and with drag torque.

5.1.3.1 High voltage electronics

The *2+1* fault-tolerant motor requires a power electronic controller lane for each phase winding and an aircraft-representative power supply for each controller. At the time of the project conception, the specification of the power supply was based on the A380, i.e. three-phase variable frequency ac at $115V_{rms}$, with harmonic distortion required to follow the profile shown in Figure 2-6, *pp.39.*

The subsequent emergence of dc as a possible power source (see *1.5.1*) led to a decision not to focus on ac power supply interfacing, so a diode bridge rectifier was deemed suitable for ac-dc conversion on the demonstrator. Basic rectification remained to allow operation from the aircraft-representative $115V_{rms}$, v.f. power supplies at FR-Hi-TEMP, demonstrating operation of the power electronics and motor with a 270V dc link.

The power circuit for a power electronic converter module is shown in Figure 5-8.

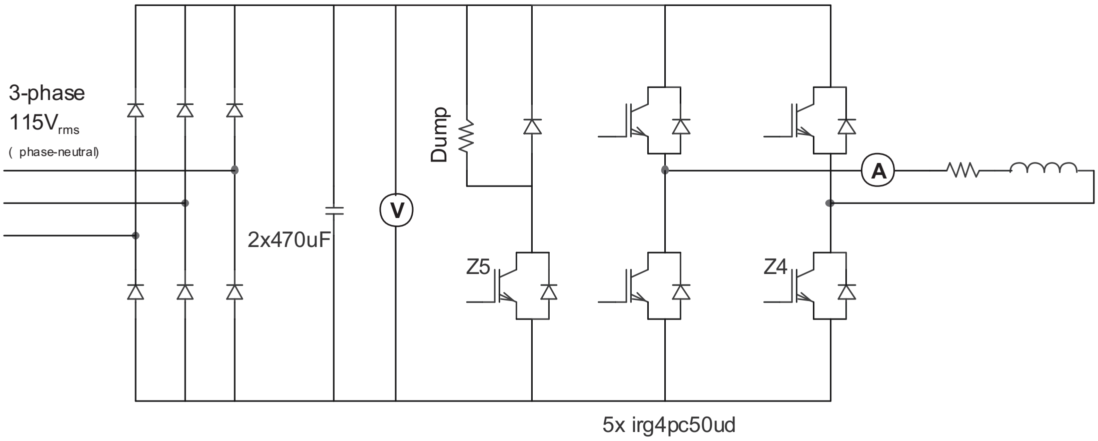

Figure 5-8: Circuit diagram of a DEAWS power module.

One module consists of a 3-phase rectifier, a capacitor bank, a single-phase IGBT H-bridge, a dump resistor circuit, voltage measurement and current measurement. With regeneration of power undetermined for the aircraft application, but required on the test rig power supplies, the dump resistor bank is external to the drive.

Electrolytic capacitors were used for the 270V dc link within the drive. Due to lifespan and atmospheric performance issues these would not be acceptable in an aerospace-grade prototype, but for a concept-stage demonstrator it was deemed unnecessary to focus on capacitor minimisation and use of polymer or ceramic technologies. Each power converter contains 940μF of capacitance, although this value is a result of selecting electrolytic capacitors for their ripple current rating and is considered massively in excess of what would actually be required in terms of capacitance. More research on this is presented in section 7.2. The additional capacitance helps filters the additional voltage ripple when developing the system on a 50Hz test supply and ensures a steady 270V throughout testing.

A detailed description of the components within each power module is given in Appendix C, pp. 215.

5.1.3.2 Processing and low-voltage electronics

For development purposes it was decided that a single processing unit would be used to operate all three power electronic lanes. Funds were focused on a development system with relatively limitless processing capability to provide versatile control development. Code is structured to emulate a triplex system in software, simplifying future porting of code to individual processors and also to aid in development and validation of fault-tolerant control algorithms.

The processing system is by Sundance Multiprocessor Technologies featuring a TMS320C6701 floating point digital-signal-processor, operating at 160 MHz and capable of 1 billion floating point operations a second. Communications and analogue measurement signals are passed directly to the system, while an external FPGA board generates PWM signals, handles shutdown logic, interfaces to the three resolver demodulation circuits and operates auxiliary contactors.

A more detailed description of the control software and hardware is given in Appendix C, section11.1.

5.1.3.3 Communications

With just one processor, inter-module communications cannot be physically represented. Instead, as the 3 lanes are represented in software, shared variables are stored in global memory and accessed during the execution of the code for each lane, where the data is consolidated with median select voters.

Three physical communications links to the flap control computer are required to demonstrate operation after the loss of a link.

Three of the RS232 UART channels on the Sundance system are used for bi-directional communications to the flap control computer and each channel is allocated to an internal 'software module'. A fourth UART channel is used for PC-based diagnostics and for control without an FCC present. This allows detailed monitoring of drive parameters, including commutation waveforms and the ability to disable power electronic lanes to test faulted conditions (Figure 5-9). With three control lanes emulated within the DSP, viewing of all internal parameters is critical for developing and debugging the triplex control software.

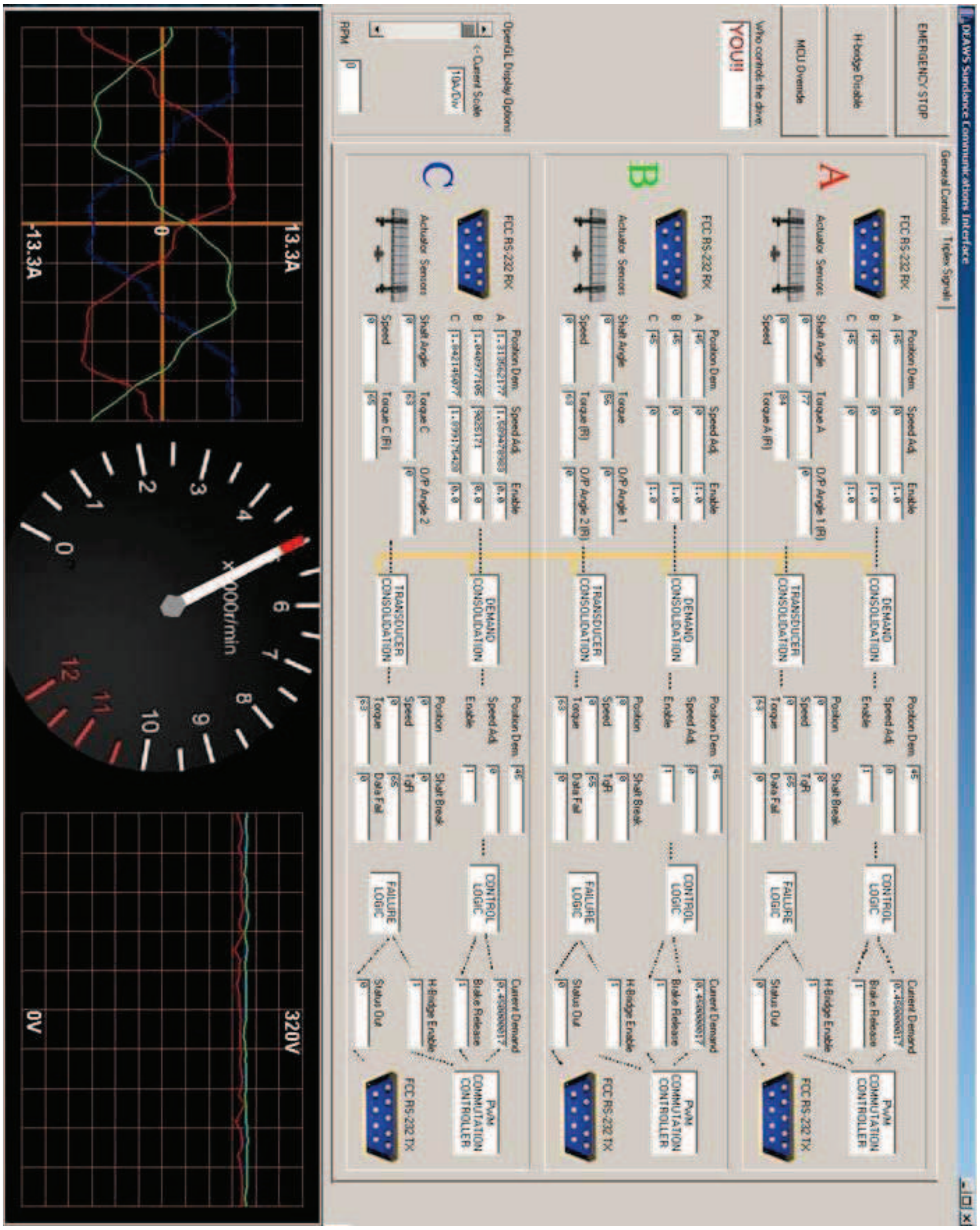

Figure 5-9: DEAWS PC diagnostics interface

The control computer links transmit and receive at 10ms intervals, corresponding to the sampling rate of the position controllers within each lane. The selected baud rate is 115200bps, the fastest possible speed of the UART devices. This is well in excess of the required speed to transmit the position, speed and enable demands from the FCC, but allows for additional parameters in future and keeps the signal transmission period short.

5.1.3.4 Brake driver electronics

As the DEAWS system is a demonstrator, the control electronics for the brake driver and voting circuitry (*see 4.2.2*) were placed in an external 'break out box' to the motor drive unit (Figure 5-10). The operator can toggle switches to impose real-time faults on the brake drive circuitry to demonstrate the fault tolerance of the voters.

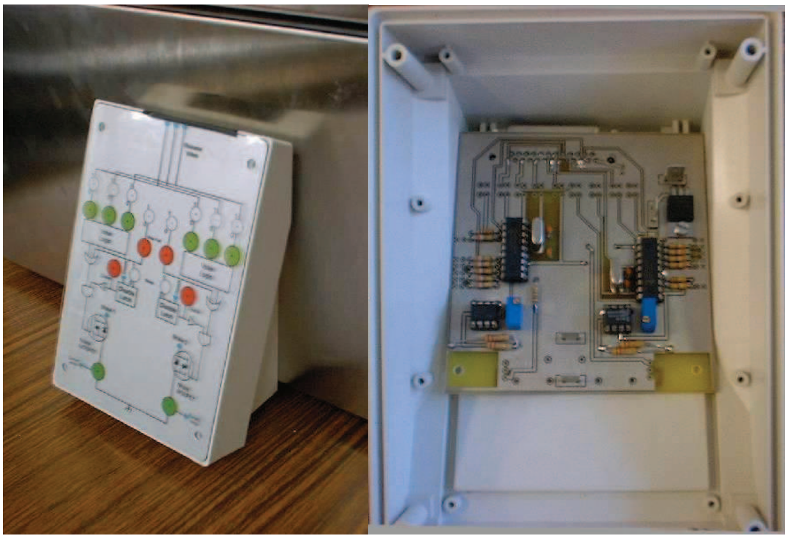

Figure 5-10: Brake driver box (left) and internal electronics (right).

It is foreseen that, due to the safety critical nature of the brakes, the 2/3 brake voters of a flight-standard system would require housing in external, galvanically isolated packages to the control electronics. With the actuator featuring a pair of dual-wound brakes, four voting circuits would be required for each actuator, although only one brake was used for the demonstrator, requiring two identical circuits within the break-out-box. Trade studies by BAE Systems deemed it necessary to include additional fault monitoring to avoid failure of two voters releasing the brakes - a catastrophic condition which must be less than 1×10^{-10} per flight hour. Figure 5-11 shows the circuitry for a brake voter with feedback monitoring by the control lanes – this effectively mirrors the brake voter logic in the control lane processor so if the brake voter makes an unspecified decision then a second transistor is opened to unpower the circuit and hold the brakes on – a condition far safer than an unscheduled release. The voting logic in the brake out box is represented by PIC microcontrollers.

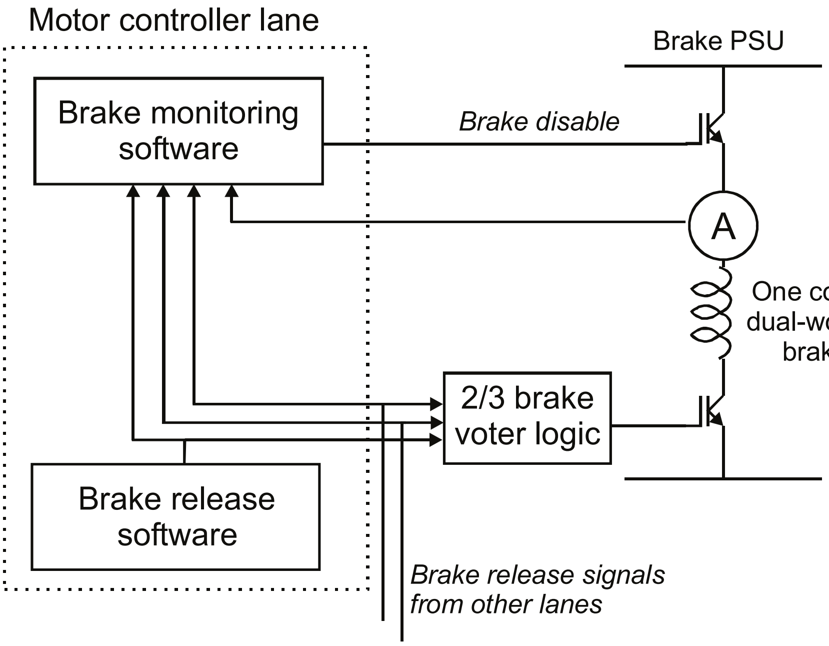

Figure 5-11: Internal logic of brake driver (c/o BAE systems).

5.1.3.5 *Overall Layout*

The arrangement of the DEAWS laboratory controller is shown in Figure 5-12. To drive the low-voltage electronics, a 240V ac to 12V PSU is included in the controller, a process that would ultimately be derived from the aircraft supply in each controller lane. Another demonstrator addition is an isolator PCB, to galvanically isolate the DSP system from the PC to reduce common-mode interference when debugging. Figure 5-13 shows photographs of a constructed controller and actuator.

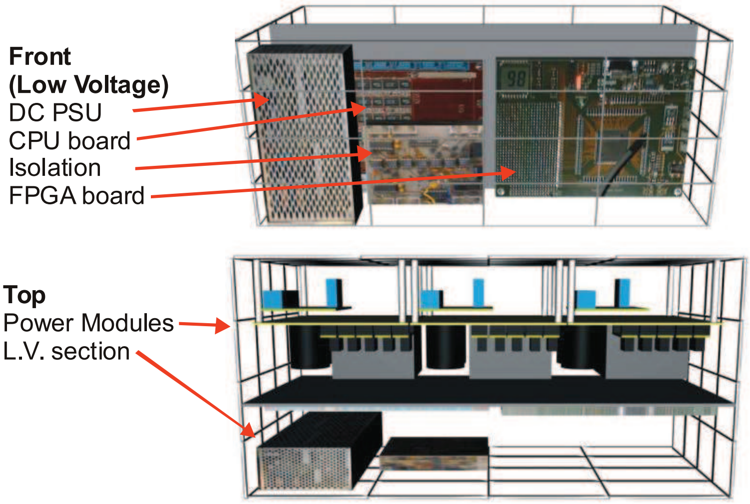

Figure 5-12: Layout of DEAWS controller.

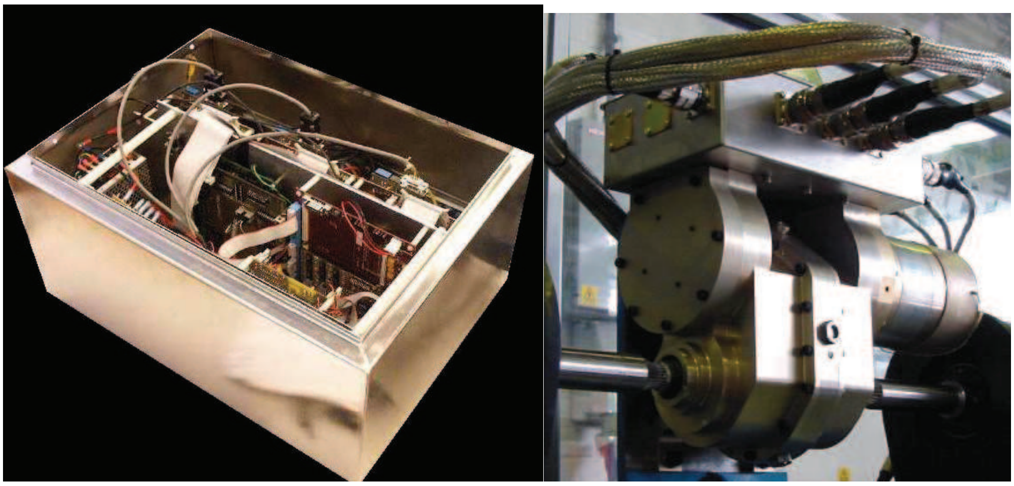

Figure 5-13: A constructed DEAWS controller (left) and actuator (right).

5.2 DESIGN OF THE ELGEAR NOSE WHEEL STEERING

Research, design and construction of the ELGEAR nose wheel steering was split between two parties. Goodrich Actuation Systems were responsible for design of the fault-tolerant motor, gearbox, clutch and the actuator. Newcastle University were responsible for the fault-tolerant power electronic controller.

ELGEAR was intended to be more representative of an aerospace system, with a higher technology readiness level than DEAWS, achieved by more representative components, packaging and design.

As with DEAWS, the fault-tolerant aspects of ELGEAR were focused on the actuator operation, rather than internal motor faults and specific power switching device failures. Converter level faults can be imposed by software disabling of electronics and removal of power supplies or communications links. Motor faults are performed off-line by applying a link to short all 3 motor terminals together – the mechanism conventionally employed to limit fault currents from inter-winding turn faults within the motor [29] and which will provide a drag torque, as described in section 3.4.

5.2.1 Design of the actuator and motor

Based on the outline specifications shown in section 2.2.3, a nose wheel actuator system was designed, capable of load torque in excess of 7000Nm and an operating speed in excess of 18°/s. The actuator is based around a 595:1 gearbox, housed within the centre of the *3+3* motor. The gearbox is an existing Goodrich design, but interfaces to a new planetary clutch arrangement (Figure 5-14).

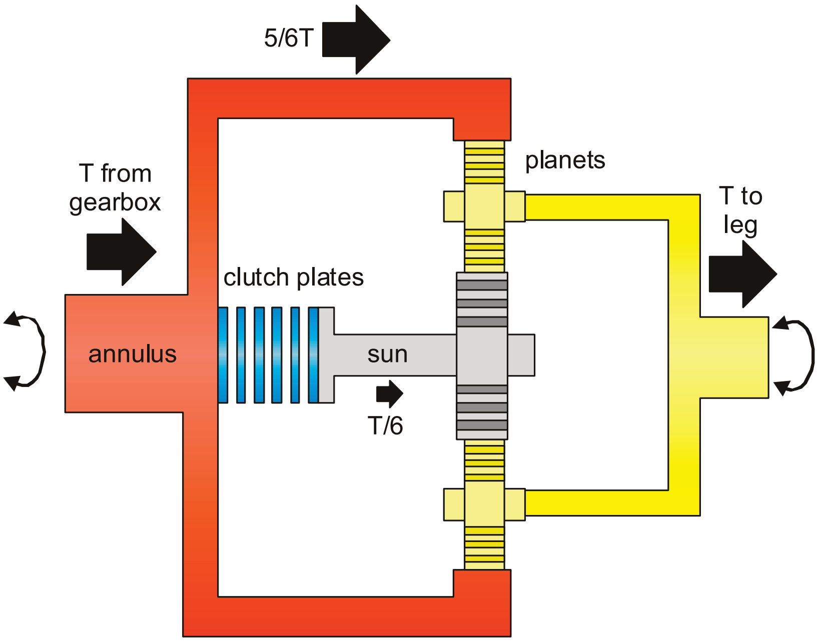

Figure 5-14: ELGEAR planetary clutch.

When engaged the clutch locks the sun to the annulus, forcing the planets and the output shaft to rotate. When disengaged, the planets and sun rotates freely. The gear ratio results in the sun transferring 1/6 of the output torque, resulting in a much smaller clutch design.

Goodrich Actuation systems were responsible for the design of the fault-tolerant *3+3* phase motor. A permanent magnet synchronous machine was selected due to the high power density and scope for fault-tolerance.

Calculations in section *3.4* predict a *3+3* motor to be 4× larger than a normal 3-phase motor. This over-sizing factor is mainly because each motor lane must be rated to provide output torque at all speeds and also overcome the drag torque from the other motor, should it be short-circuited after a fault.

With some data based on simulation predictions by Goodrich, the specifications of the motor are given in Table 5-4.

Stator teeth	24
Magnet poles	20
Outside diameter	230mm
Stack length	20mm
Coils per phase	2
Back EMF constant	0.276V per r/min $_{\text{(peak, ph-ph)}}$
Phase self-inductance	21.36mH
Phase resistance	3.84Ω
Torque constant	2.315Nm/A$_{\text{(peak)}}$
Field flux linkage per 3-ph module	0.292Vs$_{\text{(rms)}}$

Table 5-4: ELGEAR motor parameters

The motor is an inner rotor design, intended to sit around the actuator gearbox. (Figure 5-15). The decision was made to space the three phase windings 120^{o} apart, thus interleaving the phases of each lane. Constraining each three-phase set to half a motor would provide ideal physical isolation; however, it was feared that when operating from one lane, the imbalance of forces on the rotor would lead to increased bearing wear. Similar concerns were noted by Takorabet *et al.* [80], with alternative suggestions for grouping of phases. As it is only the inter-turn connections in ELGEAR that overlap, physical separation could be improved in future revisions with only packaging alterations, including bringing the two sets of motor connections out on alternate axial ends of the stator.

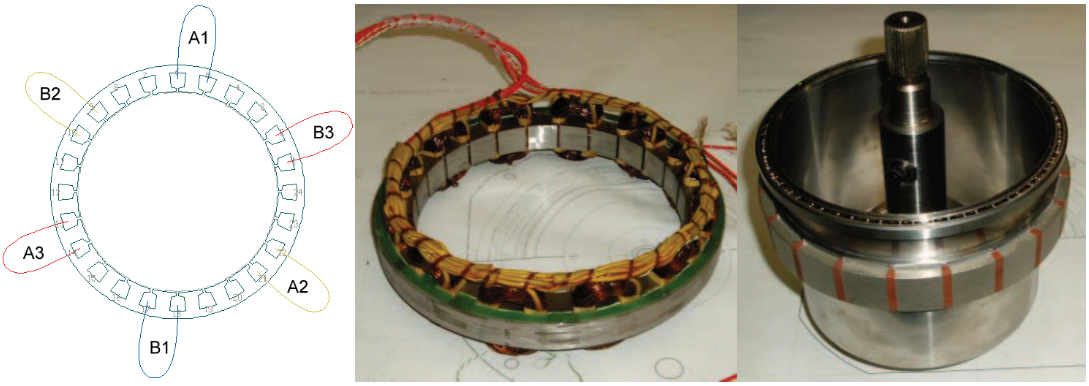

Figure 5-15: ELGEAR windings (left), stator (middle) and rotor (right) (c/o Goodrich).

With a 595:1 gearbox, 7kNm of actuator torque corresponds to 11.6Nm motor torque; however, the peak output torque is taken to be 17Nm, to allow a gearbox efficiency of 70% and to provide some over-rating margin. At 17Nm output, the peak currents per motor half are calculated to be approximately:

Normal operating condition	4.2A (per lane)
Other lane unpowered	8.4A
Other lane short-circuited	11.7A

Table 5-5: Motor peak currents to attain a peak motor torque of 17Nm.

The required torque profile for a three-phase winding set is shown in Figure 5-16. The load torque profile is calculated from the actuator torque specifications of Figure 2-11 (*pp.44*) with the 596:1 gearbox and 70% efficiency. Using the predicted inductance, resistance, field flux linkage and equation 3-18 (*pp.55*), the drag torque profile can be predicted when one three phase lane is shorted. With one motor lane failed and short-circuited, the sum of the load and drag torque profiles must be met by the remaining operational lane.

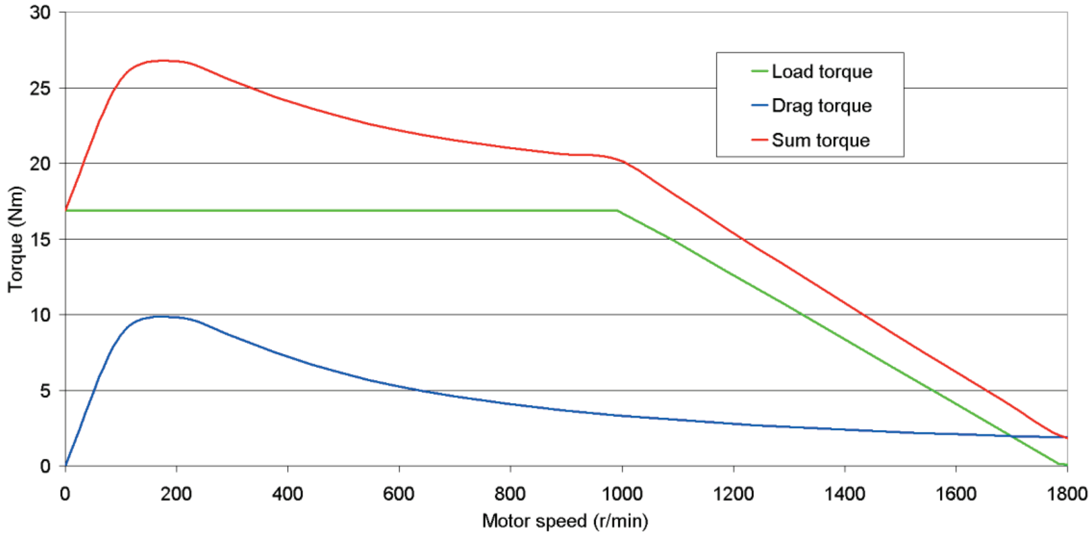

Figure 5-16: ELGEAR NWS torque vs. speed profile for a 3-phase winding module.

The actuator will effectively be commanded to operate at the greatest speed permitted by the torque/speed profile for a given torque, which at 7kNm, corresponds to a minimum of 10º/sec and 1000r/min at the motor. This is comfortably above the 200r/min region of peak drag torque, reducing the additional load and heating effects from a shorted lane. There are no specified acceleration limits, so the controller will demand a maximum torque output in order to accelerate the motor to maximum speed as quickly as possible. This is in the order of milliseconds, so the operating time around the peak drag region of 200r/min will be negligible and will not determine the thermal design of the motor or the converter heatsink requirements.

A pair of conventional resolvers are mounted on rear of the motor. Unlike DEAWS, the resolver rotors share a common shaft, as Goodrich Actuation Systems considered the probability of a resolver jam insufficient to warrant a decoupling arrangement.

A sketch of the assembled actuator is shown in Figure 5-17. The motor, gearbox and clutch are located at the top of the steering leg. The entire lower section of the leg (in red) is rotated, with position feedback given by RVDTs mounted above the torque-tube section. A torque arm couples the upper and lower sections of torque tube, which are separated internally by a shock absorber. The wheels mount to the lower axle. As with hydraulic systems, the actuator for extending and retracting the steering is at the top of the leg (green), although as the NWS motor is located at the top, the load exerted on the arm is lower than with hydraulic steering systems.

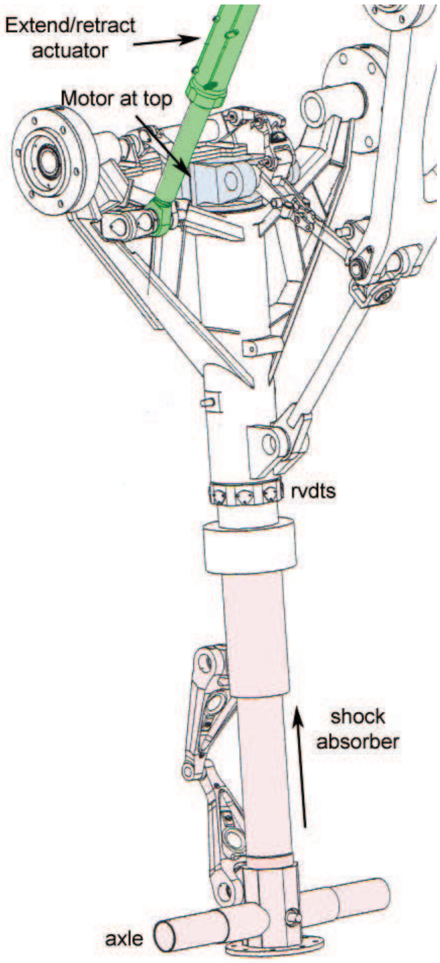

Figure 5-17: Nose wheel steering actuator. (c/o Goodrich)

5.2.2 Design of the motor drive electronics

From the outset of the ELGEAR NWS project, the physical size of the power electronic controller was considered an important factor. A compact design using completely bespoke circuit board layouts offers a better representation of a final product than an oversized laboratory demonstrator, based around commercially available control and power electronic circuit boards.

5.2.2.1 High voltage electronics

A high-voltage power-electronic main-board was designed for each power electronic lane. The power supply specifications for the NWS are relatively simple; a ±270V dc supply is available to each lane with the peak allowable current draw at 40A. During consultation with the motor designer at Goodrich, it was decided that the full 540V should be utilised, as power levels can be achieved with lower current (and therefore smaller power components and less losses) than a 270V system.

The basic circuit for the high voltage main board is shown in Figure 5-18:

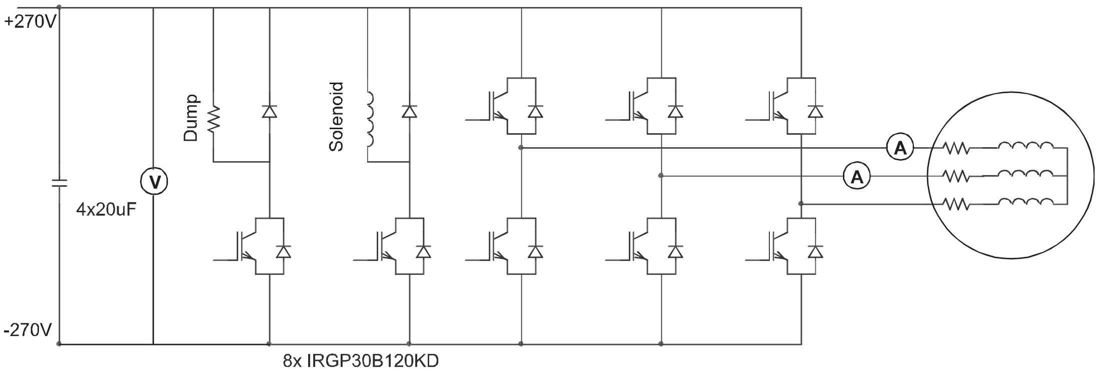

Figure 5-18: Power board circuit for a lane controller.

The motor commutation section of the circuit is a conventional 3-phase bridge, using IRGP30B120KD-P IGBTs with inbuilt 'ultrafast' soft recovery diodes, rated to 1200V and 25A at 25°C. As electrolytic capacitors are unsuitable for aviation-grade power electronics, polypropylene capacitors are used. Four Cornell-Dubliner 20μF, 750V capacitors are placed in parallel to make up an 80μF 'dc link'. Each capacitor has a ripple current rating of 19A with a peak of 740A. With a dc supply, there is no requirement to filter out ripple from rectified ac, therefore the capacitors are present to act as a lowpass filter, acting on the PWM 10-20kHz currents.

At the time of the NWS project conception, detailed power supply requirements were difficult to obtain, so estimates for acceptable input current distortion were made as the system is still a prototype. To correctly size the dc capacitors for PWM ripple filtering, the cut-off frequency must be calculated:

5-1

$$f = \frac{1}{2\pi\sqrt{LC}}$$

L is the inductance of the power supply and although an exact number is unavailable, a figure of 10μH per line was suggested by Goodrich, which ties in with the 20μH summed value used by Aten *et al*. in [41].

With 20μH in the supply, the 80μF capacitance gives a cut-off frequency of approximately 4kHz, which is comfortably lower than the intended PWM rates.

A dedicated input inductor could be included in this filter to achieve the same cut-off frequency and minimise the capacitance, so for future revisions there is allocated space in the casing to incorporate such a device in each lane.

Further work on the requirements for LC filters on dc systems is presented in section 7.2. and operational issues with a relatively low dc link capacitance are investigated in section 7.5.

Regeneration into the supply was permitted by Airbus, so there is no requirement for the controller to absorb energy when an aiding load is applied. However, as testing was at a variety of locations and not all test-rigs permit regeneration, it must be factored into the design, hence the dump resistor circuit. For a safety margin, it is assumed that regenerative loads may equal motoring loads, although they may be lower in reality as the aiding load will overcome the gearbox losses. With a peak power of approximately 1kW, regeneration can be handled relatively easily - for example a 100Ω external resistor on a 540V dc link will dissipate ~3kW and draw only 5A, which can easily be conducted through an IGBT.

Each lane must drive a solenoid to activate the clutch mechanism of the actuator. The solenoid is designed to operate from 540V and must be energized with a constant 4A to engage the clutch. A transistor circuit similar to the regeneration circuit is included for the solenoid, although as the solenoid is inductive, a larger 18A freewheeling diode, capable of conducting a continual 4A dc is required.

For additional details on the high voltage electronics, see Appendix C, section 11.2.

5.2.2.2 Processing and low-voltage electronics

From the outset, it was decided that the NWS electronics would represent a true fault-tolerant system at a hardware level – an independent control board is used with each high voltage motherboard. This is made feasible by designing a controller optimized for the task, as opposed to an excessively powerful testbench orientated system with unused I/O.

Figure 5-19 shows the entire electric drive for the NWS actuator. There are two power motherboards, each containing a stack of PCBs, the lower for the gate driver and the upper two for the processing and low-voltage electronics (subsequent revisions have combined the control boards onto one PCB).

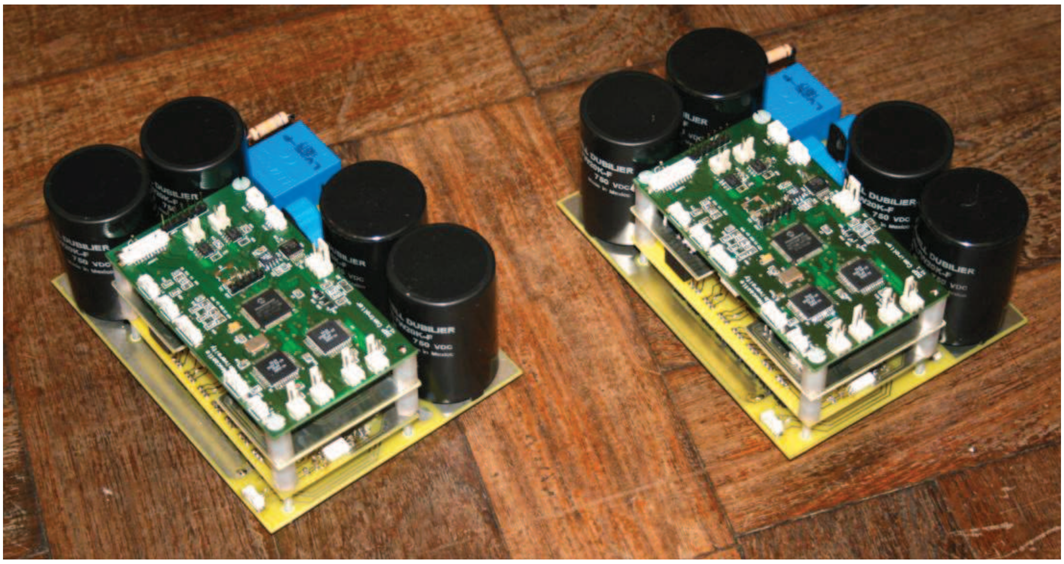

Figure 5-19: Two ELGEAR NWS power electronic controller 'MCU' lanes.

The ELGEAR control electronics is based around the dsPIC33FJ128MC708 microcontroller. This is a motor-control optimised device with on-board PWM generation and A/D conversion. 40 million instructions a second are possible, and 16k of RAM is present, although less than 25% of each are required. While this device is not aerospace-certified and a custom processor or gate array would most likely be required for future revisions, use of a dsPIC on ELGEAR highlights how only a low-cost, relatively simple processing element is required.

The microcontroller must execute the full fault tolerant control scheme of Figure 4-28 (*pp.104*) at 1kHz, requiring handling of communications, reading of RVDT position transducers and execution of the position and speed PI control loops.

It is also necessary to execute commutation code at PWM rate (10kHz), in which motor currents and dc voltage must be sampled, the resolver angle must be read from the R/D converter and the current PI loop must be executed. The current loop is a vector control scheme featuring D and Q axis PI control with a space-vector modulation scheme synthesising the output currents and allowing a 15% higher terminal voltage than basic sinusoidal commutation.

Motor temperature is also sampled by the processor for an emergency shutdown in the event of motor over-heating.

A 28V dc supply is available for all the control hardware, so a series of switch-mode power supplies convert this to 3.3V, 5V and 12V, to power all the devices on the PCB. For the demonstrator this 28V is taken from the aircraft ‘essential bus’, although for an aircraft-grade actuator the MCU would be required to derive the 28V from the ±270V dc.

Additional details on the ELGEAR control software and processing electronics are available in Appendix C, section 11.2.

5.2.2.3 Communications

Each control lane must perform a variety of communications tasks over two mediums, ARINC429 and RS-232.

There are two incoming ARINC 429 signals to a control lane and a requirement to return one transmission. Two Holt International Hi-3585 integrated circuits are used for this interface, each containing an ARINC receiver and transmitter and buffers. In addition to the NWS, other ELGEAR devices may share the same ARINC link, so the Hi-3585 can be programmed to accept only messages with the labels specific to the NWS, thus saving on unnecessary SPI transmissions to the main processor.

The ARINC arrangement is as shown earlier in, Figure 4-27 (*pp.103*). The two incoming channels are compared and data is only accepted if identical and this comparison is handled by the 1kHz main control loop within the processor. Outgoing ARINC packets are synthesized in the processor and passed serially to the Hi-3585 for transmission.

Although position control is executed at 1kHz, incoming data from the Control and Monitoring is 50Hz.

For consolidation of input signals and fault data, a cross-communications channel is present on each controller. The dsPIC features an in-built UART which allows a fully duplex transmission system between lanes using only two signal wires. A digital-magnetic-isolator device is used on each lane to galvanically isolate incoming signals (to prevent fault-propagation) while allowing a data transfer rate in excess of 1Mbps. To allow sharing of data in the 1kHz control loops, a message packet is transmitted at 2kHz. There is no synchronization method between lanes, so transmitting at 2× minimizes the sampling delay of shared parameters. A transmission length of 10 bytes was initially specified, allowing position demands and feedback, status information and room for spare parameters.

Additional research and investigation on the cross-communications requirements are given in section 7.3.

Although ARINC provides the command inputs to the controllers, a PC interface is included to allow an alternative method of control and improved diagnostics. Over 50 parameters are transmitted to the PC with a 20Hz graphical display showing the input and feedback parameters for the D-axis, Q-axis, speed and position PI control loops (Figure 5-20), allowing real-time adjustment of control loop tuning without additional diagnostic hardware.

The interface emulates the ARINC arrangement with a separate RS-232 channel to communicate to each controller lane. Replicating the Airbus ELGEAR communication protocol, in order to send a demand to both units, the user sends a side select command to both lanes to configure one lane as a master and then demands are transmitted to this lane. The master then passes the demands to the slave lane using the cross communications.

As with the DEAWS PC interface, the user can inject software faults to disable lanes and individual device failures can be monitored from Vce saturation data obtained from the HCPL-316 gate drive devices.

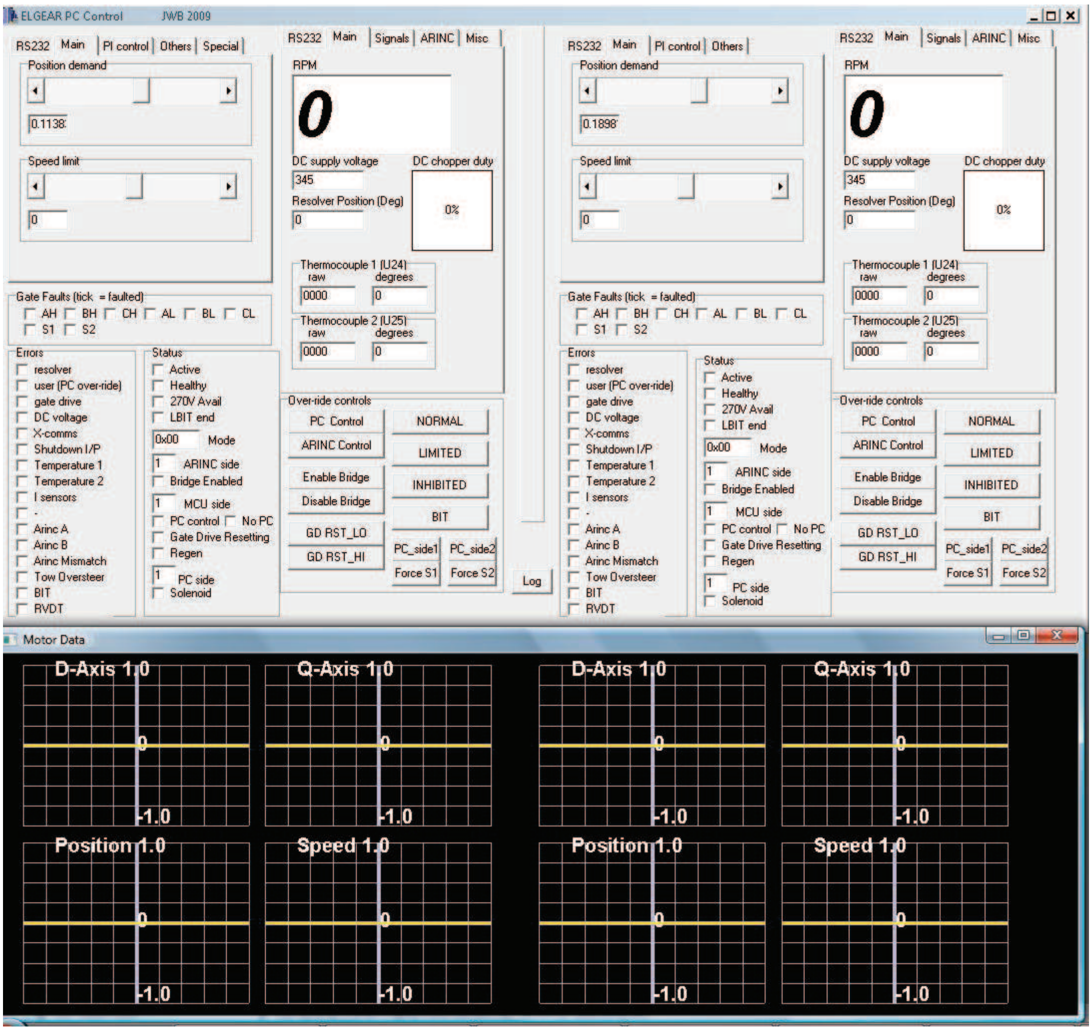

Position demand 0.1138 | 0.1898
Speed limit 0
RPM 0
DC supply voltage 345
DC chopper duty 0%
Resolver Position (Deg) 0
Thermocouple 1 (U24) raw 0000 degrees 0
Thermocouple 2 (U25) raw 0000 degrees 0
Mode 0x00
ARINC side 1
MCU side 1
PC side 1

Figure 5-20: ELGEAR PC control interface.

5.2.2.4 Packaging

Two complete MCU controller units are shown in Figure 5-21, each featuring two lanes. Both are electronically identical although the MCU on the left is a laboratory test unit, designed for future research and development and The unit on the right is packaged into a 146×200mm box, for installation on a test-rig at Airbus.

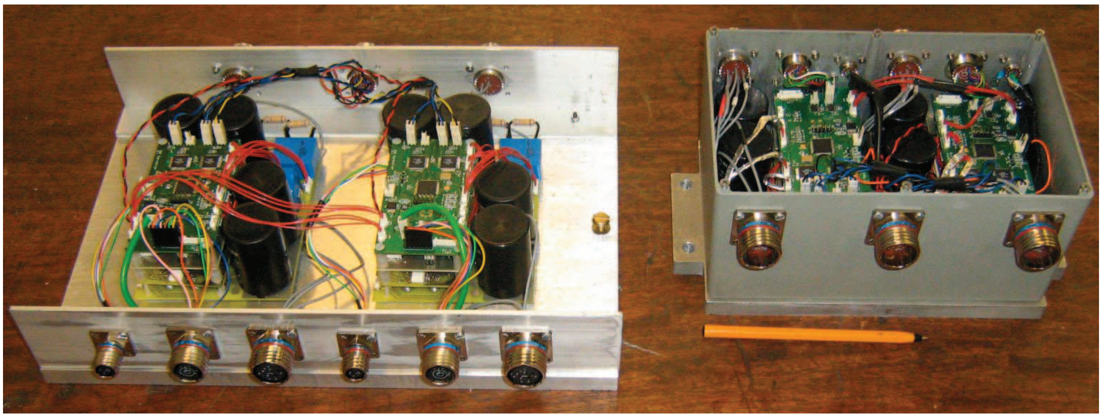

Figure 5-21: Laboratory (l) and industrial (r) MCU dual-lane controllers.

5.3 CONCLUSIONS

Two electromechanical actuators have been designed and constructed using two very different fault-tolerant configurations.

Although ELGEAR NWS and DEAWS are designed to different aerospace prototype technology levels, their resemblance to flight-grade hardware varies for different aspects of the actuators.

The packaging of the DEAWS actuator includes fitments for dual motor operation, should future research on a flap without a common shaft be required (*see section 4.2.1*) but otherwise packaging and size is comparable to a flight standard actuator for an outboard flap.

The ELGEAR NWS actuator is an entirely new nose wheel steering design, although featuring components from other Goodrich aerospace products with new additions such as the planetary clutch. Only a single clutch solenoid is present, which requires one controller to be powered at all times for loaded operation. This is acceptable for a demonstration, although faults can only be imposed on the non-controlling lane.

Both motors are reasonably representative of flight-grade motors, allowing for design optimisations and material changes. However, where DEAWS groups the three phase windings to separate sections of the motor with spacer teeth, NWS interleaves the two three-phase winding sets. For a more safety-critical application, a more significant thermal barrier between motor lane end-winding connections will be required, although this is an alteration at a packaging level rather than an electromagnetic design level.

The power electronic controllers vary significantly in their representations of aircraft hardware. The single processor system of DEAWS is a much higher-level hardware representation than the NWS, although the software algorithms and communications systems allow sophisticated fault-tolerant three-lane control with voting, using schemes presented by BAE systems, based on real safety-critical hardware systems.

The ELGEAR NWS goes a stage further than most research-level fault-tolerant drives, featuring a full duplex controller with full cross-communications and aerospace-standard ARINC 429 communications. The resulting dual-lane controller is of a size comparable to a flight-grade system. Hardware topology changes aside, it would be expected that while the electronics can be optimised, a flight-standard system would require extra filtering and suppression circuitry, potentially increasing the MCU size. Although not a flight approved component, the dsPIC offers an extremely functional device in a compact package. Demonstrating a fully-functional fault-tolerant system on a relatively simple device suggests to aerospace manufacturers that a cost-effective, compact, solution is achievable with a approved processors or logic hardware of a similar low-complexity.

The two projects are specified for two very different power supply standards, variable frequency ac and dc. With DEAWS research commencing in 2001, the variable frequency ac supply follows that of the A380, with Airbus considered a potential customer. With ELGEAR work commencing in 2007, Airbus specified dc supplies for ELGEAR. From the literature review of chapter 1, it is the view of the author that dc will become the accepted standard for actuation and this simplifies the evolution of both systems to a flight standard of hardware, with no research required on rectification technology.

Both systems will regenerate considerable amounts of power; DEAWS on retraction, as the aerodynamic loads attempt to push the flaps into the wing and ELGEAR from the corrective forces pushing the wheels straight when taxiing. There is no definite information on the quantities of regeneration allowed on a More Electric aircraft, with some sources claiming it to be completely disallowed [81], so it may be possible that the two systems could ultimately require integral dump resistors. For the demonstration test-rig, each DEAWS lane features an external dump resistor, as does ELGEAR, although as the Airbus test facilities allow regeneration via an external dump circuit, this feature is not normally in use.

The use of separate control lanes in ELGEAR NWS allows research into potential balancing and synchronisation issues of a fault-tolerant motor. Resolving any arising issues are important if the actuator is to run reliably with the lanes ‘active-active’ and tolerate all types of single electric drive faults, as intended.

Motor and power device-level fault monitoring is sidelined for the initial DEAWS and ELGEAR NWS projects in order to concentrate on system-level faults. If required, features developed from existing research can be incorporated into the projects at a later date.

6 Performance Analysis and Fault Handling

Testing of DEAWS and ELGEAR NWS is detailed in this chapter, presenting results from the fault tolerant electric drives and from the entire assembled actuation systems.

For both systems the focus of testing is at a top-level, observing fault-tolerant performance of the actuator, or multiple actuators. Motor and drive faults are confined to de-powering of converters, off-line short circuiting of motors and removal of communications links, as much research has already been undertaken on motor turn-turn short circuits and individual device failure within power converters.

6.1 DEAWS TESTING AND RESULTS

The testing of the DEAWS actuator was performed in two stages:

- A series of initial tests were performed within Newcastle University on the motor and power electronic converter.
- The motor and power electronics were transferred to a test-rig at FR-HiTEMP, where the gearbox and demonstrator flap system were connected and a series of performance tests were carried out by the author and BAE Systems to prove the functionality of the complete system.

6.1.1 Laboratory tests and results

In addition to ensuring operation, the initial laboratory tests allowed measurement of motor currents and motor output torque to observe behaviour, in particular the current shaping algorithms to overcome torque ripple at near-standstill speeds.

A load-rig was set up with the DEAWS motor mechanically coupled to a commercial high speed induction motor, via a torque transducer (Figure 6-1). A four quadrant commercial inverter controlled the induction motor, providing an aiding and antagonistic load to the DEAWS motor.

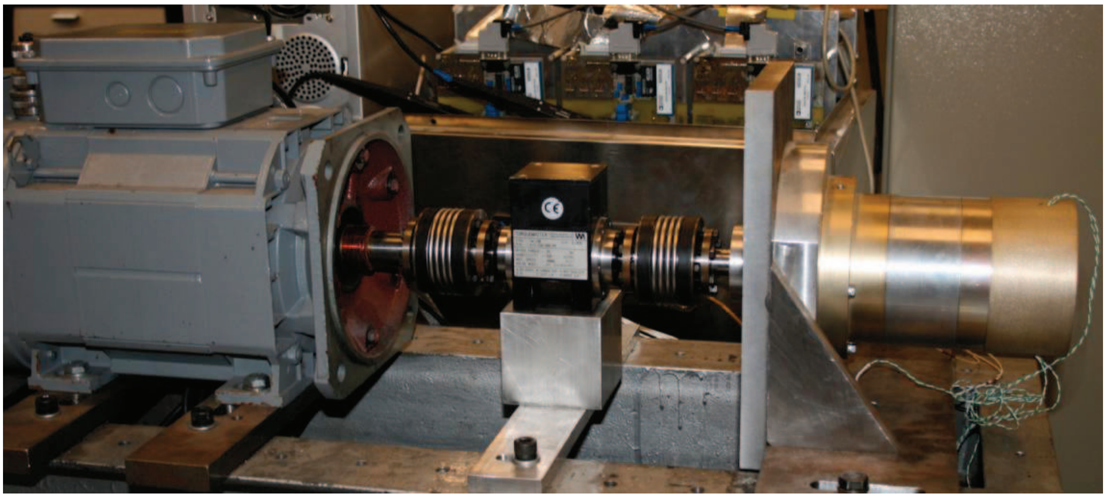

Figure 6-1: DEAWS motor (right) on laboratory test bed.

The single-channel RS232 diagnostics interface described in section 5.1.3.3 provides a 'backdoor' interface, allowing the user to issue torque demand inputs to the three lanes and also receive detailed operational status of the power electronic controller lanes. Although emulated on one processor, each of the three software control lanes can be software disabled in real-time to test the fault-handling capabilities of the triplex control scheme.

6.1.1.1 Back emf verification

The load inverter was used to rotate the DEAWS motor for back emf measurement. The emf value is critical as motor and power electronic current levels are based on a predicted 0.0158 V per r/min, i.e. 158V_{peak} at full speed, (*section 5.1.1, p.p.109*).

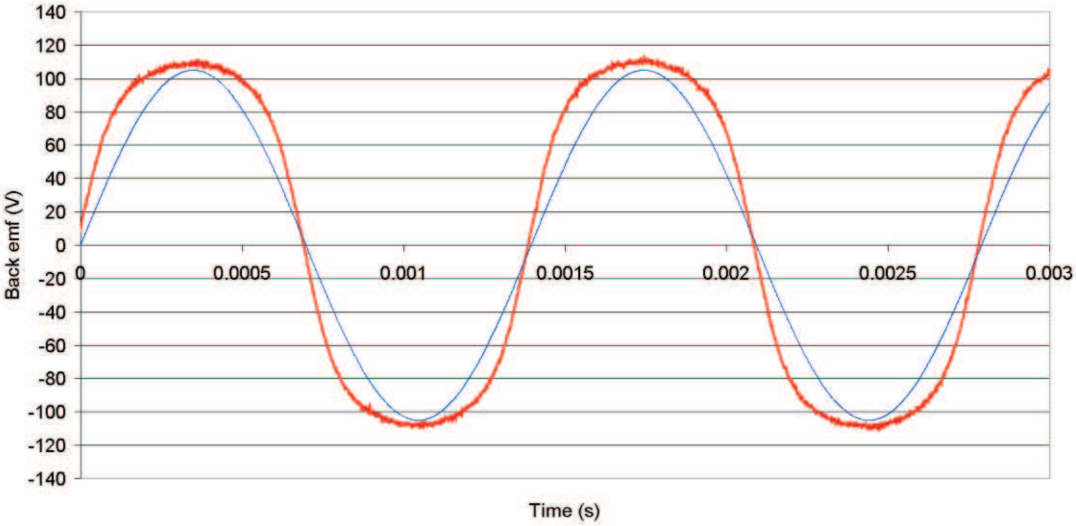

Figure 6-2: DEAWS back emf (red), ideal sine wave (blue) measured at 8500r/min.

Measured results (Figure 6-2) showed the actual back emf to be 0.0129 V per r/min, so to achieve the intended power output will require a 1.23× greater current than predicted. The predicted data in Table 5-2 (*p.p. 111*) must be revised:

Unfaulted operation	18.5 A
High speed, one phase open or short-circuit	27.7 A
Near standstill, one phase open or short-circuit	34.7 A
One phase short-circuit, low speed	36.9 A

Table 6-1: Revised motor peak currents to attain a peak torque of 3.4Nm.

While still within the device specifications for the power electronic controllers, there will be additional heating and the 36.9A short-circuit current approaches the peak measuring range of the current sensor boards. Due to discrepancies between electromagnetic simulations and the manufactured motor, the back-emf is also non-sinusoidal, which may have an effect on the low-speed torque ripple compensation.

6.1.1.2 Torque ripple tests

The DEAWS controller employs the current shaping system described in section 3.5 to overcome torque ripple from a lane failure at very low speed. Laboratory tests with a torque transducer allowed the performance of this system to be verified, as successful operation is essential for the actuator to be able to start with two lanes.

To observe the requirement for torque ripple compensation, two lanes of the controller were operated in torque control from the PC interface, with a sufficient torque demand to start the machine and accelerate with both lanes operating in sinusoidal mode (the third lane was unpowered, simulating an open circuit failure).

The load machine was set to operate as a constant drag load, representing a frictional load, while the torque transducer measured the variations in output torque from the fault tolerant motor. The applied load torque of ~2Nm was far lower than the rated torque of the *2+1* motor, but sufficient to show the resulting ripple torque when operating the motor from two phases with no ripple compensation strategy.

Acceleration in sinusoidal 2-phase mode is shown in Figure 6-3. Although the mean torque was around 2Nm, the instantaneous torque rippled between 1.5 and 3Nm. The back emf of the disabled phase is shown in green and it can be seen that the points of lowest output torque occur where this is at maximum amplitude, as expected.

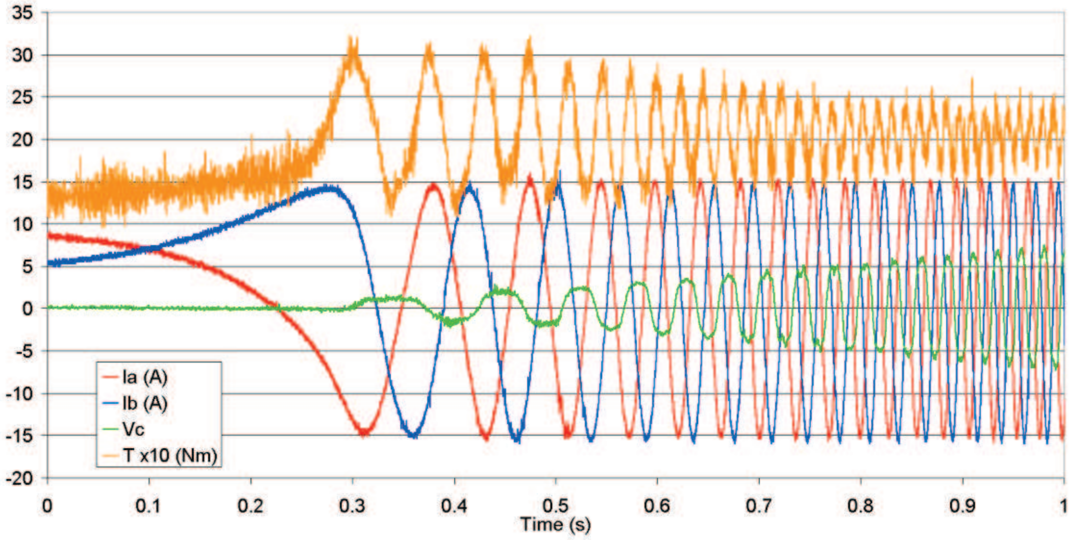

Figure 6-3: DEAWS start-up currents & torque with phase c failed open-circuit and no current reshaping.

Figure 6-4 shows the same start-up operation but with application of the current reshaping method described in 3.5, pp.57 (*see Appendix A for derivation*). The resulting torque was much flatter than in the sinusoidal case, although slight spikes were evident between the peaks of the two phase currents.

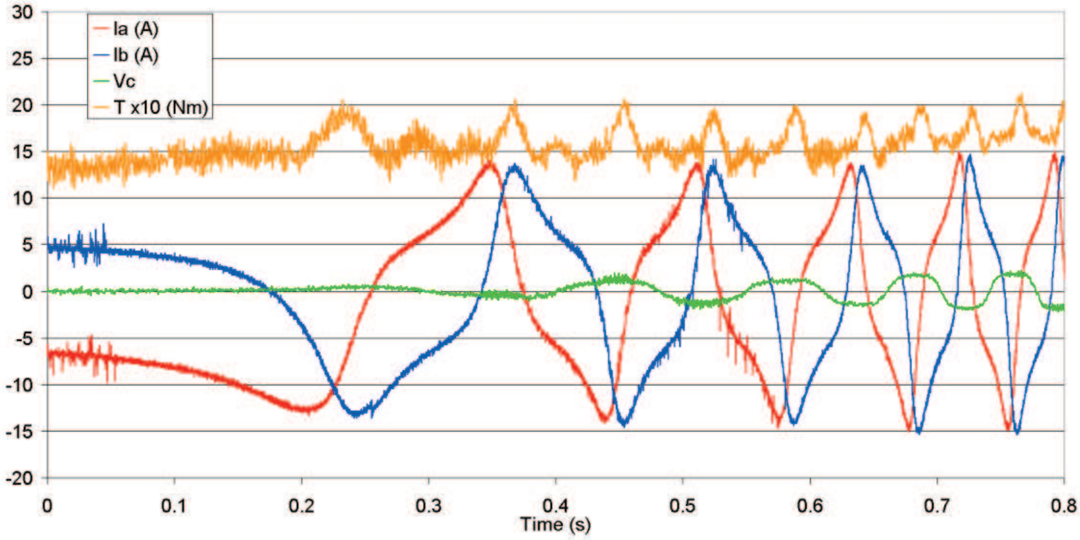

Figure 6-4: DEAWS start-up currents and torque with current reshaping.

To determine the source of these remaining torque ripple spikes, the current shaping techniques were simulated using the same algorithms, but applying the measured back emf data from the motor. As the measured emf was non-sinusoidal, but the reshaped currents are intended to compensate a sinusoidal drop in torque from the failed phase, there is a possibility that the waveforms are not ideal for the motor.

Results of this are shown in Figure 6-5. By normalising measured back emf data and applying the sinusoid-based reshaping system to the readings, it can be seen that the additional 3rd harmonic components of the emf result in periods where there are torque spikes above the target mean of 1.5 P.U. The location of the torque peaks in this data correspond with the peaks measured in the laboratory tests.

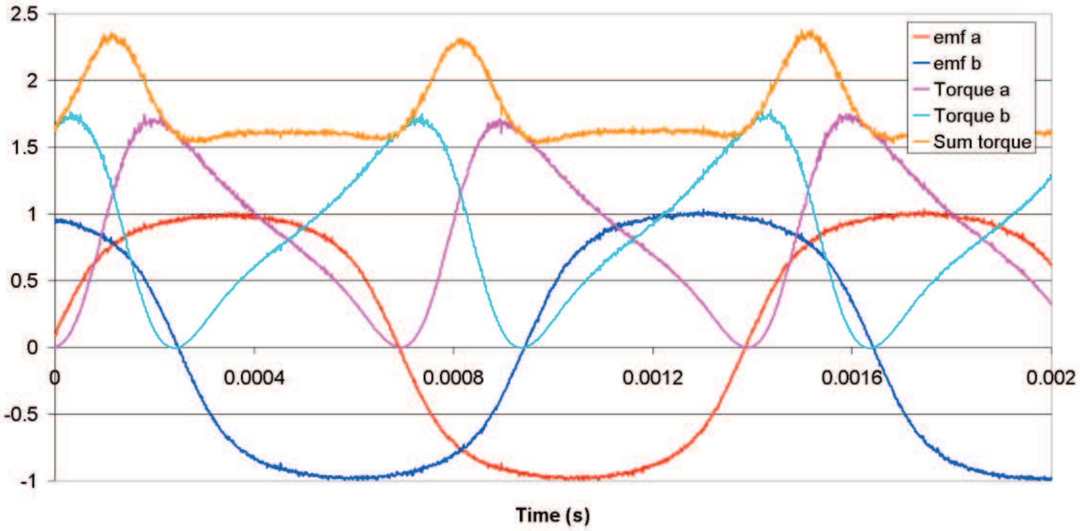

Figure 6-5: Predicted torques from sinusoidal reshaping using non-sinusoidal back emfs.

It is clear that, to obtain a flat torque output at low speeds, a current reshaping scheme such as that described in [63,64] is necessary, based on a measured back emf model of the motor, rather than idealised sinusoids.

A dynamic comparison of the torque ripple between sinusoidal and reshaped currents can be made by operating the drive at low speeds and alternating between modes (Figure 6-6). The same torque demand was present before and after the switchover. Results show this peak output of approximately 1.8Nm was only attained by the sinusoidal system at periods where the instantaneous power of the failed phase (Vc, back emf shown in green) would have been zero – i.e. the deviations in the torque output follow the profile of the failed phase. With reshaping, the torque was significantly flatter and close to the demanded level. As the resulting mean torque was higher, the motor began to accelerate, hence the sudden increasing of frequency post switchover.

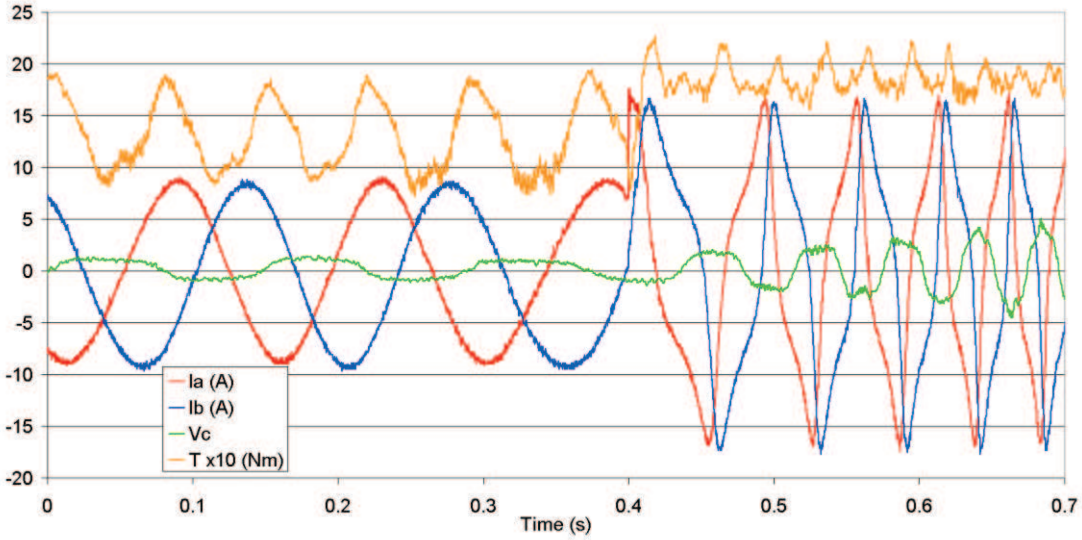

Figure 6-6: Measured results when alternating between sinusoidal and reshaped currents.

6.1.1.3 Drag torque tests

In the case of a motor winding short circuit, fault currents are minimised to 1P.U. by applying a terminal short-circuit. To measure the drag torque resulting from the short-circuit, one phase of the motor was manually short-circuited at the terminals and the motor was rotated by the load machine while torque and short-circuit current were measured. The results of this are shown in Figure 6-7. The motor was operated to 1600r/min, as at this speed the drag torque had reduced to a mean of 0.45Nm from a peak of 2Nm at 200r/min. The short-circuit current becomes speed independent at high speed, with a peak of 28.0A.

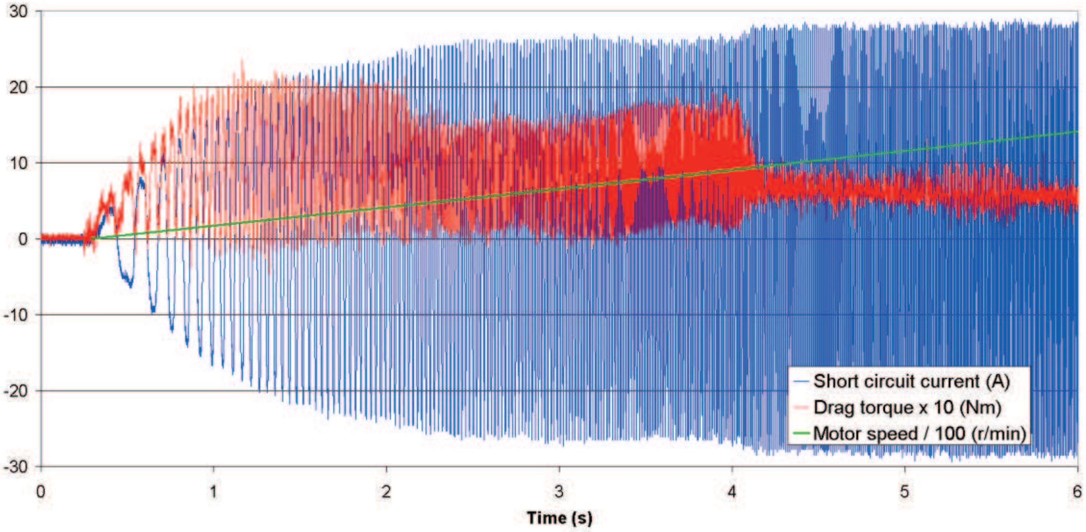

Figure 6-7: DEAWS drag torque and current from a short-circuit winding.

A close-up of the drag torque and short-circuit current waveforms is shown in Figure 6-8. The drag torque is sinusoidal and at twice the electrical frequency, as would be expected from a motoring or braking torque. Measurements and analysis were only performed at low speeds as the bandwidth limitations of the torque transducer and the inertia of the motor will eventually filter the sinusoidal components of the torque.

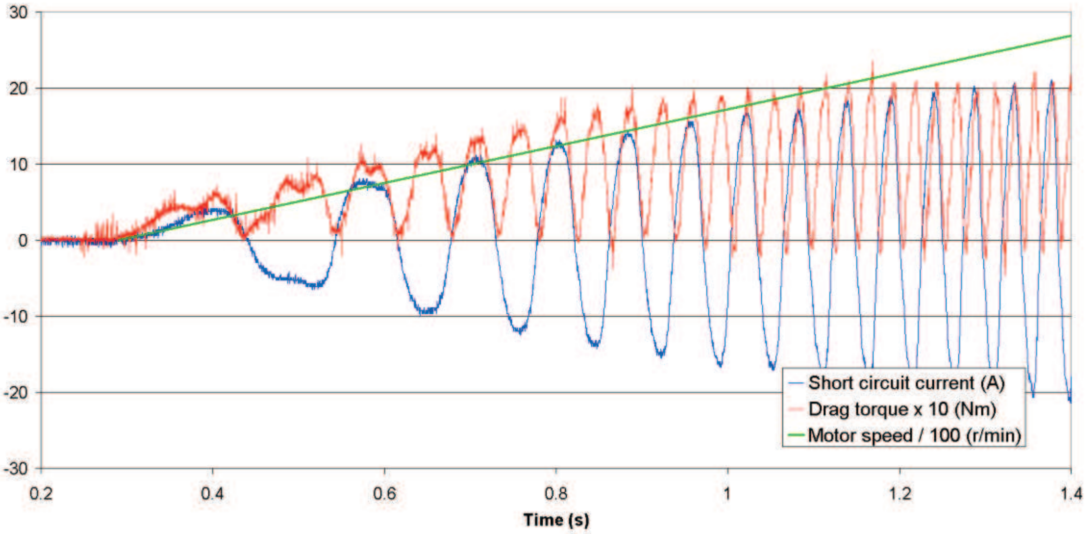

Figure 6-8: Drag torque & current from DEAWS short-circuit winding, close-up.

To test the load performance of the converter when operating with one phase lane short circuit, the maximum rated load of 3.4Nm was applied from the load motor and a start-up was performed from two phases. As the controller was operating on two lanes, the waveforms were automatically reshaped to compensate for a torque ripple due to an absent phase. The resulting torque and the envelope of the phase currents are shown in Figure 6-9.

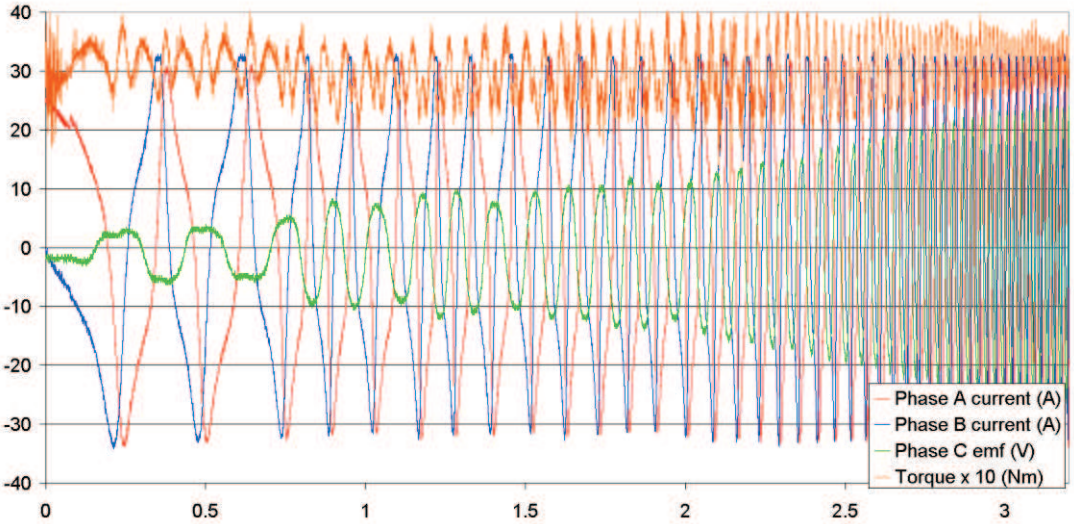

Figure 6-9: DEAWS motor start-up with 3.4Nm load and 1 phase short-circuit.

The controller was operated in torque mode, with the minimum demand applied to start and accelerate the motor through the drag torque region, which corresponded to a peak reshaped current of 33A, close to the predicted value of 36.9A given in Table 6-1 (*pp.*136).

As drag torque effects are much lower near standstill, the initial output torque is dictated only by the ability of the reshaped waveforms to overcome torque ripple to provide a mean torque of 3.4Nm. As the phase current amplitudes were fixed by the controller (for constant torque operation), the effects of the drag torque at higher speeds would only be observable through reduced acceleration. It should be re-emphasised that the currents are not reshaped to overcome the sinusoidal nature of the drag torque. With the additional inertia provided by a complete actuator, it is expected that the inertia of the system will be sufficiently high for only the mean drag torque to be overcome. Additionally, if desired, the reshaped currents could revert to sinusoidal waveforms once sufficient speed is attained in order to reduce peak currents in the power devices.

6.1.2 DEAWS Industrial test setup

The industrial test-rig for the DEAWS project was designed and constructed by Comar Engineering Services and resides at FR Hi-TEMP (now Eaton) in Titchfield (Figure 6-10).

Friction loading was considered initially, but as an actual flap will experience considerable aiding loads, an active hydraulic system allowed aiding and antagonistic loads. Using PC control, representative load profiles can be applied.

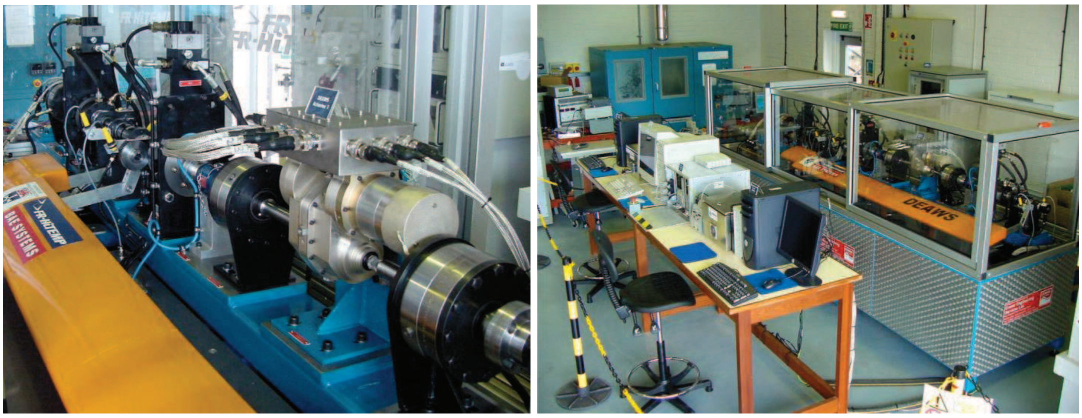

Figure 6-10: Photographs of the DEAWS actuator (l) and the DEAWS test rig (r).

Loading a flap with representative aerodynamic loads will require a hydraulic rig capable of up to 20-30kNm, which would require excessively large hydraulics. Instead loads were applied to the output shafts of the DEAWS actuator (at the output of the 37:1 gearbox), bypassing the 318:1 flap gearbox and mechanism, but reducing the loading torque accordingly. Miniature 318:1 gearboxes were included to allow movement of an unloaded, visual representation of a flap arrangement, providing a flap position signal via LVDTs and RVDTs which was fed back to the motor controllers.

A crucial element of DEAWS is the ability to demonstrate symmetry between flap surfaces. To demonstrate this, the test rig consisted of two full actuators, representing actuators on the outboard flap of either wing. To reduce test-rig complexity, one actuator featured only a single-sided output drive to a half-flap. Representative load could still be applied to the half-flap and it offered the same actuator functionality as the full flap, other than an ability to demonstrate skewing. The complete flap test arrangement is illustrated in Figure 6-11.

It should be re-emphasised that while the two control electronic boxes reside outside the test unit, a flight standard actuator would feature all electronics within the junction box on the housing.

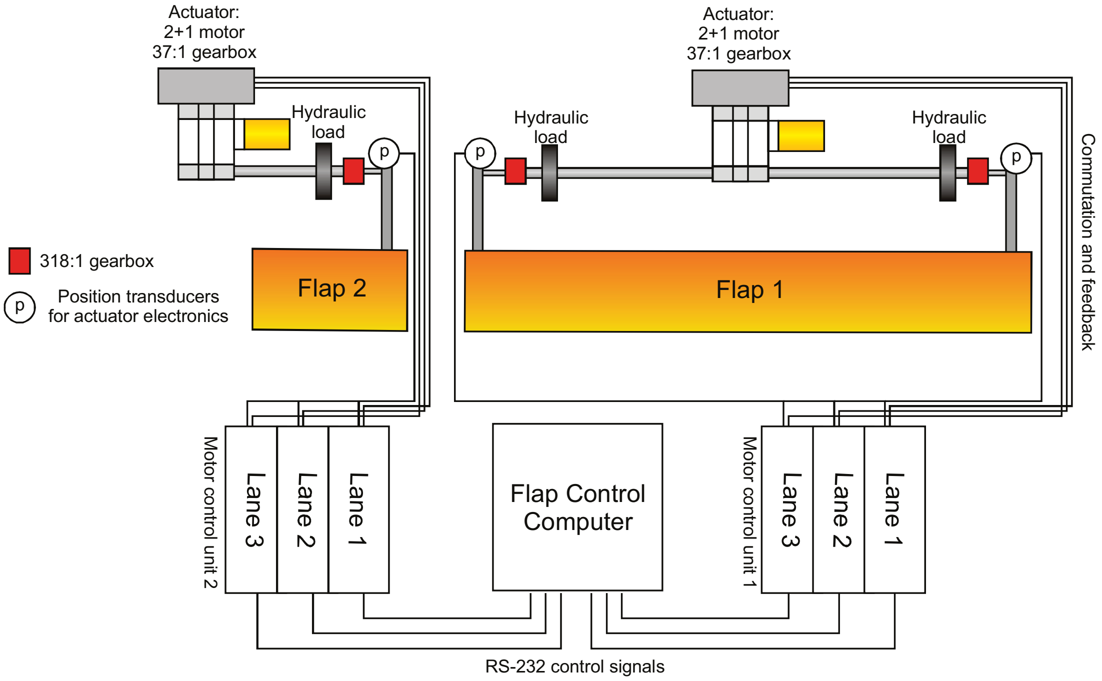

Figure 6-11: DEAWS industrial test rig configuration.

The Flap Control Computer is designed to control a real flap mechanism; hence position demands in the tests were issued for deployment angles of an actual flap. As DEAWS uses a rotary flap mechanism, with position feedback sensors on the 318:1 gearbox outputs, a non-linear look-up table converts the flap demands into rotary angles (see Figure 4-24, *pp.97*). The relationship between the rig angle and an actual flap arm are shown in Figure 6-12.

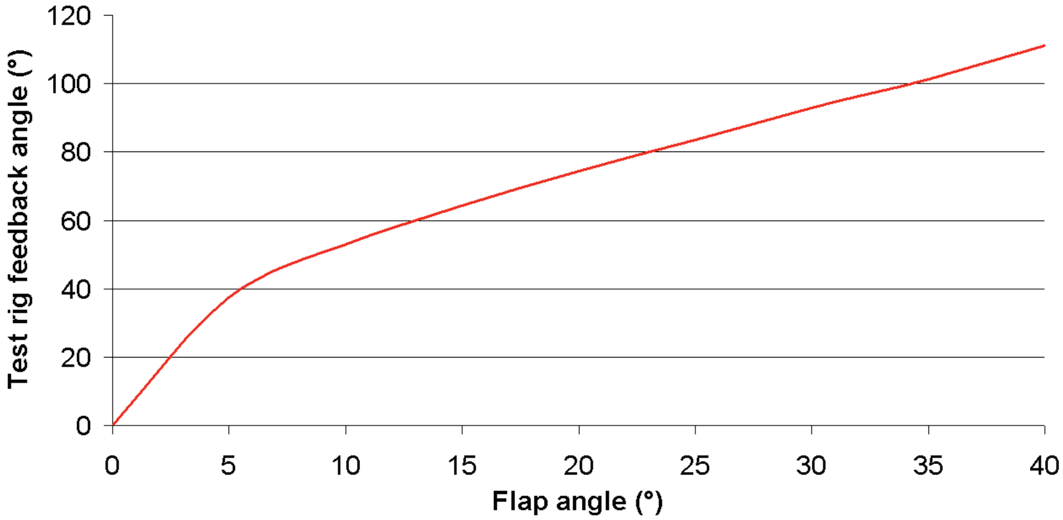

Figure 6-12: Relationship between test rig arm and actual flap,

Data from test rig results was recorded with independent transducers on the hydraulic loading system, using software integration to calculate the flap angle downstream of the 318:1 gearboxes. These rig transducers provided verification of the DEAWS position transducers (*see Figure 4-23, pp.96*). Position monitoring data was returned from three locations; each side of the full flap ('1L' and '1R') and the half-flap ('2').

Five sets of results are presented here, showing normal and faulted operation:

- Positional accuracy of the flaps.
- Performance (time to extend, retract and respond to step demands).
- Response under varying loads.
- Symmetry control between flaps.
- Thermal response under long term, repeated duty cycles.

The load profiles for the tests were based on those shown in 2.1.3 (*pp.38*), but scaled as loading was upstream of the 318 gearbox (which is estimated to have an efficiency of 75%). The profiles for the two stations of the outboard flap were used as the actuator was designed for these higher loads. Flap 1 must drive an equivalent load of station 4 on the left side and station 3 on the right. Flap 2 must drive the equivalent load of station 3. Although the actuator on Flap 1 must simply drive the sum of the two torques, applying different loads to each side allowed testing for skewing of the actuator mechanism.

In the worst-case, the actuator on flap 1 will be required to drive a peak torque of 95Nm when the peak sum of loads on the two sides is the equivalent of 22800Nm flap arm loading. At this point the electric motor will be required to output around 3.4Nm, taking into account the 37:1 actuator gearbox and an efficiency of 75%.

6.1.2.1 Full speed slew from end to end

Demanding a full flap extension from both flap surfaces demonstrates the extension time. By disabling symmetry control, the variation in speed between the two, theoretically identical, actuators can be compared.

Prior to recording, the FCC demanded 0º on both flaps to fully retract the surfaces. A full extension (110º) was demanded on both flaps and once at the full extension, the flaps were allowed to settle for a few seconds before being fully retracted to 0º. The test was repeated for a selection of load conditions including faulted operation. Figure 6-13 shows the flap angles for a 30% load condition, where the actuator on flap 1 experienced a total load from both sides of approximately 28Nm at the peak of the load profile. No errors were imposed on the system for this test.

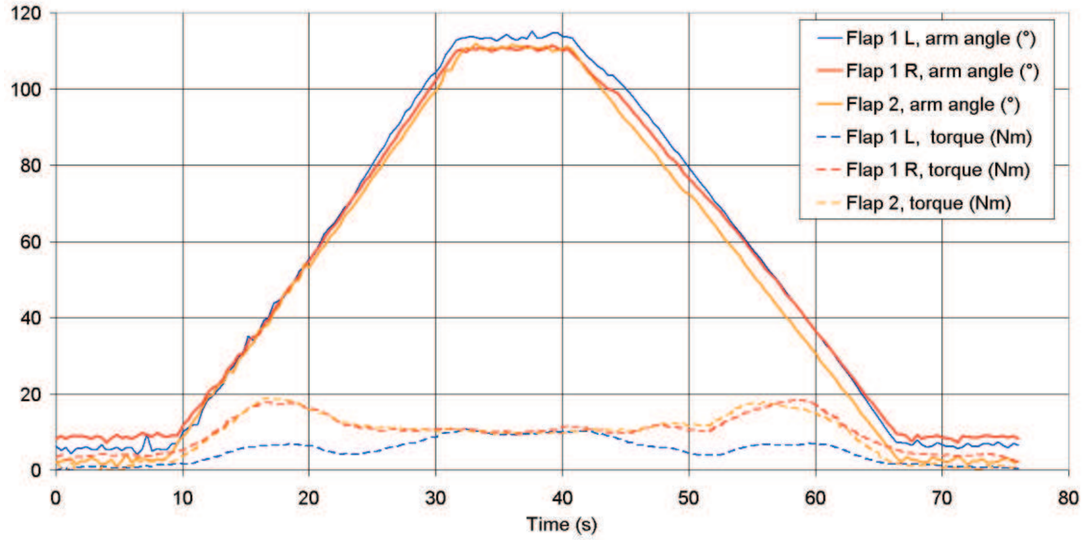

Figure 6-13: Extension and Retraction. 28Nm peak load, no symmetry correction.

Even without symmetry control, the arms of the two flaps moved together and remained reasonably close, although the settling angles varied by more than the allowable 5% (5.5º arm angle) (*see section 2.1.2*). As a representative flap load profile was applied, the torque varied across the range of movement, although the arm angles did not reflect this variation which implies good torque/speed control.

The grouping of the position signals was significantly worse at the retracted position. For the two sides of flap 1, this would imply an unacceptable level of skew across the flap. From investigation, the variation was attributable to extreme levels of backlash in the 318:1 gearboxes between the actuator output and the flap arms. Although a failing of the test rig, rather than the actuator, the backlash proved more of a problem for later positional accuracy tests than for extension and retraction times.

The flap extension times under the various loads are shown in Figure 6-14. Results were taken for both flaps and also for the full flap ('1') with one electrical lane disabled to operate the motor from 2 phases.

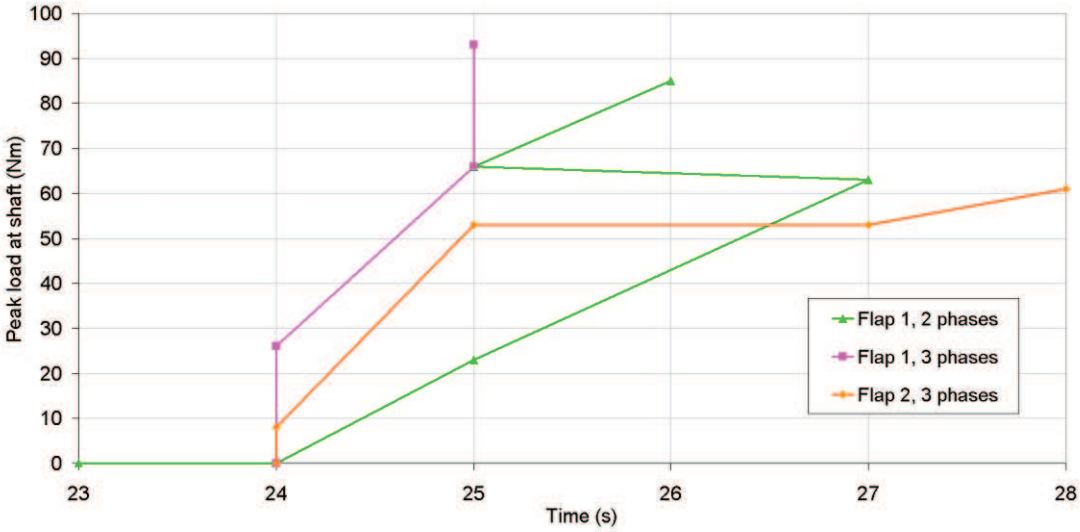

Figure 6-14: Extension time of flaps under varying loads.

Flap 2 showed a slightly greater variation in extend times than flap 1. On post-test analysis this was believed to be due to different speed-loop control parameters – the integrator scaling (K_i) being larger in the flap 1 controller software at the time of testing. Flap 1 operating on two or three phases showed the smallest variation in extend times, although one spurious 27 second extension was recorded when operating on two phases. Results were collated over a period of days, with minor adjustments and test condition variations forming possible causes for the seemingly random jumps in some of the traces.

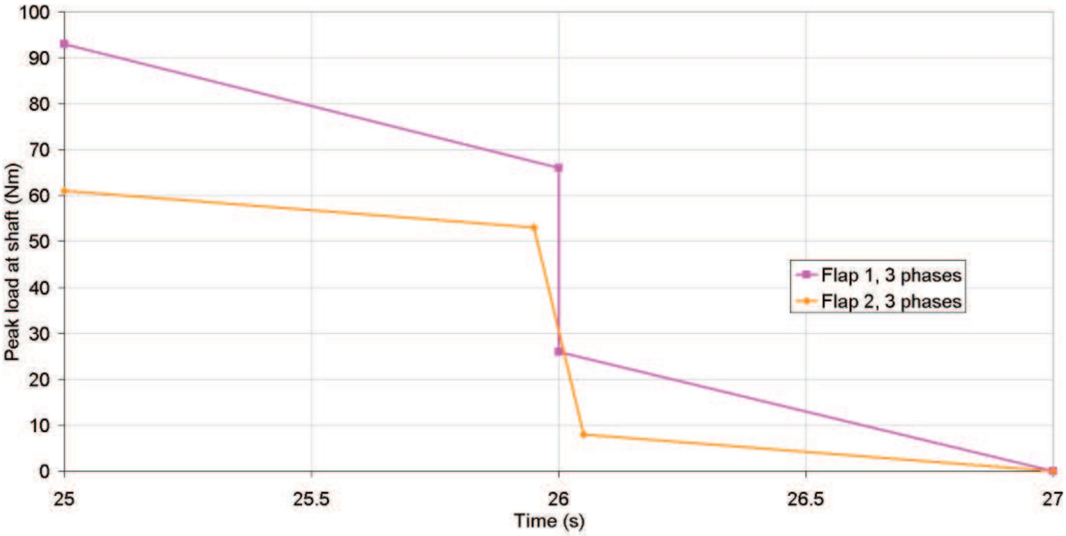

Figure 6-15: Retraction time of flaps under varying loads.

Figure 6-15 shows the retract times for the various loads, although data was only complied from the three phase conditions for both flaps. Where both flap readings were taken at a particular shaft load, the time variations were minimal. Retract times can decrease with higher shaft loads as the aerodynamic forces are assisting the flap on retraction (i.e. attempting to push the surfaces back into the wing). The actuators are operating in a regenerative mode, dissipating the assisting power into dump resistor banks.

The target extension and retraction times were both 22 seconds (*section 5.1*), based on gearing ratios and the motors operating at 10,000r/min. Although the recorded extension and retraction times were within the 30 seconds permitted in the initial specifications (section 2.1.3), there were still significant deviations from the target. In retrospect this can be attributed to inadequate tuning of the software control loops within the controllers, resulting in a failure to meet the demanded motor speeds.

6.1.2.2 Step position demand

By demanding a series of positions in 5º stages, the step response of the actuator was noted. Once each angle demand was reached the actuator applied the friction brakes and switched off the motor. To reduce the effects of backlash, the test was performed in one direction. Results were obtained for the full flap (‘1’) to show the variation between transducers on both sides. The maximum flap load profile was applied with a peak sum of 95Nm.

The position demands were in 5º flap angle steps; however, as the measured rig angles were rotary values and follow a non-linear relationship (*shown back in Figure 6-12*); the demands were transposed into rig angles for the results in Figure 6-16.

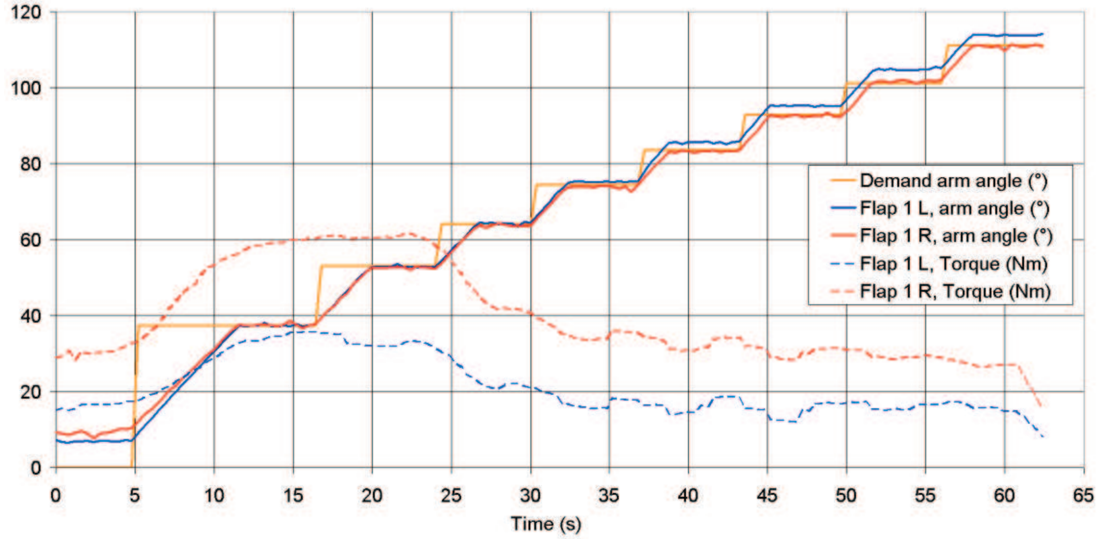

Figure 6-16: 5º step flap angle demands under 95Nm total peak load.

The results would appear slow for a conventional step response; however, this is simply due to the limitation of the maximum rate of flap travel (around 5º/s, set by the 10,000r/min of the motors). Good position holding was visible at each step, suggesting accurate position control to reach the demanded angle and successful apply the friction brakes – which was visually verified at each stage. Unfortunately the unequal and significant backlash of the measurement system remained apparent in the results towards the two extremities of movement, particularly for the left side of the flap. Again, this was a test-rig issue rather than with the actuator and an actual flap gearbox and track mechanism would not suffer such quality issues.

6.1.2.3 Symmetry Control

Probably the most critical test for the flap actuators is proving that symmetry can be maintained, as it is a crucial safety requirement (*section 2.1.2*), with a variation limit of 5% (of full travel) allowed between surfaces. For maintaining symmetry, the worst-case real-life condition is with both flaps loaded, but one actuator operating on two phases due to a fault.

A typical load profile of normal operating conditions (~53Nm peak) was applied and Figure 6-17 shows the extension profiles of the two flaps with symmetry control switched off. Flap 2 was operated using 2 motor phases. A 2 second time delay between reaching the destination angle was visible as the two flaps gradually drifted apart, giving a peak 10º variation in rig arm angle, clearly in excess of the 5% allowed error on 110º of travel.

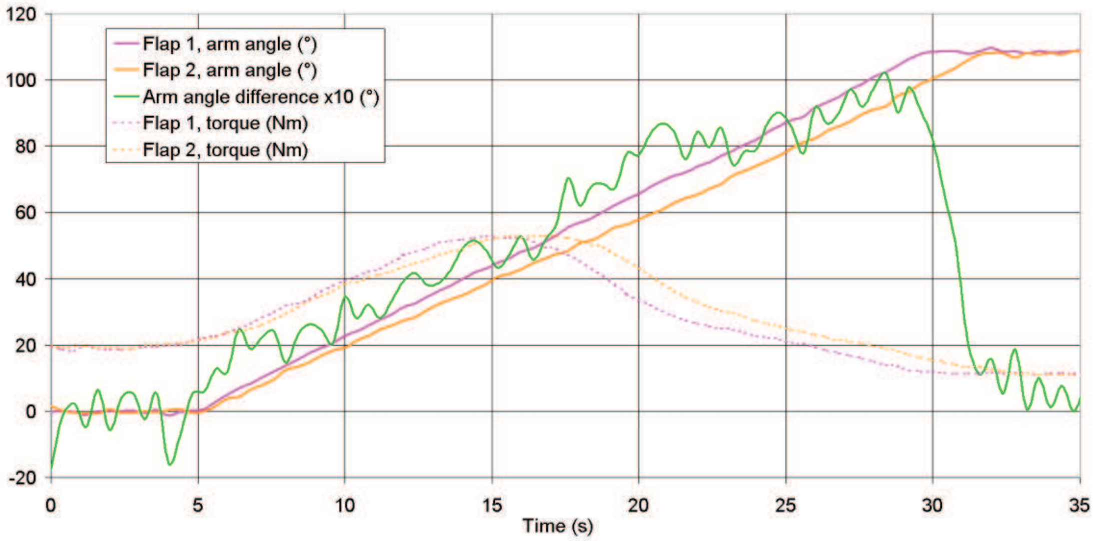

Figure 6-17: Extension of 2 flaps without symmetry control, 53kNm peak load.

For the results shown in Figure 6-18, the symmetry controller in the FCC was switched on and attempting to maintain symmetry. The symmetry controller takes the returned positions from the two actuators and limits the maximum motor speed of whichever flap is nearer the demanded position, allowing the slower flap to catch-up.

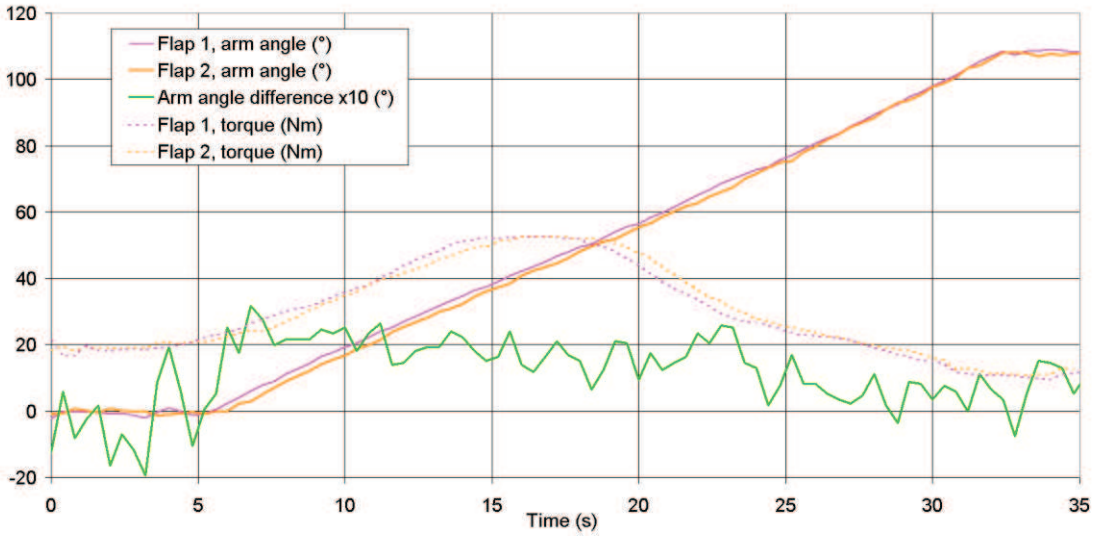

Figure 6-18: Extension of 2 flaps with symmetry control, 53kNm peak load.

Both flaps moved much closer together, with the 3-phase flap (‘1’) increasing its extension time from the previous test to match the faulted flap (‘2’). Even when not considering effects of measuring noise and backlash in the results, the peak variation was around 3º, comfortably within the allowed tolerance.

6.1.2.4 Flap jam

The most severe symmetry test is to jam one of the flaps while performing an extension. In order to prevent uncontrolled movement, the FCC should detect the excessive asymmetry and apply the brakes to all flaps on the aircraft.

To test the jam condition, a hydraulic brake on the test rig was applied to the half-flap (2), midway through an extension. The unloaded condition best demonstrates the symmetry error response as both the flaps will be moving at their maximum speed.

The jam response (Figure 6-19) appeared instant, with both flaps stopping movement at the same point. The torque reading from flap 2 is shown as it highlights the point where a jam occurs. The flap control computer estimated the asymmetry to be within 0.5° for the estimated flap arm angle.

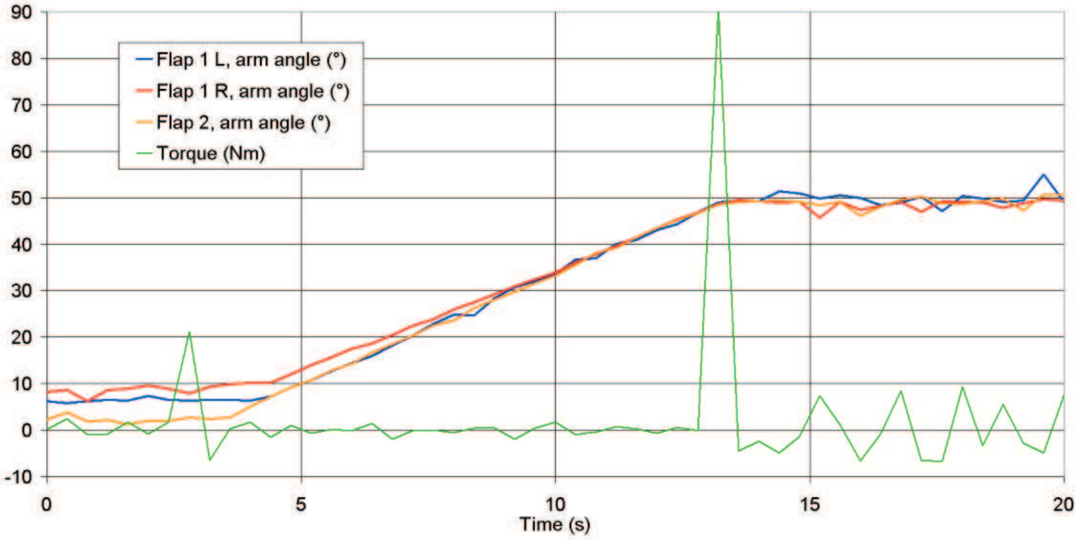

Figure 6-19: Flap 2 jammed at 13s, unloaded.

Unfortunately results were hampered again by backlash in the rig position transducers, which was particularly evident at the initial 0° position. A large degree of noise appeared on the traces after the system applied the brakes, although actual movement was zero as all points were locked by the hydraulic or friction brakes.

6.1.2.5 Communications link failure

A production DEAWS actuator would contain considerably more data links than the demonstrator actuator, as three completely separate power electronic controllers would be used for each motor, with processors communicating via isolated links (*see 4.1.5*). Although inter-drive links are not physically present on the single DSP test system, the three communications links from the FCC to each virtual drive within an actuator can be tested. As data is cross-compared between the three lanes for signal fault tolerance (*section 4.1.5*), loss of one signal channel should have no noticeable effect. This was the case when tested, so for a visible demonstration of the communications links, one serial link to Flap 2 was removed prior to testing and then a second unplugged mid-extension. The same 30% load as in 6.1.2.1 was applied.

As Figure 6-20 shows, at the point of the second link removal (around 15 seconds) both flaps halted immediately. As the cross-comparison system cannot generate a 'true' value from one out of three variables, the lanes disable and send a fault signal back to the FCC, which immediately shuts down the entire system (both flaps) with the power-off brakes. Unfortunately the rig transducers suggested noticeable asymmetry at the point of failure; however, the FCC measured a peak of only 0.5º asymmetry from the actuator sensors, so the error was attributed again to the backlash on the actuator gearboxes and sensors, rather than the control response.

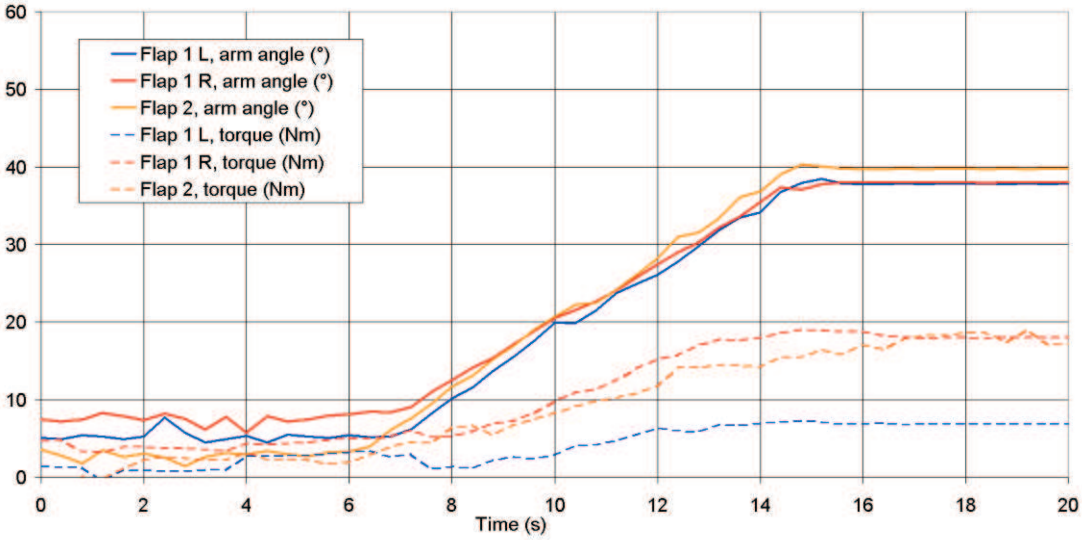

Figure 6-20: Removal of 2 serial links.

6.1.2.6 Endurance Testing

An endurance test was necessary to determine the thermal performance of the system under a realistic performance duty-cycle, although the system must also be able to cope with the worst-case load conditions. A composite load profile was therefore applied to the demonstration flap system, consisting of a typical extension load, with 7 spoiler-extension loads overlaid, which are 3.5× the normal extension torque, but only for 20% of the overall duty cycle. The 3.5× loads were spread across the extension profile as a series of spikes to even out the loading and to exercise the ability to cope with sudden load changes. The resulting load profile is shown in

Figure 6-21. As in previous tests, the test rig applied different loads to the left and right sides ('stations') of flap 1 and the greater of these loads was also applied to flap 2.

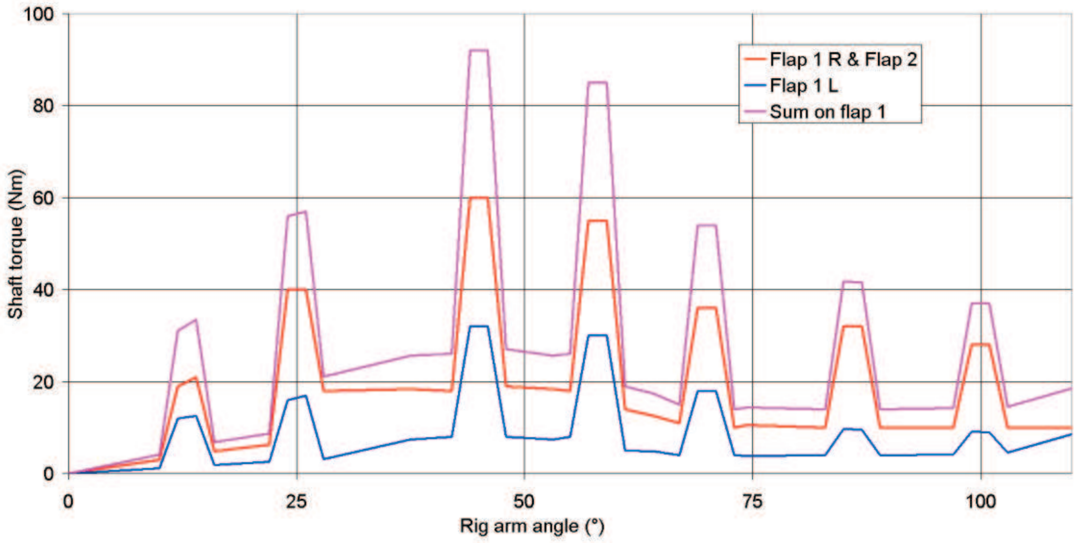

Figure 6-21: Load profile for duty cycle thermal test.

The load profile was applied repeatedly to obtain a thermal profile of the system and Figure 6-22 shows the two minute duty cycle, with an extension, pause, retraction and then a 60 second delay.

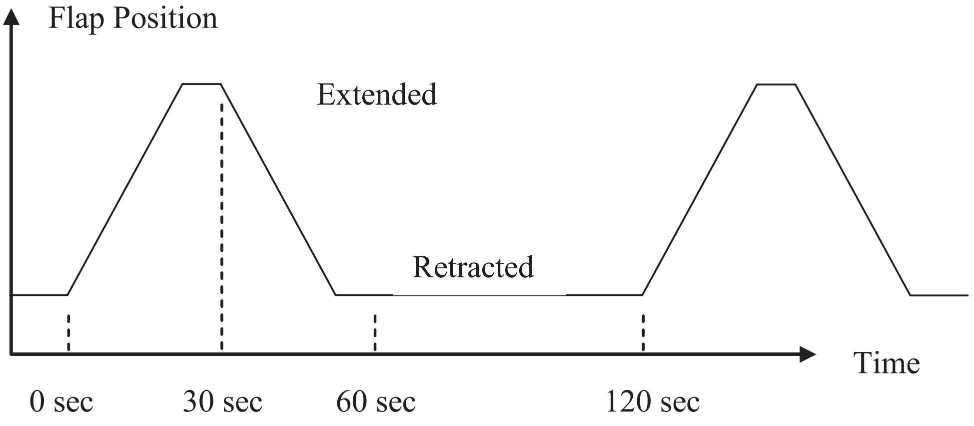

Figure 6-22: DEAWS duty cycle.

Twenty five of the two minute load cycles were run consecutively and thermocouples inside the two actuators monitored the winding and iron temperatures. Flap 2 was operated by two phases to monitor any effects of operating in the reversionary mode and to see the thermal transfer to the dormant phase (U).

The results are shown in Figure 6-23. Midway through the tests flap 2 suffered a failure of a motor drive dump resistor bank, but the tests were allowed to continue with the motor disabled as it demonstrated the cooling profile of the system.

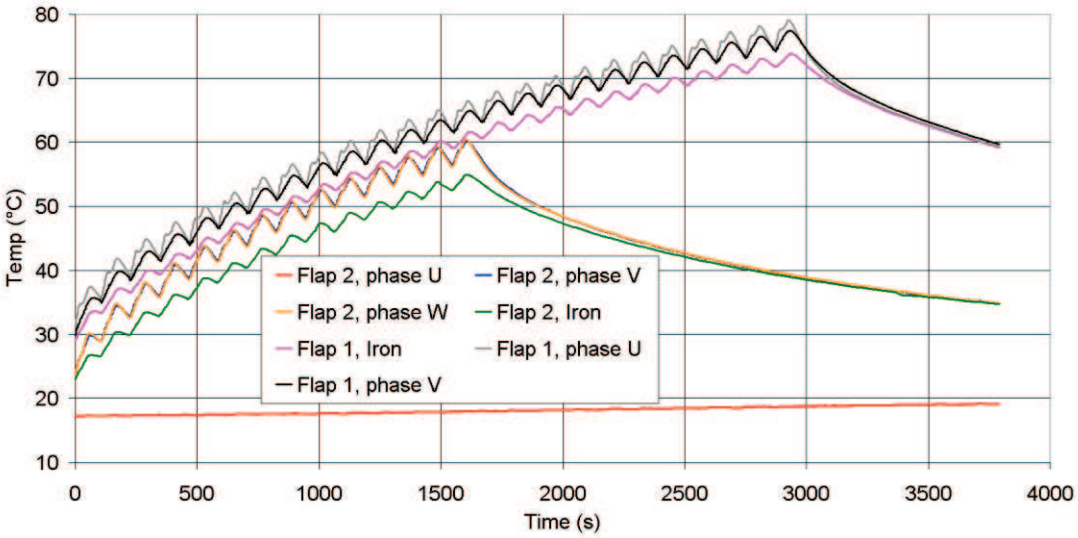

Figure 6-23: Thermal profile from DEAWS duty cycle testing.

The results show typical thermal curves and extrapolation predicts that flap 1 will reach steady-state around 90°C. Each spike on the curves was due to the short-term heating of the load profile. The minimal heating of dormant phase U on flap 2 highlighted the successful thermal isolation between motor windings of the fault-tolerant motor.

6.2 ELGEAR NWS TESTING AND RESULTS

A key difference between DEAWS and ELGEAR testing was that the nose wheel steering could be fully tested as a stand-alone item – for performance testing there were no requirements for multiple landing gear actuators to be tested simultaneously.

There were three parts to testing, all conducted by the author:

- Initial testing of motor and drive-electronics at Newcastle University.
- Unloaded testing of completed actuator at Goodrich Actuation Systems, Wolverhampton.
- Hydraulic load testing of completed actuator at Airbus, Filton.

Using a dynamometer test-rig at Newcastle, the fault tolerant motor was loaded with representative loads of the final system, including varying profiles. Without the actuator, the only control-related aspects that could not be tested were the clutch solenoid and the position feedback (although the latter could be simulated by counting motor revolutions).

The majority of the results presented were performed at Newcastle on a dynamometer rig, using a torque transducer and an induction motor load (Figure 6-24), although results at Goodrich and Airbus are described subsequently.

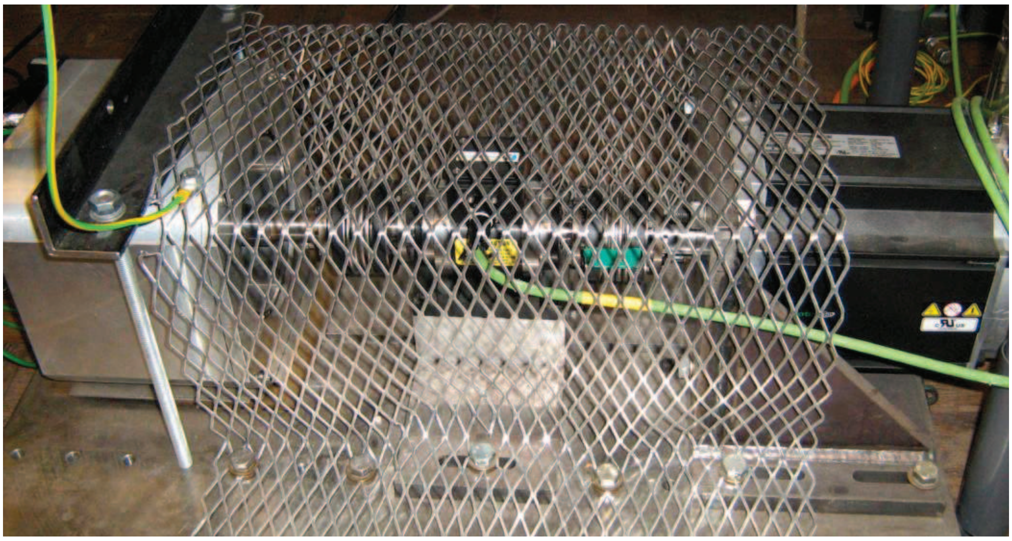

Figure 6-24: ELGEAR motor (left) on laboratory dynamometer.

The completed actuator is shown in Figure 6-25, at Goodrich initially (left) and finally at Airbus (right).

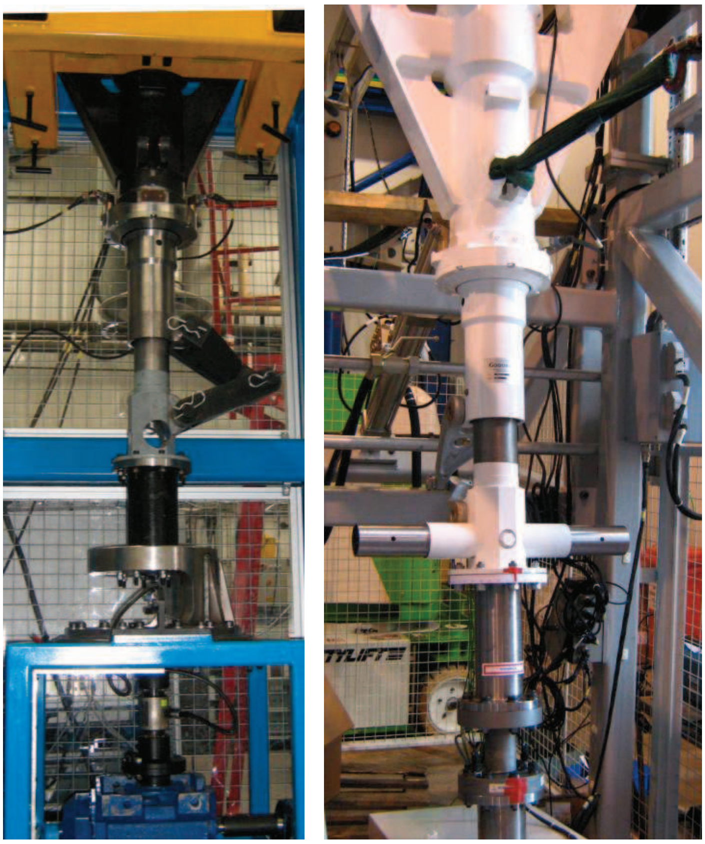

Figure 6-25: Photograph of ELGEAR actuator at Goodrich (l) and at Airbus (r).

6.2.1 Newcastle University tests

A large suite of approval tests were performed on the MCU and a test motor at Newcastle. From the ELGEAR specification (*see section 2.2.3*) the peak actuator load is 7000Nm and taking the 596:1 gearbox into account, with a predicted efficiency of 70%, this results in a 17Nm load on the output shaft of the test motor. Operation was repeatedly tested at this torque for a variety of test conditions and at a variety of operating speeds, including some in excess of the required load/speed profile.

However, for the results presented in this section the test motor was operated to represent an actuator load of 5000Nm at 10º/s, corresponding to 12Nm, 1000r/min at the motor. The loading system offered better stability in this less harsh condition, enabling better analysis of performance. Evidence of operation at full torque can be observed in the Airbus tests (*section 6.2.3*).

Control signals were input using the debugging interface described in section 5.2.2.3. The controllers were configured in software to operate in speed control mode, unless otherwise stated.

6.2.1.1 Back emf test

As with DEAWS, establishing that the back emf of the motor was within specification was important in verifying all subsequent loaded testing. The motor was driven by the loading system and operated at 1500r/min (the maximum speed available from the induction machine load). The back emf was measured phase-phase from two output terminals and results are shown in Figure 6-26.

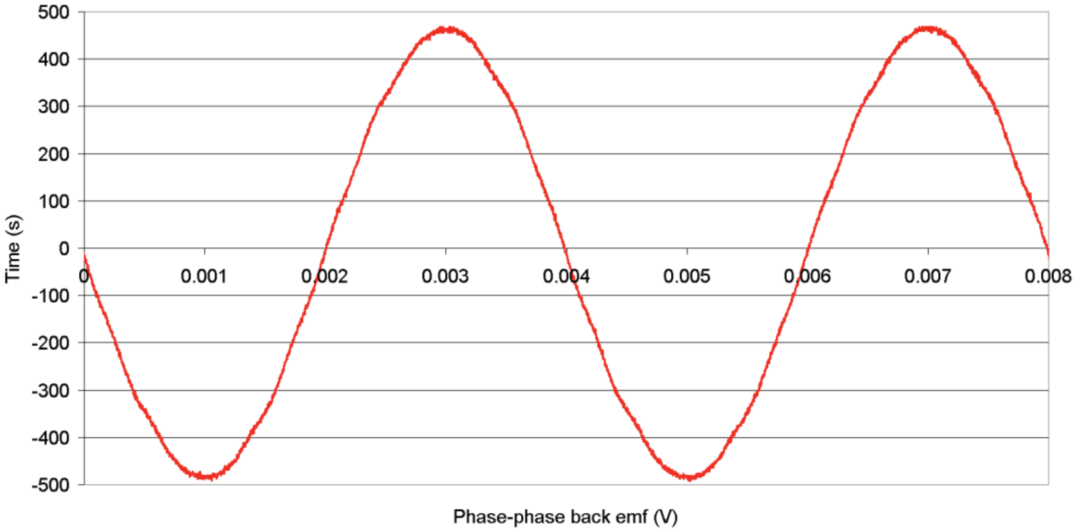

Figure 6-26: ELGEAR back emf at 1500r/min.

A peak of 465V was measured and with the electrical frequency at 250Hz this corresponds to 0.31V per r/min. This is 1.12× the 0.27V per r/min predicted in section 5.2.1. When measured with an LCR bridge, the phase inductance was 23mH and the phase resistance 3.0Ω.

6.2.1.2 Lane failure transient response

The response of the motor drive electronics to the switch-off of a winding set is demonstrated in Figure 6-27. At around 0.3 seconds lane B was instructed via the PC diagnostics interface to switch off all output phases. There is no specific software mechanism for handling the loss of a winding set. Instead the speed controller in Lane A inherently compensates for any resulting drop in speed by increasing the torque output. After a dip of nearly 200r/min, the speed returned to 1000r/min after ~0.5 seconds. The response time of the NWS can be potentially improved by adjusting the settings of the 1kHz speed control loop, which can output up to 15A of current (equating to nearly 40Nm of torque), for a much more severe acceleration, although this is restricted for mechanical and thermal reasons. As there are no formal requirements for recovery time after a fault, the system is considered acceptable if the settings allow it to achieve frequency response requirements (*section 6.2.2.2*).

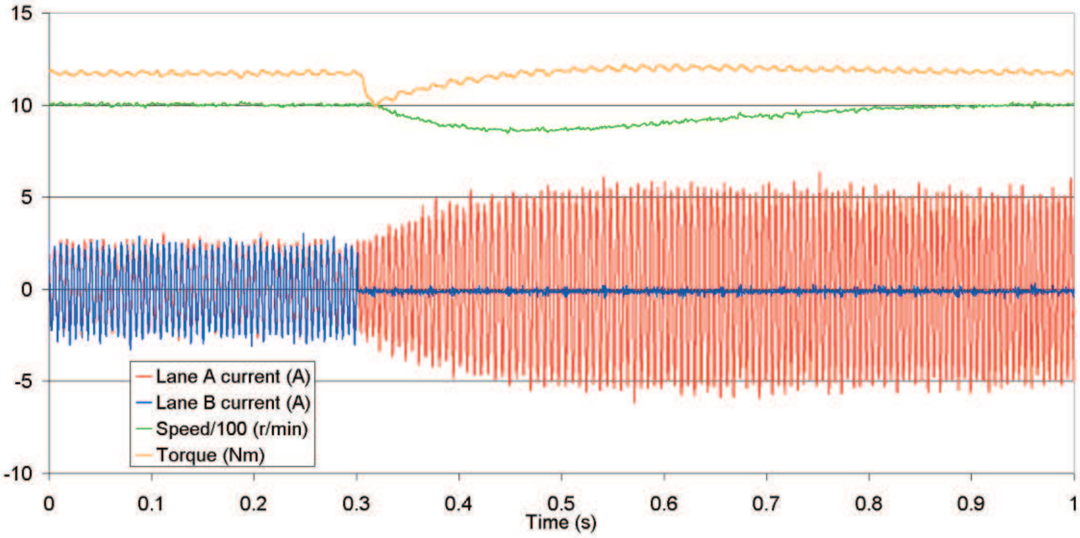

Figure 6-27: NWS response to an electric drive lane switch off, with 12Nm load.

A close-up view of the lane switch-off is shown in Figure 6-28. The currents for lane A and lane B were measured by hall-effect probes on the corresponding 'U' phases of each motor half and therefore due to magnetic symmetry, should be in phase at all times. This is evident from the trace, prior to switch-off. At switch-off the amplitude of lane B falls to zero immediately and A begins to ramp up.

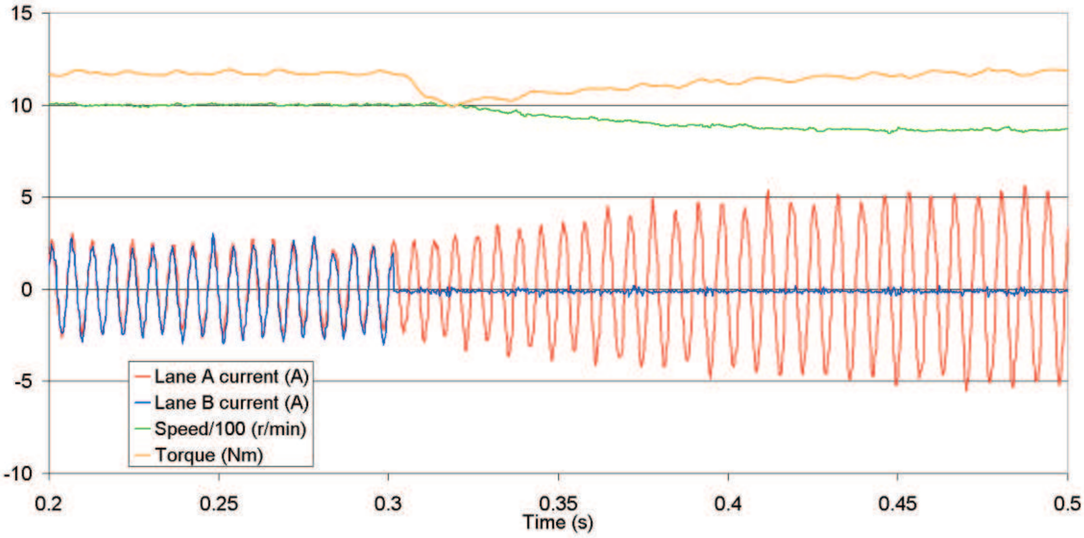

Figure 6-28: Close-up of 2 lanes after switch off of B at 0.3 seconds.

For a condition more representative of an aircraft-level failure, the 540V supply to lane A was unplugged for the results shown in Figure 6-29.

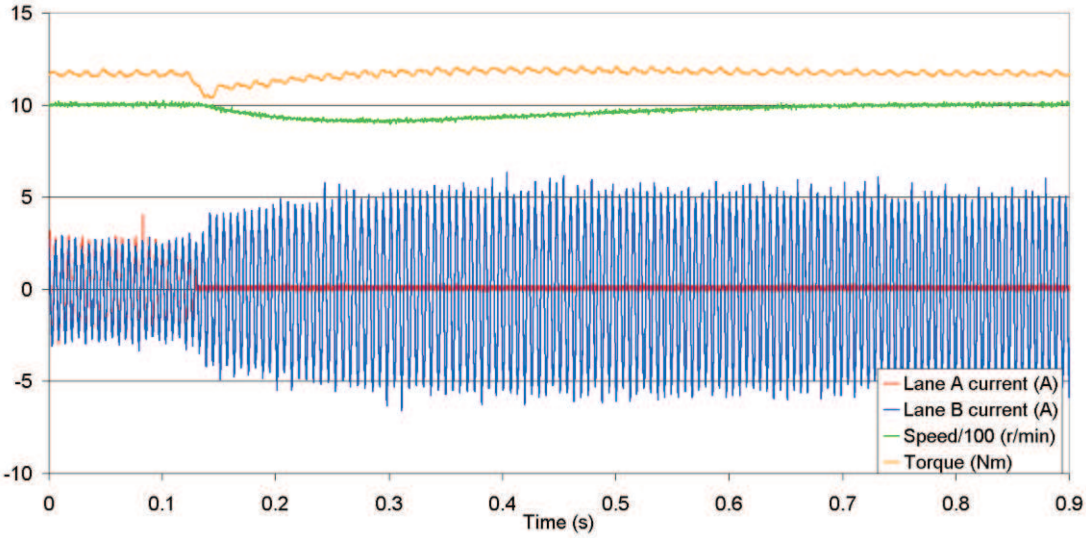

Figure 6-29: Step response after removal of DC supply to lane A, with 12Nm load.

As expected, the results were almost identical to the software switch-off, although the torque and speed variations appeared slightly less, suggesting a softer change in response. The much shorter time base of Figure 6-30 reveals the subtle differences.

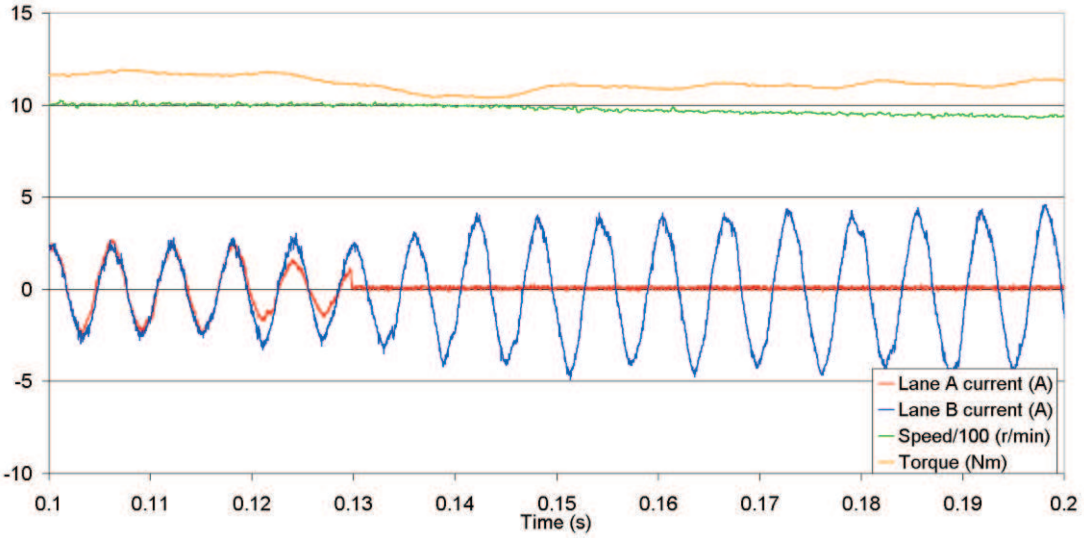

Figure 6-30: Close-up of lane A disconnection.

Although the point of power supply removal was not recorded, the fall in current magnitude of lane A and corresponding increase in lane B can be witnessed around 0.12 seconds. With a supply unplugged, the drive will continue to operate post-fault until the polypropylene capacitor voltage falls to 400V, at which point the motor is switched off, with a ‘270V failure’, occurring at approximately 0.13 seconds in the test.

6.2.1.3 Speed step response with two lanes active

For this 'active-active' test, from standstill, a target speed of 1000r/min was simultaneously issued to both lanes (Figure 6-31).

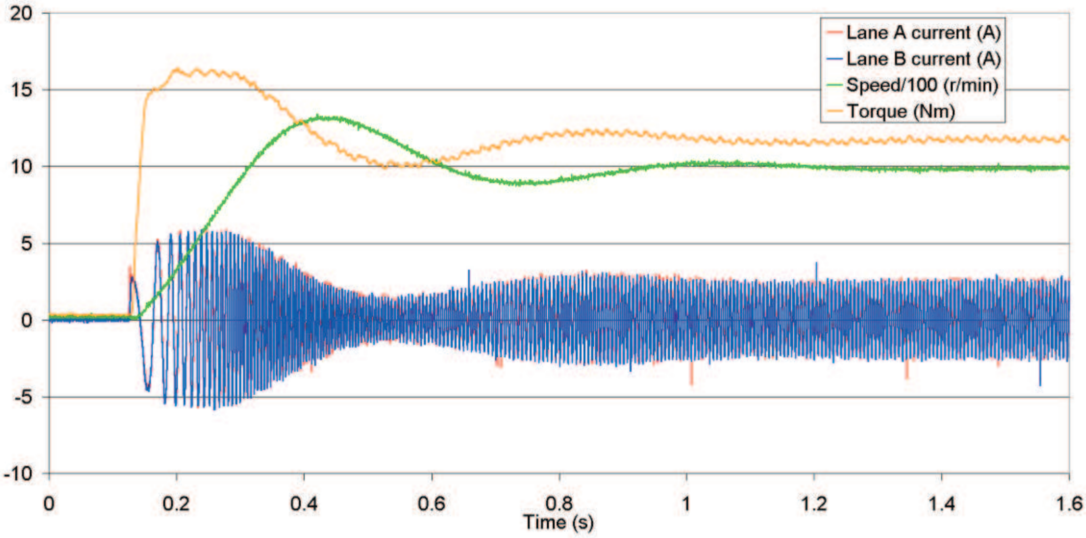

Figure 6-31: 12Nm loaded speed step response with both lanes active.

There are no speed ramps specified in the software, so acceleration is limited only by the controller software current/torque limits. Control loops are tuned to meet bandwidth specifications described in section 6.2.2.2. When an active lane detects another active lane, via the cross-communications, peak winding current is restricted to prevent excessive output torque which could potentially damage the actuator.

With the controllers effectively operating in torque saturation due to the huge speed error at turn-on, both outputted their peak currents, which active-active corresponded to 6A (capable of driving up to 14Nm per lane). The 16Nm initial load torque was a result of the motor fighting the inertia of the load machine and the applied 12Nm load. Despite a notable over-speed, a result of overshoot in the speed PI control software, the motor accelerated to 1000r/min in 200ms and the current envelopes of the two lanes were identical (*see 7.3 for more discussion*). Peak currents were around 2.5A in each lane, which using the predicted torque constant of 2.315Nm/A (section 5.2.1) should correspond to 6.6Nm per lane, or 13.2Nm in total, 10% higher than the measured torque.

6.2.1.4 Speed step response with one lane unpowered

The step response test was repeated for Figure 6-32, but with lane B inhibited ('active-standby'). When lane A receives an inactive status signal from lane B, the output current limit is doubled to 12A. As shown in the previous transient fault-responses, the speed controller will inherently increase current output, should the load increase; however, an increase in the peak torque limit is necessary to allow one lane to drive up to the rated 17Nm load with an acceptable overhead for acceleration of inertia.

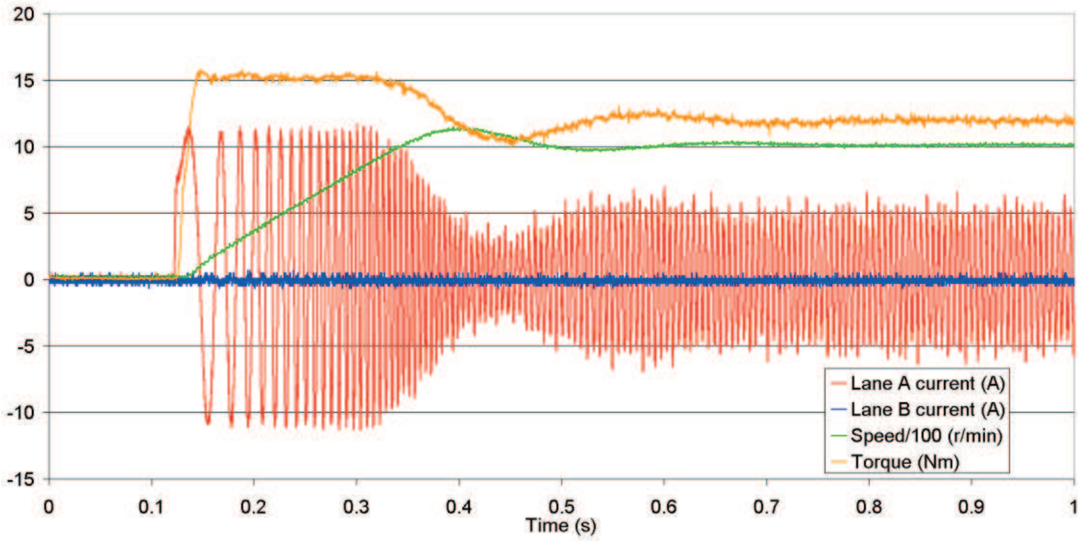

Figure 6-32: 12Nm loaded speed step response with only lane A active.

As a result of the peak current increasing from 6A to 12A, the acceleration of the motor was near-identical to the active-active condition. The speed controller output remained in saturation, demanding the maximum output current until 1000r/min was reached. The peak steady state current was 5A, double the active-active condition, as expected with only one lane providing the torque.

6.2.1.5 Speed step response with one lane short-circuited

To demonstrate the drag torque effects of a shorted winding set, prior to power-up the motor windings for lane B were disconnected and all three phase terminals were shorted together. A current probe remained on the U phase of the shorted lane to display the short circuit currents (Figure 6-33).

With a shorted lane, the speed stabilisation and acceleration times were substantially longer than the ‘active-active’ and ‘active-standby’ conditions, with the motor taking 400ms to reach 1000r/min. Again, the output current saturation limit of 12A could be increased to improve the acceleration; however, with no formal requirements for operation with a shorted winding set, the system performance can be considered acceptable.

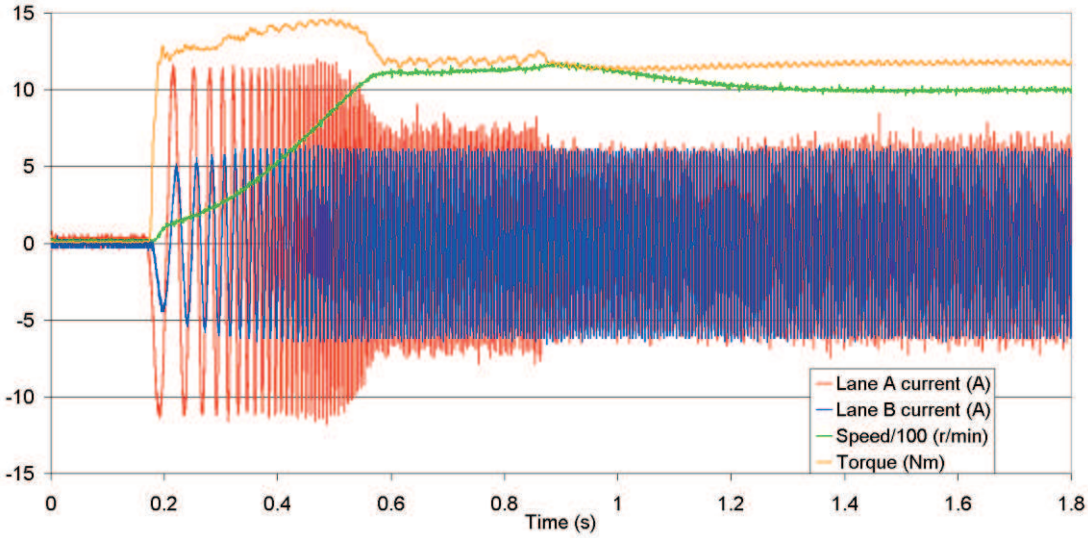

Figure 6-33: 12Nm loaded speed step response with lane B short circuited

Based on the drag torque predictions in section 5.2.1, at around 100r/min the active motor lane should require a peak current of 1.4× the 5A required in active-standby test in order to drive the 12Nm load and overcome the peak drag torque. This was not apparent in the results since the controller was in current saturation throughout acceleration to 1000r/min. Instead a non-linear acceleration profile can be observed, where the rate of acceleration increases at higher speeds as the effects of drag torque reduce. It can also be observed that the steady state current requirement has risen slightly over the active-standby test. From predictions, the drag torque should be around 3Nm at 1000r/min, corresponding to a 1.25× increase over the active-standby value of 5A, requiring 6.25A which ties in with the currents observed.

Figure 6-34 shows a close-up of the acceleration section of the waveform.

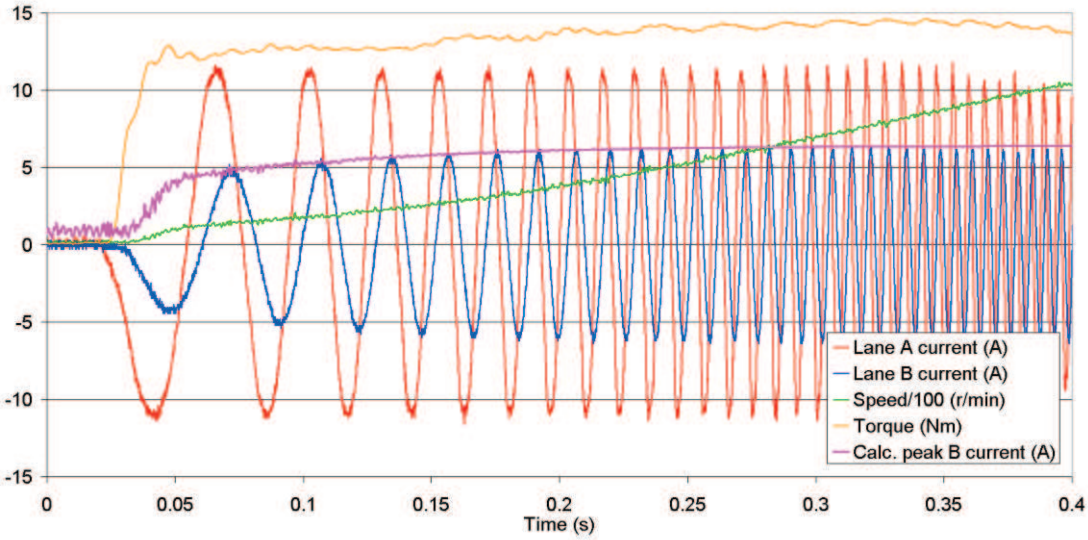

Figure 6-34: Close-up of 12Nm loaded speed step response, showing short-circuit current of B.

The peak short-circuit current in lane B (purple) is a predicted value, calculated by taking equation 3-14 (*pp.54*) for the voltages within a short-circuited winding and re-arranging in terms of *i*:

$$i = \sqrt{\frac{\omega_e^2 k_e^2}{\left(R^2 + \omega_e^2 L^2\right)}} \tag{6-1}$$

Measured values of k_e= 0.296V/rad/s, R= 3.0Ω and L=23mH were used and the value of ω_e was obtained from the speed measurement of the load rig (green trace). Despite the effects of low speed noise in the speed measurement, the measured short circuit currents follow the predicted values closely.

As the speed increases, the resistive term becomes negligible and the current profile tends towards:

$$i = \frac{k_e}{L} \tag{6-2}$$

This predicts a constant peak short-circuit current of 6.43A at higher speeds, tying in with the measured value of 6.1A.

6.2.1.6 Thermal duty cycle tests

To test the thermal response of the actuator a repeatable duty cycle was devised by Goodrich, based on worst-case data from Airbus. A target of 50 minutes continuous taxiing, with the steering loaded at all times, was set. A composite motor load profile was applied, consisting of 7Nm, 11Nm and 13Nm loads over 150 seconds (Figure 6-35), repeated 20 times, or until the actuator failure.

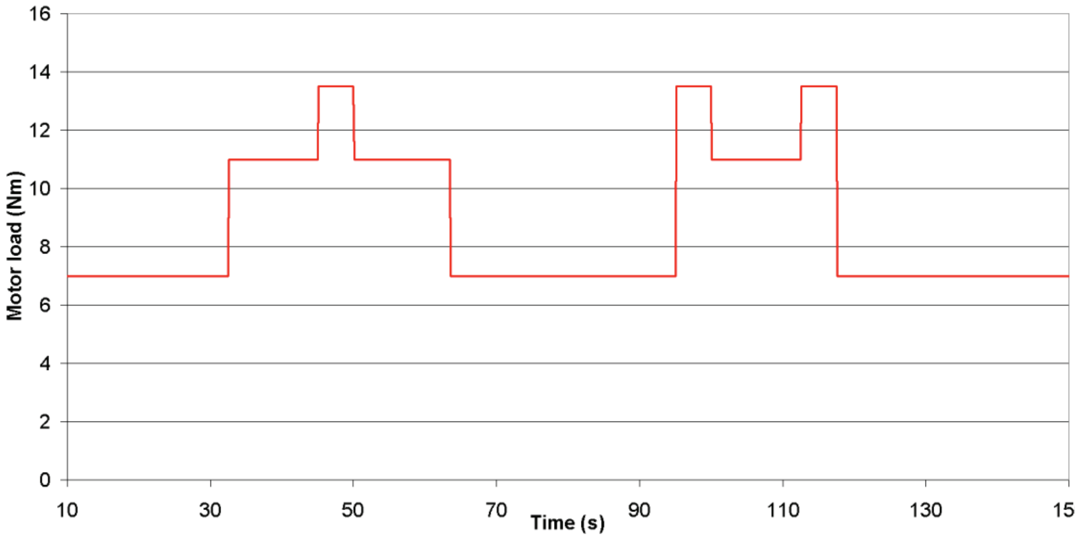

Figure 6-35: ELGEAR duty cycle.

The motor was operated with a maximum speed 1400r/min, above the required torque/speed profile, but specified by Goodrich to test the speed and torque over-rating margins of the drive.

The test was performed three times at Newcastle, firstly with both controller lanes active, then with one side unpowered and finally with one side short-circuited at the motor terminals. Motor temperatures were recorded with thermocouples on the end windings of an equivalent phase of each lane and the controller IGBT temperatures recorded using a thermal camera, focusing on the device casings.

Tests were performed on a test motor and the prototype controller which was ultimately delivered to Airbus. The controller was bolted to a heatsink of 200×300×50mm for the tests, as the original 10mm aluminium base plate was considered insufficient for continued operation over 20 minutes and the controller will ultimately be bolted to a metal airframe in an aero application.

The motor thermal profile is shown in Figure 6-36.

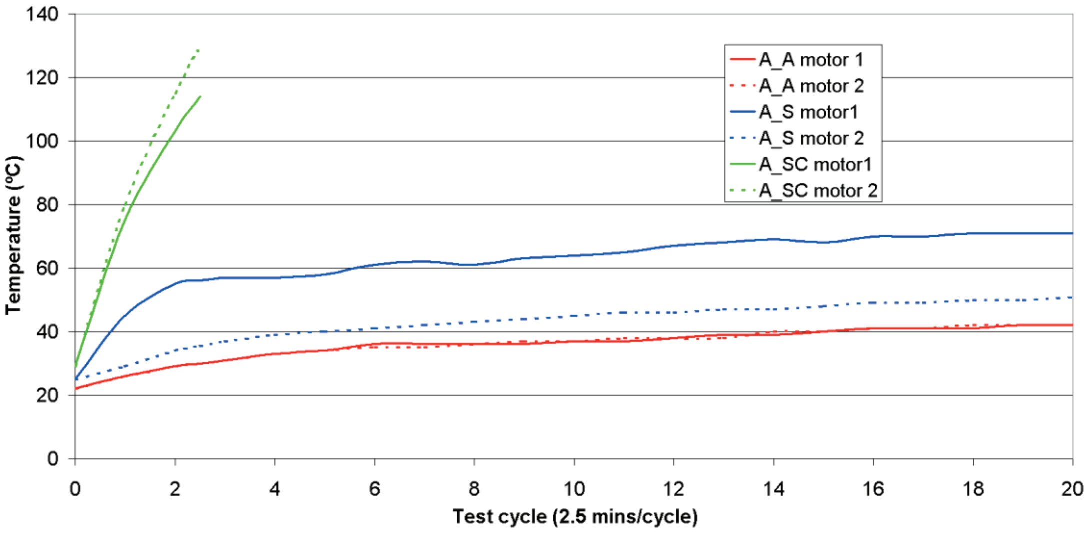

Figure 6-36: Thermal response of ELGEAR motor to a repeated duty cycle.

The A_A traces show both motor sides active and heating by an identical amount. A temperature rise of 20°C was measured after 50 minutes.

The A_S traces show motor 1 active and motor 2 in standby. The active phase was hotter, as expected, although only experiencing a 46°C rise after 50 minutes. It can also be noted that the temperature of the standby phase increased by 26°C. This may be partially attributed to the end winding overlapping of the two motor phase sets and the resulting heat transfer.

The A_SC traces show motor 1 operating and motor 2 short-circuited at the terminals. This test was aborted after 6 minutes as the heating was excessive and potentially damaging to the insulation of the test motor. A target of 20 minutes operation was desired for this condition, so either a higher temperature insulation, improved motor design or improved heat transfer method are required to fulfil this, if prolonged operation is required at the test conditions.

The short-circuited motor experienced a greater heating effect than the active motor, although the tests of 6.2.1.5 show the fault current to be 6.1A - within predictions. The lower temperature of the active lane can be attributed to the mean torque of the profile being 8.5Nm and only 2.5Nm of drag torque at the test speed of 1400r/min. This requires a peak current of only 4.8A to drive the motor.

The IGBT temperatures for the same tests are shown in Figure 6-37. The results correspond with the apparent trends in the motor temperatures, although the initial rise was sharper, but the following gradient more shallow. The active-active condition registered a transistor short-circuit failure around 17 cycles, although this was immediately reset by the operator, assuming an nuisance trip; however, the controller appeared to be heating up much faster subsequently, suggesting damage.

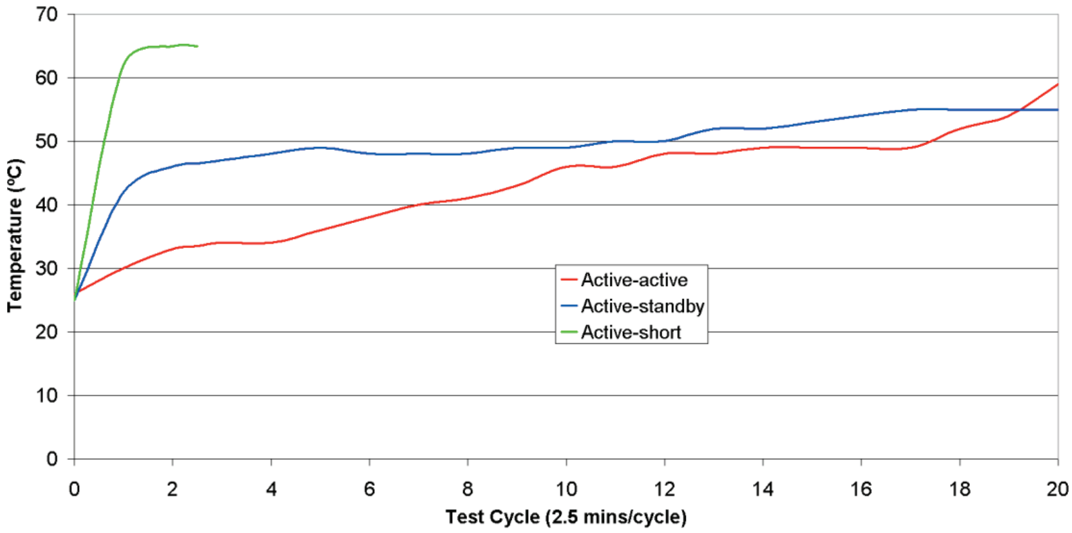

Figure 6-37: Thermal response of ELGEAR Lane A IGBTs to a repeated duty cycle.

In the active-short-circuit test the controller appeared to overcome the initial 40°C rise after 2 test cycles; however, conclusions on the thermal profile could not be made due to the limited scope of the results. With no formal Airbus requirements for operating with a short-circuited winding set, it was not deemed a high priority to improve the motor to obtain a longer operating interval.

Later discussions with Airbus suggested the thermal tests were overly-harsh and it was unlikely the actuator would ever be subject to 50 minutes continued operation at such high loads.

6.2.2 Tests at Goodrich Actuation Systems

With no facility for loading the actuator, the tests at Goodrich were confined to functionality checks of the full assembled actuator, namely mechanical operation, clutch solenoid and position control via the gearbox and position sensing RVDTs.

6.2.2.1 Full speed steering transitions

Steering the actuator to all degrees of travel demonstrates the position control. Demands for -75° and +75° were input via ARINC to rotate the steering. Both lanes were powered for the initial test but as there was no active load, currents were small since the actuator must only overcome its own inertial and frictional losses.

Figure 6-38 shows the results. The position and speed traces were obtained from transducers mounted on the test rig, while the currents were measured from the U phases of the two motor drive lanes. The currents have been artificially offset by -20A on the graph for clarity of waveforms. The measured winding currents were negligible as the system is unloaded, increasing only when the motor was required to change velocity. The acceleration time was negligible, resulting in linear changes of position as the actuator operated at an unloaded speed of ±14°/s (1400r/min at the motor), accelerating and decelerating almost instantly on the recorded time base.

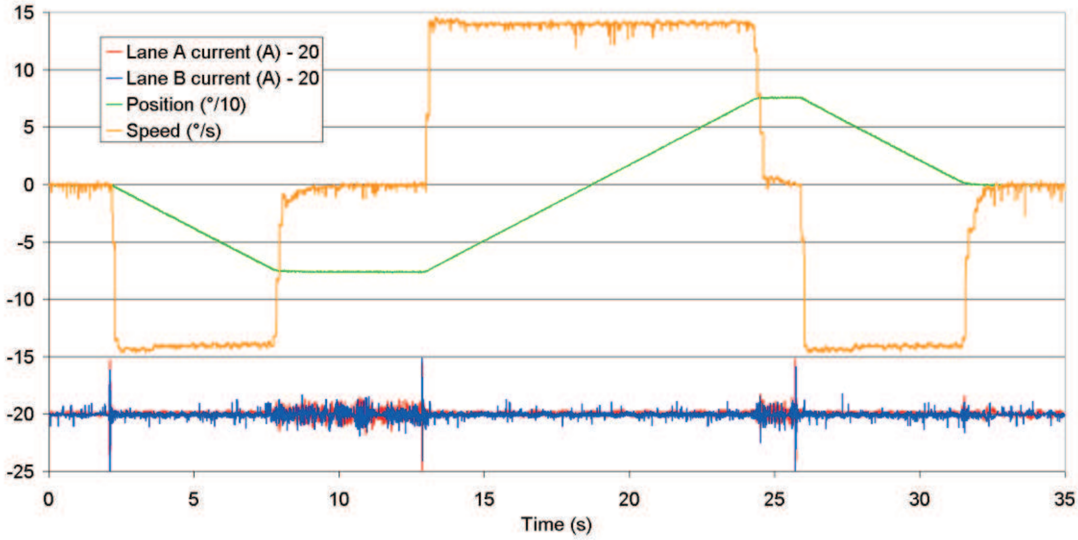

Figure 6-38: Side-to-side NWS full actuator transition.

Although the scope for testing at Goodrich was limited, a side-to-side transition was performed with one winding unpowered mid-travel (Figure 6-39).

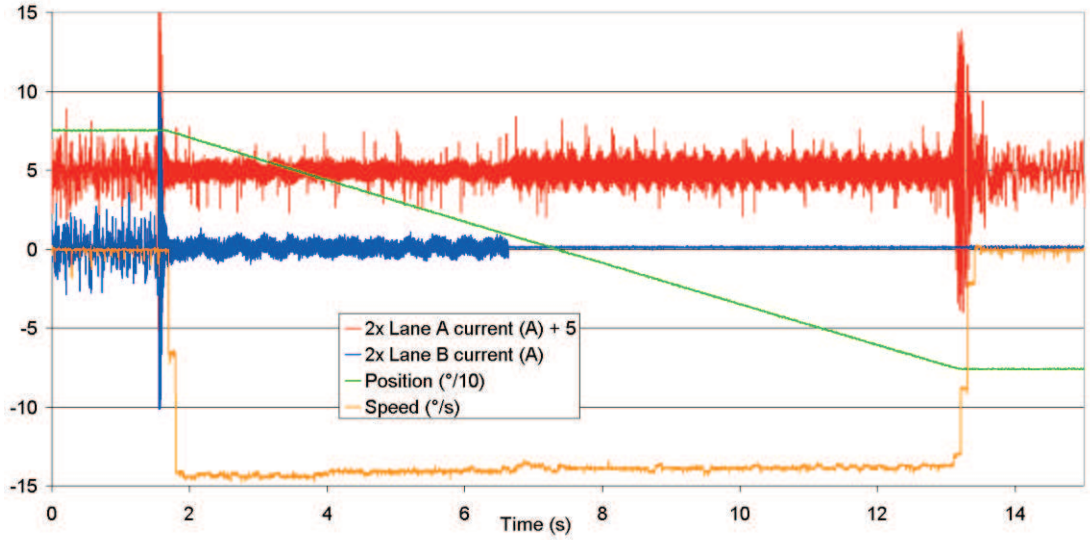

Figure 6-39: Side-to-side NWS actuator travel with lane B fault at 6.5s.

The fault was imposed on lane B via the PC diagnostics interface at around 6.5 seconds and the resulting current envelope increase is visible on lane A (which has been offset by 5 amps for clarity). Any change in the speed rate was minimal so there were no discernable effects on the actuator transition. The effects of a failure could be more pronounced with a loaded actuator, although they would be expected to follow the fast-responding trends shown in section 6.2.1.2.

6.2.2.2 Frequency response

The Airbus frequency response requirements for the actuator specify a -3dB gain point at 1Hz and a phase lag of 90° at 2.5Hz. To test the response, an unloaded actuator was injected with a position demand signal from a frequency analyzer and the measured position (from the rig transducer) was fed back. A sine-wave position demand of 4° was directly input to the A/D converter of the processor on one lane (with the other lane receiving this demand via the cross-communications link) and the response monitored as the frequency ramped from 0.1Hz to 10Hz.

The time-domain response is shown in Figure 6-40, with the demand and feedback signals offset from the current waveforms for clarity. As expected, the actuator ability to follow the demanded waveform eventually faltered as the frequency increased. Although not shown in detail, the lane currents (both near identical) increased to saturation levels as the system lost tracking. This was due to the position error within the controller rapidly increasing towards a peak of 4° as the gain and phase errors increased, which, due to the high proportional gain, resulted in a saturation of the speed and current loops.

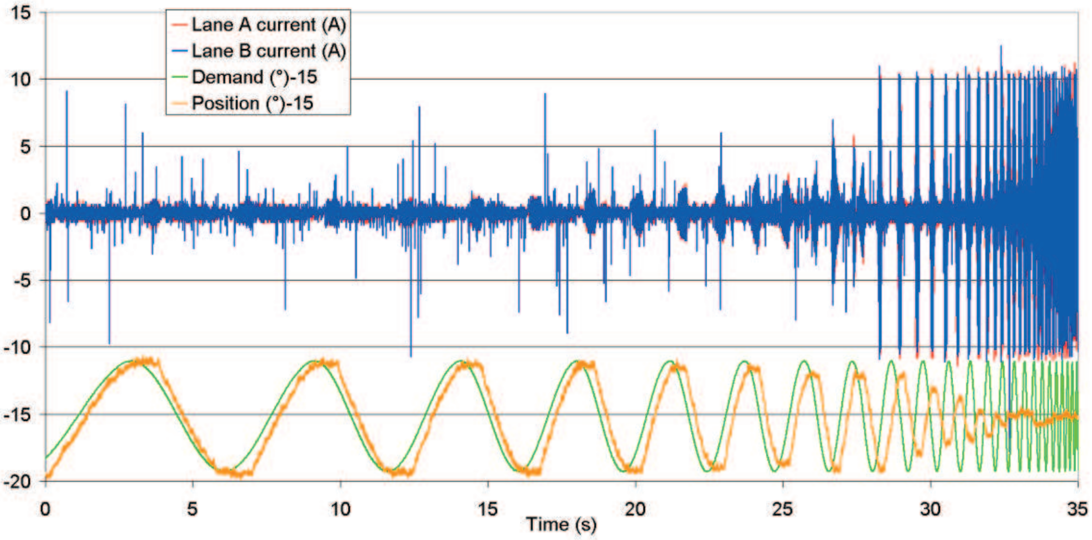

Figure 6-40: NWS frequency response test.

The outputs of the frequency response analyzer are shown in Figure 6-41 and Figure 6-42. The actuator gain fell by 3dB at approximately 1.5Hz and the phase error exceeded 90° by 0.8Hz. As the frequency headed towards 10Hz, the system was completely incapable of tracking the demand so the gain and phase errors rapidly increased and results appeared almost random.

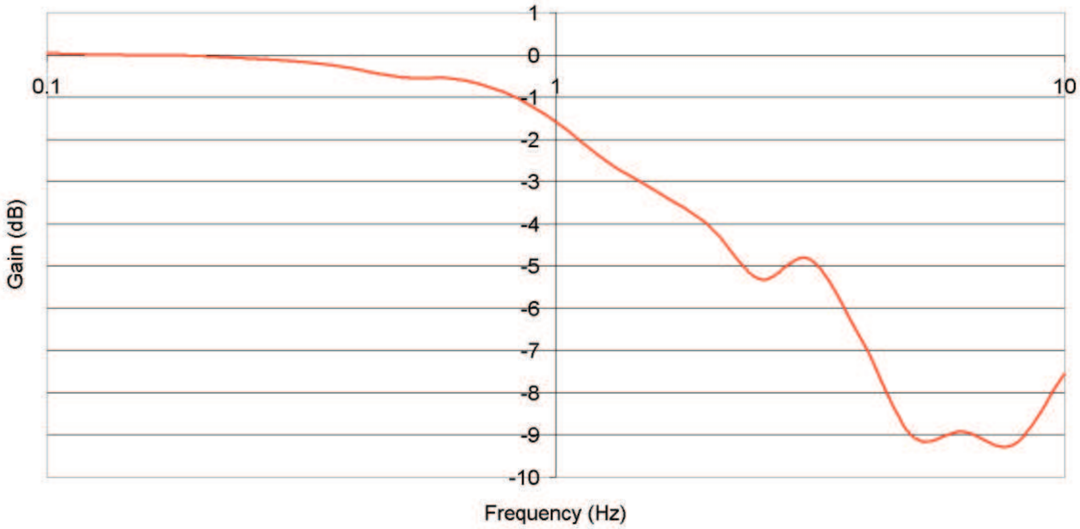

Figure 6-41: NWS gain plot.

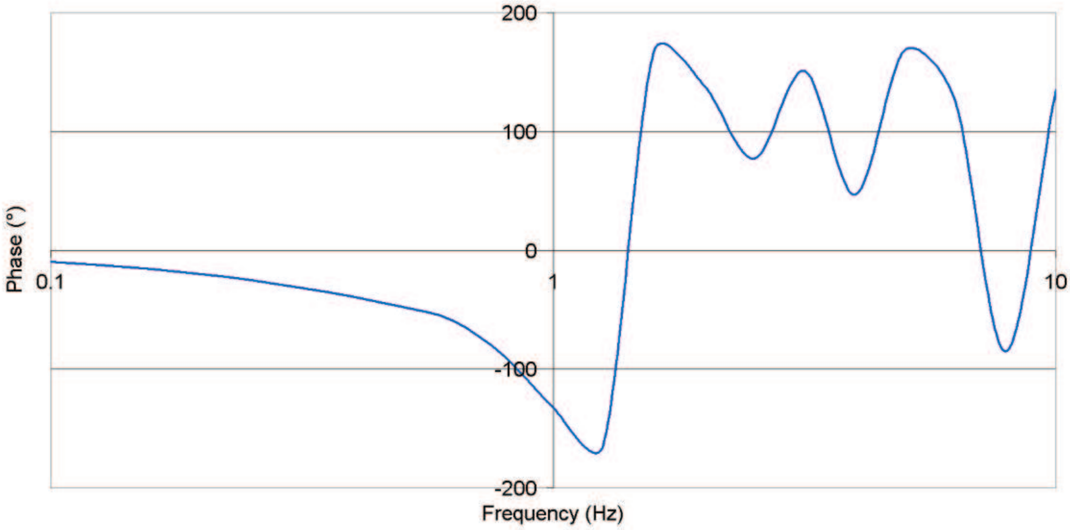

Figure 6-42: NWS phase plot.

Although the gain response was acceptable, the phase margin fell some way short of the 2.5Hz target. From observing the system, some failings appeared to be within the actuator, rather than the response of the controller. There was a measured 2.5° of backlash and twist between the motor output and the base of the nose wheel leg. The RVDTs were positioned on the output of the gearbox so the position feedback involved a true measurement of the output angle; however, the motor must overcome the backlash every time a directional change is required. Although 2.5° corresponds to 4.1 motor revolutions, at 1000r/min this adds 0.25 seconds to the response time.

6.2.3 Tests at Airbus

At the time of writing, only commissioning and basic tests were performed at Airbus. Test facilities included a full Control and Monitoring System (CMS) prototype with full ARINC communications links and a hydraulic loading system.

The most comprehensive test for the actuator was to apply the maximum rated torque of 7kNm in one direction and to demand, via CMS, 75° output angle in a clockwise and anti-clockwise direction. The default speed limit of 20°/s was instructed from the CMS, signalling the NWS to operate as fast as possible, depending on load. It was decided that the operating speed of the NWS would be internally limited to 10°/s to remain within the torque/speed profile (*see section 7.4 for more discussion*). The results of this slew are shown in Figure 6-43. As with previous Newcastle and Goodrich tests, the acceleration times were minimal, resulting in a trapezoidal position profile, as the actuator moved at the 10°/s limit. There was an offset in the demand and measured position, due to variation between the measuring sensors on the hydraulic load and the RVDTs on the NWS, although this can be easily corrected for future testing.

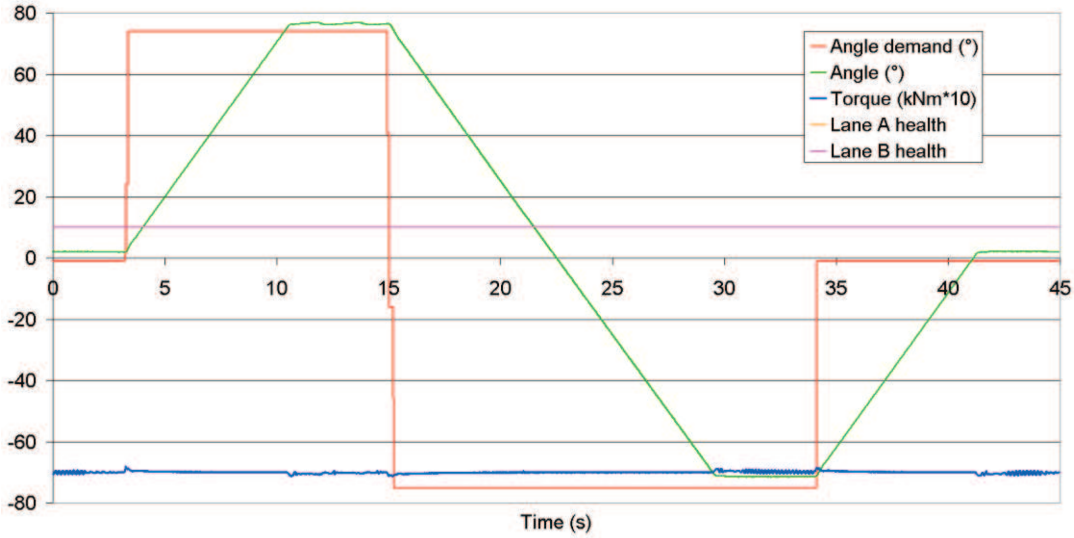

Figure 6-43: 7kNm loaded end-end slew.

To demonstrate the effects of a fault, end-end slews were demanded again, but the ±270V contactors for lane A were disconnected mid-slew (Figure 6-44).

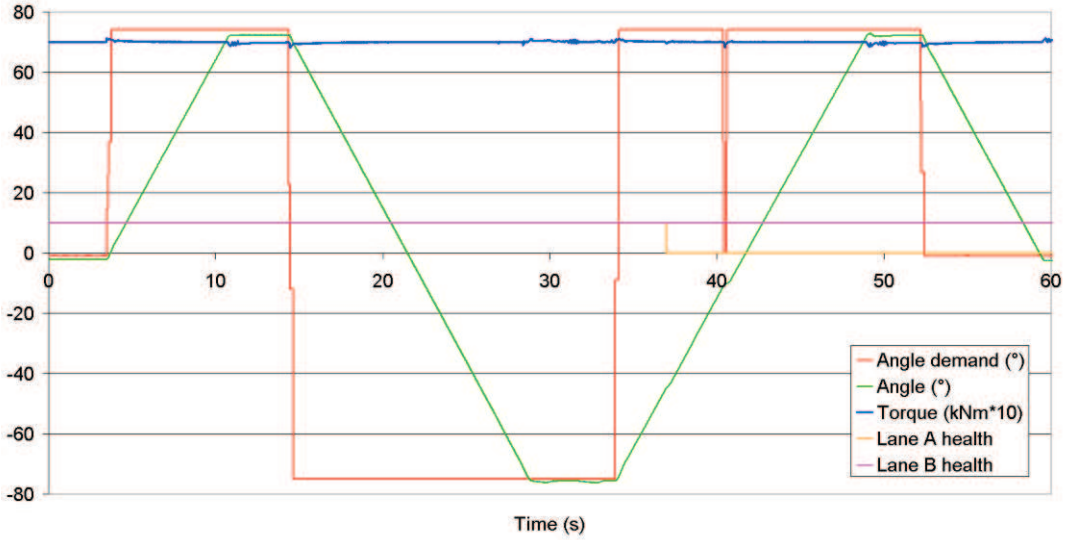

Figure 6-44: 7kNm loaded end-end slew. S1 faulted at ~37s.

The disconnection can be observed in the lane A health signal. Up until 37 seconds, both lane health values were 10V – i.e. healthy. At 37 seconds the supply was removed to lane A and the health signal fell to 0V. The response to the loss of a lane exceeded expectations with a near-seamless transition and the output angle blip almost undetectable. A minor disturbance in the movement occurred around 40s due to the CMS responding to the unhealthy lane A by changing the ARINC transmission to lane B and briefly demanding zero position. This was attributed to an error in the CMS rather than the NWS electronics.

It must be noted that the 28V to both control electronics was connected throughout the test; hence lane A remained capable of transmitting error signals back to the CMS and to lane B. In an aerospace-grade actuator the 28V would be derived from the ±270V, so the system would have to react to a complete loss of signals from the faulted lane. Theoretically the software could be altered to regard a missing lane as faulted; however, in an active-active duplex configuration if one lane loses communications with the other it cannot determine whether the communications or the other lane is at fault, so potential failure modes involving such conditions will need to be further considered.

6.3 CONCLUSIONS

A full suite of tests for two fault tolerant electromechanical actuators was presented, including results from industrial aerospace test facilities. Results show motor and actuator responses for a variety of loads under normal and faulted conditions.

The DEAWS project shows the performance of a fault-tolerant *2+1* drive, based on multiple single phases. Results verify the predicted torque ripple and drag torque effects discussed in chapter 3 and show how current reshaping can overcome torque ripple and help start the motor under rated load and with one phase short-circuited.

The test facility at Fr-HiTEMP demonstrated how a pair of actuators can respond to a series of faults. Operation is shown with simulated faults in the motor and power electronics, demonstrating that full operational performance following a single electrical fault is possible – essential to meet the *failure to operate* probability requirement of 1×10^{-5} per flight hour. Although only simulated on a DSP development system, the control and monitoring was representative of a true triplex control and monitoring scheme and provided a high integrity flap demonstrator, capable of 3-way voting on parameters for real-time fault identification and handling. Safety critical operation was shown, where flap symmetry was post-fault and the system shuts down in the event of a double-failure, using power-off brakes.

The ELGEAR NWS project demonstrated a physically representative dual-lane fault tolerant system with two separate drive lanes controlling a single actuator with only an isolated cross-communications link to share data. Motor and actuator response was demonstrated under faulted conditions, highlighting the rapid recovery from simulated and real error conditions on a test bench and on a loaded actuator at Airbus. The sharing of data between the two, otherwise independent, controllers is essential for simultaneous operation of both lanes and fault handling. The challenges involved in implementing this are presented in section 7.3.

Both systems meet their associated industrial performance specifications. The nature of the industrial-driven tests and measured results highlight how response rates are critical for gearbox-based actuator applications, with controllers continually operating in speed and current saturation regions.

Results for both systems were impeded by mechanical issues. In the case of DEAWS the backlash of the 318:1 gearbox resulted in positional measurement errors. This is a result of demonstrator-only, unloaded gearboxes, intended for a visual flap representation and such backlash would not exist in an actual rotary flap gearbox. The associated difficulties inspired the testing of a basic motor-turns counting system as a backup sensing method. Although unable to provide a position at power-up, turns counting provided a noticeable improvement in the accuracy of position control and could be considered as an additional measurement signal in a future flap system project. Such a system could not be implemented in the NWS due to the presence of the clutch, decoupling the motor from the RVDTs (*see section 4.1.4.*)

In the NWS, the frequency response of the actuator was limited by the considerable backlash in the system. Some degree of backlash will always be present in a system with a high ratio gearbox, but this will require minimising on the NWS if the frequency response is deemed a strict requirement.

Temperature monitoring proved a major failure in the NWS project. A decision to use k-type thermocouples to allow the MCU controllers to monitor motor winding temperatures resulted in temperature monitoring unable to cope with EMC radiated from the motor drive. This prevented any testing of thermal shutdown capabilities and other sensing methods such as Resistive Thermal Devices will be considered for future projects. Where thermal results are present, monitoring was performed using thermocouples and monitoring hardware independent and shielded from the controller.

The thermal data from the two projects highlights the effects of thermally isolating phases in a fault-tolerant motor, with the NWS demonstrating significant transfer of heat between the motor winding sets. As noted in chapter 5, packaging and wire distribution could be altered to improve the motor lane segregation in the NWS. A redesign of the NWS will be required if the target of 20 minutes operation with a lane short-circuited is to be met, although, like the 50 minutes duty cycle test, this may be ultimately considered excessive for requirements.

Goodrich mechanical data revealed that the ultimate loading torque of the NWS is 8500Nm and exceeding this may damage the actuator. From this, a decision was made to impose a current limit in each control lane, so that when operating active-active, both lanes were restricted to an equivalent actuator output of 4250Nm and when only one lane is operating, the torque is 8500Nm. The operational mode is determined by fault data transferred between the two lanes; however, future research may be necessary to assess the reliability of this system, as any error which incorrectly allows both lanes to contribute full torque will result in 19,000Nm.

For both actuators, a method of coping with regenerative energy was required, even when unloaded, due to the inertia present. To evolve DEAWS and ELGEAR to aerospace products, a firm specification on regeneration of energy into the supplies will be required and if it not permitted, then sizeable braking resistors will need to be incorporated into the power electronic controllers.

While most of the predicted and measured values of motor parameters were close, the back emf of both systems was notably different from predictions. Whereas $158V_{peak}$ was predicted for DEAWS, the resulting $128V_{peak}$ required considerably more current to attain torque levels and the additional 3rd harmonic reduced the effectiveness of the sinusoid-based torque ripple compensation scheme. In ELGEAR the back emf was 12% higher than predicted, which although having minimal effect on the current levels, presented difficulties in attaining the torque-speed profile for the actuator. This and other implementation challenges are discussed in detail in chapter 7.

7 Implementation Considerations for Electromechanical Actuators

During the development and testing stages of DEAWS and ELGEAR, a number of issues were resolved or highlighted for future consideration in evolving the technologies towards implementation on an aircraft. This chapter presents some of the more significant issues.

7.1 CURRENT SHIFTING FOR TORQUE RIPPLE COMPENSATION

When operating a fault-tolerant electric drive based on *n+1* single-phase modules at low speeds, reshaping of the current waveforms (*see sections 3.5 and 6.1.1.2*) is not the only method of achieving a constant torque at all angles following loss of a lane. Constant torque may also be achievable by altering the phase angles of the currents.

As with current reshaping, phase angle shifting assumes that the motor speed is near standstill and the drag torque from a short-circuit phase is negligible. Example calculations will be presented for the *2+1* motor of the DEAWS system for comparison with the current reshaping method presently implemented.

The per-unit currents, motor voltages (back emf) and torque profile for a *2+1* motor with one failed phase are shown in Figure 7-1. Phases a and b are healthy and phase c is faulted and producing zero torque (c is omitted from the graph, for clarity).

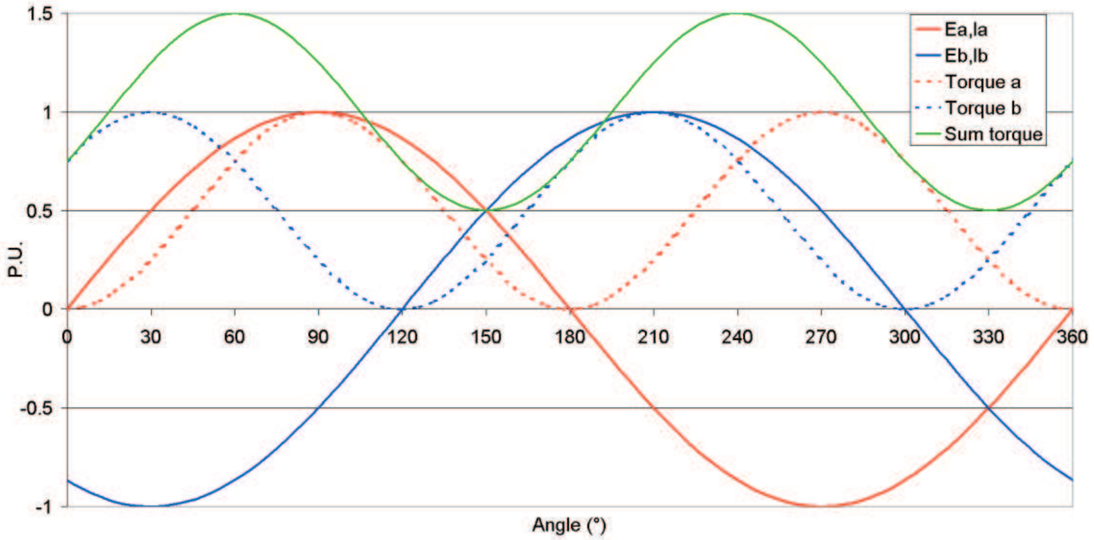

Figure 7-1: Uneven torque in a 2+1 motor with failed phase 'c' (at 270°).

Observing the position of the torque dips from the nominal value of 1.5 P.U., it is apparent that shifting the torque profiles of phases a and b towards the dip at 150° will result in more even torque distribution. If it is possible for the resultant torques of a and b to be separated by 180°, then the torque distribution will be even at all positions. Moving the torque angles requires altering of the current waveforms as the back emfs (E_a,E_b) are fixed by the motor.

For the example in Figure 7-1, consider the effects of advancing the phase angle of current I_a and retarding angle of current I_b by an equal amount, λ, to shift them towards torque dip resulting from the absent current c.

The torque from phases a and b with is given by:

7-1

$$T = \left(I_a E_b + I_b E_b\right) / \omega_m$$

Making everything variables of the electrical angle, x:

7-2

$$T = \left(I \sin(x) \cdot E \sin(x) + I \sin(x - 120°) \cdot E \sin(x - 120°)\right) / \omega_m$$

Adding the shifting constant λ to the current:

7-3

$$T = \left(I \sin(x - \lambda) \cdot E \sin(x) + I \sin(x - 120° + \lambda) \cdot E \sin(x - 120°)\right) / \omega_m$$

The terms of phase b can be expressed as cosines, reducing the angle values and allowing the equation to be re-arranged to:

7-4

$$T = \frac{IE}{\omega_m}\left[\sin(x - \lambda)\sin(x) + \cos(x - 30°)\cos(x - 30° + \lambda)\right]$$

A value of λ resulting in an equation that no longer varies with x will produce equal torque at all angles. If 30° is substituted for λ, the equation is simplified slightly to satisfy the difference formula identity:

$$\cos(A-B)=\sin A\sin B+\cos A\cos B \tag{7-5}$$

Substituting λ *=30°*:

$$T=\frac{IE}{\omega_m}\left[\sin(x-30°)\sin(x)+\cos(x-30°)+\cos(x)\right] \tag{7-6}$$

Now taking A as *(x-30°)* and B as *(x)* and applying the difference identity gives:

$$T=\frac{IE}{\omega_m}\left[\cos(x-30°-x)\right] \tag{7-7}$$

The result cancels out x and gives an equation independent of electrical angle:

$$T=\frac{IE}{\omega_m}\frac{\sqrt{3}}{2} \tag{7-8}$$

With I,E and ω_m at 1P.U, the resulting torque is 0.866 P.U., rather than the nominal 1.5 P.U. with 3 unfaulted phases. Adding a scaling factor to the shifted currents will result in a torque of 1.5 P.U.:

$$T=\sqrt{3}\times\frac{IE}{\omega_m}\frac{\sqrt{3}}{2}=1.5\frac{IE}{\omega_m} \tag{7-9}$$

The results of a 30° shift and a $\sqrt{3}$ scale are shown in Figure 7-2.

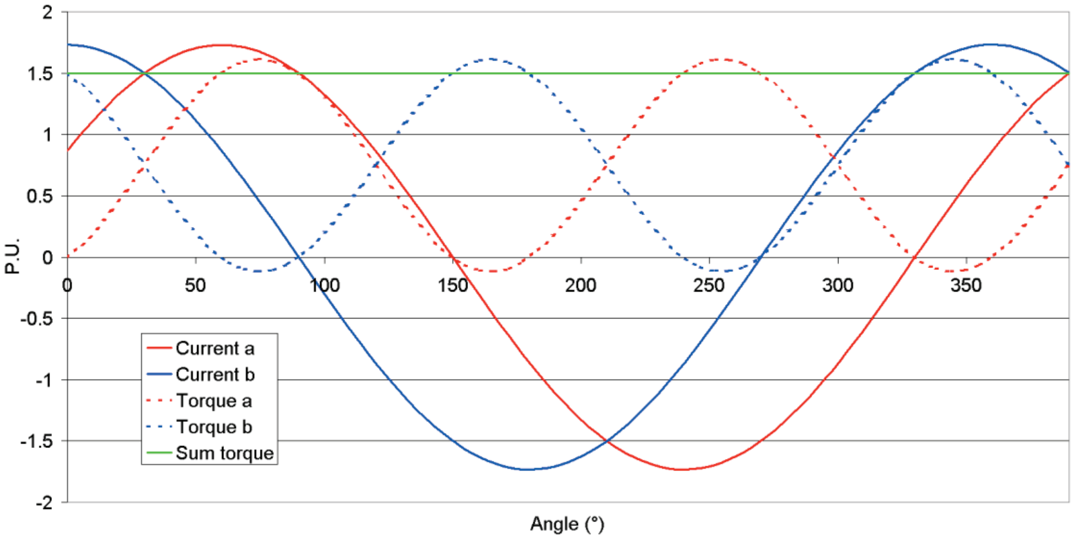

Figure 7-2: Torque of 2+1 machine with a and b currents shifted 30° and scaled by $\sqrt{3}$.

This current shifting method can be compared with the current shaping discussed in section 3.5 to determine the optimum reversionary method. Power dissipation is a main consideration, as whichever scheme provides rated torque with minimal current is preferable, so by considering the instantaneous squares of the altered currents, the proportions of resistive (I^2R) losses can be compared.

Figure 7-3 shows the I^2 values of a *2+1* motor with phase c failed open circuit and the remaining phases shifted by 30° and scaled by $\sqrt{3}$. The peak level of the summed I^2 values is 4.5 P.U and the cycle mean 3 P.U.

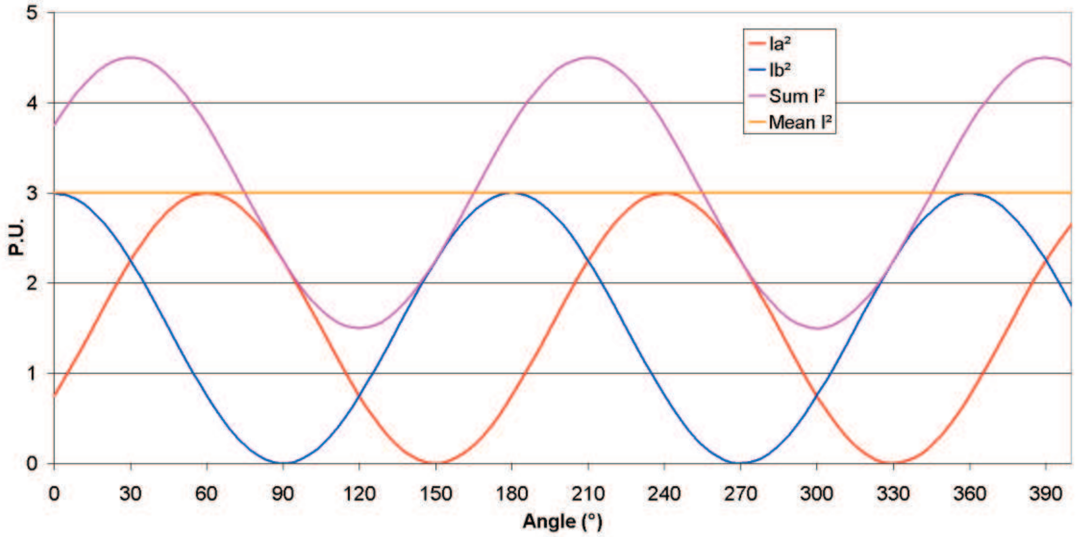

Figure 7-3: Power loss estimation for current angle shifting.

Figure 7-4 shows the squares of the equivalent reshaped currents in a *2+1* motor (*pp.60*). The peak level of the summed I^2 values is 4.5 P.U. and the mean 2.6 P.U.

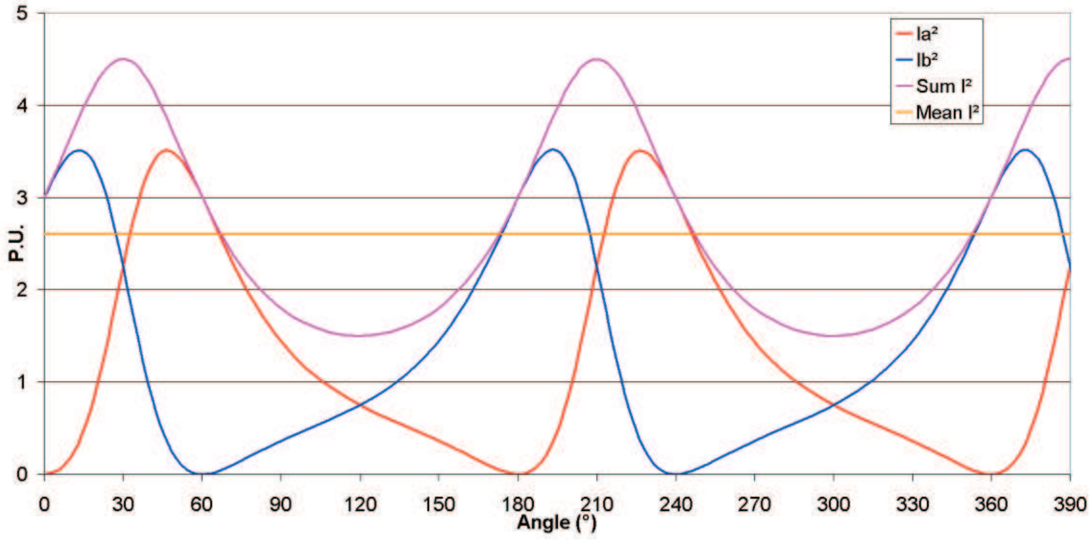

Figure 7-4: Power loss estimation for current re-shaping.

The mean I^2 differences infer that for the same output torque, current shifting requires more current and thus incurs more losses. Figure 7-2 also shows brief periods where one phase is outputting a motoring torque and the other an opposing torque. The phase with the opposing torque will be regenerating energy and the implications of this must be considered. As each phase will most likely operate from a different power supply, energy will not be locally circulated, so the system will require a means to either dissipate, store, or return this energy to the supply (if permitted). Storing of this energy may present difficulties at lower speeds as the regenerative periods of rotation will be longer.

Table 7-1 provides a comparison for current shifting on three, four and five-phase machines, with the phase shift and current increase required to achieve rated torque at all angles. In the *3+1* machine the phase at 180° to the failed phase is not shifted, while the two other phases are moved by ±60°. In the *4+1* machine all four phases are shifted by ±18° to achieve optimal torque sharing.

It can be observed that the I^2 values are consistently higher with current shifting than by employing reshaping techniques. The required peak currents are equal or slightly lower when current shifting, but as currents are scaled equally at all angles, there are higher mean losses compared to the reshaping scheme, where current is increased only at the required angles.

Motor	**Optimum phase shift**	**Peak current when current shifting (P.U.)**	**Sum of mean I^2 when current shifting (P.U.)**	**Peak current when current reshaping (P.U.)**	**Sum of mean I^2 when current reshaping (P.U.)**
2+1	30°	1.732	3	1.88	2.6
3+1	60° (+0°)	2	6	2	2.81
4+1	18°	1.3143	3.455	1.49	3.22

Table 7-1: Current shifting and reshaping for *n+1* motors with one faulted phase.

It can be concluded that, as a method of overcoming torque ripple at low speeds, current shifting can offer slightly lower peak device currents than current reshaping; however, losses are higher and bidirectional power flow may occur. Nevertheless, in the case of a geared EMA, the typical motor acceleration is so high that a speed will be reached where inertia overcomes any torque ripple in milliseconds and neither scheme will be required for a significant time period, so any extra heating from adopting a current shifting system would be negligible.

7.2 INPUT POWER QUALITY FOR MULTIPLE SINGLE PHASE DRIVES

The prototype DEAWS system does not focus on the interfacing of motor drive electronics to aircraft supplies for reasons stated in section 5.1.3.1 (*pp.115*). One area where the design impact of supply interfacing was not initially considered is the input filtering requirements for fault tolerant electric drives, where each lane is operated from a separate power supply.

The instantaneous power delivered by each phase of a conventional electric drive is dependent on the electrical angle of the motor. As the phases are electrically displaced to give a constant motor torque at all angles of rotation, the power drawn from the supply is the sum of these powers and balances to a dc quantity. This is illustrated for a three phase converter in Figure 7-5. Where the drive is interfaced to an ac bus with a converter capable of minimal distortion and unity power factor, the current drawn will be sinusoidal and of constant amplitude. Fault tolerant drives consisting of multiple three-phase lanes (*section 3.2*) behave in this conventional manner as each lane is effectively a conventional three phase electric drive.

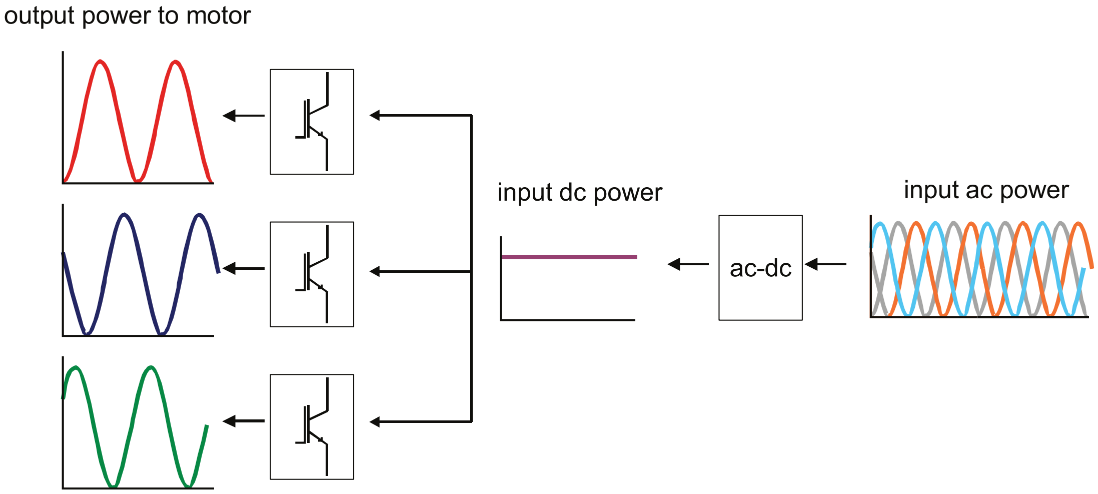

Figure 7-5: Input and output power balance for a conventional three phase converter.

In the case of a fault tolerant drive consisting of multiple single phases, each phase lane will typically be connected to an independent power supply. Where insufficient filtering is present on the system, the instantaneous power supplied to the motor will be pulled directly from the supply, resulting in a supply current harmonic at twice the motor electrical frequency (Figure 7-6). Where the drive is connected to an ac bus, the power drawn from the supply will be modulated by this ripple effect.

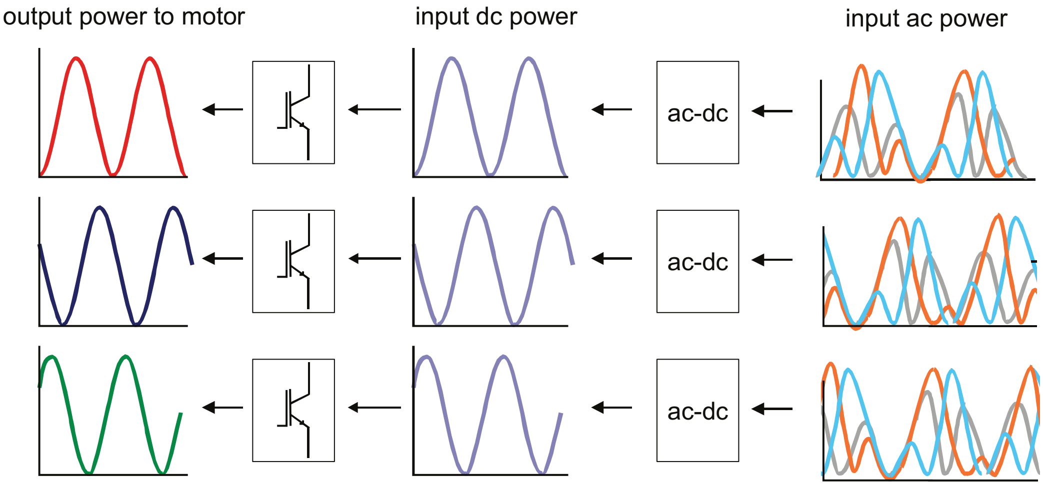

Figure 7-6: Power in a converter with three independent phases and insufficient filtering.

In aerospace applications there are considerable mass and size penalties for large passive filters, particularly as larger alternatives to electrolytic capacitors are used, such as polypropylene.

To assess what impact this effect will have on the DEAWS system, a simulation can be performed to model the power requirements for a variety of input filters. Research was undertaken by Khatre *et al*. [82] into modelling the DEAWS system with an active rectifier input, capable of interfacing to a variable frequency aircraft supply and with a more representative filter than the 940μF electrolytic bank of the laboratory demonstrator. Unfortunately these simulations model the DEAWS motor with a conventional three phase motor drive, so are unrepresentative of a true isolated single phase system and the filter requirements must be reassessed.

A Matlab Sim Power Systems model can be created for one power lane of DEAWS. For simplicity of modelling and with dc power supplies featuring on new aircraft, the lane is interfaced to a 270V dc supply and dc input currents are monitored. As shown in Figure 7-6, any distortion on the dc input would manifest itself as a modulation effect on an ac-connected system, so results are relevant to both supplies.

As a basis for establishing input filter values representative of an actuator on a real aircraft an aerospace standard will be used. The RTCA, DO-160f document contains guidelines for input power quality on new ±270V dc systems and states an allowed distortion level of 0.14× for devices drawing between 1 and 10kW [83]. The 0.14 is a multiple of the mean current drawn when the device is operating in a steady state condition at maximum load. In the case of DEAWS, this is where the controller is operating from two lanes, each outputting a 27.7A sine-wave at 10,000r/min (an electrical frequency of 833Hz) into a back emf of 128V. The model of the lane is shown in Figure 7-7 with the power electronic H-bridge, digital controller, input inductor and dc link capacitor, the latter two sized to filter the input current to the DO-160f standard. A supply impedance of 20μH, 0.04Ω is also included, based on values stated by Goodrich for the cabling between an actuator and a power supply (also equalling the value stated by Aten *et al* [41] when simulating an actuator). Where possible, commercially available capacitor and inductor values are used in this study as, although not optimal, they prove the system can become a physical reality and also give a basic representation of volume and mass.

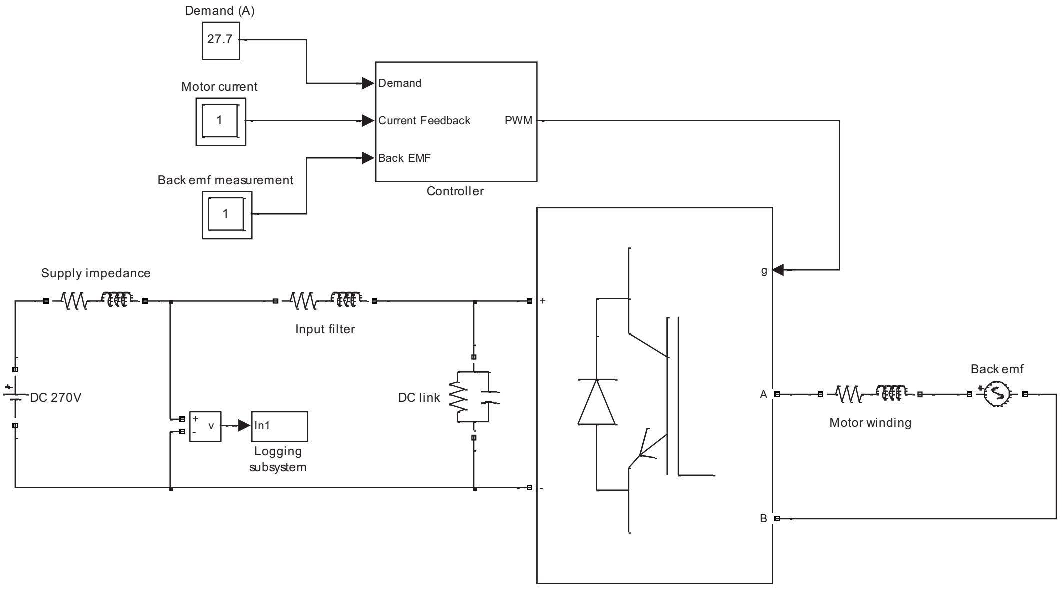

Figure 7-7: Matlab Sim Power model of a single DEAWS module.

A 10kHz PWM controller (Figure 7-8) represents the control scheme used in the prototype demonstrator. The controller is tuned to produce a winding current in phase with the motor back emf, for optimal power output. To allow a settling time for the simulation, a ramp block restricts the output for a brief start-up period, although all the results presented here are taken once the system is in a steady state.

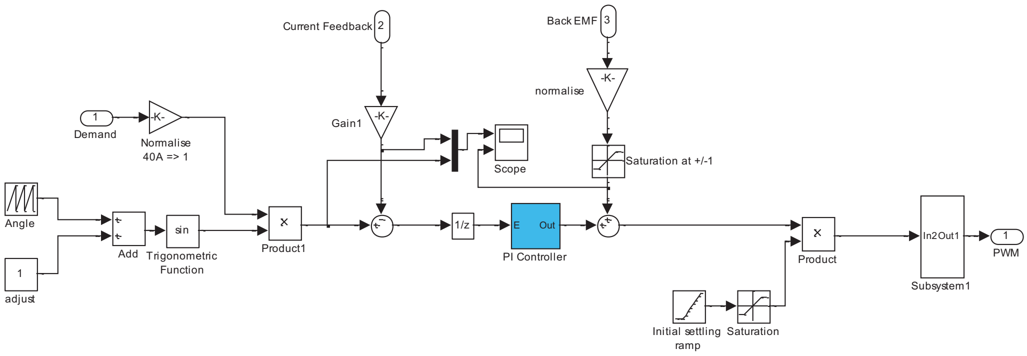

Figure 7-8: Current controller model.

For the first run of the simulation the input filter physically implemented on the ELGEAR NWS system is used (*see section 5.2.2.1*) to allow a direct comparison. This consists of an 80μF dc link capacitor and no input inductor, relying only on the 20μH supply impedance for filtering. Results are shown in Figure 7-9.

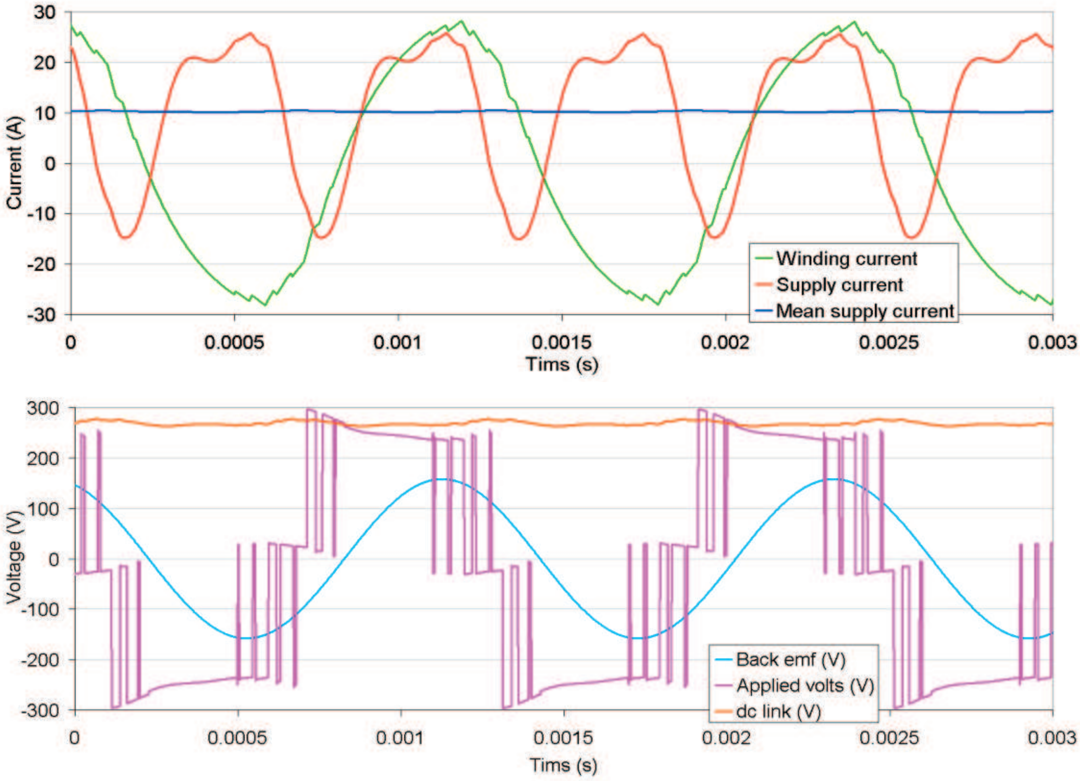

Figure 7-9: Simulated DEAWS current and voltage waveforms with 80μF and 20μH.

Although the controller successfully synthesises a 27.7A sine-wave, there is an excessive ripple at 2× motor electrical frequency on the dc input supply current, peaking at 25A, considerably higher than the 10.1A mean current and 18× higher than the allowable 0.14× limit. This arrangement could not be a practical reality and the input filter must be adjusted.

For a visual comparison, results were obtained experimentally from a single three-phase lane of the ELGEAR NWS system, operating at a nominal speed of 1000 r/min and 12Nm of motor load. The existing 80μF dc link capacitor bank remains and 20μH of supply inductance is added to represent the cabling in an aircraft and to match the simulation of the DEAWS system. Results are shown in Figure 7-10, with one of the three output phase currents displayed.

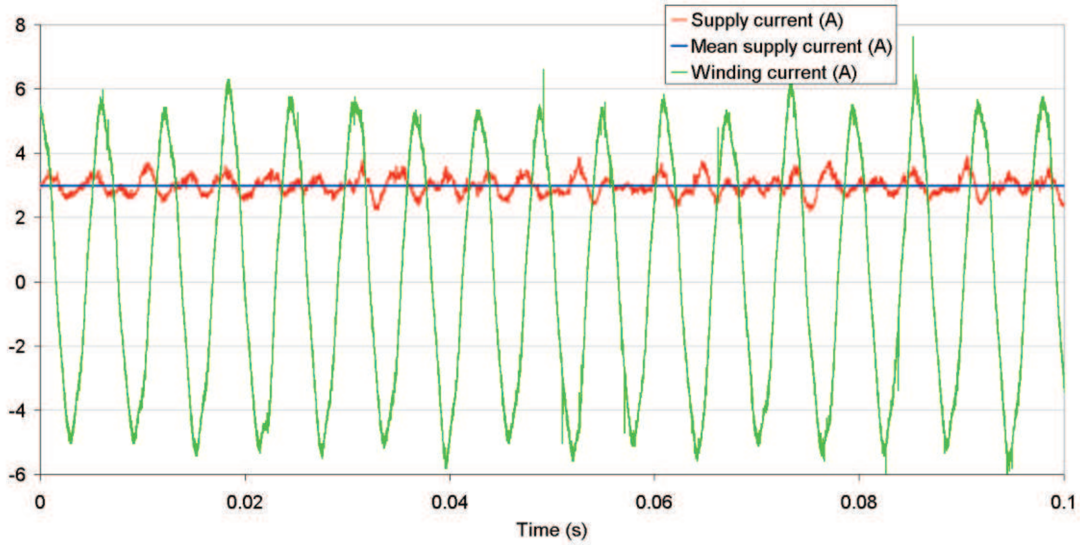

Figure 7-10: Measured ELGEAR NWS input current distortion with 80µF and 20µH.

The distortion present on the input current is due to the tracking of the current PI controllers within the converter and is non periodic. Although exceeding the 0.14× requirement at points, the input current is significantly smoother than the DEAWS simulation and is as-expected for a system with multiple motor phases driven from a common supply.

The 1200V, 4×20µF polypropylene capacitor bank of the ELGEAR system is governing factor in the physical size of the converter and adding anything physically larger to DEAWS would compromise the space envelope of the actuator. Using the same commercial capacitor range as in ELGEAR [84], a 600V, 3×30µF capacitor bank is achievable, so this will be used as an initial capacitance value for an improved filter.

Simulations were run with an assortment of inductor values, with the results shown in Figure 7-11 obtained with a 1.1mH inductor.

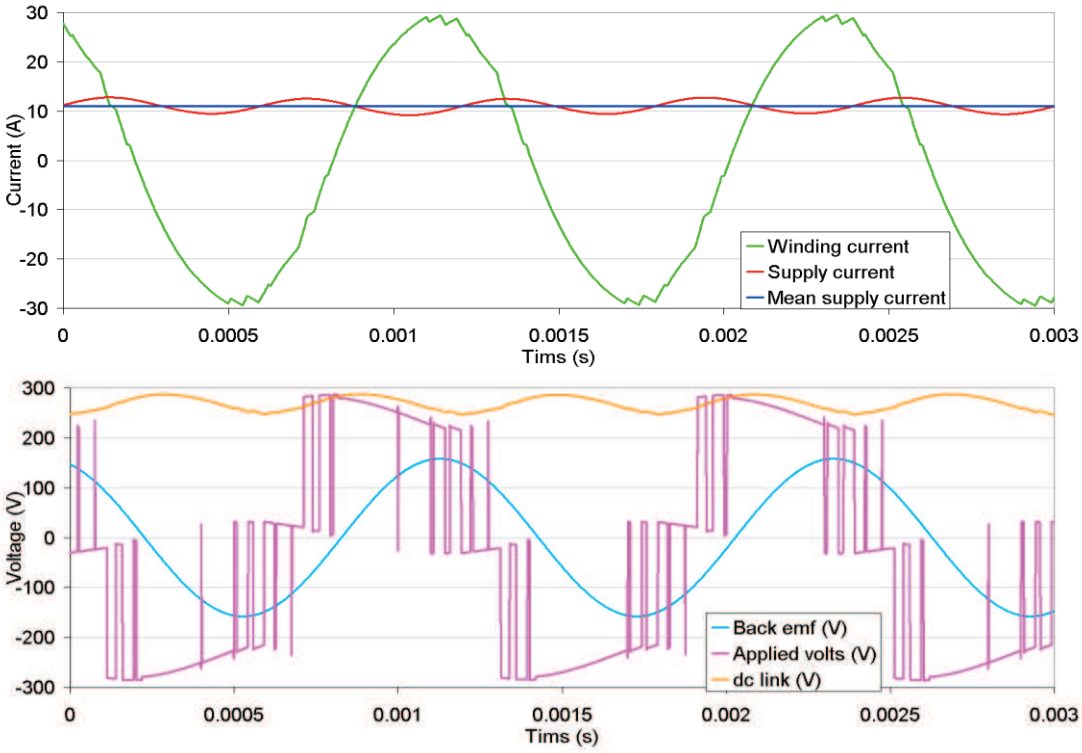

Figure 7-11: DEAWS current and voltage waveforms with 90μF capacitance, 1.1mH inductor.

With the new filter, the input current distortion is reduced to 14% of the 11A mean value, so the system is just on the limit of acceptability for DO-160f, although an 11A dc, 1.1mH inductor is significant in volume and weight. From observing available components on the EPCOS power line choke datasheet [85], a 1.1mH, 12A inductor can be made up with two 2.2mH 6A inductors in parallel. With one inductor measuring 40×111×51mm (*l*×*d*×*h*) and weighing 600g, this is a considerable size and weight to add to a single converter lane, with a total of 3.6kg required across the three H-bridges of the *2+1* system.

The designer can alter the ratio of inductance to capacitance to maintain the same level of input distortion, although a size/mass trade-off occurs. For example, the same input current ripple level can be obtained with a 16A, 0.29mH inductor and 360μF of capacitance, resulting in a 600g inductor weight reduction, but incurring a 300% capacitor volume increase.

It can be concluded that there is a considerable additional input filter requirement for a fault tolerant system based on single-phase bridge modules where each phase is supplied independently. Although the required filtering is physically achievable, it represents a considerable weight and volume disadvantage over systems based on multiple three-phase winding modules.

7.3 ELGEAR LANE SYNCHRONISATION

When running the ELGEAR NWS motor drive ‘active-active’, the issue of synchronisation between the two controller lanes is a significant consideration. Although overlooked in many fault tolerant prototypes, particularly where single processing units are used for convenience, even early dual-lane electromechanical actuators, such as those demonstrated by Thompson [86], featured sharing of motor current demands between processing electronic lanes.

On the ELGEAR NWS a 1Mbit, isolated RS-232 channel is the sole method of communications between lanes and with an absolute maximum limit of 100 bits per PWM cycle (at 10kHz), the amount of data which can be exchanged is limited.

It is necessary to determine the points in the control scheme where a synchronisation method is required, so the three PI control loops within each lane are considered, with parameters listed in Table 7-2. Numbers are normalised and handled as fractions within the dsPIC software, with ±1.0 representing the full range of a 16-bit register.

Controller	Demand	Feedback	Scale	Resolution	Sample rate	K_p	K_i	Output Range
Position	ARINC	RVDT	180° = 1.0	0.1°	1kHz	38.3	0	±0.5
Speed	Position output	Resolver	2000r/min = 1.0	14.7r/min	1kHz	0.64	0.01	±0.6
Current D and Q	Speed output	Hall sensors	15A = 1.0	0.03A	10kHz	1.36	0.02	SVM 540V to motor

Table 7-2: ELGEAR control loop parameters.

The software follows the conventional arrangement of nested position, speed and current PI loops similar to that shown back in Figure 4-7 (*pp.77*), but with two identical PI loops for the ‘D’ & ‘Q’ parameters of the vector current control. When determining synchronisation requirements the inputs and outputs of each loop can be considered separately:

- **Position demand:** At the outermost level, the ARINC position demand inputs to the two lanes are identical as a result of multiple ARINC inputs for noise elimination and a master-slave arrangement which ensures the input parameters for the selected ‘master’ lane are used by both lanes (*pp.104*).
- **Position feedback:** The two lanes receive an actuator angle measurement from independent RVDTs and there will be variations in this data, owing to sensor alignment, accuracy and noise. At best, the resolution of the angle measurement

is limited to 0.1° (of ±75° full-scale) by the 10-bit A/D converter of the dsPIC, although testing showed a measurement error of up to 2.4° at the outer ranges of actuator travel, introduced by the RVDT demodulation circuitry. For dynamic response (6.2.2.2, *pp.165*) only a proportional controller is used in the position loop, with a very high gain value and output saturation at ±1000 r/min. Therefore any minor measurement variation will result in considerable speed and torque demand variations between lanes. A simulation is shown in Appendix D, highlighting the potential variations. Consequently for the NWS it has been assumed essential to share position feedback between lanes, each taking an average to ensure identical data. A tolerance band identifies a large variation between measurements and a potential sensor error.

- **Speed demand:** With identical position demand and measurement data ensured through synchronisation, the resulting speed demand data should be identical for each lane.
- **Speed feedback:** At 1000r/min, the 12-bit AD12S200 resolver interface is counting through 68266 steps per second. For a fast dynamic response, the speed loops within the controllers operate with a 1kHz sampling rate, which results in 68 resolver steps between each sample at 1000r/min, corresponding to a speed resolution of only 14.7r/min. With an integrator present within the speed controller, the effects of even a 14.7r/min variation between the lanes can result in a large wind-up, resulting in an equally large variation in torque output between lanes (see Appendix D for examples). Although the sampling rate can be decreased to improve the speed measurement accuracy, integrator wind-up can still occur with smaller disagreements. The integrator could be eliminated and the proportional gain increased, resulting in a much harsher controller operating at the saturation thresholds of the torque demand, but a simpler option is to share data to ensure a common speed value in each lane. If demand and feedback data is made identical for both lanes then the resulting torque demands will be identical.
- **Torque/current demand:** An alternative to consolidating position or speed feedback data is to simply consolidate the torque demands between lanes. Although the current loops operate at 10kHz, the input demands are produced in the speed loop, so the consolidation is only required at 1kHz.

- **Torque/current feedback:** Although when active-active, both converters should be synthesizing identical sets of three-phase currents, there are no obvious control benefits in attempting to share current feedback signals between the two lanes, or to consolidate PWM output demands. Although comparison of winding currents and resolver signals could be used to highlight faults, exchanging data at the 10kHz rate of the current controller will require a much higher data bandwidth than exchanging data at the position or speed controller rates.

For the NWS prototype it was decided to consolidate torque demands between the lanes when running active-active. To demonstrate the need for synchronisation the controller was operated on the Newcastle test-rig under speed control with no synchronisation. A 1000r/min speed demand was issued to both lanes and a 12Nm load was repeatedly applied and removed. The envelope of the resulting currents is shown in Figure 7-12, showing a symmetrical phase in each controller (the current in lane A is offset by -6 amps for clarity).

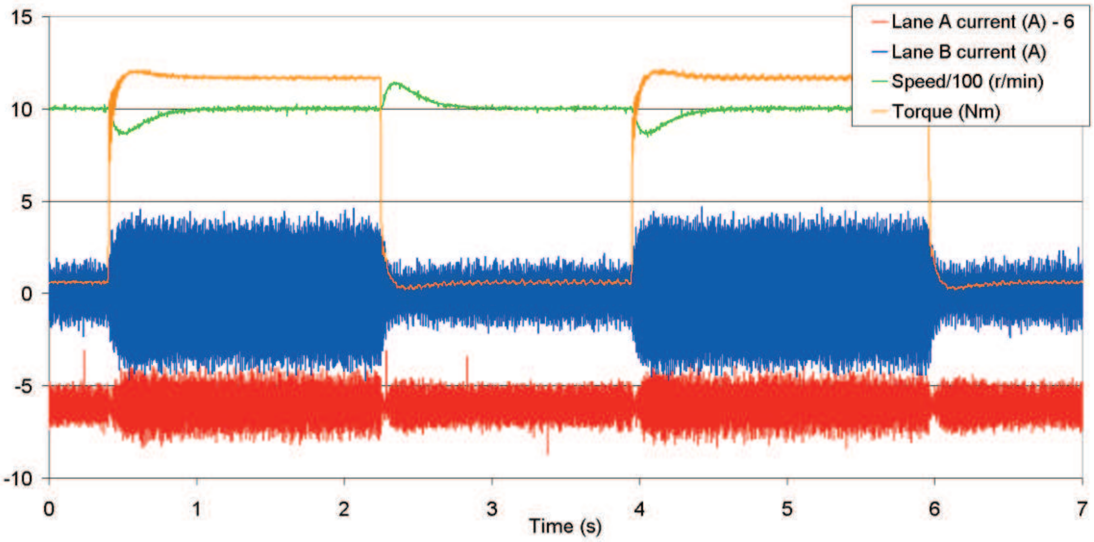

Figure 7-12: Speed control with applied steps of torque, no synchronisation.

It is clear that lane B draws twice the current of lane A when the load is applied.

A close-up of the transition from loaded to unloaded is shown in Figure 7-13. At the start of the trace both lanes are outputting currents in the same direction, although of unequal magnitude. Following the removal of the load, the currents in the two lanes are opposing and the lanes effectively force-fighting, with one producing an accelerating torque and the other a braking. Although the net torque is zero, the braking lane will be regenerating energy into the supply and both lanes will be wasting heat energy as a result of unnecessary power flow.

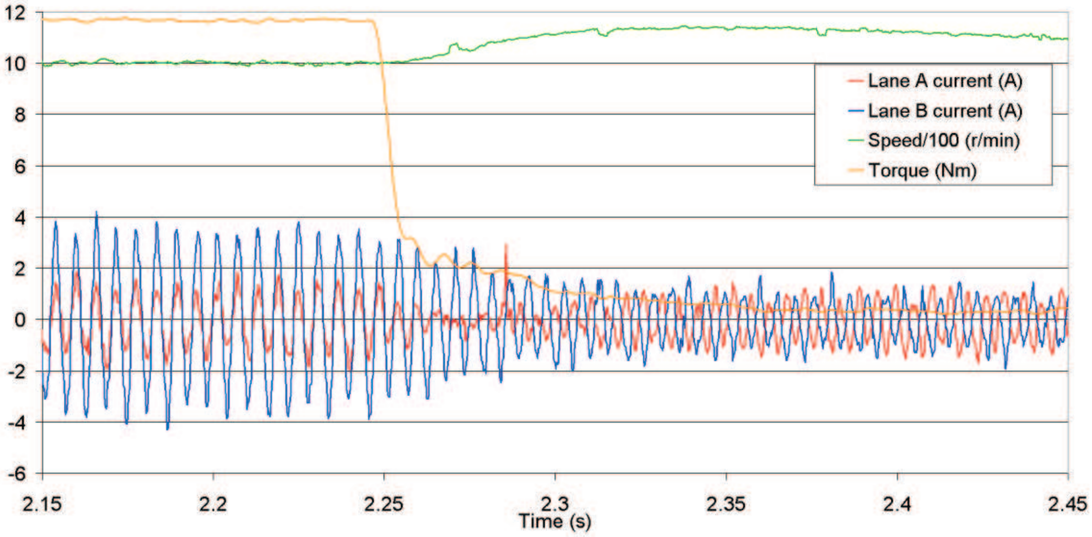

Figure 7-13: Close-up of speed control with applied steps of torque, no synchronisation.

With the torque demand synchronisation applied, each lane will simply perform a mean between its own speed loop output and that of the other lane, using the result as the current controller demand. The effect of this is near 50:50 torque sharing, as shown in Figure 7-14.

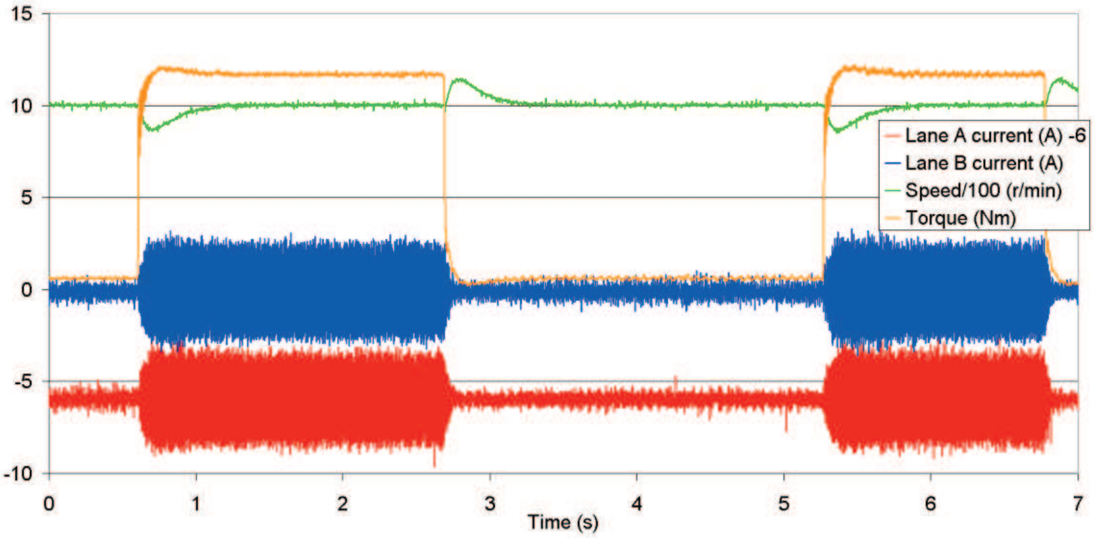

Figure 7-14: Speed control. Lane currents with applied steps of torque, torque-sharing on.

A close-up is shown in Figure 7-15, with both lanes demanding near-identical currents. After the load is removed the peak currents are negligible as the force-fighting has been eliminated.

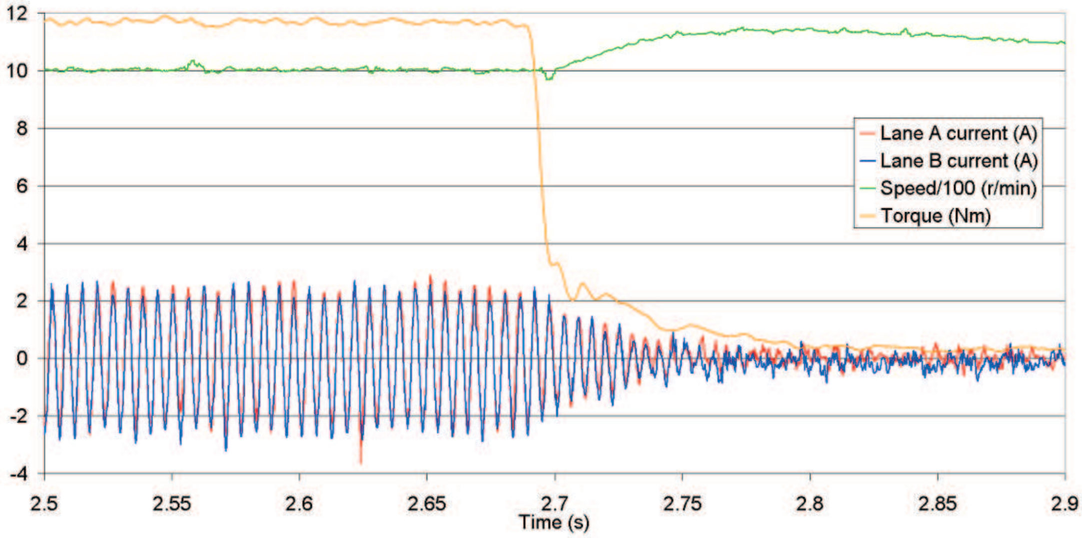

Figure 7-15: Close-up of lane currents with applied steps of torque. Torque-sharing on.

The torque sharing feature was deemed a requirement for optimum thermal performance and implemented during the development stages of ELGEAR. It is present for all results in this thesis and features on the completed actuator installed at Airbus. When a lane is faulted, or the controller deliberately operated in active-standby, the operating lane will synthesise and apply its own current demands.

It could be argued that linking the current demands of the two lanes compromises fault-tolerance, as one lane could inform the other of an incorrect demand, thus resulting in two incorrect outputs. This is more a restriction of a duplex system, as a triplex arrangement can provide a median torque value and identification of any out-of-tolerance data from a lane.

7.4 IMPLEMENTING AN ACTUATOR WITH A TORQUE/SPEED PROFILE

Each motor controller lane of the ELGEAR NWS was initially designed for a torque/speed profile derived from the Airbus specification shown in section 2.2.3. Unlike DEAWS, which is sized for the same peak torque at all speeds, the ELGEAR motor torque/speed profile decreases from 1000r/min upwards (see Figure 5-16, *pp.124*).

The actuator was intended to operate at speeds up to 1800r/min, reducing speed as load is applied. From the torque/speed profile a power graph can be derived for a single electric drive (Figure 7-16), operating in isolation and against the drag torque from a motor terminal short of the other lane. It should be noted that when operating active-active, the power requirement is halved as the torque is proportioned 50:50 between lanes.

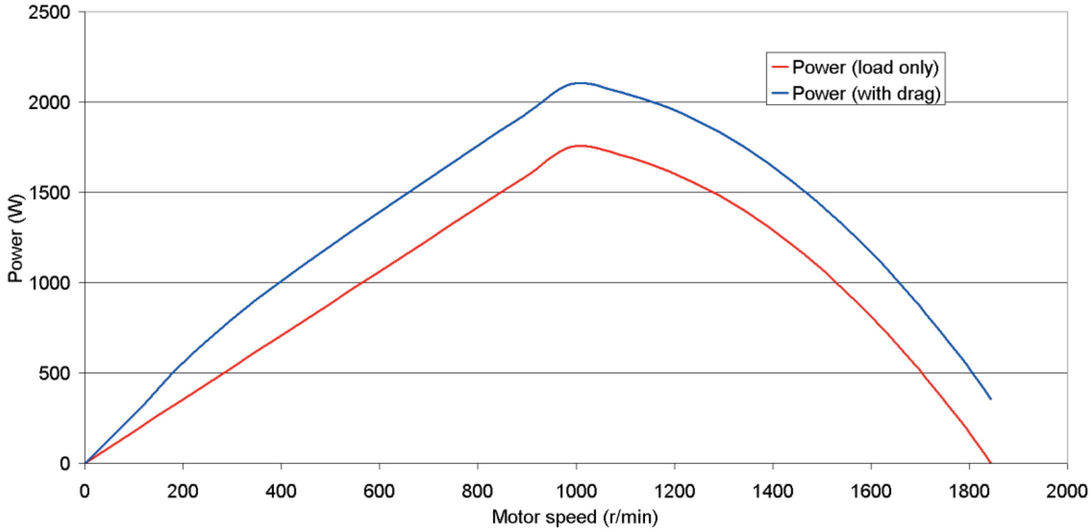

Figure 7-16: ELGEAR power profile.

Neglecting the required power profile and designing a drive capable of full torque at all speeds (as with DEAWS), would result in a rating for 17Nm at 1834r/min and a >70% larger drive. It is therefore optimal to design the system to follow the torque/speed profile.

7.4.1 Implementation of a torque limiter

The optimal design for a motor specifies a sufficiently high back emf to maintain rated torque at rated speed, with a minimal winding current. The balance of voltage vectors is shown in the phasor diagram of Figure 7-17, with the vector controller within the motor drive maintaining the quadrature axis current in phase with the motor back emf.

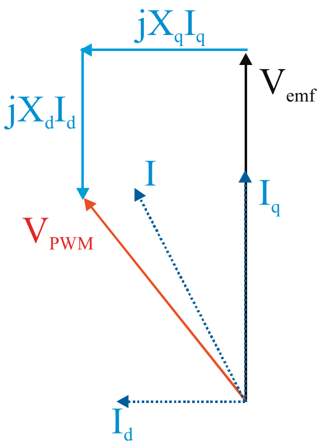

Figure 7-17: Phasor voltages for zero current angle.

When a torque is specified out of the working range of the electric drive, there is insufficient PWM voltage available to overcome the back emf and synthesise the required winding currents. From practical experience, insufficient voltage can result in instability of current control with non-sinusoidal waveforms, resulting in rough operation and motor heating.

Although it may appear unreasonable to apply a load out of range of the actuator, such conditions are unavoidable when following a torque/speed profile where the actuator is commanded to move as fast as possible, dependent on load torque. If the torque is minimal then the motor may achieve 1800r/min; however, it is entirely feasible for a load to be subsequently applied that can only be attained at 1000r/min and the actuator will be forced out of range and must respond quickly by reducing speed.

To stay within the operating range of the drive, the controller must adopt one of the following two options:

a) **Current limit:** For the measured supply voltage and the measured operating speed, the current/torque output does not exceed the rating of the controller.

b) **Speed limit**: For the measured supply voltage and the measured torque, the speed output does not exceed the operating range of the controller.

With the nested control loops of the controller following the conventional order of position → speed → current, restricting the current output for a given speed is far more logical than inserting additional feedback control to alter the speed demands, depending on the current demands. Hence option a) is selected.

From the torque/speed profile of the ELGEAR controller and the motor parameters, the operating currents for a single lane can be calculated, as in Figure 7-18.

The figure shows the peak currents available without field weakening and when field weakening applies an optimum d-axis current of 5.5A to overcome the back emf. 540V is assumed in the calculations, although the ratings will fall if the supply drops. It is clear that the torques at lower speeds cannot be maintained throughout the full operational speed range and that field weakening is required to attain the required torque at the highest speeds, although up to 1400r/min is otherwise achievable. Field weakening was not implemented for the demonstrator as the speeds obtained without were considered sufficient for research and development.

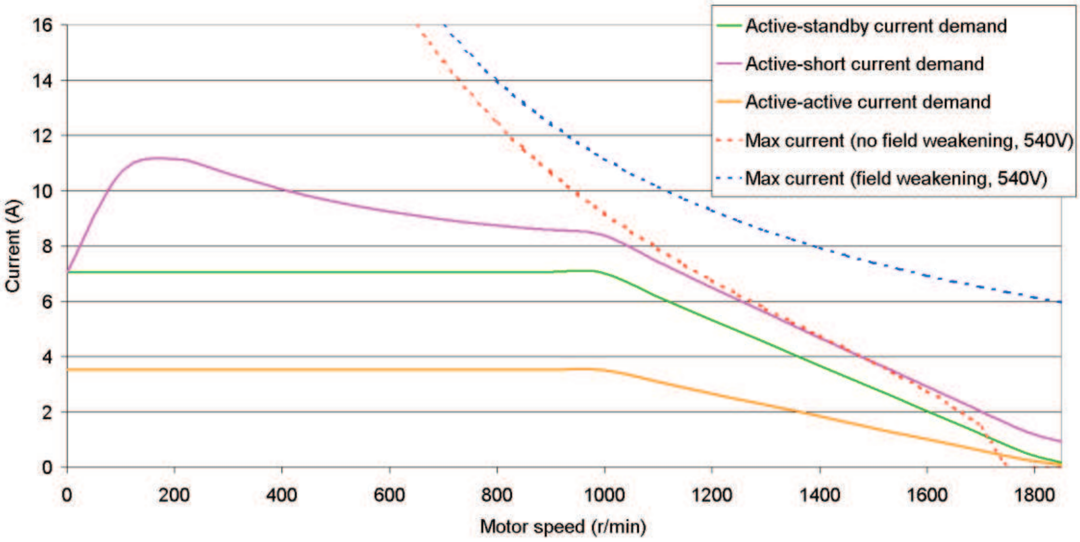

Figure 7-18: ELGEAR NWS motor/converter current limits.

To implement the current/torque limiter, a three-dimensional look-up-table was implemented. The table consisted of peak current vs. speed curves for a selection of supply voltages between 415 and 540V with software interpolation between points.

Although the measured back emf was higher than predicted, it is notable that the NWS prototype motor was specifically designed to require field weakening at higher speeds. The use of field weakening on a fault tolerant drive raises a point of concern, noted by Mellor *et al.* on a two-lane fault tolerant traction drive [87]. If the drive is operating on one lane, using field weakening to attain high speeds, then at the point where the back emf of the unpowered lane exceeds the supply voltage, regeneration will occur. As the NWS is connected directly to a stiff 540V dc supply, a braking torque will be exerted at these higher speeds. To avoid this, the standby/faulted controller must impose a three-phase terminal short-circuit, requiring the controller to have failed in such a manner that this remains achievable.

7.4.2 Operation under aiding load

As per the specifications (*section 2.2.3*), the NWS must operate with antagonistic and aiding load. The motor must therefore act in motoring and generation modes, respectively. The torque limiter was initially designed and tested with antagonistic loads.

Aiding loads attempt to accelerate the actuator in the direction of travel and where aiding load is applied outside the safe operating region; the torque limiter will act to reduce the torque output of the lane. Unfortunately a drop in torque results in the aiding load accelerating the actuator, moving even further from the safe operating region. The actuator effectively ‘runs away’ until the aiding load is reduced to a level within the operating range of the drive. This is a critical failing of the torque limiter.

Some factors lessen the effects of aiding loads:

- As the aiding load is transferring energy to the actuator, the actuator motor does not have to apply torque to overcome the losses in the gearbox as these are overcome by the aiding load. In the case of the NWS, a 70% gearbox efficiency results in a 7000Nm aiding load requiring 8.2Nm of torque from the motor, compared to a 7000Nm antagonistic load requiring 16.8Nm.
- The controller is in a regenerative mode of operation when the load is aiding. This can result in a dc link above the supply rating and a higher PWM voltage, increasing the operating range of the drive. However, in the case of the NWS, the controller is configured to regenerate energy directly to the Airbus dc power supply, which is held at 540V, so the converter voltage will not exceed this.

For the timescale of the NWS project it was ultimately deemed sufficient to remove the torque limiter and reduce the peak operating speed of the controller to 1000r/min, where maximum aiding or antagonistic load of 7000Nm can be applied without exceeding the safe operational range. Although this is acceptable for demonstrative purposes, to evolve the project further to attain the desired operation under a torque/speed profile, a balance must be reached:

- A torque limiter is required for antagonistic load at motor speeds over 1000r/min as conditions will occur which exceed the output capabilities of the controller and the speed must drop accordingly.
- With aiding loads, the torque limiter profile may still be applied, but rather than removing torque once the profile is exceeded, a method to increase the operational range must be considered. Field weakening would be a potential solution, although for the NWS this would still not accommodate the sudden application of rated low-speed torque at 1800r/min.

7.5 TURN-OFF REGENERATION IN LOW CAPACITANCE DRIVES

With electrolytic capacitors widely considered unsuitable, physically larger polypropylene capacitors are used for high-altitude aerospace electric drives, so it is particularly important to minimise this capacitance. Although a more aerospace representative design than DEAWS, the 80μF capacitor bank of the ELGEAR NWS was specified to operate in conjunction with 20μH of supply inductance to filter out 10kHz PWM ripple (*see 5.2.2.1 and 7.2*) and in a production converter, an inductor could be included in the drive to allow a trade-off between capacitor volume and inductor mass.

When testing the NWS controller at Newcastle, a number of motor controllers were damaged when attempting to change the direction of the motor. In order to perform a speed reversal, even when unloaded, the inertial energy within the motor must be dissipated via the controllers to bring the motor to a standstill, before rotating in the opposite direction.

Due to the unidirectional limitation of the 540V power supply at Newcastle, each lane of the NWS is equipped to drive an external dump resistor to dissipate regenerative energy. An external diode is present on the supply to each lane to prevent regeneration and therefore the dc link capacitors can rise above 540V. Although the power supply at Airbus allows regeneration and is ‘stiff’ at 540V, the Newcastle arrangement represents a typical non-regenerative setup for a fault tolerant actuator.

When examining the damaged converters, IGBTs were found to be damaged. As failure occurred when performing an unloaded speed reversal, any motor currents were brief and within the specified 15A software limits of the controller. Rather than current overload damage, the possibility of excessive dc link voltage was considered.

Haskew and Hill [88] discuss the concept of switch-level regeneration within motor drives and this is of particular relevance to aerospace-designed converters with minimal dc link capacitance.

Electric drive regeneration occurs in multiple stages and these can be shown on a single-phase H-bridge for simplicity. For this example, it is assumed that due to prior regeneration, the voltage across the dc link capacitor, V_c is higher than the dc supply voltage, so the capacitor can be considered as the supply source, with the supply regeneration-blocking diode (not shown) reverse biased.

The first stage is controlled switching of the IGBTs, as in Figure 7-19. The converter is actively regenerating from the motor in this example, with the back emf acting as a source. This effectively sums the dc link capacitance and the back emf voltages and connects them across the motor windings. This will rapidly build up the current within the winding inductance.

The voltage across the inductor is given by:

7-10 $$V_L = V_C + V_{emf} - IR$$

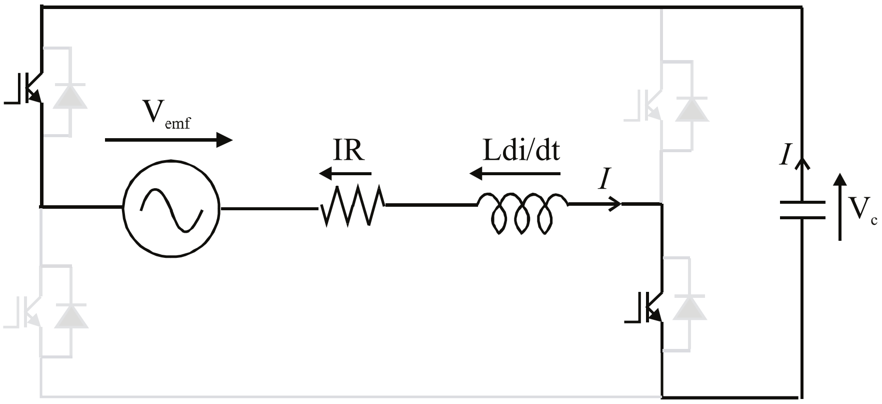

Figure 7-19: Switching IGBTs to sum back emf with supply.

During this stage the current in the inductor will build up following:

7-11 $$\frac{\partial i}{\partial t} = \frac{V_L}{L}$$

The build-up of current is not perfectly linear as the circuit is effectively a series RLC arrangement, so discharging of the capacitor and increasing current through the phase resistance will dynamically alter the values of V_c and IR. It should be emphasised that at this initial stage, the energy transferred to the inductor is from both the dc capacitor and the motor back emf source, with the ratio proportional to their voltages (for example, if V_{emf} is 270V and V_c is 540V, then 66% of the additional inductor energy is from the capacitor).

As ELGEAR windings are switched with 10kHz unipolar PWM, the next stage of operation is to switch on both top or bottom IGBTs to enable a freewheeling path for the inductor current (Figure 7-20). The current will continue to rise during this transition, but at a lower rate, driven only by the motor back emf.

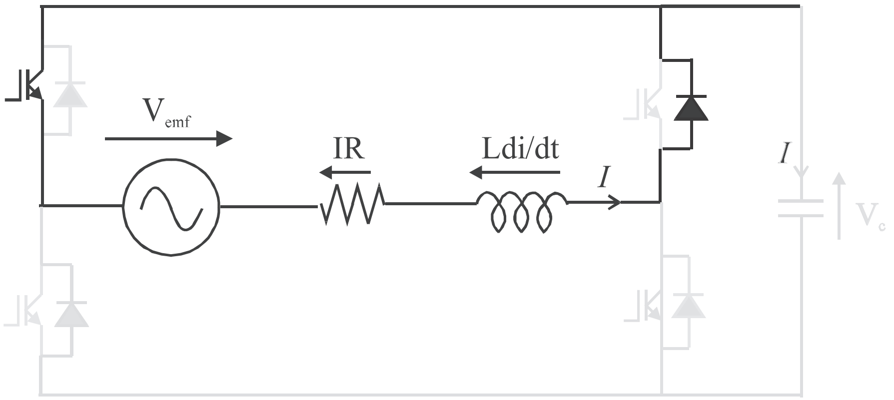

Figure 7-20: IGBT controlled freewheeling.

The final stage of regeneration is to switch on the bottom left and top right IGBTs. As anti-parallel diodes are fitted to prevent damaging reverse conduction of the IGBTs, the current will continue to flow using these diodes, back into the dc link capacitor (Figure 7-21). This will attempt to increase the voltage in the capacitor.

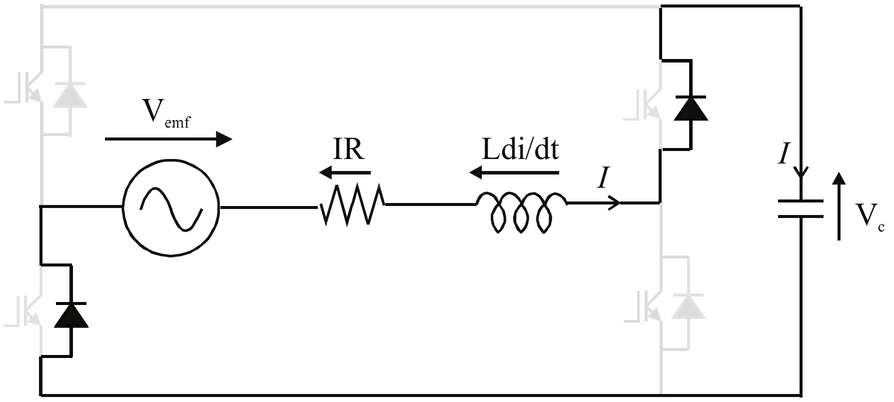

Figure 7-21: Turn-off of transistors and freewheeling path.

As with the first stage, the circuit is now an RLC arrangement and:

7-12 $$V_{emf} - V_L - IR = V_C$$

Current flows in the same direction through the inductor and into the capacitor, increasing the stored charge and V_c, but as V_c is > V_{emf}, V_L becomes negative and the inductor current decreases. If the commutation controller dictates, this process will occur until the inductor current reaches zero and if the two parallel IGBTs remain switched on, the inductor current will eventually flow in the negative direction, discharging the capacitor.

This multi-stage process results is an increased capacitor voltage from charge provided by the motor back emf. Although this process is controlled, the alternative is that, should all IGBTs be switched off during regeneration (i.e. during a failure), then the last stage of the process will involuntarily occur, remaining until all the energy within the motor inductance is transferred to the capacitor, via the anti parallel diodes. When an electric drive is controlling a dump resistor, this may also be disabled at this point, resulting in an uncontrolled rise of the capacitor voltage. While a controller can offer fully independent operating of the motor and dump resistor circuits, the logical regeneration fail-safe when the controller cannot maintain the dc link below a safe threshold is to depower the motor and dump resistors.

In the case of the NWS, the dump resistor is switched across the dc capacitor bank when V_c exceeds 590V and should the dump resistor fail to dissipate enough energy; the drive will shut down all motor and resistor IGBTs at 680V to prevent over-voltage damage. It is the subsequent transfer of energy at this 'fail-safe' shut-down point that must be considered.

A laboratory demonstration of this operation is shown in Figure 7-22, with a close-up in Figure 7-23. The NWS is operating without a brake resistor present to highlight the over-voltage shutdown events.

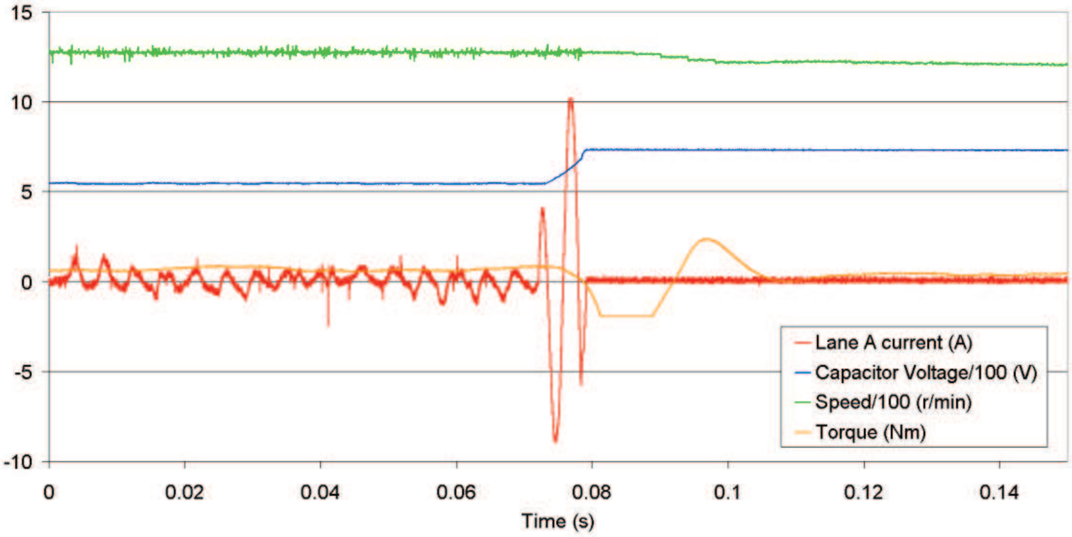

Figure 7-22: Regeneration, then switch-off.

The initial rise in current and dc link voltage at 0.07s is controlled regeneration, as the NWS drive absorbs power from the aiding load into the dc link capacitor. At 0.784s, the capacitor voltage exceeds the shutdown threshold of 680V and all IGBTs are switched off. The current in lane A (showing a single phase of the motor) collapses and the capacitor voltage continues to rise, but following a different profile. From this point the energy within the motor inductance is transferring to the capacitor through the anti-parallel diodes and as the motor current falls, the capacitor voltage increases.

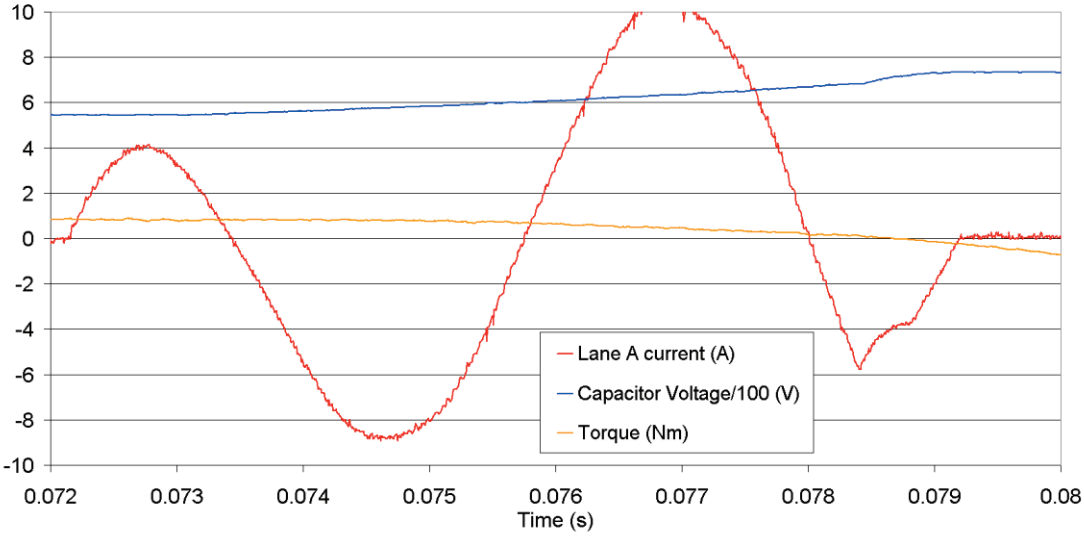

Figure 7-23: Close-up of regeneration, and switch-off spike. 730V on capacitor at end of process.

Although a relatively minor increase in voltage, this process is uncontrolled and must be considered when specifying the dc link capacitor value for a converter. On the ELGEAR NWS demonstrator the capacitor bank is rated for 750V and this test condition has raised the capacitor voltage close to this limit. In reality the 750V rating voltage of the capacitor bank is under-specified; however, even with higher rated components; the voltage increase is still an additional step towards the breakdown voltage of the power transistors, which must be considered.

Designers of aerospace converters with fault tolerant permanent magnet motors of inherently high inductance and electric drives where capacitance is minimised, should consider these uncontrolled energy transfers when specifying components.

7.6 CONCLUSIONS

Through research and design of the ELGEAR NWS and DEAWS, a series of design considerations have been presented in this chapter. All are of relevance beyond the scope of their associated project, as part of the myriad of challenges when implementing fault tolerant electric drives and actuators for aerospace applications.

Current shifting, to overcome torque ripple in faulted multiple single-phase drives, could be considered more of a software option than a design consideration. Although torque ripple can theoretically be eliminated and the peak currents are slightly lower than current reshaping, the higher power dissipation makes current-shifting a less attractive proposition; however, there may be applications where sinusoidal currents are preferred to relatively complex reshaped waveforms.

A very significant consideration when designing a fault tolerant system is the additional input current distortion for drives based on single phase winding modules. The extra inductance and capacitance required for a system such as DEAWS to attain aerospace requirements makes the filter considerably larger than an equivalent multiple three-phase system. This presents a considerable disadvantage for single-phase based systems, which may nullify the merits of a potentially smaller motor and converter than a three-phase alternative.

The requirement for data sharing in a fault tolerant control system was presented in this chapter. The criticality of minor signal variations between lanes, such as speed sensing, may not be apparent on many laboratory fault tolerant systems where multiple control lanes are simulated on a single processor. Information sharing must be considered for any drive running all lanes simultaneously. The torque sharing method applied to the ELGEAR NWS is very simple and although effective, poses a few additional questions regarding the fault-tolerance of such a scheme on a duplex controller, should one controller give false information to the other about the torque output. This will be a future consideration in the evolution of the system or any other duplex active-active system.

Difficulties in designing an electric actuator to follow a torque/speed profile and dynamically adjust the speed, depending on load, have been presented. This could be considered an uncommon method of operation as an actuator could be designed to operate at a fixed speed and known load, but allowing an actuator to increase speed where possible could be advantageous in reducing movement time. Such a mode of operation may be inappropriate for actuators used on flight control surfaces due to the resulting unpredictability of the rate of movement.

The turn-off regeneration observed on the ELGEAR NWS controller is symptomatic of electric drives with low capacitances. Although the rise observed in the dc link voltage of the NWS cannot be confirmed as damaging, designers of aerospace electric drives must account for the discharging of motor energy when attempting to minimise quantities of capacitance.

Many of the considerations presented highlight the difficulties faced in transferring laboratory prototype fault tolerant systems to aerospace products. It could be questioned whether aerospace manufacturers will ultimately approve electric drives requiring complicated post-fault mitigation strategies, such as torque ripple compensation, or even imposing short-circuits to overcome limit the impact of winding faults.

Similarly, there may be difficulties in assessing all the potential failure modes of fault tolerant drives where high bandwidth cross-communication is required and where disabled or faulted electronic lanes remain capable of generating high dc link voltages or drag torques in the motor.

8 Conclusions

The existing research and development of actuation for the More Electric Aircraft has been assessed, with safety the dominating factor in the airworthiness of new actuation technologies. The application of electromechanical actuation in existing aircraft is limited as reliability is not considered as high as hydraulic and electro-hydraulic actuation.

Whereas hydraulic actuators will revert to a failsafe damping mode, allowing a surface to 'blow back' to a safe position or parallel actuators to continue movement, electromechanical ball or roller screw actuators may suffer a jam within the screw, gearbox or motor.

Two very different electromechanical actuation systems have been presented in this thesis, for systems where a mechanical jam can either be overcome by decoupling, or does not present a significant safety risk when handled correctly. As a result, both the DEAWS electrical flap system and the ELGEAR nose wheel steering provide a more viable step towards aerospace acceptance than many 'blue sky' research projects.

With a degree of fault tolerance foreseen for both projects and permanent magnet motors selected for optimum torque density at the required power levels, fault tolerant permanent magnet drive topologies have been researched with two variants of drives identified: $n+1$ (single-phase drives) and $3n+3$ (3-phase) drives.

The sizes of the motor and power electronics were assessed for both these drive topologies under three operating conditions, high speed, low speed and near standstill. Use of multiple single phase lanes ($n+1$ drives) presents a disadvantage at low speed due to the torque ripple resulting from a failed phase; however, multiple three phase lanes ($3n+3$ drives) require a higher component count for the same motor size and power converter KVA rating.

A table of electronic converter and motor sizes for all viable $n+1$ and $3n+3$ drives has been presented, allowing selection of the optimum permanent magnet drive topology for an application.

Aspects of the trade study process for both actuation systems have been discussed, with safety calculations presented for both, highlighting the potential failure modes.

For DEAWS, as subsequent flight is possible, the failure-to-operate probability of a flap system is 1×10^{-5} per flight hour, a significantly less stringent condition than the $<1\times10^{-10}$ expected for a primary flight control surface. It has been shown that the jam probability of an electromechanical actuator is sufficiently low to achieve this requirement but that a fault tolerant electric drive is required to reduce the associated failure probability by overcoming a single electrical failure of the motor, control electronics, signalling or power supplies.

The probability of an uncommanded flap movement, either due to aerodynamic forces following loss of power or an incorrect actuator operation is specified as 1×10^{-10} per flight hour, as this could result in a roll of the aircraft. To attain this, it has been shown that power-off brakes and three lanes of control electronics are required. The *2+1* electric drive was identified as an ideal topology for DEAWS as it provides an optimum balance of size and component count, whilst providing full motor control following a fault. The three processing elements in the *2+1* system allowed triplex monitoring and voting of the flap position sensors and high integrity control, allowing the system to apply the brakes following a disagreement between the two remaining lanes in the event of a second fault.

The ELGEAR nose wheel steering employs a clutch to decouple the nose leg from the actuator mechanism in the event of a failure, including a jam. As the steering is only required for taxiing, failure of the electronics or removal of the power supplies will release the clutch and allow a safe landing or takeoff. Although specific safety requirements are not discussed, the steering is required to operate after any single electrical fault, therefore the minimum option of a duplex system was selected. The *3+3* electric drive was selected as a three lane motor drive such as that of DEAWS was considered to have an excessive component count and the relatively high 4× over-sizing of the *3+3* motor was not deemed significant in respect to the overall actuator mass.

In assessing the safety requirements of the actuation systems it is clear that the failure of a power supply or control signal must be considered as critical as that of an electric drive lane, therefore true fault tolerant systems must use independent power supplies and control signals for each lane. It is also apparent that three or more lanes allow voting of parameters, so two lane systems may require extra measures to avoid deadlocks in the event of a disagreement.

Prototype actuators were produced for both systems, each featuring fault tolerant motors, gearboxes, actuator mechanisms and power electronic converters. The latter has been described in detail in this thesis, including the necessary fault tolerant control schemes. Cost and development restrictions limited the power electronic controller of DEAWS to a single DSP emulating three processing elements, although fully independent H-bridges were implemented for each lane and the powerful processor allowed rapid implementation of current reshaping waveforms and a representation of an aerospace triplex control scheme with 'high integrity' monitoring of the actuator. This safety critical control aspect leaves much scope for future research. With the ELGEAR NWS a true duplex converter arrangement was produced, with completely independent motor drive electronic lanes and real-time synchronization. The NWS converter is far more compact than the earlier DEAWS system and features much simpler processing devices, yet maintains the full functionality required for the Airbus demonstrator with ample code and processing headroom for evolving the system to handle motor winding short-circuit faults and even model-based algorithms for improved fault detection. The fully independent processing lanes of the ELGEAR control electronics highlighted the need for synchronisation when operating both lanes simultaneously, a requirement not apparent on DEAWS as emulating multiple processors in a single DSP can mask data and timing variations.

A series of laboratory tests were performed on the electric drives of DEAWS and ELGEAR, using a dynamometer to demonstrate the fault-handling of the two systems in response to open circuit conditions and the performance under normal, open circuit and terminal short-circuit conditions. Results were also presented from successful demonstrations on actuator test benches at FR-HiTemp and Airbus, showing loaded actuator performance and failure responses.

The development and testing highlighted a series of implementation considerations for both systems, the most critical being the requirement for additional filtering on $n+1$ based fault tolerant electric drives, which could result in a considerable size and weight penalty.

In hindsight, the question could be asked:

"Which fault tolerant system is best for an actuator application, the DEAWS *2+1* or the ELGEAR *3+3*?"

There is no clear answer and the two actuator applications are very different, but the advantages of each system for their application can be compared:

DEAWS advantages

- Although only intended to tolerate one motor or power converter lane failure, the *2+1* system provides three-way sensor monitoring and allows majority voting of variables and detection of a faulted lane. This is critical to ensure the brakes are applied in the event of a second fault and difficulties may arise in ensuring this will always occur with a two lane system, such as the ELGEAR *3+3* controller. Additional monitoring and voting hardware could be added to a *3+3*, without adding lanes of power electronic controllers or motors, but the *2+1* offers a more elegant solution.

- The *2+1* fault tolerant motor is half the size of an equivalent *3+3* due to the lower drag torque effect of a short-circuit within a lane at low speed and rated torque. As multiple actuators will be present across the wingspan, a 50% saving in motor mass is significant. A triple three-phase drive (*2×3+3*) would require the same motor size as the *2+1* but has a 50% higher power electronic device count, although no torque ripple compensation would be required and the input filter requirements would be much smaller.

ELGEAR advantages:

- Only two electric drives are required for a duplex system and although the power device count is the same as the *2+1*, only two sets of control electronics and power supplies are required, with much reduced signalling from the Control and Monitoring and between controllers.

- Torque ripple does not occur following loss of a lane. There is no requirement for an active lane to reshape and scale the winding currents to maintain a smooth torque at very low speeds.

- The *3+3* attains the target of operation after one fault. With no safety requirement given in ELGEAR for handling of a second fault, the *3+3* is sufficient. The ultimate fail-safe condition is to release the clutch and with steering only required when taxiing, this can be performed by removal of both power supplies, if desired. Additional monitoring can be added to handle potential deadlocks of a 2-way system, but in the case of steering when taxiing, three lanes of monitoring is excessive and pilot intervention could toggle between lanes, if required.

- The *3+3* system has a far smaller input filter requirement than the DEAWS single phase systems. Although not considered at the time of design, the DEAWS *2+1* filter requirement is significant and will result in a considerable mass and volume penalty.

If a drive topology for a more generalised actuator were to be designed then a combination of both technologies could be considered. While the *3+3* is larger, this is offset by the reduced control complexity, a much lower filter requirement and no requirement to compensate for torque ripple at low speeds. A third lane could be introduced for monitoring and voting but with no power electronic capability and although a third power supply and communications link would be required, this would eliminate the deadlocks of a two lane system.

Would this generalised actuator be suitable for all aircraft surfaces? No. With existing roller or ball screws, the mechanical safety of the actuator mechanism would be considered unsuitable for primary surfaces and even if mechanical failure were deemed impossible, it would be a considerable task designing and verifying a fault tolerant electric drive capable of tolerating multiple faults in order operate with a failure rate below 1×10^{-10} per flight hour.

With the safety of mechanical actuation technologies (in particular roller screws) constantly being reassessed, the challenges in the aerospace approval of fault tolerant electromechanical actuators must be considered.

The DEAWS and ELGEAR NWS avoid the failings of many ‘fault tolerant’ drives by using topologies allowing independent lanes of power with independent power supplies, signals and processing, rather than attempting fault tolerance within a single drive [60]. By requiring only two or three power supplies (i.e. one to each lane), the difficulties in commissioning fault tolerant drives with higher lane numbers (e.g. [20]) are also avoided.

Research is required to assess all the failure modes and effects within fault tolerant drives. Where synchronisation is employed, a detailed analysis of potential common failures must be undertaken. Synchronisation can be sidestepped by operating electric drives in active-standby, the mode of operation for the alternative ELGEAR NWS actuators produced by Nottingham/G.E.[89], with two fully independent motors and power electronics proposed. The NWS presented in this thesis is also capable of operating in active-standby, although full independence of controllers (no cross-communications) would remove the ability to compare position sensors and other fault cross-monitoring, relying on a drive which detects all its own faults, requiring overseeing electronics to detect anomalies, or the pilot to realise and switch lanes. A notable active-active benefit, demonstrated by the NWS presented here, is the fast system recovery following a fault, although it could be argued this is unnecessary for a system used only during taxiing.

Another potential hurdle for fault tolerant systems is the requirements and behaviour post-fault. Where a motor short-circuit has occurred, a lane must remain powered to actively short-circuit the motor terminals and minimise fault currents [29]. The acceptability of this must be considered, in particular the heating effects on the motor following a second failure resulting in loss of transistor operation. An unpowered lane will also become live, should the connected motor be rotated from another lane and this may be undesirable. These faults are limited to permanent magnet machines and there may be future research into considering the advantages of switched reluctance motors in smaller actuators. Some of the additional motor mass of the SRM may be offset by the absence of faulted drag torque, while torque ripple issues may be avoided by parallel multiphase configurations similar to the ELGEAR *3+3*.

It can be concluded that, while the two actuators presented here are a step forward, there is scope for much further research into actuators for More Electric Aircraft.

As an epilogue, it may be noted the DEAWS system was ultimately deemed unacceptable to Airbus, not due to the design of the fault tolerant electronics, but due to concerns over placing the brakes on the high speed side of the gearbox, which would involve holding the flap from one side following a gearbox disconnection, something considered unsafe. A revised design was proposed to address these concerns and work has been undertaken by the author on a successor to the project.

To summarise, this thesis has presented an application-level analysis of actuation in commercial aircraft, considering systems from a safety perspective to show where electromechanical actuators can be applied and where fault tolerance is necessary. New methods of determining the optimum permanent magnet electric drive topology have been presented, alongside their associated fault-tolerant control strategies and the aircraft-level constraints upon drive designs. Two industrial projects were presented, showing application of two very different fault tolerant actuators and their associated electric drives, both of which were compared and contrasted. Through experimentation, fault tolerant control schemes were verified, including algorithms to compensate for torque ripple and synchronisation between fault tolerant lanes in a drive. Additional findings were also presented, providing further information into the challenges involving laboratory based research projects for viable aircraft hardware.

9 Appendix A

9.1 MINIMUM SPEED NEEDED TO OVERCOME TORQUE RIPPLE

Rotational energy is given by:

9-1 $$E = \tfrac{1}{2} I\omega^2$$

Moment of inertia, I, of a solid cylinder of radius r, length l and density ρ:

9-2 $$I = \tfrac{1}{2}\pi\rho l r^4$$

9-3 $$\therefore E = \tfrac{1}{4}\pi\rho l r^4\omega^2$$

Estimation of energy required to overcome a torque ripple:

In the worst case, assume that a failed phase no longer contributes to torque for one quarter of an electrical cycle (healthy torque is sinusoidal so average output was only for ½ a cycle and at twice the electrical frequency.) If there are P pole pairs then the energy associated with this loss of torque is given by:

9-4 $$energy = T\delta\theta = T\frac{2\pi}{4P}$$

For the fault tolerant drive described in 3.4 (and also in [29]), with a nominal peak phase torque of 2Nm and 8 poles, this energy is

9-5 $$\frac{2\times 2\pi}{4\times 4} = 0.785J$$

The rotor dimensions and density are r=0.054m , l=0.08m, ρ=7800kg/m^3

Hence, using equation 9-3, the stored inertial energy in the rotor is

9-6 $$\frac{\pi}{4}\times 0.08\times 7800\times 0.054^4\omega^2 = 4.2\times 10^{-3}\omega^2$$

The rotational mass could be far greater when shaft, gearbox and actuator rotating mass are included, but just taking the motor alone, the minimum speed needed to overcome the torque ripple is given by:

9-7 $$0.785 = 4.2\times 10^{-3}\omega^2,$$
$$\omega = 13.7\ \textit{rad/s, i.e. 131 r/min.}$$

9.2 EXAMPLE OF CURRENT RESHAPING

Consider the instantaneous torque of a 2+1 machine operating with all three phases:

9-8 $$T = (P_a + P_b + P_c)/\omega_m$$

$$T = \frac{[I\sin\alpha \times E\sin\alpha] + [I\sin(\alpha+2\pi/3)\times E\sin(\alpha+2\pi/3)] + [I\sin(\alpha-2\pi/3)\times E\sin(\alpha-2\pi/3)]}{\omega_m}$$

We can rearrange to separate out the angle-varying power components:

9-9 $$TIE\omega_m = [\sin\alpha\times\sin\alpha] + [\sin(\alpha+2\pi/3)\times\sin(\alpha+2\pi/3)] + [\sin(\alpha-2\pi/3)\times\sin(\alpha-2\pi/3)]$$

In a three phase machine, the sum of the three angle varying components is nominally a constant 1.5. When a phase fails, such as c in this example, the resulting sum of the angle-varying components is equal to the failed component subtracted from the nominal constant value:

9-10 $$1.5 - [\sin(\alpha-2\pi/3)\times\sin(\alpha-2\pi/3)]$$

Making the assumption that the failed phase current and back emf would have been sinusoidal, the equation simplifies to.

9-11 $$1.5 - \sin^2(\alpha-2\pi/3)$$

The deviation from the nominal value of 1.5 is given by:

9-12 $$\frac{1.5-\sin^2(\alpha-2\pi/3)}{1.5}$$

The reciprocal of this can be applied as a scaling to the remaining phases to increase their angle-varying components to the nominal value of 1.5 at all angles.

9-13 $$TIV\omega_m = \left[\frac{1.5}{1.5-\sin^2(\alpha-2\pi/3)}\right][\sin\alpha\times\sin\alpha] + \left[\frac{1.5}{1.5-\sin^2(\alpha-2\pi/3)}\right][\sin(\alpha+2\pi/3)\times\sin(\alpha+2\pi/3)]$$

As the back emf of the remaining phases is fixed, only the currents may be altered to increase the angle-varying power. We can re-arrange and simplify the equation to

9-14 $$T = \frac{\left[\frac{1.5I\sin\alpha}{1.5-\sin^2(\alpha-2\pi/3)}\right]V\sin\alpha + \left[\frac{1.5I\sin(\alpha+2\pi/3)}{1.5-\sin^2(\alpha-2\pi/3)}\right]V\sin(\alpha+2\pi/3)}{\omega_m}$$

Thus the currents for the two remaining phases, a and b, in this *2+1* motor are:

9-15 $$\frac{1.5I\sin\alpha}{1.5-\sin^2(\alpha-2\pi/3)} \textit{ and } \frac{1.5I\sin(\alpha+2\pi/3)}{1.5-\sin^2(\alpha-2\pi/3)}$$

9.3 TORQUE AND CURRENT WAVEFORMS FOR N+1 PHASE MOTORS.

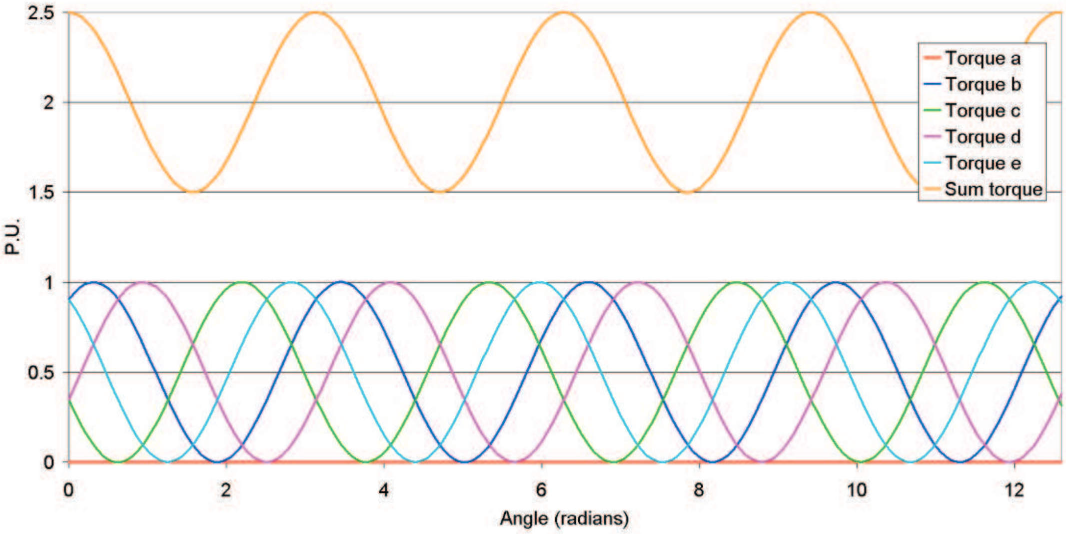

Figure 9-1: 4+1 phase motor torque waveforms with phase a open circuit and no current reshaping.

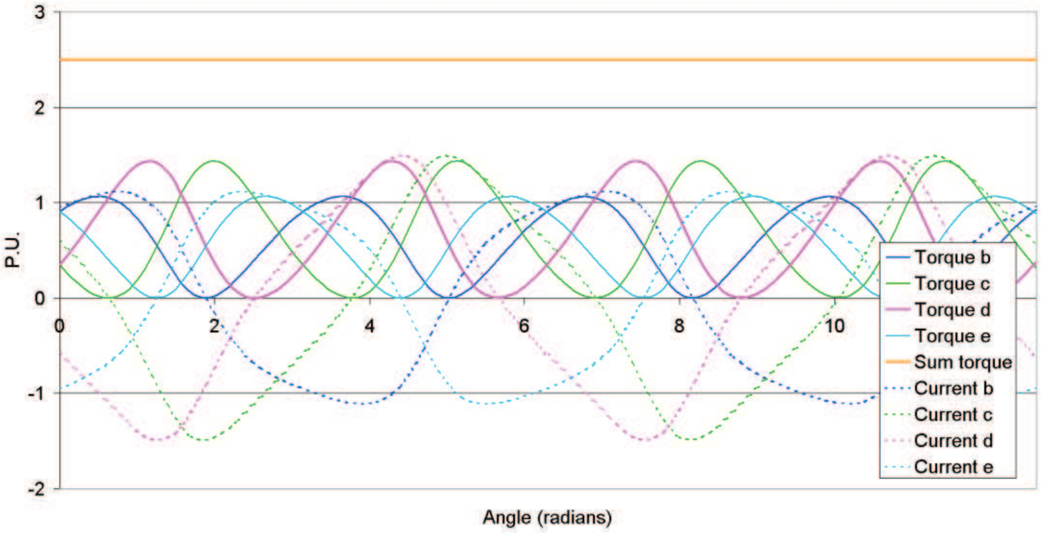

Figure 9-2: 4+1 phase motor with current reshaping.

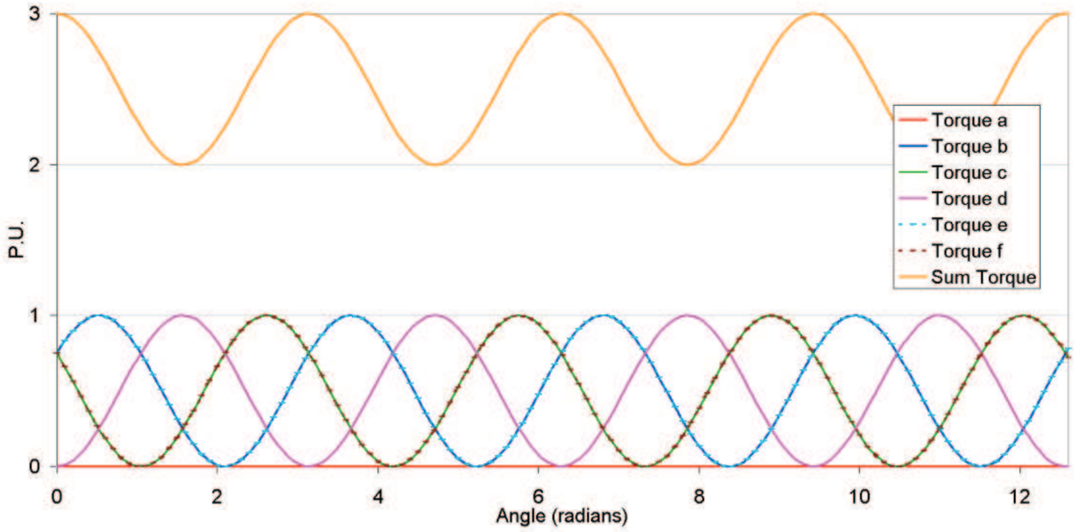

Figure 9-3: 5+1 phase motor torque waveforms with phase a open circuit and no current reshaping.

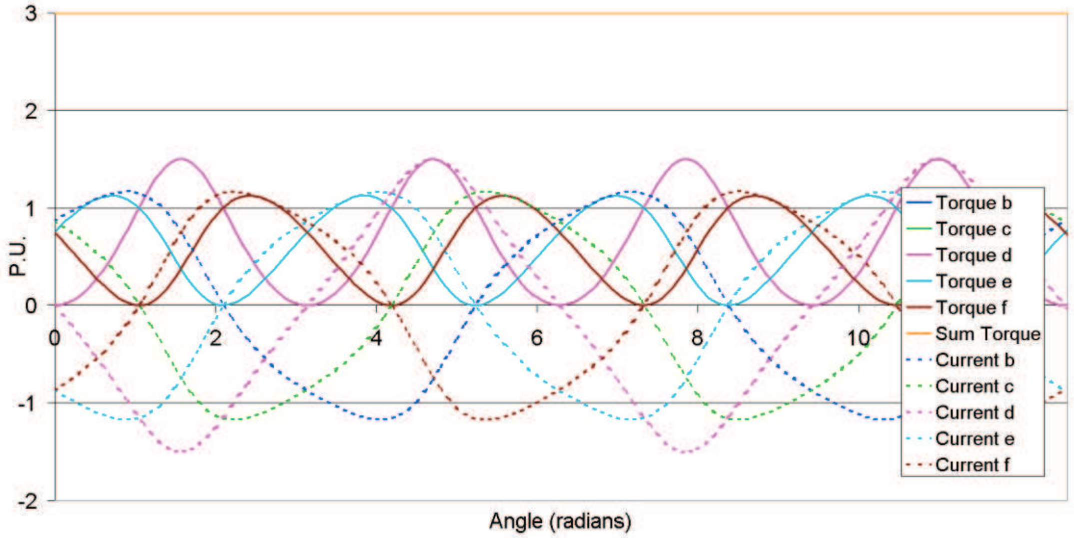

Figure 9-4: 5+1 phase motor with current reshaping.

10 APPENDIX B

10.1 DEAWS FLAP OPERATION

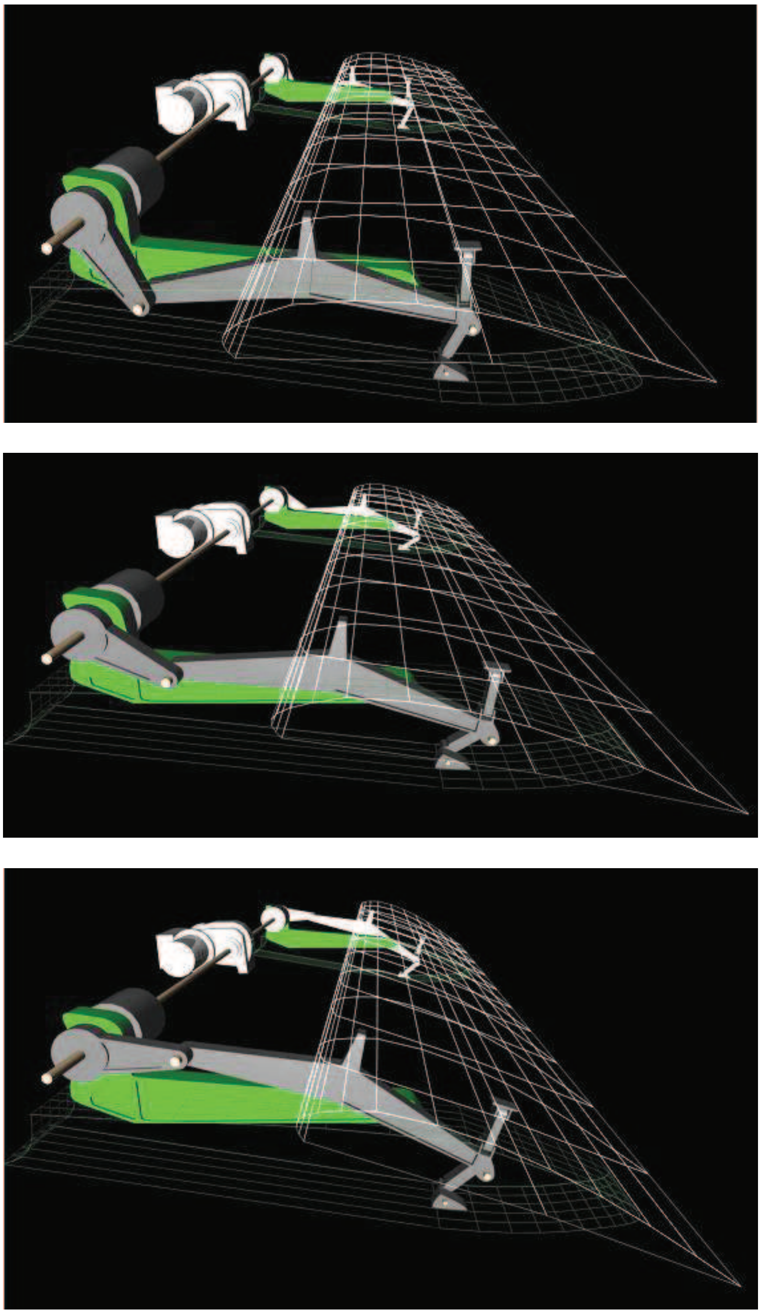

Figure 10-1: Operation of DEAWS rotary flap mechanism.

11 Appendix C

11.1 FURTHER DETAILS ON DEAWS HARDWARE AND SOFTWARE

11.1.1 DEAWS control software

The control scheme for a single lane of the DEAWS controller is shown in Figure 11-1. Each control lane contains an identical software control scheme with nested proportional-integral (PI) loops for position, speed and current.

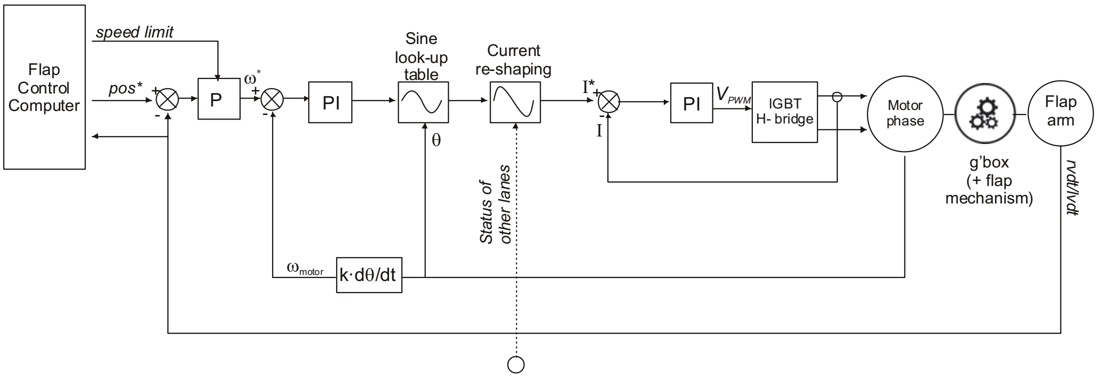

Figure 11-1: DEAWS control diagram.

The position controller compares a demanded flap angle from the flap control computer against the measured flap angle from the RVDT and LVDT transducers on the flap mechanism. Whilst full position control is performed in each of the drive lanes, the symmetry controller in the FCC also receives a copy of the position data from each lane, allowing detection of anomalies and determining of a ‘true’ flap angle. A speed limit parameter is transmitted from the FCC, allowing the motor speed to be reduced from a maximum of 10,000r/min. The symmetry controller is within the BAE Systems FCC, so considered out of the scope of this thesis, however it’s basic function is to compare the flap angles of corresponding actuators on each wing, adjusting the speed limits to slow the faster flap so it remains in symmetry with the slower flap. When symmetry deviates beyond an acceptable tolerance, a brake signal is transmitted to all lanes on all flaps, applying the friction brakes and locking the entire flap system.

Identical PI controller code is used for the position, speed and current loops, following the conventional arrangement shown in Figure 11-2. Constants are set for the proportional and integral gains (k_p and k_i), with values obtained by real-time tuning of the drive on a testbench and on the flap test rig (*see section 6.1*), using the user interface shown in Figure 5-9 (*pp. 117*).

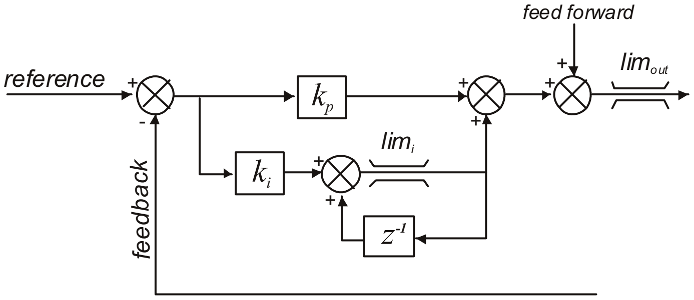

Figure 11-2: PI controller diagram.

All parameters are stored in RAM and are adjustable via the user interface. In the position control PI loop, the speed limiter parameter (from the FCC), controls the motor speed by writing to the output limit parameters (±$\mathrm{lim}_{\mathrm{out}}$). In the current PI loop, the predicted back EMF of the motor (calculated from the motor speed, commutation angle and a look-up-table) is added as a feed-forward term for improved control stability.

It should also be noted that, prior to use in the PI control loops, the data from the FCC (position demand, speed limit and control logic) is cross-voted between lanes to ensure identical parameters are used in each lane. This voting scheme is shown in Figure 4-24 (*pp.97*).

As the speed loop output is a DC current demand, a sinusoidal current demand is derived using the motor angle (via a resolver). In the case where current must be reshaped at low speeds, following a lane failure (*see section 3.5*) a current reshaping block scales the sinusoidal current reference to produce a reshaped waveform. Two reshaping routines are present in the block since the required reshaping is dependent on which of the other 2 lanes has failed, and therefore the status of all lanes is cross-communicated at this point (simply an exchange of variables between function blocks when performed within the single DSP lab demonstrator). The current PI controller attempts to synthesise the pure or reshaped sine-wave current demand by controlling the modulation of the PWM output.

The position and speed loops are sampled at 100Hz, while the current loop and current shaping are calculated at PWM rate (10kHz). As three lanes are simulated on a single processor, the sampling of the control loops in all of the lanes is inherently synchronised to common interrupts, so no specific inter-lane synchronisation method is required.

11.1.2 DEAWS control hardware

A Sundance Multiprocessor Technologies development system controls all three power electronic lanes in the DEAWS prototype. The system consists of a series of processing cards and a base-board:

- **SMT335 CPU board**: TMS320C6701 DSP, with SPI communications header.
- **SMT397 Data Acquisition board:** 12× 12-bit 50ksps A/D converters and 4× 12-bit DACs.
- **SMT118 Motherboard:** 4× RS232 UARTs and power supplies to other boards.

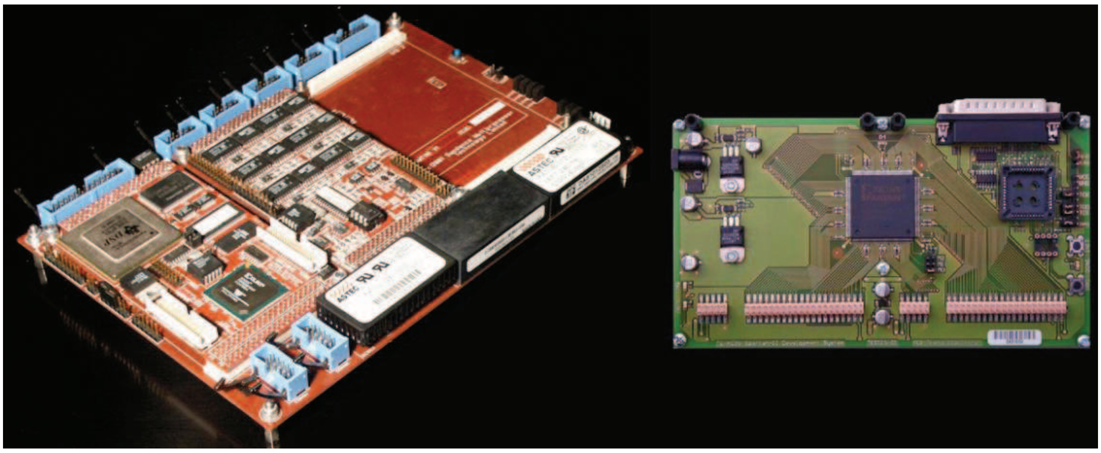

Figure 11-3: Sundance DSP system (l) and FPGA development board (r).

Communications between boards is via the ‘Sundance data bus’, in which devices on all boards are allocated to memory addresses accessible by the DSP. All inter-board control is made transparent to the user by factory-programmed mapping and sequencing ASICs.

The TMS320C6701 is not a motor-control specific processor, hence the requirement for the SMT397 to perform analogue-digital conversions. This is also apparent in the lack of digital inputs and outputs and pulse width modulation.

For the control of an H-bridge, two PWM channels are required for each power electronic module, as independently modulated leg signals allow unipolar switching. Each channel must also be split into two inverse signals for complementary switching of an IGBT pair, incorporating dead-time delays to prevent shoot-through when transitioning between an upper and lower device. A signal to the braking resistor IGBT and a fault-feedback signal from every IGBT is additionally required while it is also necessary to have fast shutdown capability in the event of a fault. It is desirable to implement this shutdown logic in hardware, rather than software, as a processor failure could result in a fault propagating and damaging the expensive CPU development system and any connected systems. In total, across the 3 lanes, 12 PWM, 3 braking and 15 feedback signals are required. Signals for contactors and other ancillaries are also needed.

To perform all this hardware control, a Field Programmable Logic Array (FPGA) is used as it allows user-defined logic and timing hardware to be implemented on a single device (often with 200+ reconfigurable pins). The FPGA selected for the prototype is a Xilinx Spartan 2, 50,000 gate, development board (Figure 11-3). The FPGA code is self-written and intended to interface to the Serial Peripheral Interface on the TMS320C6701. The SPI is a high speed, direct link to the DSP, with data appearing in directly accessible registers. The SPI can be operated at sufficient clock speeds to allow megabits of data transfer.

A 10kHz PWM trigger pulse is generated in the FPGA and sent to an external interrupt pin on the DSP. This synchronises the A/D sampling on the SMT397 and the current commutation algorithms in the DSP, leading to a series of SPI transmissions to pass PWM demand data to the FPGA and to return status and other data.

Another task for the FPGA is resolver interfacing. Each winding module is assigned to a resolver *(section 4.1.3)* and each resolver must have an excitation and demodulation circuit with and an interface to the DSP. Although the DEAWS prototype uses only one DSP, to represent the three lane modular approach, each resolver must be fed back to the DSP and handled by a representative software lane.

Three AD2S80 resolver-digital converter chips are connected to the FPGA. The converter chips are mounted on a custom-made daughterboard which plugs onto the FPGA development board. Also present on the converter board is a sinusoidal excitation signal for each resolver. Each AD2S80 provides a 13-bit conversion of the connected resolver position. The 13-bit data is converted to SPI packets and sent to the DSP, along with the fault data.

11.1.3 DEAWS power electronic hardware

Figure 11-4 shows a constructed power electronic module for a lane within the DEAWS demonstrator.

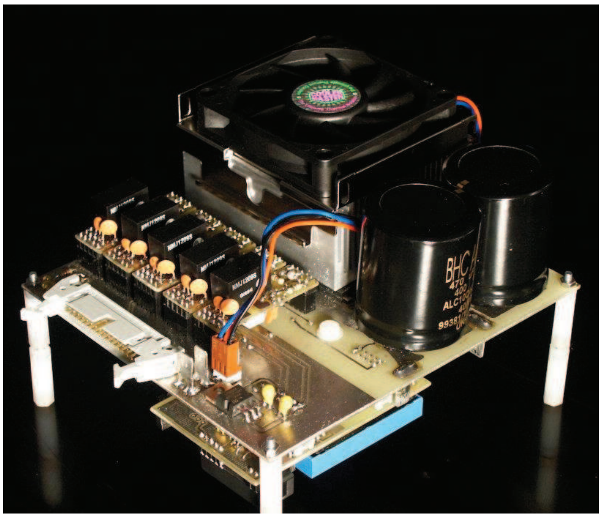

Figure 11-4: Photograph of a single phase power electronic module.

The motor winding is driven from an H-bridge of four IRG4PC50UD IGBTs while an additional IGBT drives an external braking resistor to dissipate power from aiding loads, since the on-board diode rectifier can not regenerate into the AC supply. All IGBTs and diodes are in T0-247 discrete packages, with IGBTs featuring internal fast-recovery diodes. Discrete packages may take up more collective area than combined modules, but they can be easily arranged to suit converter layouts and can be individually replaced after a failure. To keep the design compact, a heatsink/fan arrangement cools the power devices, although in an aircraft version only passive cooling would be permitted; via the outside casing of the converter.

Each IGBT has a plug-in gate-drive PCB, based around an HCPL-316 optocoupler and a dc-dc converter. The output stage of the gate drive is galvanically isolated from the low-voltage input side for operator safety reasons and to prevent processor damage after catastrophic failure of a high-voltage device. Unlike ‘bootstrap’ circuits, the dc-dc converter arrangement allows indefinite gate-drive power, providing a permanent high-side drive if over-modulation is required. V_{ce} saturation detection is also a feature of the HCPL-316, providing an automatic IGBT turn-off after ~3μs if excessive current causes the on-state voltage of the IGBT to exceed 7V (e.g. in the case of a device short-circuit). Fault data is returned to the CPU/FPGA controller where the switching logic is configured to disable the entire lane module following any single device fault.

A measurement board on the underside of the module employs an LTS15-NP hall-effect current transducer to measure the output currents of the H-bridge. A 200 kHz bandwidth provides a generous margin for the 10 kHz sampling rate of the processor current control loop.

An AN101 op-amp allows a galvanically isolated measurement of the dc link voltage, using a high-voltage potential divider network as the signal input.

The measurement board uses on-board operational amplifiers to scale all signals to the ± 10V levels for processor A/D interfacing.

11.2 FURTHER DETAILS ON ELGEAR HARDWARE AND SOFTWARE

11.2.1 ELGEAR control software

The basic control scheme for the dual-lane ELGEAR drive is shown in Figure 11-5.

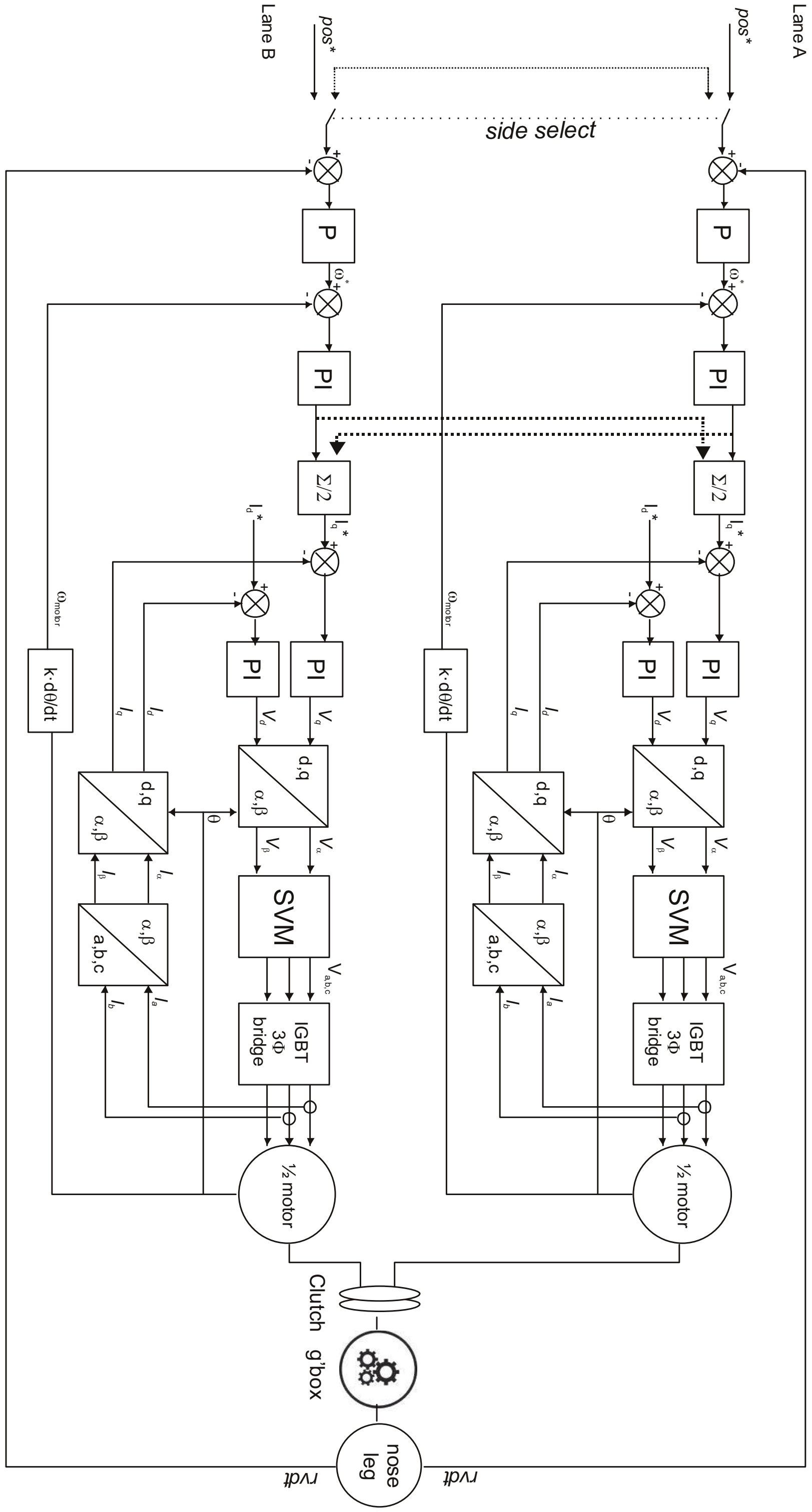

Figure 11-5: ELGEAR control scheme.

Both control lanes contain identical software, each employing nested position, speed and current control loops. Vector control with space vector modulation is employed for improved current control and to attain a 15% higher voltage than sinusoidal PWM [61]. The position and speed loops are computed at a 1kHz iteration rate, while the current vector loops are computed at the 10kHz the PWM iteration rate.

Identical PI controller code is used for the position, speed and current loops, following the conventional diagram shown in Figure 11-2 (*pp.212*). The k_p and k_i constants for the position, speed and current loops can be set by the debugging interface shown in Figure 5-20, (*pp.131*) and were defined by real-time tuning of the controller on laboratory and industrial test-rigs (*see section 6.2 for tests, while PI constants are listed in Table 7-2, pp. 183*). Integrator and output saturation limits are also set ($\pm lim_i$, $\pm lim_{out}$ respectively) and in the case of the position loop, the output limit can be adjusted via the ARINC communications input for external control of the maximum speed of the actuator (a possible feature in a later revision of the CMS). In addition, the output limits of the speed loop are internally configured to values representing 0.5× or 1× rated torque, dependant on whether the actuator is operating in active-active or active-standby mode respectively. This prevents excessive output torque when operating in active-active mode (these variable torque limits can be observed in the results of section 6.2.1.2, *pp.155*).

Cross-communications links can also be observed in the control scheme of Figure 11-5. Each lane receives ARINC input data, including a ‘side select’ command (*see Figure 4-28, pp.104 for more details*). The side select will define one lane as master, and the other as slave, with the slave obtaining its inputs from the master lane via the cross-communications. This allows dual-lane operation following an ARINC failure to one lane, as the control and monitoring system can change the master lane.

11.2.2 ELGEAR control hardware

Further details on the hardware outlined in section 5.2.2.2 are listed below:

- **A/D converters.** 10 A/D channels are sampled by the dsPIC33FJ128MC708 in each ELGEAR controller lane, including motor currents, dc link voltage, RVDT position sensors, solenoid current and a test input for frequency response analysis. All channels are sampled at PWM frequency and the entire process is automated via DMA, so the user software can simply read the converted data from an array, once all conversions are complete.

- **Motor resolver.** The motor resolver is interfaced to the dsPIC using an AD2S1200 12-bit Resolver to Digital converter chip, providing excitation signals and demodulation in a compact 12mm² surface mount package. The converter is configured to communicate using an SPI link and on each execution of the current commutation code, the motor angle is sampled by the processor.
- **RDVT position transducer.** The RVDTs used for actuator output angle sensing are modulated with an AD598 device, which also demodulates the measured angle to a dc voltage, which is fed back to the aforementioned processor A/D inputs via an op amp circuit. In retrospect, this arrangement was not ideal, as the A/D converter has only 10-bit precision, leaving only 1024 steps to measure a 190º movement, thus a resolution of 0.19º. This was just on the verge of acceptability for positional accuracy; however, there is little scope for noise in the signalling, conversion, scaling or sampling process.
- **Motor temperature.** Two AD590 thermocouple interface ICs allow direct connection of k-type thermocouples to the controller, with data is converted to a digital value and sent via SPI to the dsPIC.
- **Communications.** The dsPIC handles two ARINC channels of data using HI 3585 transceiver devices which communicate to the processor via SPI. Two on-board UART devices are also used for cross-communications between lanes and for a PC diagnostics interface. More information is given in section 5.2.2.3.

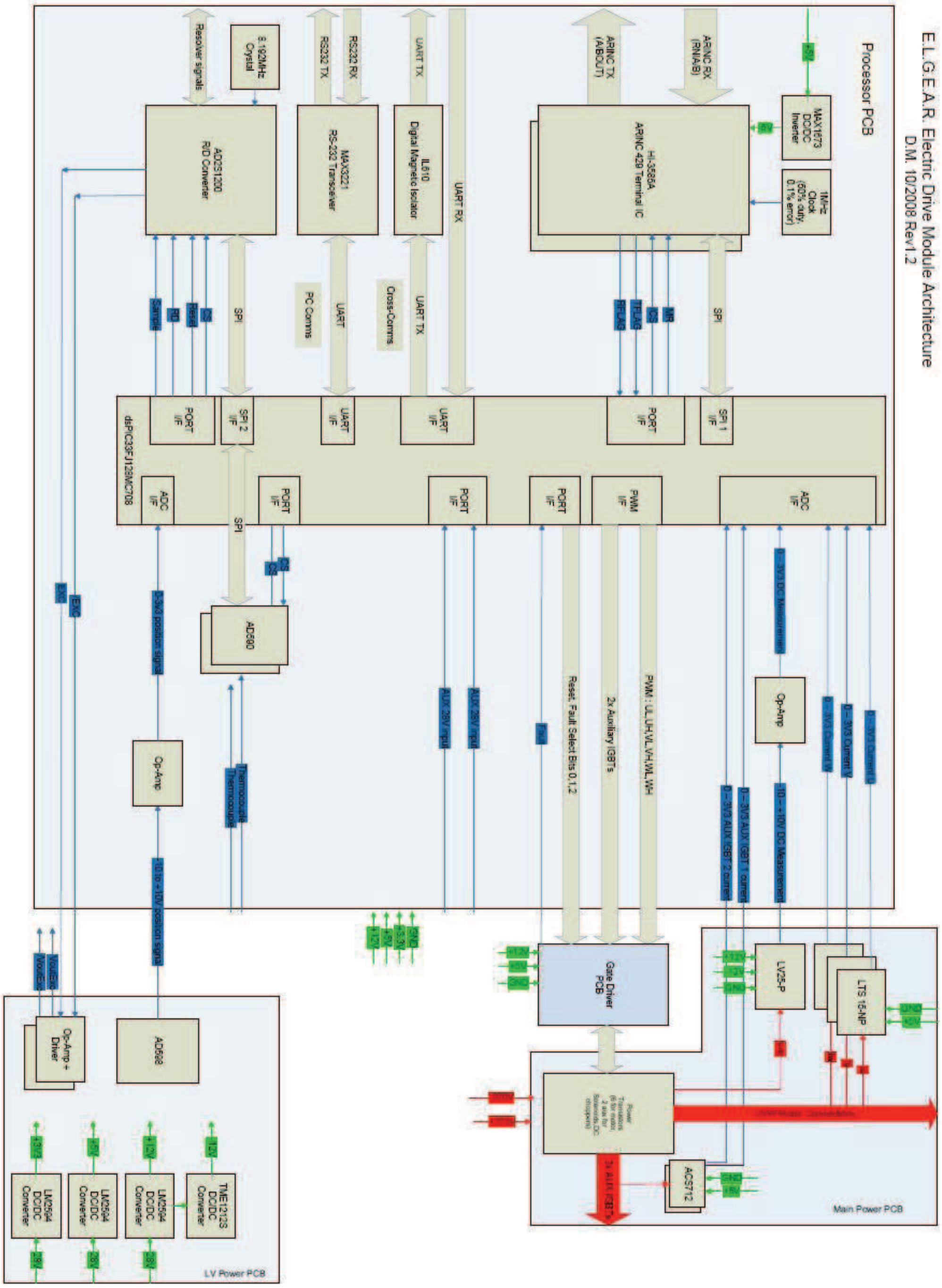

Figure 11-6: ELGEAR control schematic.

11.2.3 ELGEAR power electronic hardware

Further details on the hardware outlined in section 5.2.2.1 are presented here:

Current sensing in the ELGEAR electronic controllers is performed by LTS15-P hall-effect current sensors, present on two of the motor phase legs and providing measurement of up to 15A. These are fed via potential dividers straight to the main processors. A hall-effect current transformer measures the voltage at the dc link capacitors via a 54kΩ load resistor, drawing a nominal current of 10mA at 540V. Both sensors provide galvanic output isolation between the processing hardware and the high voltage hardware.

All power electronic components are arranged as shown in Figure 11-7, with the power devices on the underside of the PCB, which is then clamped onto an aluminium bedplate of 8×146×222mm, allowing short-term use of the controller, although it should be clamped to a larger heatsink for repeated use at high loads.

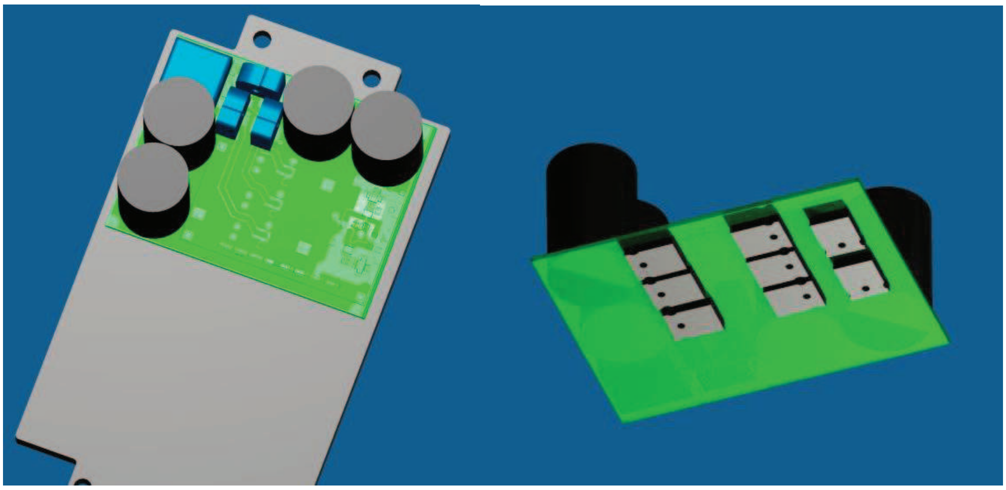

Figure 11-7: Power PCB arrangement (l) and power transistor location (r).

The capacitors and sensors are on the top-side of the main PCB and spaced to allow for a stack of control boards proving the control hardware.

A 135×80mm gate drive board plugs into the power PCB and contains 8 isolated driver circuits to switch the 8 IGBTs on the main board. Each gate driver features an HCPL-316 optocoupler, while an arrangement of NTA1215 dc-dc converters provide isolated power for low and high side devices. As with DEAWS (*pp.215*), these circuits provide isolated control of the transistor gates and automatic shutdown in the event of transistor over-currents, via V_{ce} saturation monitoring. The gate drive board is configured to switch off all 8 devices in the event of any failure, although this can be reset by the processor, should unfaulted devices be required to switch on for post-fault handling.

12 Appendix D

12.1 SIMULATION OF DUAL LANE OPERATION OF ELGEAR NWS

A MATLAB simulation of the dual-lane control scheme of the NWS is shown in Figure 12-1. The motor model contains only an inertial effect and the actuator is unloaded. The sampling and quantisation of the resolver-digital-converters is modelled for both lanes and a digital error can be injected to the lower lane (A). Similarly a position feedback scaling error can also be injected into lane A. Figure 12-2 shows the control scheme within a lane subsystem, sampled at 1kHz. Only the position and speed loops are simulated, with the torque output of the speed loops used to drive the very simple load model, rather than including a current/torque loop and detailed electric motor drive model. The switch within the control loops allows enabling of synchronisation, which is disabled for all results to highlight the variation in torque demands between the two lanes when variations in measured signals occur.

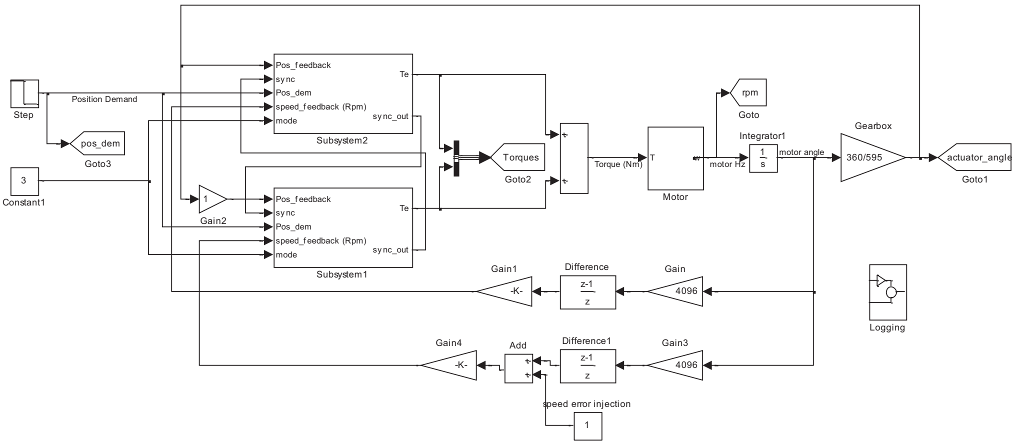

Figure 12-1: NWS Dual-lane controller simulation schematic.

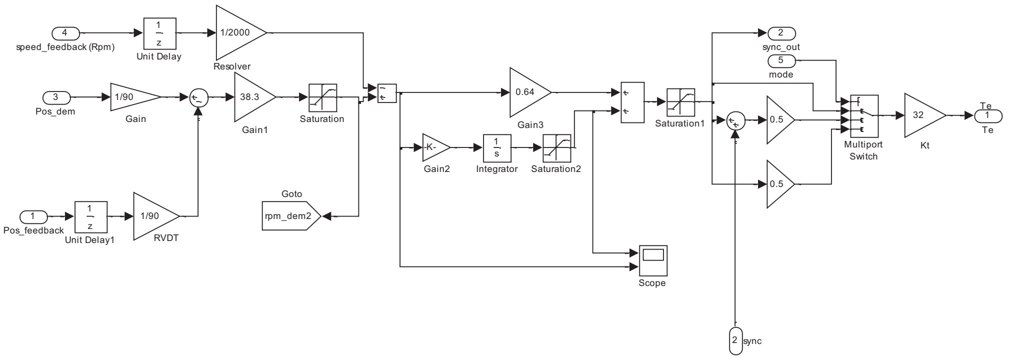

Figure 12-2: Speed and position control loops within one NWS lane.

Figure 12-3 shows a transition of the actuator from 0° to 75° and back to 0°. Identical measurements are used for both lanes, so this can be considered the ideal situation.

Acceleration is rapid, as in the real system, with an initial overshoot before the speed settles at 1000r/min. The position controller relies on a high proportional gain and saturation of the output, so the speed demand is almost always 1000r/min (shown as 10 on the lower traces). With identical feedback signals to both lanes, the speed demands and torque outputs are identical (hence lane A values are not visible on the lower trace). With no load, torque is only exerted to accelerate the inertia..

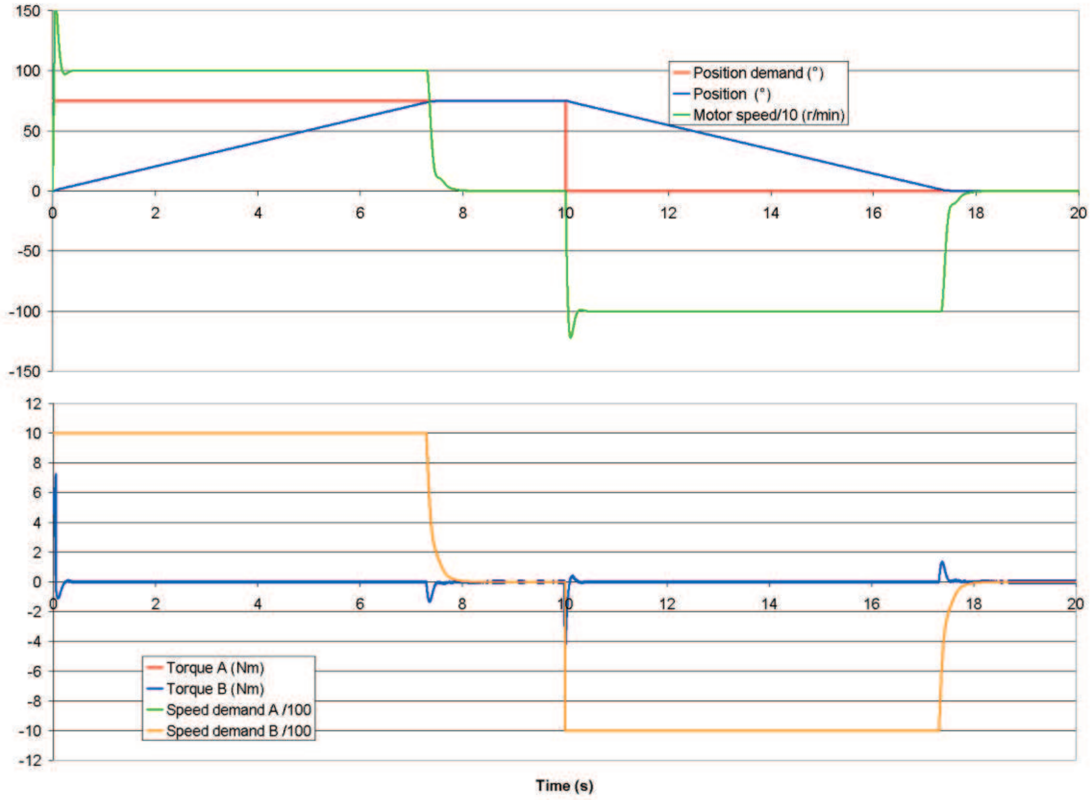

Figure 12-3: Simulation of NWS operation with identical measurements to both lanes.

The effects of a 1% measurement error applied to the position feedback of lane A (data is multiplied 1.01) are shown in Figure 12-4. The output from both lanes is identical while the speed controller is in saturation (1000r/min) and the actuator is accelerating towards 75°. A problem arises at 75° where the 1% variation in feedback results in the two lanes force-fighting to move the actuator to their own slightly different interpretations of 75°. Speed integrator wind-up occurs as both lanes are unable to overshoot and settle the actuator at the target position, resulting in severe torque fighting as the actuator continues to operate.

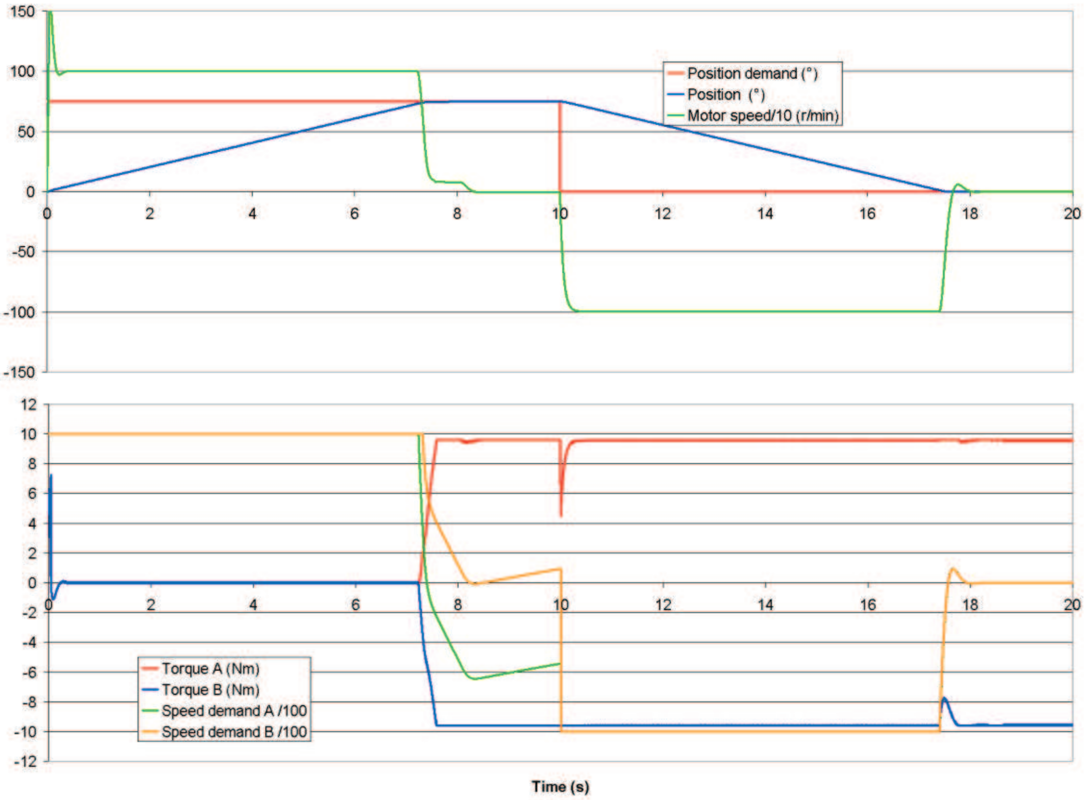

Figure 12-4: Simulation of NWS operation with 1% measurement variation between lanes.

The resulting effects of a 1-bit resolver position error producing a speed measurement variation between lanes is shown in Figure 12-5. The position feedback signals are made identical for both lanes. The resolver error effectively adds a constant 14.7r/min onto the speed calculation for lane A, resulting in a wind-up of the speed integrator as the motor is considered to be moving at the incorrect speed. With the integrator resulting in an increasing torque demand, the other lane has to counteract this to maintain correct position control. Although in reality a more random variation in speed measurements could be expected than a constant error, the simulation shows how rapidly integrators will wind-up with a relatively small error.

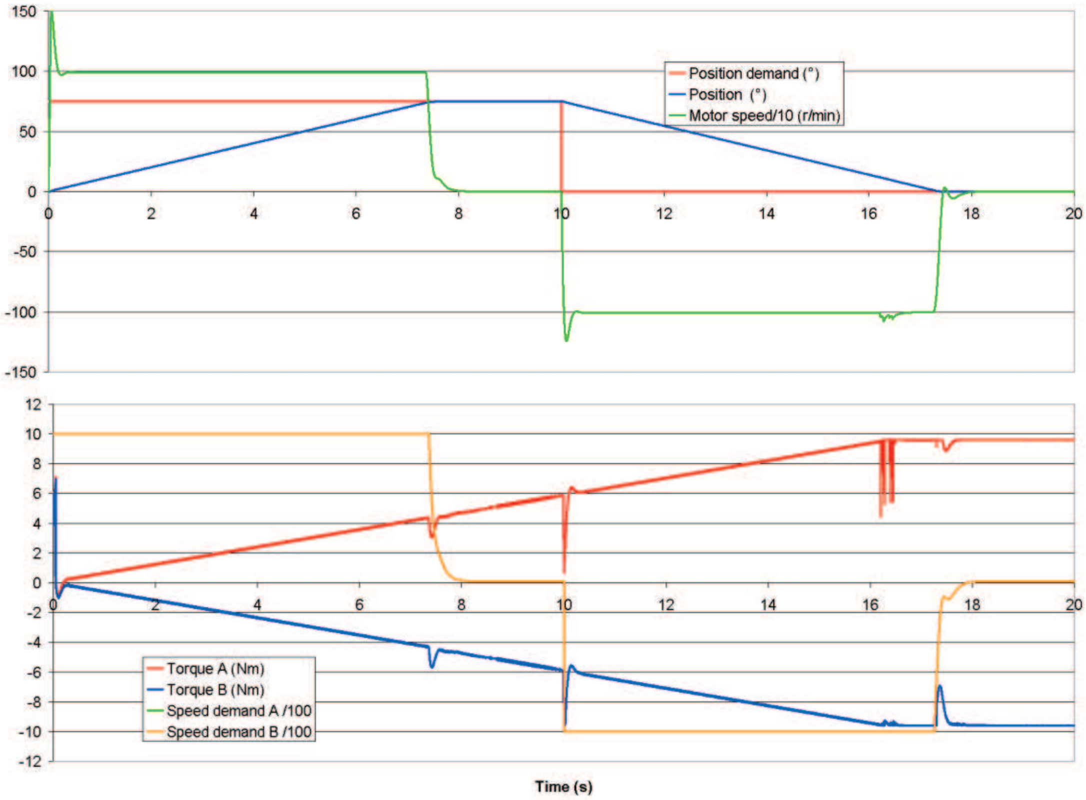

Figure 12-5: Simulation of NWS operation with speed measurement variation between lanes.

13 Index of Figures

14 References

1 Jones, R.I. Coll. of Aeronautics, Cranfield University. “The More Electric Aircraft: the past and the future?”, IEE Colloquium on Electrical Machines and Systems for the More Electric Aircraft, (Ref. No. 1999/180), pp.1/1-1/4.

2 Mecrow, B.C, Bennett, J.W, Jack, A.G, Atkinson D.J, Freeman, A.J, “Very High Efficiency Drives for Solar Powered Unmanned Aircraft”,18th International Conference on Electrical Machines, 6-9 Sept, 2008, pp.1-6.

3 Choi, B.B. Brown, G.V. “Fuel-Cell-Powered Electric Motor Drive Analyzed for a Large Airplane”, NASA R&T report, http://www.grc.nasa.gov/WWW/RT/2004/RS/RS11S-choi.html.

4 Hoffman, A.C. Hansen, I.G. Beach, R.F. Plencher, R.M. Dengler, R.P. Jefferies, K.S. Frye, R.J. “Advanced Secondary Power System for Transport Aircraft” NASA technical paper 2463, May 1985.

5 Weimer, J.A. “The Role of Electric Machines and Drives in the More Electric Aircraft”, IEEE International Electric Machines and Drives Conference, 1-4 June 2003, pp.11-15.

6 Cutts, S.J. “A Collaborative Approach to the More Electric Aircraft”, International Conference on Power Electronics, Machines and Drives 2002, (Conf. Publ. No. 487), 4-7 June 2002, pp.223- 228.

7 Churn, P.M. Maxwell, C.J. Schofield, N. Howe, D. Powell, D.J. “Electro-Hydraulic Actuation of Primary Flight Control Surfaces”, IEE Colloquium on All Electric Aircraft (Digest No. 1998/260), 17 Jun 1998, pp.3/1-3/5.

8 Collins, A. “EABSYS: Electrically Actuated Braking System”, IEE Colloquium on Electrical Machines and Systems for the More Electric Aircraft (Ref. No. 1999/180), 29 October 1999, pp.4/1-4/5.

9 Robin, T. “From Fly by Wire to Power by Wire More Electric for Green Plane”, SKF presentation to Pollutec, Dec 2009.

10 Adams, C. “A380 ‘More Electric’ Aircraft”, Avionics Magazine, October 1, 2001, http://www.aviationtoday.com/av/issue/feature/A380-More-Electric-Aircraft_12874.html

11 Moir, I. Seabridge, A. “Aircraft Systems: Mechanical, Electrical and Avionics Subsystems Integration”, Published by John Wiley and Sons, 2008, ISBN 0470059966, 9780470059968.

12 Crowder, R.M. “Electrically powered actuation for civil aircraft, Actuator Technology: Current Practice and New Developments”, IEE Colloquium on (Digest No: 1996/110), 10 May 1996, pp.5/1-5/3.

13 Heney, P.J. “A380 Pushes 5000 PSI into the Realm of the Common Man”, Hydraulics and Pneumatics Magazine, http://www.hydraulicspneumatics.com/200/Issue/Article/False/6497/Issue

14 Moir, I. “The All-Electric Aircraft-Major Challenges”, IEE Colloquium on All Electric Aircraft, 17 Jun 1998, pp.2/1-2/6.

15 Rea, J. “Boeing 777 High Lift Control System”, IEEE Aerospace and Electronic Systems Magazine, Aug 1993, Volume: 8, Issue: 8, pp.15-21.

16 Nystrom, B. Austrin, L. Ankarback, N. Nilsson, E. “Fault Tree Analysis of an Aircraft Electric Power Supply System to Electrical Actuators”, International Conference on Probabilistic Methods Applied to Power Systems, 2006, 11-15 June 2006, pp.1-7.

17 Olaiya, M. Buchan, N. “High Power Variable Frequency Generator for Large Civil Aircraft”, IEE Colloquium on Electrical Machines and Systems for the More Electric Aircraft (Ref. No. 1999/180), 1999, pp.3/1-3/4.

18 Provost, M.J. “The More Electric Aero-Engine: a General Overview from an Engine Manufacturer”, IEE Power Electronics, Machines and Drives Conference, April 2002, Bath, UK, pp.246-251.

19 Powell, D.J. Jewell, G.W. Howe, D. Atallah, K. "Rotor Topologies for a Switched-Reluctance Machine for the 'More-Electric' Aircraft Engine", IEE Proceedings on Electric Power Applications, May 2003, pp.311- 318.

20 Hall, R. Jack, A.G. Mecrow, B.C. Mitcham, A.J. "Design and Initial Testing of an Outer Rotating Segmented Rotor Switched Reluctance Machine for an Aero-Engine Shaft-Line-Embedded Starter/Generator", IEEE International Conference on Electric Machines and Drives, May 2005, pp.1870-1877.

21 Mitcham, A.J. Cullen, J.J.A. "Permanent magnet generator options for the More Electric Aircraft", International Conference on Power Electronics, Machines and Drives (Conf. Publ. No. 487), 4-7 June 2002, pp.241- 245.

22 Wang J, Sun Z, Ede J.D, Jewell G.W, Cullen J.J.A, Mitcham A.J, "Testing of a 250-kilowatt fault-tolerant permanent magnet power generation system for large aeroengines", AIAA Journal of Propulsion and Power, Vol. 24(2), 2008, pp.330-335.

23 Todd, R. Abd Hafez, A.A. Forsyth, A.J. Long, S.A. "Single Phase Controller Design for a Fault Tolerant Permanent Magnet Generator", IEEE Vehicle Power and Propulsion Conference (VPCC), Sept 3-5, 2008.

24 Burrow, S.G. Mellor, P.H. Churn, P. Sawata, T. Holme, M. "Sensorless Operation of a Permanent-Magnet Generator for Aircraft", IEEE Transactions on Industry Applications, Jan.-Feb. 2008, Volume: 44, Issue: 1, pp.101-107.

25 Cossar, C. Sawata, T. "Microprocessor Controlled DC Power Supply for the Generator Control Unit of a Future Aircraft Generator with a Wide Operating Speed Range", 31 March-2 April 2004, pp.458- 463, Vol.2.

26 Nelson, T. "787 Systems and Performance", Boeing Commercial Airplanes.

27 Cotton, I. Nelms, A. Husband, M. "Defining safe operating voltages for aerospace electrical systems", Electrical Insulation Conference and Electrical Manufacturing Expo, 2007, 22-24 Oct. 2007, pp.67-71.

28 Avery, C.R.; Burrow, S.G.; Mellor, P.H. "Electrical generation and distribution for the more electric aircraft", 42nd International Universities Power Engineering Conference, 4-6 Sept. 2007, pp.1007 – 1012.

29 Haylock, J.A. Mecrow, B.C. Jack, A.G. Atkinson, D.J. "Operation of a Fault Tolerant PM Drive for an Aerospace Fuel Pump application", Eighth International Conference on Electrical Machines and Drives (Conf. Publ. No. 444), 1-3 Sep 1997, pp.133-137.

30 Mecrow, B.C. Jack, A.G. Atkinson, D.J. Green, S. Atkinson, G.J. King, A. Green, B. "Design and Testing of a 4 Phase Fault Tolerant Permanent Magnet Machine for an Engine Fuel Pump," IEEE Transactions on Energy Conversion, vol. 19, no. 4, Dec. 2004, pp.671–678.

31 Atkinson, G.J. Mecrow, B.C. Jack, A.G. Atkinson, D.J. Sangha, P. Benarous, M. "The Analysis of Losses in High-Power Fault-Tolerant Machines for Aerospace Applications", IEEE Transactions on Industry Applications, Sept.-Oct. 2006 Volume: 42, Issue: 5, pp.1162-1170.

32 Green, S. Atkinson, D.J. Jack, A.G. Mecrow, B.C. King, A. "Sensorless Operation of a Fault Tolerant PM Drive", IEE Proceedings on Electric Power Applications, Mar 2003, Vol. 150, Issue: 2, pp.117- 125.

33 Green, S. Atkinson, D.J. Mecrow, B.C. Jack, A.G. Green, B. "Fault Tolerant, Variable Frequency, Unity Power Factor Converters for Safety Critical PM Drives", IEE Proceedings on Electric Power Applications, 7 Nov. 2003, Vol. 150, Iss. 6, pp.663- 672.

34 Jensen, C. Jenney, G.D. Raymond, B. Dawson, D. "Flight test experience with an EMA on the F18 systems research aircraft", 19th Digital Avionics Systems Conference, 7-13th Oct 2000.

35 Atallah, K. Caparrelli, F. Bingham, C.M. Schofield, N. Howe, D. Mellor, P.H. Maxwell, C. Moorhouse, D. Whitley, C. "Permanent Magnet Brushless Drives for Aircraft Flight Control Surface Actuation", IEE Colloquium on Electrical Machines and Systems for the More Electric Aircraft (Ref. No. 1999/180), 1999, pp.8/1-8/5.

36 Cossar, C. Kelly, L. Miller, T.J.E. Whitley, C. Maxwell, C. Moorhouse, D. “The Design of a Switched Reluctance Drive for Aircraft Flight Control Surface Actuation”, IEE Colloquium on Electrical Machines and Systems for the More Electric Aircraft (Ref. No. 1999/180), 1999 pp.2/1-2/8.

37 Fronista, G.L. Bradbury, G. “An Electromechanical Actuator for a Transport Aircraft Spoiler Surface”, 27 Jul-1 Aug 1997, Vol. 1, pp.694-698.

38 Lemor, P.C. “The roller screw, an efficient and reliable mechanical component of electro-mechanical actuators”, Proceedings of the 31st Intersociety Energy Conversion Engineering Conference, 11-16 Aug 1996, pp.215-220, vol.1.

39 Garcia, A. Cusido, J. Rosero, J.A. Ortega, J.A. Romeral, L.”Reliable Electro-Mechanical Actuators in Aircraft”, Aug. 2008, Volume: 23, Issue: 8, pp.19-25.

40 Gerada, C. Bradley, K.J. “Integrated PM Machine Design for an Aircraft EMA”, IEEE Transactions on Industrial Electronics, Sept. 2008, pp.3300-3306.

41 Aten, M. Whitley, C. Towers, G. Wheeler, P. Clare, J. Bradley, K. “Dynamic Performance of a Matrix Converter Driven Electro-Mechanical Actuator for an Aircraft Rudder”, Second International Conference on Power Electronics, Machines and Drives, 2004. (PEMD 2004), (Conf. Publ. No. 498), 31 March-2 April 2004, Vol. 1, pp.326- 331.

42 de Lillo, L. Empringham, L. Wheeler, P. Clare, J. Bradley, K. “A 20 KW Matrix Converter Drive System for an Electro-Mechanical Aircraft (EMA) Actuator”, 2005 European Conference on Power Electronics and Applications, pp.6.

43 Ziegler, N.; Matt, D.; Jac, J.; Martire, T.; Enrici, P. “High force linear actuator for an aeronautical application. Association with a fault tolerant converter”, International Aegean Conference on Electrical Machines and Power Electronics, 10-12 Sept. 2007, pp.76 - 80

44 Ertugrul, N. Soong, W. Dostal, G. Saxon, D, “Fault Tolerant Motor Drive System with Redundancy for Critical Applications”, IEEE 33rd Annual Power Electronics Specialists Conference 2002, Vol. 3, pp.1457- 1462.

45 Kamath, G.R. Runyan, B. Wood, R. “A Compact Autotransformer Based 12-Pulse Rectifier Circuit”, The 27th Annual Conference of the IEEE Industrial Electronics Society 2001, Vol. 2, pp.1344-1349.

46 Gong, G. Heldwein, M.L. Drofenik, U. Minibock, J. Mino, K. Kolar, J.W. “Comparative Evaluation of Three-Phase High-Power-Factor AC-DC Converter Concepts for Application in Future More Electric Aircraft”, IEEE Transactions on Industrial Electronics, June 2005, Vol. 52, Iss. 3, pp.727- 737.

47 Wheeler, P W Kearns, P Bradley, K J de Lilo, L Robson, P Whitley, C Clare, J C Empringham, L Pickering, S Lampard, D Towers, G “An Integrated Machine and Matrix Converter based High Power Rudder EMA”, The 3rd IET International Conference on Power Electronics, Machines and Drives, Mar. 2006, pp.167-171.

48 Huang, X. Bradley, K. Goodman, A. Gerada, C. Wheeler, P. Clare, J. Whitley, C. “Fault-Tolerant Brushless DC Motor Drive For Electro-Hydrostatic Actuation System In Aerospace Application”, Conference Record of the 2006 IEEE Industry Applications Conference, 41st IAS Annual Meeting, 8-12 Oct. 2006, Vol. 1, pp.473-480.

49 Thomas. J, Maxwell.C, Benarous.M, “Electrically Actuated Landing Gear for a Civil Aircraft Application”, UK Magnetics Society More Electric Aircraft Seminar, 2 April 2009, pp.1.

50 Cannon, W.E. “A Pictorial Tour of the 146/RJ Flap Circuit”, BAE Systems document, 2000.

51 Ferland, G. Chikhani, A. Cartier, J.C. “Harmonic and Transient Analysis of an Aircraft Electrical Distribution System”, Canadian Conference on Electrical and Computer Engineering, 14-17 Sep 1993, pp.668-671.

52 Messier-Bugatti “LEHGS, Local Electro-Hydraulic Generation System”, www.messier-bugatti.com.

53 Han, L. Wang, J. Howe, D. “Stability Assessment of Distributed DC Power Systems for ‘More-Electric’ Aircraft”, 4th IET Conference on Power Electronics, Machines and Drives, 2008, 2-4 April 2008, pp.661-665.

54 Sadeghi, T. Lyons, A. “Fault Tolerant EHA Architectures”, IEEE Aerospace and Electronic Systems Magazine, Mar 1992 Volume: 7, Issue: 3, Part 1 pp.32-42.

55 Jahns, T.M. “Improved Reliability in Solid-State AC Drives by Means of Multiple Independent Phase Drive Units”, IEEE Transactions on Industry Applications, May 1980, Volume: IA-16, Issue: 3, pp.321-331.

56 Miller, T.J.E. “Faults and Unbalance Forces in the Switched Reluctance Machine”, Conference Record of the 1993 IEEE Industry Applications Society Annual Meeting, 1993, 2-8 Oct 1993, Volume 1, pp.87-96.

57 Spee, R.; Wallace, A.K. “Remedial strategies for brushless DC drive failures”, Power Electronics Specialists Conference, 11-14 April 1988 pp.199 – 206, vol.1

58 Tavner, P.J. Hasson, J.P. “Predicting the Design Life of High Integrity Rotating Electrical Machines”, Ninth International Conference on Electrical Machines and Drives, 1999, pp.286-290.

59 Jack, A.G.; Mecrow, B.C.; Haylock, J.A. “A comparative study of permanent magnet and switched reluctance motors for high-performance fault-tolerant applications”, IEEE Transactions on Industry Applications, Vol. 32, Iss. 4, July-Aug. 1996, pp.889 - 895

60 Welchko, B.A. Lipo, T.A. Jahns, T.M. Schulz, S.E. “Fault tolerant three-phase AC motor drive topologies; a comparison of features, cost, and limitations”, IEEE International Electric Machines and Drives Conference, 1-4 June 2003, pp.539- 546 vol.1.

61 van der Broeck, H.W. Skudelny, H.-C. Stanke, G.V. “Analysis and realization of a pulsewidth modulator based on voltage space vectors” IEEE Transactions on Industry Applications, Jan/Feb 1988, pp.142 – 150.

62 Bennett, J.W. Jack, A.G. Mecrow, B.C. Atkinson, D.J. Sewell, C. Mason, G. “Fault-Tolerant Control Architecture for an Electrical Actuator”, IEEE 35th Annual Power Electronics Specialists Conference, 20-25 June 2004, pp.4371- 4377 Vol.6.

63 Ede, J.D. Atallah, K. Wang,J. Howe, D. “Effect of Optimal Torque Control on Rotor Loss of Fault-Tolerant Permanent-Magnet Brushless Machines”, IEEE Transactions on Magnetics, Sep 2002, pp.3291- 3293.

64 Ede, J.D. Atallah, K. Wang, J.B. Howe, D. “Modular Fault-Tolerant Permanent Magnet Brushless Machines”, International Conference on Power Electronics, Machines and Drives, 4-7 June 2002. pp.415- 420.

65 Zhu, J.W. Ertugrul, N. Soong, W.L. “Fault Analysis and Remedial Strategies on a Fault-Tolerant Motor Drive with Redundancy”, IEEE International Electric Machines & Drives Conference, 3-5 May 2007, pp.1119-1124.

66 Yeh, Y.C. “Triple-Triple Redundant 777 Primary Flight Computer”, IEEE Proceedings on Aerospace Applications Conference, 3-10 Feb 1996, pp.293-307, vol.1.

67 J.R. Sklaroff, "Redundancy Management Technique for Space Shuttle Computers”, IBM Journal of Res. and Dev., Vol. 20, Jan.1976, pp.20-25.

68 Pieters, P. Riikonen, J. “Case study: To eliminate major root causes of failures with VSDs installations”, 5th Petroleum and Chemical Industry Conference Europe - Electrical and Instrumentation Applications, 10-12 June 2008, pp.1-7.

69 Lemor, P.C. “The roller screw, an efficient and reliable mechanical component of electro-mechanical actuators”, Proceedings of the 31st Intersociety Energy Conversion Engineering Conference, 11-16 Aug 1996, pp.215-220, vol.1.

70 Acarnley, P.P. Watson, J.F. “Review of position-sensorless operation of brushless permanent-magnet machines”, IEEE Transactions on Industrial Electronics, April 2006, Vol. 53, Iss. 2, pp.352-362.

71 Johnson, J.P. Ehsani, M. Guzelgunler, Y. “Review of sensorless methods for brushless DC”, Industry Applications Conference Annual Meeting, 3-7th Oct 1999, pp.143-150, vol.1.

72 Kim,e-H. Lee, H-W. Ehsani, M. “State of the art and future trends in position sensorless brushless DC motor/generator drives”, 31st Annual Conference of IEEE Industrial Electronics Society, 6-10 Nov. 2005, pp.1728-1725.

73 Chen, L. Avizienis, A. “N-Version Programming: A Fault Tolerance Approach to Reliability of Software Operations”, IEEE 8th Annual International Symposium on Fault-Tolerant Computing, 1978, pp.13-19.

74 D. M. Blough and G. F. Sullivan, “A comparison of voting strategies for fault-tolerant distributed systems”, IEEE Proceedings of 9th Symposium on Reliable Distributed Systems, Oct. 1990, pp.136-145.

75 Latif-Shabgahi, G. Bennett, S. and Bass, J. M. “Smoothing voter: A novel voting algorithm for handling multiple errors in fault-tolerant control systems”, Microprocessors and Microsystems, 27(7), pp.303-313.

76 Gersting, J.L. Nist, R.L. Roberts, D.B. Van Valkenburg, R.L. “A Comparison of Voting Algorithms for n-version Programming”, Proceedings of the 24th International Conference on System Sciences, 8-11 Jan 1991, pp.253-262, vol.2.

77 Lawson, M. Chen, X. “Fault tolerant control for an electric power steering system”, IEEE International Conference on Control Applications, 3-5 Sept. 2008, pp.486-491.

78 Dumont, P.E. Aitouche, A. Merzouki, R. Bayart, M. “Fault Tolerant Control on an Electric Vehicle”, IEEE International Conference on Industrial Technology, 15-17 Dec. 2006, pp.2450-2455.

79 Haylock, J.A. Mecrow, B.C. Jack, A.G. Atkinson, D.J. “Operation of fault tolerant machines with winding failures”, IEEE International Electric Machines and Drives Conference Record, 18-21 May 1997, pp.MC3/10.1-MC3/10.3.

80 Takorabet, N. Caron, J.P. Vaseghi, B. Nahid-Mobarakeh, B. Meibody-Tabar, F. Humbert, G. “Study of Different Architectures of Fault Tolerant Actuator Using a Double-Star PM Motor”, Industry Applications Society Annual Meeting, 5-9 Oct. 2008, pp.1-6.

81 Imayavaramban, M.; Wheeler, P.W. “Avoiding Regeneration with a Matrix Converter Drive”, IEEE Power Electronics Specialists Conference, 17-21 June 2007, pp.2529 - 2534

82 Khatre, M. Jack, A.G. “Simulation of PMSM VSI Drive for Determination of the Size Limits of the DC-Link Capacitor of Aircraft Control Surface Actuator Drives”, International Conference on Power Electronics, Drives and Energy Systems, 12-15 Dec, 2006 pp.1-6.

83 RTCA, “DO-160F. Environmental Conditions and Test Procedures for Airborne Equipment”. Aviation industry standards and procedures document, 2007. pp.16-41

84 CDE Cornell Dubliner “Type UNL ElectroFilm High Current Capacitors”, product datasheet.

85 EPCOS “Power line chokes”, product datasheet.

86 Thompson, K. “Notes on `The electric control of large aeroplanes'” IEEE Aerospace and Electronic Systems Magazine, Dec 1988, pp.19-24.

87 Mellor, P.H. Allen, T.J. Ong, R. Rahma, Z. “Faulted behaviour of permanent magnet electric vehicle traction drives”, IEEE International Electric Machines and Drives Conference, 1-4 June 2003, pp.554- 558, vol.1.

88 Haskew, T.A. Hill, E.M. “Regeneration mechanisms in a DC motor with an H-bridge inverter”, International Conference on Electric Machines and Drives, May 1999, pp.531-533.

89 Wijekoon, T. Empringham, L. Wheeler, P.W. Clare, J.C. Whitley, C. Towers, G. “Aircraft Electrical Landing Gear Actuation Using Dual-output Power Converter with Mutual Power Circuit Components”, 24th IEEE Applied Power Electronics Conference and Exposition, 8-10 Sept. 2009, pp.1-10.